A thiol-disulphide switch in the regulation of cytoskeletal dynamics

Inauguraldissertation

zur

Erlangung des akademischen Grades eines

Doktors der Naturwissenschaften (Dr. rer. nat.)

der

Mathematisch-Naturwissenschaftlichen Fakultät

der

Ernst-Moritz-Arndt-Universität Greifswald

vorgelegt von

Manuela Gellert

geboren am 21.06.1981

in Suhl

Greifswald, Mai 2017

Dekan: Prof. Dr. Werner Weitschies

1. Gutachter: Prof. Dr. Christiane A. Helm
2. Gutachter: PD Dr. Christopher H. Lillig
3. Gutachter: Prof. Dr. Marcel Deponte
4. Gutachter: Prof. Dr. Jan Riemer

Tag der Promotion: 28.08.2017

Every great advance in science has issued from a new audacity of imagination.

John Dewey (The Quest of Certainty, 1929)

To my family.

Table of contents

1 Introduction

The ability to receive and interpret signals from the environment as well as the coordinated and specific response to these signals is of primary importance for every living cell. Many diseases, such as degenerative and malignant disorders, arise from errors or misinterpretations in this signal transduction. The common principle of signal transduction includes sensing of signalling molecules by an intra- or extracellular receptor, transduction of this signal through the activated receptor by activation of transducer molecules and subsequent regulation of second messenger molecules or effector proteins, that, in the end, trigger a biological effect. These sophisticated pathways enable adaption, modulation, and amplification of signal and response. Besides the well established signalling mechanism through reversible phosphorylation, the reversible redox modification of protein side chains as key mechanism, affecting essentially all signalling pathways, came into focus in recent years (1–3). Redox modifications appear to be rapid, compartmentalised, reversible and highly specific (1,4–7). None of these post-translational redox modifications occur randomly, they need to be catalysed by specific enzymes (2).

1.1 Redox signalling

In the past, the measure of the change in Gibb's free energy (ΔG) during a chemical reaction has been used to characterise redox modifications with the help of redox potentials. This concept is based on the assumption of an equilibrium between pro- and anti-oxidants within the cell. An imbalance favouring the oxidation of biomolecules was defined as oxidative stress (8,9). Oxidative stress was held responsible for a variety of pathological conditions such as neurodegenerative diseases or cancer, supported by the apparent accumulation of oxidised molecules (10–12). During the last decade, however, the paradigm started to shift from oxidative stress to well defined and very specific redox signalling mechanisms. These mechanisms depend on rapid, compartmentalised, reversible and specific redox modifications of target molecules and proteins (4–7). Signal transduction depends on reaction kinetics and enzymatic catalysis, that are not determined by ΔG. In this new concept, based on specific redox dependent modifications, the enzyme family of oxidoreductases as well as reactive oxygen, nitrogen, and sulphur species came into focus as key elements of redox signalling (3,13–15). The cysteinyl thiol group is a major target in redox signalling due to its unique chemistry (16).

1.1.1 Redox modifications of cysteinyl side chains

The cysteinyl side chains are the major target of redox signalling (Fig. 1, left side). Oxidation of protein thiols can lead to the formation of inter- or intramolecular disulphides. A disulphide may also be formed with small molecular weight thiols, such as glutathione (GSH), the most abundant

cellular thiol compound, a process known as S-glutathionylation (2). Reaction of endogenously produced nitric oxide with thiols, catalysed by metals, can induce S-nitrosylation of protein thiols. Another way for S-nitrosylation is the transfer of S-nitroso groups to other protein thiols, *i.e.* trans-nitrosylation (17,18). Cysteinyl thiols may also be oxidised to sulphenic acid, or even further to sulphinic or sulphonic acid, by reaction with hydrogen peroxide or peroxy nitrite (19). Sulphinic and sulphonic acid occur at specific target sites but are considered to be irreversible (20). The described modifications are specific for the redox active compound, for example second messenger molecules, as well as the cysteinyl side chains of transducer and effector proteins (21). The molecular environment of the thiol group and the enzymes involved in the reaction determine this specificity (1).

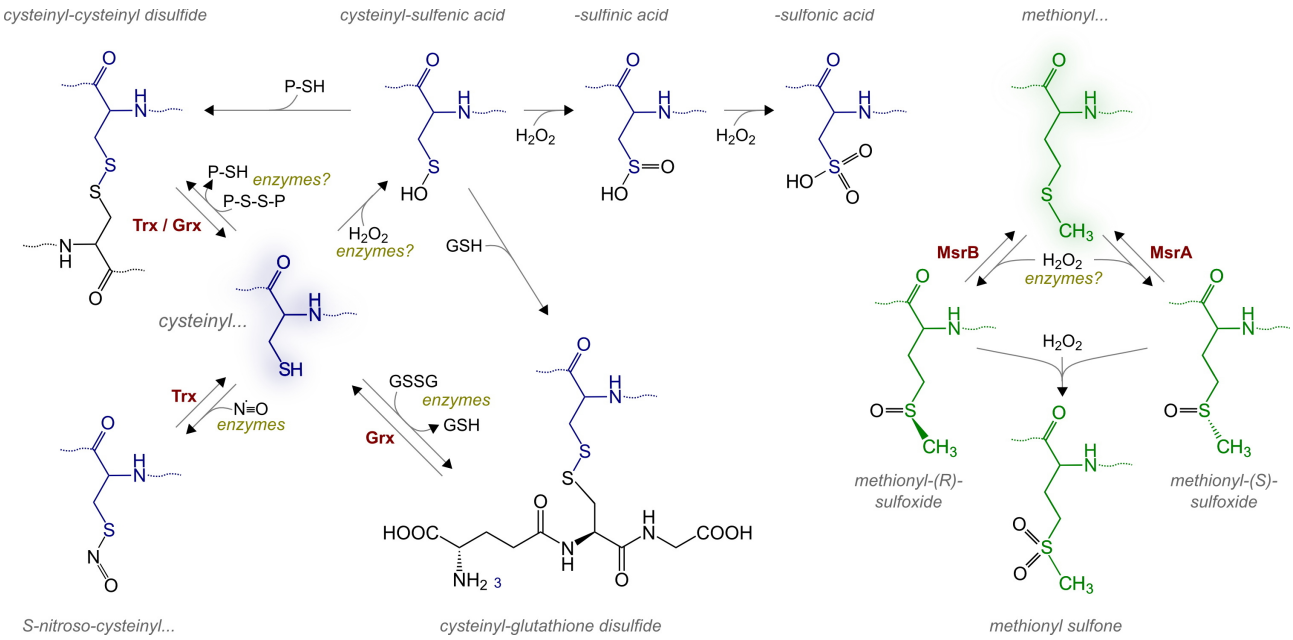

Fig. 1: Redox modifications of protein cysteinyl and methionyl residues. In the presence of another thiol (SH), the cysteinyl residue (left site, blue) can be modified to a protein (cysteinyl-cysteinyl) disulphide, that can be reduced by Trxs and Grxs, or cysteinyl-glutathione mixed disulphides. Protein cysteinyl residues can be oxidised to sulphenic acid (R-SOH) by peroxides or (at least in some cases) by specific enzymes. In the presence of excessive peroxides this may be irreversibly 'over'-oxidised to sulphinic ($R\text{-}SO_2\text{-}H$) and sulphonic acid ($R\text{-}SO_3\text{-}H$). Cysteinyl-glutathione disulphides may also be formed through thiol-disulphide exchange reactions with glutathione disulphide or by specific enzymes, *e.g.* Grxs that also specifically catalyse the reduction of these disulphides. Nitric oxide (·NO) in general can only lead to the nitrosylation of cysteinyl residues through the catalysis during which one electron is transferred from the ·NO to a recipient, *e.g.* a metal cofactor. S-nitrosylation can be reversed by trans-nitrosylation to another protein thiol, *e.g.* to the active site of Trxs. Methionyl residues (right site, green) are oxidised stereo-selective to R- or S-methionyl-sulphoxides. These are specific substrates for methionine sulphoxide reductases (Msr) B and A, respectively. Further oxidation of methionyl sulphoxides results in methionyl sulphone, a step that has to be considered irreversible. From Gellert et al.: Redox regulation of cytoskeletal dynamics during differentiation and de-differentiation (article IV in this thesis). (1)

1.1.2 Methionine sulphoxidation

The thioether group of methionine can be reversibly oxidised to methionine sulphoxide (Fig. 1, right side), a modification also recognised as a redox signalling mechanism (22). Oxidation of the methionyl residues is also specifically catalysed by enzymes suggesting a fine tuned activation or

inactivation of protein functions via the methionine sulphoxide formation (22,23). Oxidation of the methionine thioether group results in a mixture of methionine-S-sulphoxide and methionine-R-suphoxide, the two diastereomers. The stereospecific reduction of methionine-S-sulphoxide is catalysed by methionine sulphoxide reductase (Msr) A, in a mechanism that requires three cysteinyl residues in the catalytic centre. Methionine-R-sulphoxide, on the other hand, is stereospecifically reduced by MsrB, the activity of which requires only two cysteinyl residues (24). Human MsrA is expressed in various isoforms and localised in different compartments (25–27). The oxidised enzyme is reduced by thioredoxins (Trxs) or glutaredoxins (Grxs) (24,28). Of the three MsrB genes that most mammalian genomes posses, MsrB1 exhibits the highest activity. MsrB1 contains a selenocysteinyl residue in its active site instead of the catalytic cysteinyl residue. MsrB2 and 3 are less catalytically efficient and contain cysteinyl residues only (29,30). Oxidised MsrB is reduced by Trxs or Grx, directly or via a glutathione-mixed disulphide (24,28,29). An overview of the reaction mechanism of MsrA and B is depicted in Fig. 2C. In contrast to the two separate mammalian MsrA and B enzymes, the two enzymes are translationally fused as MsrAB in some bacteria, such as *Streptococcus pneumoniae*, *Neisseria gonorrhoeae* and *Haemophilus influenzae* (31–33). Oxidised MsrAB is subsequently reduced by Trxs (34–36). Fused *Sp*MsrAB2 also carries a transmembrane domain that anchors the protein to the membrane. Both catalytic domains reduce stereo-specific methionyl sulphoxides as described above (Fig. 1). The cytosolic NADPH pool provides electrons, that are shuttled between cytosolic Trx and integral membrane proteins to two surface-exposed thioredoxin-like lipoproteins (Etrx1/2), to keep pneumococcal surface proteins in the reduced state. The molecular architecture of Etrx1 and Etrx2 and their redox partner *Sp*MsrAB2, in *S. pneumoniae* will be presented later in this thesis [article II].

1.1.3 The thioredoxin-fold family of proteins

Many key enzymes of redox signalling, which catalyse the modifications of thiol groups, *e.g.* disulphide reduction, glutathionylation or trans-nitrosylation, are members of the so called thioredoxin family of proteins. The name-giving Trxs as well as Grxs and peroxiredoxins (Prx) belong to this protein family, with isoforms expressed ubiquitously in all organisms, tissues, cells and organelles (37–40). Their common structural motif, the thioredoxin fold, that, in its most basic form, consists of a central four stranded β-sheet surrounded by three α-helices, defines the Trx family of proteins (41).

Trxs were discovered in *E. coli* around 1968 as electron donor for ribonucleotide reductase (RNR) (42,43). The small, approximately 12 kDa proteins are characterised by their highly conserved Cys-Gly-Pro-Cys active site motif. About a decade later, Grxs were identified as GSH-dependent alternative electron donor for RNR in *E. coli* (44–46). Additionally, Grxs are divided in

two major subfamilies, depending on their active site motif. Dithiol-Grxs (Cys-Pro-Tyr-Cys) and monothiol-Grxs (Cys-Gly-Phe-Ser) both require GSH for their extensive functions in redox signalling and iron metabolism, respectively (37). Proteins of the third branch of the Trx family of proteins, Prxs, reduce peroxides rather than protein disulphide (3).

Both, Trxs and dithiol-Grxs use the Cys-X-X-Cys active site, located on the loop connecting sheet 1 and helix 1 (bacterial Grx numbering), to catalyse the reduction of protein disulphides in the so called dithiol mechanism (see Fig. 2, A and B). The low pK_a value of the N-terminal active site

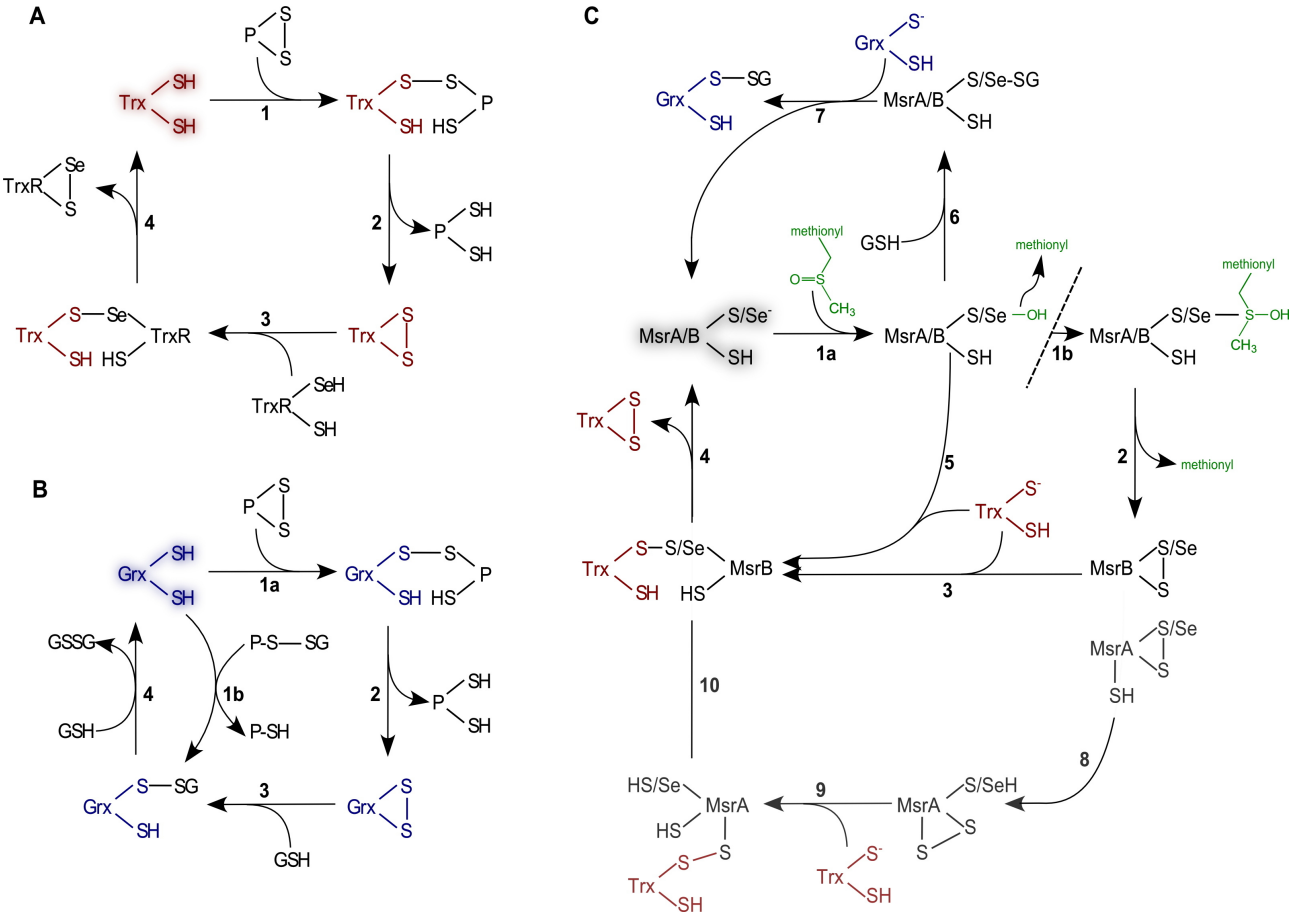

Fig. 2: Reaction mechanisms of thioredoxins, glutaredoxins, and methionine sulphoxide reductase. (A) Trxs (red) reduce protein disulphides in the dithiol mechanism using both active site thiols (SH). The N-terminal active site cysteinyl residue forms a covalent mixed disulphide intermediate with the oxidised substrate protein (A 1), which is reduced in the second step by the C-terminal active site cysteinyl residue, releasing a reduced protein (A 2). The disulphide in the active site of oxidised Trx is reduced by NADPH-dependent TrxR in a similar reaction sequence (A 3 and 4). (B) Grxs (blue) also reduce protein disulphides, similar to Trxs, but their active site disulphide is reduced by two molecules of glutathione (GSH) (B 1a-4). In addition, Grxs reduce protein-cysteinyl-glutathione mixed disulphides in the so called monothiol mechanism (B 1b and 4), that only depends on the N-terminal active site cysteinyl residue. This thiolate attacks the GSH moiety and forms a GSH-mixed disulphide intermediate itself (B 1b), that is subsequently reduced by another GSH molecule (B 4). (C) The catalytic active site sulphenic cysteinyl residue of MsrAs and Bs (black/grey) reacts with methionine-R/S-sulphoxide yielding a sulphenic acid intermediate (C 1a) or a methionyl-bound intermediate (C 1b). Both are attacked by the second cysteinyl residue leading to the formation of a disulphide with the catalytic cysteinyl residue (C 2). In case of MsrAs, this disulphide is attacked by a third cysteinyl residue leading to a disulphide between the second and third cysteinyl residues (C 8). In either case, the disulphide in the active sites of the MsrA and MsrB is a substrate for Trxs or Grxs (C 3-4 or 8-10). Alternatively, the sulphenic/selenenic intermediate may react with GSH yielding a glutathione mixed disulphide (C 6), that is reduced by Grxs (C 7). From Gellert et al.: Redox regulation of cytoskeletal dynamics during differentiation and de-differentiation (article IV in this thesis). (1)

thiol allows the initiation of a nucleophilic attack on one of the sulphur atoms of the substrates disulphide, leading to the formation of a transient mixed disulphide intermediate (47). In the second reaction step, this mixed disulphide intermediate is reduced by the second C-terminal cysteinyl residue, resulting in the release of a reduced substrate and an oxidised Trx or Grx, respectively (38). The oxidised active site of Trx is regenerated by NADPH-dependent thioredoxin reductase (TrxR) (48). Oxidised Grx, on the other hand, is reduced by NADPH via the glutathione reductase (GR) and GSH (49). Reversible (de-)glutathionylation, exclusively catalysed by dithiol Grx and few monothiol Grx, depends only on the N-terminal active site cysteine (50,51). The nucleophilic attack of this N-terminal active site thiol on the sulphur atom of the GSH in the glutathionylated protein leads to the release of the reduced target protein and the formation of a mixed disulphide between Grx and GSH (Fig. 2B). This mixed disulphide is subsequently reduced by a second GSH molecule (52,53). In the third branch of thioredoxin family proteins, six mammalian peroxiredoxins that are divided into 3 groups, based on their structure and catalytic mechanism, have been described. They are categorised as 2-Cys Prx (Prx1-4), atypical 2-Cys Prx (Prx5), and 1-Cys Prx (Prx6) (54,55). Prxs are highly abundant proteins with a peroxidase activity but alternative functions have been proposed. Most Prxs function as homodimers, but also form decamers and stacks of decamers (2-Cys Prx) (3).

1.1.4 Cytosolic thioredoxin

One cytosolic and one mitochondrial Trx/TrxR couple are encoded in the mammalian genome (3). Trxs catalyse the protein disulphide reduction via the two cysteines in the highly conserved Cys-Gly-Pro-Cys active site, discovered in 1968 (56). As depicted in Fig. 2A the N-terminal cysteinyl residue induces the formation of a mixed disulphide intermediate via nucleophilic attack of a target protein disulphide. This mixed disulphide is reduced by the C-terminal active site cysteine, resulting in the release of a reduced target protein and an oxidised Trx (57). In addition to the active site cysteines, Trx1 contains three structural cysteinyl residues that have been implicated in the formation of Trx1-dimers as well as regulatory functions (58,59). Although Trx1 is a cytosolic protein without a nuclear localisation sequence, the translocation to the nucleus has been observed under certain conditions (60,61). It has also been demonstrated that Trx1, even though it lacks a signal sequence for secretion via the endoplasmatic reticulum (ER), is secreted in a non-classic pathway involving neither the ER nor the Golgi apparatus and is independent of the redox state of Trx1 (62,63).

Oxidised Trxs are reduced by TrxR using electrons derived from NADPH in a similar reaction mechanism. Mammalian TrxRs are selenoproteins containing a flavin adenine di-nucleotide (FAD) domain as well as an NADPH binding domain. TrxRs form homodimers in a head-to-tail

conformation and possess two active site motifs, the selenocysteine containing active site (Gly-Cys-Sec-Gly) being located at the C-terminus of the protein (64,65). The second active site motif (Cys-Val-Asn-Val-Gly-Cys) is located at the N-terminus, adjacent to the FAD domain (65).

1.1.5 Mammalian glutaredoxins

Four different mammalian Grxs have been identified, so far. All four of them are well conserved in other vertebrate species. Two Grxs, Grx1 and 2, are classical dithiol Grx and two monothiol Grx, Grx3 (also known as PICOT (PKC-interacting cousin of thioredoxin) or TXNL-2 (thioredoxin-like2)) and Grx5 (66–69). The multidomain monothiol Grxs are restricted to eukaryotic cells only, whereas dithiol and single domain monothiol Grxs are ubiquitously present in all kingdoms of life (37).

The dithiol Grx1 is the most well characterised mammalian Grx with a widely conserved Cys-Pro-Tyr-Cys active site motif. The protein of about 12 kDa is considered to be located in the cytosol, the nucleus and the mitochondrial intermembrane space (70,71). Glutaredoxin 1 has been shown to support RNR with electrons and general dithiol-disulphide exchange reactions (72). It was also demonstrated to be involved in dehydroascorbate reduction, cellular differentiation, regulation of transcription factors, and apoptosis (38,73–79).

Grx2, about 14 kDa in size (18 kDa unprocessed), shares 34% sequence homology with Grx1. The active site of Grx2 consists of Cys-Ser-Tyr-Cys, with an exchange of the prolyl for a seryl residue (67,80). This altered active site sequence results in an increased affinity of Grx2 for glutathionylated proteins and therefore leads to an increased catalytic efficiency compared to Grx1. Grx2 can be reduced by either GSH or TrxR, combining characteristics of Trxs and Grxs. It was also described as the first Trx family protein that complexes an iron-sulphur cluster (81–83).

The monothiol Grx3 is a multidomain protein of about 37 kDa, that is located in the cytosol. It consists of an N-terminal Trx domain, with a redox inactive active site and two C-terminal monothiol Grx domains, that posses highly conserved Cys-Gly-Phe-Ser active sites (51,69).

Grx5 is a single domain monothiol Grx located in mitochondria. It is comparable in size to the dithiol Grxs with the same active site motif as the monothiol Grx3 (Cys-Gly-Phe-Ser). Neither Grx5 nor Grx3 catalyse mono- or dithiol mechanism reactions (51). Both proteins, Grx3 and 5, are important for iron homoeostasis and the synthesis of iron-sulphur proteins in vertebrates and yeast, respectively (3,84–87).

1.1.5.1 Glutaredoxin 2 isoforms

In 2001, the mammalian Grx2 (Gene: GLRX2) was identified and proposed to have two isoforms differing in their first exon (67,80). The GLRX2 gene consists of five exons, including two

alternative first exons (Ia and Ib). The core domain of Grx2, including the active site, is encoded by exon II-IV. Alternative transcription and splicing results in three transcript variants. Exon Ia encodes a mitochondrial localisation sequence and is part of the mRNA variant GLRX_v1 (exon Ia-II-III-IV). This mitochondrial Grx2a is ubiquitously expressed. GLRX_v2 and v3 are products of two alternative splice donor sites of the alternative exon Ib, they encode the nuclear and cytosolic isoforms Grx2b and Grx2c. The expression of Grx2b and Grx2c is restricted to testis, in adult human tissues, but has also been demonstrated in various cancer cell lines (88). In contrast, the mouse GLRX2 gene consists of six exons, three constitutive exons (II, III, IV), two alternative first exons (Ia, Ib) and one single cassette exon. Five transcript variants encoding for three protein isoforms arise through alternative transcription and splicing, but the mitochondrial Grx2a and the nuclear/cytosolic Grx2c are conserved from mouse to man. Testis-specific Grx2d is unique to mouse (89).

1.1.5.2 Cytosolic glutaredoxin 2

Also genomes of other vertebrate species, like zebrafish for instance, contain genes encoding homologues to the cytosolic Grx2 isoform. It has been demonstrated, that this cytosolic zfGrx2 is essential for brain development. Zebrafish with silenced expression of cytosolic Grx2 lose essentially all types of neurons by apoptotic cell death and fail to develop an axonal scaffold (90). Only the re-introduction of wildtype Grx2c could rescue the defects, but neither of the redox-inactive active site mutants, that are not able to catalyse protein disulphide reduction (90). Overexpression of Grx2c in SH-SY5Y neuroblastoma cells during retinoic acid induced differentiation increases axon length by a factor of 1.5 to 2 and the number of branching points 2-fold (90). Cytosolic Grx2 has an essential function also for vascular development and maintenance of cardiovascular function (50,91). Zebrafish lacking cytosolic Grx2 have an impaired heart looping and defects in heart functionality due to a failed migration of cardiac neural crest cells (92). This heart looping defect could be rescued by introduction of the active site mutant of zfGrx2 that is still able to catalyse monothiol mechanism reactions (92). Grx2c has also an essential function in spermatogenesis, a process that includes the migration of spermatogenic cells through the close Sertoli cell formation (88). Taken together, all these findings suggest that Grx2c may promote cell motility as well as invasion behaviour of cells in general. Characterisation of a HeLa cell line overexpressing Grx2c at moderate levels (HeLa Grx2c^{+} cells, (93)), which induces dramatic alterations in cell morphology, motility, and invasion, will be presented in [manuscript VI].

In a proteomic approach, Schütte et al. were able to identify target proteins, that undergo thiol-disulphide exchange reactions catalysed by Grx2 in the dithiol reaction mechanism (94). One potential target protein identified was collapsin response mediator protein 2 (CRMP2). As part of

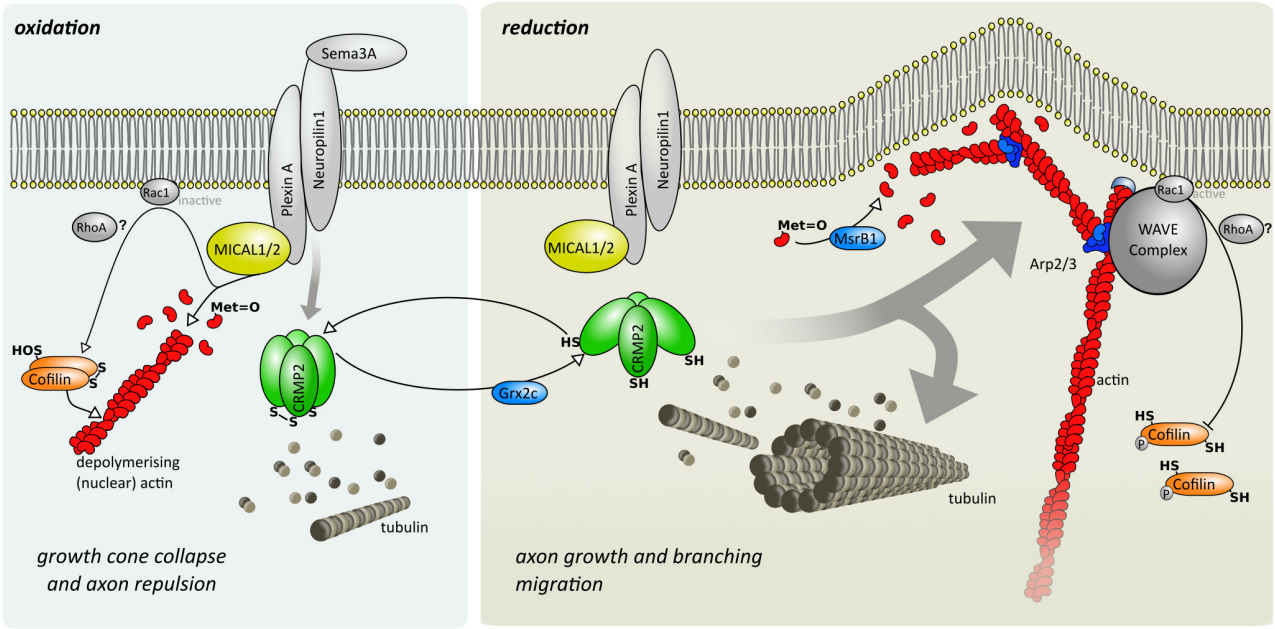

Fig. 3: Redox switches in semaphorin signalling, cofilin, and actin dynamics. Sema3A binding to NP1 activates PlexA and the semaphorin signalling cascade. Activated PlexA interacts with MICAL1/2 that then leads to actin de-polymerisation, through cofilin activation or the proposed sulphoxidation of methionyl residues of β-actin. CRMP2 is another mediator of the Sema3A signalling cascade that induces growth cone collapse and axon repulsion (left side: 'oxidation'). Without ligand binding, MICALs are not activated by the NP1/PlexA receptor. The reduction of CRMP2 by cytosolic Grx2c leads to a conformational change of the homotetramer. This conformational change causes (directly or indirectly) the polymerisation of actin and tubulin. MsrB1 is able to reduce the sulphoxides of methionyl residues of β-actin, allowing polymerisation. The WAVE complex is activated close to the membrane by active Rac1 and binds Arp2/3 which leads to actin polymerisation and branching. Activated Rac1 also leads to the phosphorylation and therefore inactivation of cofilin. The absence of Sema3A and the resulting changes of the cytoskeletal dynamics lead to axon outgrowth and branching as well as enabling active migration (right side: 'reduction'). From Gellert et al.: Redox regulation of cytoskeletal dynamics during differentiation and de-differentiation (article IV in this thesis) (1)

the semaphorin3A-signalling cascade and regulator of cytoskeletal dynamics, CRMP2 has critical functions for both axon guidance and cell migration (95,96). In agreement with these results, CRMP2 was significantly more oxidised in zebrafish lacking the cytosolic form of Grx2 (90).

1.2 Collapsin response mediator protein family

The collapsin response mediator protein family consists of 5 homologous cytosolic proteins. The proteins of this family were identified by various authors and have been named in many different ways, *e.g.* TOAD-64 (turned on after division, 64 kDa), Ulip (uncoordinated 33-like protein), and DRP or DPYL/DPYSL (dihydropyrimidinase-related protein), but the most frequently notation used today is CRMP (97,98). CRMP1-4 share about 75% homology with each other and function as tetrameric complexes, while CRMP5 shares only 50% homology and may form heterodimers with CRMP1-4 (99,100). Additionally, CRMP1, 2, and 4 can be expressed in two alternative isoforms, derived from alternative splicing, leading to alternative N-termini (100). The C-terminal regions of the proteins were predicted to be rather unfolded, however, these regions contain binding sites for

the two major proteins of the cytoskeleton, *i.e.* tubulin and actin (99), and various regulatory phosphorylation sites (97). The CRMPs do not function as enzymes, instead they are thought to function as scaffolds for specific protein-protein interactions (97–99). All CRMPs are highly expressed in the nervous system with distinct spatio-temporally controlled expression patterns and localisations during development (101–103). Particularly in this phase, the proteins are required for, *e.g.*, axon formation and extension (CRMP1), axon guidance, elongation, and branching (CRMP2 and 4), as well as filopodial dynamics and the development of growth cones (CRMP5).

1.2.1 CRMP2

The first identified, most abundant, and also the most widely studied protein of the CRMP family is CRMP2 (DPYSL2). CRMP2 regulates and controls various physiological processes such as cell signalling, metabolism, cell migration and trafficking, growth, and immune function. All of these functions, however, come down to the proteins function as a scaffold for protein-protein interactions, primarily for proteins that control cytoskeletal dynamics, *e.g.* cell adhesion and migration (97–99, 123). Alternative first exons give rise to two different CRMP2 isoforms (CRMP2A and B) with opposing activities, contributing to cell morphology and axonogenesis by microtubule remodelling (105). The subcellular localisation of these isoforms depends on cell type, developmental stage, and neuronal compartment (106). In general, ‘CRMP2’ refers to the canonical isoform CRMP2B (unless otherwise stated).

CRMP2 forms homo- as well as heterotetrameric complexes (107–110), the formation of CRMP2 homotetramers *in vitro* will also be presented in [article I]. Binding of tubulin-heterodimers and the promotion of microtubule assembly during axonal outgrowth is an established function of CRMP2 (111). It also directly interacts with the specifically Rac1-associated protein 1 (Sra1)/WASP family veroprolin-homologous protein 1 (WAVE1) complex, a regulator of actin dynamics (112). CRMP2 affects axon outgrowth also through the kinesin 1-dependent transport of the Sra1/WAVE1 complex via direct interaction between CRMP2 and the light chain of kinesin 1 (112). The activity of CRMP2 is modulated by α2-chimaerin in the regulation of bipolar transition and neuronal migration (113). Direct interaction of CRMP2 with N-type Ca^{2+} channels modulates the Ca^{2+} influx into the nerve terminals, and therefore the synaptic strength (114). In non-neuronal cells, MICAL-L1 (MICAL-like protein 1) has been identified as interaction partner of CRMP2 (115).

1.2.1.1 Posttranslational modifications of CRMP2

CRMP2 is regulated via various posttranslational modifications. Foremost, several phosphorylation sites, mostly located in the C-terminus of CRMP2, affect its function in the semaphorin 3A (Sema3A)-signalling pathway (see below) (97). These differential phosphorylation events modulate the contribution of CRMP2 to cytoskeletal remodelling during neuronal

development as well as to the chemokine-directed T-cell migration (116). The priming phosphorylation of Ser522 by cyclin-dependent kinase 5/p35 (CDK5) facilitates the phosphorylation of Thr509, Thr514, and Ser518 by glycogen synthase kinase-3 beta (GSK3β) (117–121). Phosphorylation of Tyr32 is catalysed by tyrosine-protein kinase Fyn (122). These five phosphorylation events control, among other functions, the binding of CRMP2 to tubulin (117–119). In contrast, the promotion of microtubule assembly by CRMP2 is turned-off by phosphorylation of CRMP2 at Thr555 by Rho kinase (123,124). The chemokine stromal cell-derived factor-1α (CXCL12) leads to a decreased phosphorylation of GSK3β targeted residues (Thr509/514) of CRMP2 as well as to an increased phosphorylation at Tyr479 by the proto-oncogene Src-family tyrosine-protein kinase Yes (116). The de-phosphorylation of CRMP2, on the other hand, has only been demonstrated as a function of the protein phosphatase 2A (PP2A) (125). Recently, SUMOylation (small ubiquitin-like modifier) has been described for CRMP2 at Lys374, that is enhanced by prior phosphorylation by CDK5 (126). Phosphorylation by Fyn, on the other hand, prevented SUMOylation. Modification of CRMP2 by SUMOylation may be involved in the regulation of the voltage-gated sodium channel NaV1.7 (126,127).

Another recently discovered regulatory posttranslational modification is the reversible formation of an intermolecular disulphide between two subunits in the homotetrameric CRMP2 complex (128). This regulatory dithiol-disulphide switch between the Cys504 residues of two adjacent subunits leads to a profound conformational change of the CRMP2 homotetramer (128). Grx2c has been identified as specific reductase of this intermolecular disulphide both *in vivo* and *in vitro* (90,94,128). The identification of this CRMP2 dithiol-disulphide switch will be presented in [article I]. The currently available crystal structures contain only the rigid body of CRMP2 but lack the flexible C-terminus, including the described regulatory sites (108,129). The structural characterisation of the conformational change by molecular dynamics simulations combined with *in vitro* analysis will be presented in [manuscript V].

1.2.1.2 Functions of CRMP2 in the nervous system

In neuronal development, CRMP2 is crucial for axon outgrowth and guidance, to determine axon-dendrite fate, and therefore for establishment and maintenance of neuronal polarity (95,130). As early as 1992, Li *et al.* identified mutations in the unc-33 gene of *Caenorhabditis elegans* to be responsible for uncoordinated movements and severe abnormalities in axon outgrowth and guidance (131). Three years later, Goshima *et al.* identified a collapsin response mediator protein (CRMP-62, 62 kDa protein) required for semaphorin 3A (Sema3A) signal transduction in chick dorsal root ganglia (132). This CRMP-62 shared homology not only with the nematode neuronal protein unc-33 (uncoordinated protein 33), but also with human proteins termed hCRMP1 and hCRMP2 (132).

Around the same time, Minturn and collaborators discovered that rat TOAD-64 (Turned On After Division, 64 kDa protein) was a homologue of unc-33 gene from *C. elegans* (133). TOAD-64 was described to be specifically localised in lamellipodia and filopodia of growth cones with a thigh but not strict membrane association (133). In cultured hippocampal neurons, CRMP2 is enriched in the distal part of growing axons. Overexpression of CRMP2 induces the formation of multiple axons (130). In 2005 Chung et al. identified a 58 kDa calpain-cleaved form of CRMP2 (134). This short isoform of CRMP2 has been shown to be derived from C-terminal processing and is formed during brain development. While CRMP2 is localised in the cytoplasm only, the short form has been identified in the nuclear fraction of brain extracts as well (135). Calpain-cleaved CRMP2 has been reported to be inhibiting neurite regeneration after traumatic brain injury (136,137).

1.2.1.3 The semaphorin signalling pathway

CRMP2 acts downstream of the semaphorin 3A receptor. Semaphorins (Sema's) are secreted signalling proteins involved in the control of organogenesis and cellular differentiation. Ureteric bud branching and podocyte-endothelial crosstalk are modulated by Sema3A, for instance (138). Sema3A controls migration of developing thymocytes within the thymic lobules as well as adult T-cell polarisation and migration (139,140). The role of Sema3A signalling in bone remodelling is discussed for example in (141) and (142). Sema signalling is involved in the development of the lymphatic and blood vascular system, indicating signalling pathways similar to those involved in the nervous system (143). Sema3A was the first vertebrate semaphorin identified. It can cause growth cone collapse and acts therefore primarily as axon guidance cue (144). A heterodimer consisting of neuropilin-1 (NP1), the high-affinity ligand binding partner, and a class A plexin (PlexA), the signal transducing part, is the Sema3A receptor (Fig. 3) (144). Varying receptor complexes for class 3 semaphorins were discussed to be important for their various biological functions (145). Goshima and collaborators identified the chicken CRMP-62 (CRMP2) to be essential, mediating the repulsive effect of Sema3A (collapsin-1) (132).

1.2.1.4 Interaction of CRMP2 with MICAL proteins

MICAL (Molecule interacting with CasL) is a direct interaction partner of PlexA and is required for signal transduction in the Sema3A pathway (146). The mammalian MICAL protein family consists of three MICAL proteins and two MICAL-like homologues. From invertebrates to vertebrates, MICAL proteins are highly conserved (147). MICALs are large cytosolic multidomain proteins including an N-terminal flavin monooxygenase domain (146,148). Through NADPH consumption, the FAD cofactor is reduced to $FADH_2$ which can react with molecular oxygen, yielding peroxyflavin (149). One of these oxygen atoms may be transferred to a nucleophilic substrate, *e.g.* reaction with protein thiolates may yield sulphenic acids. Another potential reaction

way that has been discussed before is the dissociation of the peroxyflavin yielding H_2O_2 (149). The production of H_2O_2 by MICAL was even suggested to occur in response to receptor activation (150,151). Oxidation of the CRMP2 redox switch was suggested to occur after H_2O_2 production by MICAL (151). The second order rate constant of CRMP2 oxidation by H_2O_2 is about 0.82 $M^{-1}s^{-1}$, as described in [manuscript V]. The peroxidatic cysteinyl residue in the active site of peroxiredoxins possess a rate constant from $3x10^5$ to 10^7 $M^{-1}s^{-1}$ for the reduction of H_2O_2. This is five to seven orders of magnitude higher compared to 'regular' cysteines, *e.g.* Cys504 of CRMP2. *In vivo*, H_2O_2 will therefore react with the thiol groups of dedicated peroxidases primarily, unless H_2O_2 would be produced in the ultimate vicinity of the thiol group (152). This suggests additional transducer proteins that may be involved in the signal transduction from MICALs to CRMP2.

In 2010, Hung et al. identified MICAL as necessary and sufficient for semaphorin mediated F-actin remodelling (153). Further characterisation revealed that actin methionyl residues 44 and 47 are oxidised to methionine sulphoxides by MICAL, leading to the disassembly of actin filaments (154). MICAL1 and MICAL2 generate methionine-*R*-sulphoxide, which is stereo-specifically reduced by MsrB1 (155). The efficiency of F-actin disassembly due to oxidation via MICAL is accelerated by the increased binding of cofilin upon actin oxidation, suggesting that MICAL and the severing protein cofilin act synergistic in F-actin disassembly (see Fig. 3) (156).

1.2.1.5 Regulation of actin and tubulin dynamics

Axon outgrowth and guidance, growth cone collapse, and cell migration share many similarities with respect to the morphological changes as well as the underlying regulatory dynamics. These processes require a very fine tuned regulation of cytoskeletal dynamics. Numerous actin binding proteins, which stabilise or severe filaments, promote elongation or nucleation of new filaments have been described before (157,158). One of theses proteins is the actin-related protein (Arp)2/3 complex, consisting of seven subunits, that promote a network of branched actin filaments, the tips of which push the cell membrane forward (159). The Arp2/3 complex is activated by so called nucleation promoting factors of the Wiskott-Alrich syndrome protein (WASP) and WASP-family veropolin-homologous protein (WAVE) families of proteins (160,161). In response to a variety of signalling pathways, these WASP/WAVE complexes are recruited to the membrane and activated by the action of Ras (rat sarcoma) family GTPases, *e.g.* Rho (Ras homologue family member), CDC42 (cell division control protein 42), or Rac (Ras-related C3 botulinum toxin substrate) (162). When phosphorylated by CDK5 and GSK3β, CRMP2 interacts with cytoplasmic FMR1-interacting protein 1 (Cyfip1), also referred to as Sra1 (163). Active Rac recruits Cyfip1 and, in turn, this complex activates the Arp2/3 complex-dependent WAVE nucleation activity (164).

Downstream of the Sema3A signalling pathway (see above), the remodelling of the cytoskeleton involves the regulation of Rac1 as well as cofilin activity. The FARP proteins (FERM, RhoGEF (ARHGEF), and pleckstrin domain protein) are major players in this pathway (165,166). FARP1 activates Rac1 and promotes F-actin assembly to promote dendrite outgrowth of developing motor neurons (165), FARP2, on the other hand, is a mediator of axon guidance. Both, FARP1 and 2 act as transducers of the semaphorin signalling pathway (165,167). The guanine nucleotide exchange factor Trio, that interacts with and activates Rac1, mediates axonal development (168). In the characterisation of HeLa-Grx2c cells, that will be presented in [manuscript VI], we identified Trio as one of the most affected proteins in a proteomic and phospho-proteomic approach. Noteworthy, Hall *et al.* demonstrated, that effects and morphology induced by a dominant active Rac1 mutant can be rescued by overexpression of CRMP2 (169). This suggests an interaction of CRMP2, which is predominantly oxidised in the absence of Grx2c (see [manuscript VI]), with Cyfip1/WAVE, antagonising its sequestration by active Rac1.

Dimers of α/β-tubulin assemble end to end at centromers and form microtubules (usually consisting of 13 protofilaments). Similar to actin dynamics, microtubule-associated proteins (MAP) stabilise or destabilise microtubules, facilitating microtubule dynamics (170). Microtubules in dendrites and axons are likely to have a stable minus and dynamic plus ends, and are involved in maintaining the plasticity of neurons (170). CRMP2 has been characterised as MAP itself (171). One of the primary microtubule functions is the cargo transport throughout the cell, by motor proteins such as dynein or kinesin (170). CRMP2 has also been described to be involved in dynein as well as kinesin dependent transport (112,115). Both α- and β-tubulin are potential protein disulphide substrates for Grx2c, which possesses crucial functions in neuronal development itself, as described before (see 1.1.5.2) (94).

More detailed insights in the complex redox regulation of actin and tubulin dynamics, cofilin as actin severing protein, and an overview of the Sema3A signalling pathway, CRMP2 and MICALs is presented in [article IV].

1.3 Relevance of CRMP2s redox switch in physiology and pathophysiology

Over the last decade, a change of paradigms – from oxidative stress to the spatio-temporal resolved, localised, and very specific redox signalling – took place. As major regulators of the redox state of cysteinyl thiol groups, thioredoxin family proteins hold a prominent role in these redox regulatory circuits. For instance, numerous members Trx family proteins are essential for embryonic development and their loss is embryonically lethal, *e.g.* Trx1, Trx2, Grx3, while others severely

impair development, leading to defects, *e.g.*, in the metabolism, the skeleton, or the cardiovascular system (3).

1.3.1 Neuronal de- and regeneration

The high metabolic activity and high oxygen consumption accompanied with a limited regeneration capacity explain why especially cells of the nervous system are highly susceptible to oxidative damage (3). It is therefore not surprising that many proteins of the Trx family are present in various tissues and cell types of the brain (3,172). The appearance of 8-hydroxy-guanosine, decreased glutathione levels, increased lipid peroxidation, and increasing amounts of malondialdehyde in the *substantia nigra* of the brain are suggested as oxidative damage in Parkinson's disease (173,174). Alzheimer's disease is another major neurodegenerative disorder that is connected to oxidative damage. Lipid peroxidation and malondialdehyde levels, for instance, are increased in the temporal cortex and the hippocampus in the brain of Alzheimer's patients (175). The amyloid precurser protein, that was associated with Alzheimer's disease before, reduces Cu(II) to Cu(I) in an electron-transfer reaction that could also lead to the production of hydroxyl radicals (176). Accumulation of neurofibrillary tangles leads to loss of neurons in Alzheimer's disease. A monoclonal antibody raised against these neurofibrillary tangles labelled a highly phosphorylated form of CRMP2 (177,178). The role of Sema3A in the adult nervous system is not well understood, but accumulation of Sema3A was observed in Alzheimer's disease, contributing to the progression by either direct neurodegeneration or indirect by abrogation of recovery capabilities (179). In patients suffering from amyotrophic lateral sclerosis (ALS), protein carbonylation was increased in the spinal cord and motor cortex. Elevated levels of 3-nitrotyrosine and 8-hydroxy-guanosine were described in ALS patients as well as mutations in the copper/zinc superoxide dismutase in cases of familial motor neuron diseases like ALS (180). An antibody against neuropilin 1, that prevents binding of Sema3A, inhibited growth cone collapse and resulted in the delayed appearance of motor deficits in a mouse model for ALS, indicating that the Sema3A signalling through neuropilin 1 and CRMP2 is involved in the progression of this neurodegenerative disorder (181). The Sema3A/NP1/CRMP2 signalling pathway as well as the redox regulation of CRMP2 by cytosolic Grx2c are essential for brain development, axon outgrowth and guidance (90,144). CRMP2, especially the non-phosphorylated form, might be important to maintain synaptic plasticity in adult neurons (182). Components of the Sema3A signalling cascade are therefore attractive targets in the development of new drugs to treat various neurodegenerative disorders. The natural sulphur amino acid metabolite lanthionine ketimine (LK) and its cell permeable ester (LKE) interact with CRMP2 and exhibit potent neurotrophic activity (183). In a mouse model for Alzheimer's disease, LKE treatment altered the phosphorylation status of CRMP2 and improved cognition (184). The

interaction of LKE and CRMP2 provided neuroprotective effects in mouse models of multiple sclerosis and cerebral ischemia, respectively (185,186). The interference of these compounds in the Sema3A signalling pathway, promoting the maintenance of nerve plasticity, might also have potential therapeutic value for recovery after spinal cord injury (187). Another compound reported to interact with CRMP2 is lacosamide (Vimpat®), used for treatment of epilepsy. Lacosamide reduces the neuronal excitability through-voltage gated sodium channels, but the role of CRMP2 in epilepsy as well as the interaction with lacosamide needs to be further elucidated (188). In a model for perinatal asphyxia, Trx1 and Grx2 are required to maintain the phenotype and integrity of neurons [article III] (189). The reduction of CRMP2 by Grx2c and the resulting signalling mechanisms that promote axon outgrowth and cytoskeletal dynamics might thus be of importance for neuronal regeneration.

1.3.2 Cancer progression and metastasis

Cell motility and invasion are important characteristics for neuronal cells during development and axonogenesis, but are also hallmark features for disseminating and metastasising cancer cells. Migration of cells requires a continuous re-arrangement of the cytoskeleton but also interaction with neighbouring cells and surrounding matrix. Cytosolic Grx2 regulates cytoskeletal dynamics trough the CRMP2 redox switch in neuronal development (90). In adult human tissue Grx2c is exclusively expressed in testis with an essential role in spermatogenesis (88). However, Grx2c was also expressed in about 60% of various cancer cell lines (88). Grx2c may therefore promote the migration and invasion behaviour of cells in general. The characterisation of a stable Grx2c expressing HeLa cell line, to test this hypothesis, will be presented in [manuscript VI]. This hypothesis and the results presented in [manuscript VI] are further supported by the results of a clinical pilot study that we performed. Loss of the mitochondrial isoform of Grx2 (Grx2a) increases the sensitivity of cells against doxorubicin, a common chemotherapeutic (190). The degree of differentiation in lung cancer correlates with the immuno-histochemical staining for Grx2, although it was not possible to distinguish between the cytosolic and mitochondrial isoform (191).

The same proteins described for neuronal development and involved in severe neurological disorders, modulate the behaviour of cancer cells or promote cancer progression. Sema3A inhibits the migration and spreading of breast and the invasiveness of prostate cancer cells. There were also reports suggesting contribution of Sema3A to progression of pancreatic and colon cancer (192). Reduction of Sema3A or NP1 expression or inhibition of the PlexA signalling in breast carcinoma enhanced cell migration (193). Alterations in expression and phosphorylation of CRMP2 were reported to be involved in breast cancer progression, as well (194). Research targeting the

regulation of the actin cytoskeleton by MICAL proteins could also lead to new therapeutic advances and design of novel drugs (195).

The Sema3A signalling cascade as well as the redox regulation of CRMP2 are involved in neuronal development and cancer progression. Identification of interaction partners and characterisation of reaction mechanisms will contribute to improve diagnostics and design of new drugs.

2 Conclusions

I. Article: Identification of a thiol redox switch in CRMP2

The vertebrate-specific glutaredoxin 2 (Grx2) is expressed in at least two isoforms, mitochondrial Grx2a and cytosolic Grx2c. Prior to this thesis, we demonstrated that cytosolic Grx2 is essential for embryonic brain development (92). Collapsin response mediator protein 2 (CRMP2/DPYSL2) was identified as redox-regulated target of Grx2c and this redox regulation of CRMP2 is essential for axonal outgrowth (90,94).

In article I, we identified a specific and reversible intermolecular dithiol-disulphide switch between adjacent Cys504 residues of two subunits in the homotetrameric CRMP2. This switch determines two distinct conformations of the quaternary CRMP2 complex, and is reduced specifically by Grx2c in a dithiol reaction mechanism. This switch is triggered during neuronal differentiation and controls regular axonal outgrowth.

II. Article: Pneumococcal surface oxidative resistance system

Streptococcus pneumoniae, a gram-positive human commensal, but also a respiratory pathogen, has evolved efficient mechanisms to resist oxidative stress conditions as well as to displace other bacteria in the nasopharynx. *S. pneumoniae* has a high virulence potential and can cause respiratory and life-threatening diseases, such as pneumonia, meningitis, and septicaemia.

In article II, we characterised the surface-exposed thioredoxin family lipoproteins Etrx1 and Etrx2 at physiological, functional, and structural levels. Both proteins show strong similarities in their overall fold, but also relevant differences between the active sites, *e.g.* Etrx2s hydrophobic cavity, electrostatic potential, CXXC active site motif. A structural basis for the specific interaction of Etrx with the MsrA or MsrB domain in *Sp*MsrAB is provided by these differences. A loss of function of either both Etrx proteins or *Sp*MsrAB dramatically reduced the pneumococcal virulence in a mouse model of acute pneumonia. Additionally, under these conditions, the bacterial uptake by macrophages was enhanced, and the pneumococcal killing by hydrogen peroxide or free methionine sulphoxide accelerated. Both Etrx proteins can compensate for each other, but the lack of the two Etrx redox pathways leads to an accumulation of oxidised *Sp*MsrAB. Identification of this redox-regulated system and its target proteins may therefore contribute to the design of novel antimicrobials.

III. Article: Grx2 and Trx1 contribute to neuronal integrity

Members of the thioredoxin family of proteins regulate the thiol redox state of various key proteins as well as the amount of the intracellular second messenger hydrogen peroxide. These proteins are crucial mediators of cell function and their expression, localisation and individual functions are altered under various pathological conditions.

In article III, we analysed the regulation and potential functions of Trx family proteins during hypoxia/ischemia and reoxygenation of the developing brain, in both a cellular and an animal model of perinatal asphyxia. We discovered a complex, cell-type and tissue specific, expression pattern of these proteins following hypoxia/ischemia and reoxygenation. Especially Grx2 and Trx1 showed distinct alterations during tissue recovery following the treatment. The importance of these proteins to maintain the regular neuronal phenotype was confirmed in a cellular model by siRNA mediated silencing of these two proteins and hypoxia-reoxygenation treatment. Both, Grx2 and Trx1, could be clinically relevant in neuronal damage following perinatal asphyxia, but also in many other neuronal disorders.

IV. Article: Redox regulation of cytoskeletal dynamics

In contrast to the bony skeleton of vertebrates or the exoskeleton of invertebrates, the cytoskeleton consists of a dynamic meshwork of protein filaments that spans through the cytosol of eukaryotic cells. Particularly actin filaments and microtubules provide structure and points of attachment. They are responsible for cell shape, all types of cell movement, and are the basis of intracellular transport and distribution. Through specific junctions and points of adhesions, actin filaments and microtubules join cells together to form tissues, organs, and organisms. Therefore, a very fine tuned regulation of cytoskeletal dynamics is absolutely essential for cell differentiation and developmental processes.

In article IV, we discuss the control of this dynamic remodelling by redox signalling mechanisms, focussing on recent discoveries, that demonstrated reversible thiol and methionyl switches in the regulation of actin dynamics. The dynamic remodelling of the cytoskeleton, indispensable during development and organogenesis, can be spatio-temporally controlled by various redox signalling mechanisms, *e.g.* the thiol-disulphide switch in CRMP2 and methionyl-methionyl sulphoxide switches in β-actin. These mechanisms might also contribute to a variety of pathological conditions. Over the last decade, we could witness a shift in paradigms. The redox switches that control cellular functions are not a result of random modifications by unspecific oxidants, but appear to be rather controlled by specific enzymes. Reduction and oxidation of these

distinct redox modifications is specifically catalysed by these enzymes, similar to the regulation by (de-)phosphorylation.

V. Manuscript: Structural analysis of the CRMP2 thiol switch

Collapsin response mediator protein 2 (CRMP2/DPYSL2), a mediator of semaphorin signalling, is crucial for neuronal development. The homotetrameric complex is regulated via phosphorylation by specific kinases, but also by reversible disulphide formation between two Cys504 residues of adjacent subunits. Available X-ray structures of CRMP2 contain only the rigid body of the molecule but lack the flexible C-terminus including the important sites for phosphorylation and redox regulation.

In manuscript V, we investigated the effects of the CRMP2 dithiol-disulphide redox switch on the protein using a combination of *in vitro* analysis and force field molecular dynamics. Model structures for both redox states were established, that are consistent with results gained from CD spectroscopy using recombinantly expressed CRMP2. The second order rate constant of CRMP2 oxidation by hydrogen peroxide was determined and the solvent accessible surface area of certain phosphorylation sites in both redox states simulated. The results presented in this manuscript give first detailed insight in the distinct structural changes of homotetrameric CRMP2 following oxidation. They also indicate a tight connection between the regulation by phosphorylation and redox modification.

VI. Manuscript: Cancer-specific Grx2c promotes migration and invasion

The vertebrate specific cytosolic isoform of glutaredoxin 2 (Grx2c) is essential for brain development and axonal outgrowth, spermatogenesis, and is also specifically induced in various cancer cell lines (88,90). Axonal outgrowth and transmigration of spermatogenic cells depends on the cells abilities to migrate as well as invade, hallmark features of disseminating and metastasising cancer cells. Cell motility and invasion require a very complex regulation of cytoskeletal dynamics.

In manuscript VI, we investigated the effects of Grx2c expression on cell morphology, migration, and invasion behaviour. A low expression of Grx2c in HeLa cells led to dramatic alterations in cytoskeletal dynamics, a significantly increased motility, and enabled the cells to invade a model 3D-matrix. To characterise the underlying mechanisms, we used stable isotope labelling combined with phospho-peptide enrichment and high-accuracy mass spectrometry. We identified specific changes in proteins and pathways regulating cytoskeletal dynamics, cell adhesion, and receptor-mediated signal transduction. Grx2c was also expressed with significantly higher frequency in clear cell renal cell carcinoma (ccRCC) compared to healthy kidney tissue. Tumours tested positive for

Grx2c expression had a strong trend for more locally advanced tumour stages and a clear tendency for a decreased cancer-specific survival, compared to patients without detectable Grx2c. Taken together, the results presented in this manuscript suggest a critical function of Grx2c in cell morphology, migration and invasion, and also in cancer development and progression.

3 Summary

Numerous signalling pathways orchestrate the development, the functions, and the survival of cells, mostly in response to external stimuli. An overwhelming amount of data supports the concept of specific, spatio-temporal redox signalling pathways that affect the redox state of protein cysteinyl side chains and thus the biological function of these proteins. Glutaredoxins (Grxs) and thioredoxins (Trxs) catalyse reversible thiol-disulphide exchange reactions. The cytosolic Grx2 isoform Grx2c is essential for brain development and axonal outgrowth. A reversible dithiol-disulphide switch of CRMP2 has been identified as one of the major targets regulated by Grx2c. This CRMP2 redox switch is toggled in neuronal differentiation. Reduction of CRMP2 thiols induces profound conformational changes, modifying interactions and downstream elements of this redox switch. In [article I] and [manuscript V], we identified the Cys504 of CRMP2 to be the redox regulated residue. We used various *in vitro* assays with recombinant protein and molecular dynamics simulations to characterise the conformational change. Model structures for reduced and oxidised CRMP2 confirmed the oxidation induced changes in the secondary structure detected by CD spectroscopy. The changes involve the solvent accessible surface area of at least one known phosphorylation site at the C-terminus of the protein.

In [article III], we analysed the function of Grx2 and Trx1 in a model for perinatal asphyxia. Trx family proteins exhibit a very complex, cell-type and tissue specific expression pattern following hypoxia/ischemia and reoxygenation, especially Trx1 and Grx2. SiRNA-mediated silencing of these proteins in a cellular hypoxia-reoxygenation model confirmed the importance of Grx2 and Trx1 to maintain the neuronal phenotype. The results imply the clinical relevance for both proteins in perinatal asphyxia as well as many other neurological disorders. In agreement with the results presented in [articleI], Grx2 may be required for the re-establishment of neuronal integrity and connectivity.

Cell shape, all forms of intracellular transport, and cell movement depend on the cytoskeleton, particularly on the dynamic re-arrangement of actin filaments and microtubules. The fine tuned and complex regulation of cytoskeletal dynamics is essential for cell differentiation and development. In [article IV], we discuss the redox regulation of this dynamic cytoskeletal remodelling. Taking recent discoveries into account, we focus on redox signalling mechanisms, *e.g.* reversible thiol and methionyl switches in the regulation of actin dynamics and the thiol-disulphide switch of CRMP2 (Fig. 3). These switches are specifically controlled by enzymes such as Trx1 and Grx2c, for instance, and not the result of random modification by unspecific oxidants. Methionyl sulphoxidation of actin can be reversed by methionyl sulphoxide reductase (MsrA) in a stereo-

specific manner, promoting actin polymerisation. Human cells express two different Msr enzymes (MsrA and MsrB), that can reduce S- and R-methionyl sulphoxide, respectively. In the gram-positive *Streptococcus pneumoniae*, on the other hand, both Msr genes and thus enzymes were fused during evolution. In [article II], we characterised the surface-exposed thioredoxin family lipoproteins Etrx1 and 2 and regulators of this Msr (*Sp*MsrAB). A structural basis for the specific interaction of Etrx with *Sp*MsrAB is provided by differences between the Etrx1 and 2 active sites. A loss of function of both Etrx proteins or *Sp*MsrAB dramatically reduced pneumococcal virulence, enhanced the bacterial uptake by macrophages, and accelerated pneumococcal killing by H_2O_2 or free methionine sulphoxide. Identification and characterisation of components of this redox regulated system may contribute to the design of new antimicrobials.

In [manuscript VI], we investigated the effects of Grx2c expression on cell morphology, migration, and invasion behaviour of cancer cells. Grx2c expressing cancer cells developed dramatic changes in phenotype, including alterations in cytoskeletal dynamics and significantly increased motility. The expression of Grx2c enabled the cells to invade a 3D collagen matrix. We used stable isotope labelling combined with phosphopeptide enrichment and high accuracy mass spectrometry to characterise the underlying mechanisms. Proteins and pathways regulating cytoskeletal dynamics, cell adhesion, and receptor-mediated signal transduction were detected to be specifically altered. We started a clinical pilot study with patients suffering from clear cell renal cell carcinoma (ccRCC). Grx2c was expressed with significantly higher frequency in ccRCC compared to healthy kidney tissue. Grx2c positive tumours had a strong trend for locally more advanced tumour stages and a clear tendency for a decreased cancer-specific survival, compared to patients without detectable Grx2c. These results were supported by data from 'The Cancer Genome Atlas'.

In synopsis, the results presented and discussed in these articles and manuscripts, support the concept of specific redox signalling in different models and model organisms. They also demonstrate the importance of the specific redox control of signalling pathways that, in the case of errors or misinterpretations, contribute to pathophysiological alterations. The regulation of the CRMP2 redox switch by Grx2c, for instance, is physiologically essential for brain development, but might lead to cancer progression, if 'switched on' in adult tissue. Identification of further interaction partners as well as the development of compounds modulating this redox switch and CRMP2s conformations, will be part of our future research.

4 References

1. Gellert M, Hanschmann E-M, Lepka K, Berndt C, Lillig CH. Redox regulation of cytoskeletal dynamics during differentiation and de-differentiation. Biochim Biophys Acta. 2015 Aug;1850(8):1575–87.

2. Berndt C, Lillig CH, Flohé L. Redox regulation by glutathione needs enzymes. Front Pharmacol [Internet]. 2014;5(168). Available from: http://www.frontiersin.org/experimental_pharmacology_and_drug_discovery/10.3389/fphar.2014.00168/full

3. Hanschmann E-M, Godoy JR, Berndt C, Hudemann C, Lillig CH. Thioredoxins, glutaredoxins, and peroxiredoxins--molecular mechanisms and health significance: from cofactors to antioxidants to redox signaling. Antioxid Redox Signal. 2013 Nov 1;19(13):1539–605.

4. Ghezzi P, Bonetto V, Fratelli M. Thiol Disulfide Balance: From the Concept of Oxidative Stress to that of Redox Regulation. Antioxid Redox Signal. 2005;7(7–8):964–72.

5. Jones DP. Redefining oxidative stress. Antioxid Redox Signal. 2006;8(9–10):1865–79.

6. Halvey PJ, Watson WH, Hansen JM, Go Y-M, Samali A, Jones DP. Compartmental oxidation of thiol-disulphide redox couples during epidermal growth factor signalling. Biochem J. 2005 Mar 1;386(Pt 2):215–9.

7. Go Y-M, Jones DP. Redox compartmentalization in eukaryotic cells. Biochim Biophys Acta BBA - Gen Subj. 2008 Nov;1780(11):1273–90.

8. Sies H, Cadenas E. Oxidative stress: damage to intact cells and organs. Philos Trans R Soc Lond B Biol Sci. 1985 Dec 17;311(1152):617–31.

9. H Sies. Oxidative stress: from basic research to clinical application. Am J Med. 1991 Sep 30;91(3C):31S–38S.

10. Butterfield DA, Perluigi M, Sultana R. Oxidative stress in Alzheimer’s disease brain: new insights from redox proteomics. Eur J Pharmacol. 2006 Sep 1;545(1):39–50.

11. Chinta SJ, Andersen JK. Redox imbalance in Parkinson’s disease. Biochim Biophys Acta BBA - Gen Subj. 2008 Nov;1780(11):1362–7.

12. Giles GI. The redox regulation of thiol dependent signaling pathways in cancer. Curr Pharm Des. 2006;12(34):4427–43.

13. Forman HJ, Maiorino M, Ursini F. Signaling Functions of Reactive Oxygen Species. Biochemistry (Mosc). 2010 Feb 9;49(5):835–42.

14. Gruhlke MCH, Slusarenko AJ. The biology of reactive sulfur species (RSS). Plant Physiol Biochem PPB. 2012 Oct;59:98–107.

15. Forman HJ, Fukuto JM, Torres M. Redox signaling: thiol chemistry defines which reactive oxygen and nitrogen species can act as second messengers. Am J Physiol Cell Physiol. 2004 Aug;287(2):C246-256.

16. Poole LB. The Basics of Thiols and Cysteines in Redox Biology and Chemistry. Free Radic Biol Med. 2015 Mar;0:148–57.

17. Hess DT, Matsumoto A, Kim S-O, Marshall HE, Stamler JS. Protein S-nitrosylation: purview and parameters. Nat Rev Mol Cell Biol. 2005 Feb;6(2):150–66.

18. Foster MW, Hess DT, Stamler JS. Protein S-nitrosylation in health and disease: a current perspective. Trends Mol Med. 2009 Sep;15(9):391–404.

19. Poole LB. Formation and functions of protein sulfenic acids. Curr Protoc Toxicol Editor Board Mahin Maines Ed--Chief Al. 2004 Feb;Chapter 17:Unit17.1.

20. Chang Y-C, Huang C-N, Lin C-H, Chang H-C, Wu C-C. Mapping protein cysteine sulfonic acid modifications with specific enrichment and mass spectrometry: an integrated approach to explore the cysteine oxidation. Proteomics. 2010 Aug;10(16):2961–71.

21. Leonard SE, Reddie KG, Carroll KS. Mining the thiol proteome for sulfenic acid modifications reveals new targets for oxidation in cells. ACS Chem Biol. 2009 Sep 18;4(9):783–99.

22. Drazic A, Winter J. The physiological role of reversible methionine oxidation. Biochim Biophys Acta. 2014 Aug;1844(8):1367–82.

23. Kaya A, Lee BC, Gladyshev VN. Regulation of Protein Function by Reversible Methionine Oxidation and the Role of Selenoprotein MsrB1. Antioxid Redox Signal. 2015 Oct 1;23(10):814–22.

24. Boschi-Muller S, Gand A, Branlant G. The methionine sulfoxide reductases: Catalysis and substrate specificities. Arch Biochem Biophys. 2008 Jun 15;474(2):266–73.

25. Hansel A, Kuschel L, Hehl S, Lemke C, Agricola H-J, Hoshi T, et al. Mitochondrial targeting of the human peptide methionine sulfoxide reductase (MSRA), an enzyme involved in the repair of oxidized proteins. FASEB J Off Publ Fed Am Soc Exp Biol. 2002 Jun;16(8):911–3.

26. Hansel A, Heinemann SH, Hoshi T. Heterogeneity and function of mammalian MSRs: enzymes for repair, protection and regulation. Biochim Biophys Acta. 2005 Jan 17;1703(2):239–47.

27. Lee JW, Gordiyenko NV, Marchetti M, Tserentsoodol N, Sagher D, Alam S, et al. Gene structure, localization and role in oxidative stress of methionine sulfoxide reductase A (MSRA) in the monkey retina. Exp Eye Res. 2006 May;82(5):816–27.

28. Kim H-Y. Glutaredoxin serves as a reductant for methionine sulfoxide reductases with or without resolving cysteine. Acta Biochim Biophys Sin. 2012 Jan 7;44(7):623–7.

29. Kim H-Y, Gladyshev VN. Methionine sulfoxide reduction in mammals: characterization of methionine-R-sulfoxide reductases. Mol Biol Cell. 2004 Mar;15(3):1055–64.

30. Lee BC, Dikiy A, Kim H-Y, Gladyshev VN. Functions and evolution of selenoprotein methionine sulfoxide reductases. Biochim Biophys Acta. 2009 Nov;1790(11):1471–7.

31. Delaye L, Becerra A, Orgel L, Lazcano A. Molecular evolution of peptide methionine sulfoxide reductases (MsrA and MsrB): on the early development of a mechanism that protects against oxidative damage. J Mol Evol. 2007 Jan;64(1):15–32.

32. Kim YK, Shin YJ, Lee W-H, Kim H-Y, Hwang KY. Structural and kinetic analysis of an MsrA-MsrB fusion protein from Streptococcus pneumoniae. Mol Microbiol. 2009 May;72(3):699–709.

33. Tarrago L, Gladyshev VN. Recharging oxidative protein repair: catalysis by methionine sulfoxide reductases towards their amino acid, protein, and model substrates. Biochem Biokhimiia. 2012 Oct;77(10):1097–107.

34. Hoshi T, Heinemann S. Regulation of cell function by methionine oxidation and reduction. J Physiol. 2001 Feb 15;531(Pt 1):1–11.

35. Lowther WT, Brot N, Weissbach H, Honek JF, Matthews BW. Thiol-disulfide exchange is involved in the catalytic mechanism of peptide methionine sulfoxide reductase. Proc Natl Acad Sci U S A. 2000 Jun 6;97(12):6463–8.

36. Ranaivoson FM, Neiers F, Kauffmann B, Boschi-Muller S, Branlant G, Favier F. Methionine sulfoxide reductase B displays a high level of flexibility. J Mol Biol. 2009 Nov 20;394(1):83–93.

37. Lillig CH, Berndt C, Holmgren A. Glutaredoxin systems. Biochim Biophys Acta BBA - Gen Subj. 2008 Nov;1780(11):1304–17.

38. Lillig CH, Holmgren A. Thioredoxin and Related Molecules From Biology to Health and Disease. Antioxid Redox Signal. 2007;9(1):25–47.

39. Shelton MD, Chock PB, Mieyal JJ. Glutaredoxin: Role in Reversible Protein S-Glutathionylation and Regulation of Redox Signal Transduction and Protein Translocation. Antioxid Redox Signal. 2005;7(3–4):348–66.

40. Rhee SG, Woo HA. Multiple functions of peroxiredoxins: peroxidases, sensors and regulators of the intracellular messenger H_2O_2, and protein chaperones. Antioxid Redox Signal. 2011 Aug 1;15(3):781–94.

41. Martin JL. Thioredoxin--a fold for all reasons. Struct Lond Engl 1993. 1995 Mar 15;3(3):245–50.

42. Laurent TC, Moore EC, Reichard P. Enzymatic synthesis of deoxyribonucleotides. iv. isolation and characterization of thioredoxin, the hydrogen donor from Escherichia coli B. J Biol Chem. 1964 Oct;239:3436–44.

43. Moore EC, Reichard P, Thelander L. Enzymatic Synthesis of Deoxyribonucleotides V. PURIFICATION AND PROPERTIES OF THIOREDOXIN REDUCTASE FROM ESCHERICHIA COLI B. J Biol Chem. 1964 Jan 10;239(10):3445–52.

44. Holmgren A. Glutathione-dependent synthesis of deoxyribonucleotides. Characterization of the enzymatic mechanism of Escherichia coli glutaredoxin. J Biol Chem. 1979 May 10;254(9):3672–8.

45. Holmgren A. Glutathione-dependent synthesis of deoxyribonucleotides. Purification and characterization of glutaredoxin from Escherichia coli. J Biol Chem. 1979 May 10;254(9):3664–71.

46. Luthman M, Eriksson S, Holmgren A, Thelander L. Glutathione-dependent hydrogen donor system for calf thymus ribonucleoside-diphosphate reductase. Proc Natl Acad Sci U S A. 1979 May;76(5):2158–62.

47. Roos G, Foloppe N, Messens J. Understanding the pKa of Redox Cysteines: The Key Role of Hydrogen Bonding. Antioxid Redox Signal. 2012 Jul 1;18(1):94–127.

48. Holmgren A, Björnstedt M. Thioredoxin and thioredoxin reductase. Methods Enzymol. 1995;252:199–208.

49. Holmgren A, Aslund F. Glutaredoxin. Methods Enzymol. 1995;252:283–92.

50. Berndt C, Lillig CH, Holmgren A. Thiol-based mechanisms of the thioredoxin and glutaredoxin systems: implications for diseases in the cardiovascular system. Am J Physiol Heart Circ Physiol. 2007;292(3):H1227-1236.

51. Herrero E, de la Torre-Ruiz MA. Monothiol glutaredoxins: a common domain for multiple functions. Cell Mol Life Sci CMLS. 2007 Jun;64(12):1518–30.

52. Gravina SA, Mieyal JJ. Thioltransferase is a specific glutathionyl mixed disulfide oxidoreductase. Biochemistry (Mosc). 1993 Apr 6;32(13):3368–76.

53. Holmgren A. Glutathione-dependent enzyme reactions of the phage T4 ribonucleotide reductase system. J Biol Chem. 1978 Oct 25;253(20):7424–30.

54. Rhee SG, Kang SW, Chang TS, Jeong W, Kim K. Peroxiredoxin, a novel family of peroxidases. IUBMB Life. 2001 Jul;52(1–2):35–41.

55. Seo MS, Kang SW, Kim K, Baines IC, Lee TH, Rhee SG. Identification of a new type of mammalian peroxiredoxin that forms an intramolecular disulfide as a reaction intermediate. J Biol Chem. 2000 Jul 7;275(27):20346–54.

56. Holmgren A. Thioredoxin. 6. The amino acid sequence of the protein from escherichia coli B. Eur J Biochem FEBS. 1968 Dec 5;6(4):475–84.

57. Kallis GB, Holmgren A. Differential reactivity of the functional sulfhydryl groups of cysteine-32 and cysteine-35 present in the reduced form of thioredoxin from Escherichia coli. J Biol Chem. 1980 Nov 10;255(21):10261–5.

58. Hashemy SI, Holmgren A. Regulation of the catalytic activity and structure of human thioredoxin 1 via oxidation and S-nitrosylation of cysteine residues. J Biol Chem. 2008 Jun 10;

59. Weichsel A, Gasdaska JR, Powis G, Montfort WR. Crystal structures of reduced, oxidized, and mutated human thioredoxins: evidence for a regulatory homodimer. Struct Lond Engl 1993. 1996 Jun 15;4(6):735–51.

60. Hirota K, Murata M, Sachi Y, Nakamura H, Takeuchi J, Mori K, et al. Distinct roles of thioredoxin in the cytoplasm and in the nucleus. A two-step mechanism of redox regulation of transcription factor NF-kappaB. J Biol Chem. 1999 Sep 24;274(39):27891–7.

61. Zhang Y, Chen F, Tai G, Wang J, Shang J, Zhang B, et al. TIGAR knockdown radiosensitizes TrxR1-overexpressing glioma in vitro and in vivo via inhibiting Trx1 nuclear transport. Sci Rep. 2017 Mar 24;7:42928.

62. Rubartelli A, Bajetto A, Allavena G, Wollman E, Sitia R. Secretion of thioredoxin by normal and neoplastic cells through a leaderless secretory pathway. J Biol Chem. 1992 Dec 5;267(34):24161–4.

63. Tanudji M, Hevi S, Chuck SL. The nonclassic secretion of thioredoxin is not sensitive to redox state. Am J Physiol Cell Physiol. 2003 May;284(5):C1272-1279.

64. Gladyshev VN, Jeang KT, Stadtman TC. Selenocysteine, identified as the penultimate C-terminal residue in human T-cell thioredoxin reductase, corresponds to TGA in the human placental gene. Proc Natl Acad Sci U S A. 1996 Jun 11;93(12):6146–51.

65. Arnér ESJ. Focus on mammalian thioredoxin reductases - Important selenoproteins with versatile functions. Biochim Biophys Acta. 2009 Jun;1790(6):495–526.

66. Isakov N, Witte S, Altman A. PICOT-HD: a highly conserved protein domain that is often associated with thioredoxin and glutaredoxin modules. Trends Biochem Sci. 2000 Nov;25(11):537–9.

67. Lundberg M, Johansson C, Chandra J, Enoksson M, Jacobsson G, Ljung J, et al. Cloning and expression of a novel human glutaredoxin (Grx2) with mitochondrial and nuclear isoforms. J Biol Chem. 2001 Jul 13;276(28):26269–75.

68. Wingert RA, Galloway JL, Barut B, Foott H, Fraenkel P, Axe JL, et al. Deficiency of glutaredoxin 5 reveals Fe-S clusters are required for vertebrate haem synthesis. Nature. 2005 Aug 18;436(7053):1035–9.

69. Witte S, Villalba M, Bi K, Liu Y, Isakov N, Altman A. Inhibition of the c-Jun N-terminal kinase/AP-1 and NF-kappaB pathways by PICOT, a novel protein kinase C-interacting protein with a thioredoxin homology domain. J Biol Chem. 2000 Jan 21;275(3):1902–9.

70. Lysell J, Stjernholm Vladic Y, Ciarlo N, Holmgren A, Sahlin L. Immunohistochemical determination of thioredoxin and glutaredoxin distribution in the human cervix, and possible relation to cervical ripening. Gynecol Endocrinol Off J Int Soc Gynecol Endocrinol. 2003 Aug;17(4):303–10.

71. Pai HV, Starke DW, Lesnefsky EJ, Hoppel CL, Mieyal JJ. What is the functional significance of the unique location of glutaredoxin 1 (GRx1) in the intermembrane space of mitochondria? Antioxid Redox Signal. 2007 Nov;9(11):2027–33.

72. Holmgren A. Thioredoxin and glutaredoxin systems. J Biol Chem. 1989 Aug 25;264(24):13963–6.

73. Wells WW, Xu DP, Yang YF, Rocque PA. Mammalian thioltransferase (glutaredoxin) and protein disulfide isomerase have dehydroascorbate reductase activity. J Biol Chem. 1990 Sep 15;265(26):15361–4.

74. Takashima Y, Hirota K, Nakamura H, Nakamura T, Akiyama K, Cheng FS, et al. Differential expression of glutaredoxin and thioredoxin during monocytic differentiation. Immunol Lett. 1999 Jun 1;68(2–3):397–401.

75. Bandyopadhyay S, Starke DW, Mieyal JJ, Gronostajski RM. Thioltransferase (glutaredoxin) reactivates the DNA-binding activity of oxidation-inactivated nuclear factor I. J Biol Chem. 1998 Jan 2;273(1):392–7.

76. Hirota K, Matsui M, Murata M, Takashima Y, Cheng FS, Itoh T, et al. Nucleoredoxin, glutaredoxin, and thioredoxin differentially regulate NF-kappaB, AP-1, and CREB activation in HEK293 cells. Biochem Biophys Res Commun. 2000 Jul 21;274(1):177–82.

77. Pineda-Molina E, Klatt P, Vázquez J, Marina A, García de Lacoba M, Pérez-Sala D, et al. Glutathionylation of the p50 subunit of NF-kappaB: a mechanism for redox-induced inhibition of DNA binding. Biochemistry (Mosc). 2001 Nov 27;40(47):14134–42.

78. Chrestensen CA, Starke DW, Mieyal JJ. Acute cadmium exposure inactivates thioltransferase (Glutaredoxin), inhibits intracellular reduction of protein-glutathionyl-mixed disulfides, and initiates apoptosis. J Biol Chem. 2000 Aug 25;275(34):26556–65.

79. Daily D, Vlamis-Gardikas A, Offen D, Mittelman L, Melamed E, Holmgren A, et al. Glutaredoxin protects cerebellar granule neurons from dopamine-induced apoptosis by activating NF-kappa B via Ref-1. J Biol Chem. 2001 Jan 12;276(2):1335–44.

80. Gladyshev VN, Liu A, Novoselov SV, Krysan K, Sun QA, Kryukov VM, et al. Identification and characterization of a new mammalian glutaredoxin (thioltransferase), Grx2. J Biol Chem. 2001 Aug 10;276(32):30374–80.

81. Johansson C, Lillig CH, Holmgren A. Human Mitochondrial Glutaredoxin Reduces S-Glutathionylated Proteins with High Affinity Accepting Electrons from Either Glutathione or Thioredoxin Reductase. J Biol Chem. 2004;279(9):7537–43.

82. Lillig CH, Berndt C, Vergnolle O, Lonn ME, Hudemann C, Bill E, et al. Characterization of human glutaredoxin 2 as iron-sulfur protein: A possible role as redox sensor. Proc Natl Acad Sci. 2005;102(23):8168–73.

83. Berndt C, Hudemann C, Hanschmann E-M, Axelsson R, Holmgren A, Lillig CH. How Does Iron Sulfur Cluster Coordination Regulate the Activity of Human Glutaredoxin 2? Antioxid Redox Signal. 2007;9(1):151–7.

84. Tamarit J, Belli G, Cabiscol E, Herrero E, Ros J. Biochemical characterization of yeast mitochondrial Grx5 monothiol glutaredoxin. J Biol Chem. 2003 Jul 11;278(28):25745–51.

85. Mühlenhoff U, Gerber J, Richhardt N, Lill R. Components involved in assembly and dislocation of iron-sulfur clusters on the scaffold protein Isu1p. EMBO J. 2003 Sep 15;22(18):4815–25.

86. Mühlenhoff U, Molik S, Godoy JR, Uzarska MA, Richter N, Seubert A, et al. Cytosolic monothiol glutaredoxins function in intracellular iron sensing and trafficking via their bound iron-sulfur cluster. Cell Metab. 2010 Oct 6;12(4):373–85.

87. Haunhorst P, Berndt C, Eitner S, Godoy JR, Lillig CH. Characterization of the human monothiol glutaredoxin 3 (PICOT) as iron-sulfur protein. Biochem Biophys Res Commun. 2010 Apr 2;394(2):372–6.

88. Lönn ME, Hudemann C, Berndt C, Cherkasov V, Capani F, Holmgren A, et al. Expression Pattern of Human Glutaredoxin 2 Isoforms: Identification and Characterization of Two Testis/Cancer Cell-Specific Isoforms. Antioxid Redox Signal. 2008;10(3):547–58.

89. Hudemann C, Lönn ME, Godoy JR, Zahedi Avval F, Capani F, Holmgren A, et al. Identification, expression pattern, and characterization of mouse glutaredoxin 2 isoforms. Antioxid Redox Signal. 2009 Jan;11(1):1–14.

90. Bräutigam L, Schütte LD, Godoy JR, Prozorovski T, Gellert M, Hauptmann G, et al. Vertebrate-specific glutaredoxin is essential for brain development. Proc Natl Acad Sci U S A. 2011 Dec 20;108(51):20532–7.

91. Bräutigam L, Jensen LDE, Poschmann G, Nyström S, Bannenberg S, Dreij K, et al. Glutaredoxin regulates vascular development by reversible glutathionylation of sirtuin 1. Proc Natl Acad Sci U S A. 2013 Dec 10;110(50):20057–62.

92. Berndt C, Poschmann G, Stühler K, Holmgren A, Bräutigam L. Zebrafish heart development is regulated via glutaredoxin 2 dependent migration and survival of neural crest cells. Redox Biol. 2014;2:673–8.

93. Enoksson M, Fernandes AP, Prast S, Lillig CH, Holmgren A, Orrenius S. Overexpression of glutaredoxin 2 attenuates apoptosis by preventing cytochrome c release. Biochem Biophys Res Commun. 2005 Feb 18;327(3):774–9.

94. Schütte LD, Baumeister S, Weis B, Hudemann C, Hanschmann E-M, Lillig CH. Identification of potential protein dithiol-disulfide substrates of mammalian Grx2. Biochim Biophys Acta. 2013 Nov;1830(11):4999–5005.

95. Arimura N, Menager C, Fukata Y, Kaibuchi K. Role of CRMP-2 in neuronal polarity. J Neurobiol. 2004 Jan;58(1):34–47.

96. Collette Y, Marignier R, Vuaillat C, Rogemond V, Davoust N, Malcus C, et al. A role for the neuronal protein collapsin response mediator protein 2 in T lymphocyte polarization and migration. J Immunol Baltim Md 1950. 2005 Dec 1;175(11):7650–60.

97. Yamashita N, Goshima Y. Collapsin response mediator proteins regulate neuronal development and plasticity by switching their phosphorylation status. Mol Neurobiol. 2012 Apr;45(2):234–46.

98. Tan F, Thiele CJ, Li Z. Collapsin response mediator proteins: Potential diagnostic and prognostic biomarkers in cancers (Review). Oncol Lett. 2014 May;7(5):1333–40.

99. Nagai J, Baba R, Ohshima T. CRMPs Function in Neurons and Glial Cells: Potential Therapeutic Targets for Neurodegenerative Diseases and CNS Injury. Mol Neurobiol. 2016 Jun 23;

100. Quach TT, Honnorat J, Kolattukudy PE, Khanna R, Duchemin AM. CRMPs: critical molecules for neurite morphogenesis and neuropsychiatric diseases. Mol Psychiatry. 2015 Sep;20(9):1037–45.

101. Wang LH, Strittmatter SM. A family of rat CRMP genes is differentially expressed in the nervous system. J Neurosci Off J Soc Neurosci. 1996 Oct 1;16(19):6197–207.

102. Charrier E, Reibel S, Rogemond V, Aguera M, Thomasset N, Honnorat J. Collapsin response mediator proteins (CRMPs): involvement in nervous system development and adult neurodegenerative disorders. Mol Neurobiol. 2003 Aug;28(1):51–64.

103. Ricard D, Stankoff B, Bagnard D, Aguera M, Rogemond V, Antoine JC, et al. Differential expression of collapsin response mediator proteins (CRMP/ULIP) in subsets of oligodendrocytes in the postnatal rodent brain. Mol Cell Neurosci. 2000 Oct;16(4):324–37.

104. Martins-de-Souza D, Cassoli JS, Nascimento JM, Hensley K, Guest PC, Pinzon-Velasco AM, et al. The protein interactome of collapsin response mediator protein-2 (CRMP2/DPYSL2) reveals novel partner proteins in brain tissue. Proteomics Clin Appl. 2015 Oct;9(9–10):817–31.

105. Yuasa-Kawada J, Suzuki R, Kano F, Ohkawara T, Murata M, Noda M. Axonal morphogenesis controlled by antagonistic roles of two CRMP subtypes in microtubule organization. Eur J Neurosci. 2003 Jun;17(11):2329–43.

106. Bretin S, Reibel S, Charrier E, Maus-Moatti M, Auvergnon N, Thevenoux A, et al. Differential expression of CRMP1, CRMP2A, CRMP2B, and CRMP5 in axons or dendrites of distinct neurons in the mouse brain. J Comp Neurol. 2005 May 23;486(1):1–17.

107. Wang LH, Strittmatter SM. Brain CRMP forms heterotetramers similar to liver dihydropyrimidinase. J Neurochem. 1997 Dec;69(6):2261–9.

108. Stenmark P, Ogg D, Flodin S, Flores A, Kotenyova T, Nyman T, et al. The structure of human collapsin response mediator protein 2, a regulator of axonal growth. J Neurochem. 2007 May;101(4):906–17.

109. Deo RC, Schmidt EF, Elhabazi A, Togashi H, Burley SK, Strittmatter SM. Structural bases for CRMP function in plexin-dependent semaphorin3A signaling. EMBO J. 2004 Jan 14;23(1):9–22.

110. Tan M, Cha C, Ye Y, Zhang J, Li S, Wu F, et al. CRMP4 and CRMP2 Interact to Coordinate Cytoskeleton Dynamics, Regulating Growth Cone Development and Axon Elongation. Neural Plast. 2015;2015:947423.

111. Fukata Y, Itoh TJ, Kimura T, Ménager C, Nishimura T, Shiromizu T, et al. CRMP-2 binds to tubulin heterodimers to promote microtubule assembly. Nat Cell Biol. 2002 Aug;4(8):583–91.

112. Kawano Y, Yoshimura T, Tsuboi D, Kawabata S, Kaneko-Kawano T, Shirataki H, et al. CRMP-2 is involved in kinesin-1-dependent transport of the Sra-1/WAVE1 complex and axon formation. Mol Cell Biol. 2005 Nov;25(22):9920–35.

113. Ip JPK, Shi L, Chen Y, Itoh Y, Fu W-Y, Betz A, et al. α2-chimaerin controls neuronal migration and functioning of the cerebral cortex through CRMP-2. Nat Neurosci. 2011 Dec 4;15(1):39–47.

114. Brittain JM, Piekarz AD, Wang Y, Kondo T, Cummins TR, Khanna R. An atypical role for collapsin response mediator protein 2 (CRMP-2) in neurotransmitter release via interaction with presynaptic voltage-gated calcium channels. J Biol Chem. 2009 Nov 6;284(45):31375–90.

115. Rahajeng J, Giridharan SSP, Naslavsky N, Caplan S. Collapsin response mediator protein-2 (Crmp2) regulates trafficking by linking endocytic regulatory proteins to dynein motors. J Biol Chem. 2010 Oct 15;285(42):31918–22.

116. Varrin-Doyer M, Vincent P, Cavagna S, Auvergnon N, Noraz N, Rogemond V, et al. Phosphorylation of collapsin response mediator protein 2 on Tyr-479 regulates CXCL12-induced T lymphocyte migration. J Biol Chem. 2009 May 8;284(19):13265–76.

117. Uchida Y, Ohshima T, Sasaki Y, Suzuki H, Yanai S, Yamashita N, et al. Semaphorin3A signalling is mediated via sequential Cdk5 and GSK3beta phosphorylation of CRMP2: implication of common phosphorylating mechanism underlying axon guidance and Alzheimer's disease. Genes Cells Devoted Mol Cell Mech. 2005 Feb;10(2):165–79.

118. Yoshimura T, Kawano Y, Arimura N, Kawabata S, Kikuchi A, Kaibuchi K. GSK-3beta regulates phosphorylation of CRMP-2 and neuronal polarity. Cell. 2005 Jan 14;120(1):137–49.

119. Cole AR, Causeret F, Yadirgi G, Hastie CJ, McLauchlan H, McManus EJ, et al. Distinct priming kinases contribute to differential regulation of collapsin response mediator proteins by glycogen synthase kinase-3 in vivo. J Biol Chem. 2006 Jun 16;281(24):16591–8.

120. Cole AR, Knebel A, Morrice NA, Robertson LA, Irving AJ, Connolly CN, et al. GSK-3 phosphorylation of the Alzheimer epitope within collapsin response mediator proteins regulates axon elongation in primary neurons. J Biol Chem. 2004 Nov 26;279(48):50176–80.

121. Brown M, Jacobs T, Eickholt B, Ferrari G, Teo M, Monfries C, et al. Alpha2-chimaerin, cyclin-dependent Kinase 5/p35, and its target collapsin response mediator protein-2 are essential components in semaphorin 3A-induced growth-cone collapse. J Neurosci Off J Soc Neurosci. 2004 Oct 13;24(41):8994–9004.

122. Uchida Y, Ohshima T, Yamashita N, Ogawara M, Sasaki Y, Nakamura F, et al. Semaphorin3A signaling mediated by Fyn-dependent tyrosine phosphorylation of collapsin response mediator protein 2 at tyrosine 32. J Biol Chem [Internet]. 2009 Aug 3 [cited 2009 Aug 31]; Available from: http://www.ncbi.nlm.nih.gov/pubmed/19652227

123. Arimura N, Inagaki N, Chihara K, Ménager C, Nakamura N, Amano M, et al. Phosphorylation of collapsin response mediator protein-2 by Rho-kinase. Evidence for two separate signaling pathways for growth cone collapse. J Biol Chem. 2000 Aug 4;275(31):23973–80.

124. Arimura N, Ménager C, Kawano Y, Yoshimura T, Kawabata S, Hattori A, et al. Phosphorylation by Rho kinase regulates CRMP-2 activity in growth cones. Mol Cell Biol. 2005 Nov;25(22):9973–84.

125. Zhu L-Q, Zheng H-Y, Peng C-X, Liu D, Li H-L, Wang Q, et al. Protein phosphatase 2A facilitates axonogenesis by dephosphorylating CRMP2. J Neurosci Off J Soc Neurosci. 2010 Mar 10;30(10):3839–48.

126. Dustrude ET, Moutal A, Yang X, Wang Y, Khanna M, Khanna R. Hierarchical CRMP2 posttranslational modifications control NaV1.7 function. Proc Natl Acad Sci U S A. 2016 Dec 27;113(52):E8443–52.

127. Dustrude ET, Perez-Miller S, François-Moutal L, Moutal A, Khanna M, Khanna R. A single structurally conserved SUMOylation site in CRMP2 controls NaV1.7 function. Channels Austin Tex. 2017 Feb 28;1–13.

128. Gellert M, Venz S, Mitlöhner J, Cott C, Hanschmann E-M, Lillig CH. Identification of a dithiol-disulfide switch in collapsin response mediator protein 2 (CRMP2) that is toggled in a model of neuronal differentiation. J Biol Chem. 2013 Dec 6;288(49):35117–25.

129. Majava V, Löytynoja N, Chen W-Q, Lubec G, Kursula P. Crystal and solution structure, stability and post-translational modifications of collapsin response mediator protein 2. FEBS J. 2008 Sep;275(18):4583–96.

130. Inagaki N, Chihara K, Arimura N, Ménager C, Kawano Y, Matsuo N, et al. CRMP-2 induces axons in cultured hippocampal neurons. Nat Neurosci. 2001 Aug;4(8):781–2.

131. Li W, Herman RK, Shaw JE. Analysis of the Caenorhabditis elegans axonal guidance and outgrowth gene unc-33. Genetics. 1992 Nov;132(3):675–89.

132. Goshima Y, Nakamura F, Strittmatter P, Strittmatter SM. Collapsin-induced growth cone collapse mediated by an intracellular protein related to UNC-33. Nature. 1995 Aug 10;376(6540):509–14.

133. Minturn JE, Fryer HJ, Geschwind DH, Hockfield S. TOAD-64, a gene expressed early in neuronal differentiation in the rat, is related to unc-33, a C. elegans gene involved in axon outgrowth. J Neurosci Off J Soc Neurosci. 1995 Oct;15(10):6757–66.

134. Chung M-A, Lee J-E, Lee J-Y, Ko M-J, Lee S-T, Kim H-J. Alteration of collapsin response mediator protein-2 expression in focal ischemic rat brain. Neuroreport. 2005 Oct 17;16(15):1647–53.

135. Rogemond V, Auger C, Giraudon P, Becchi M, Auvergnon N, Belin M-F, et al. Processing and nuclear localization of CRMP2 during brain development induce neurite outgrowth inhibition. J Biol Chem. 2008 May 23;283(21):14751–61.

136. Zhang Z, Ottens AK, Sadasivan S, Kobeissy FH, Fang T, Hayes RL, et al. Calpain-mediated collapsin response mediator protein-1, -2, and -4 proteolysis after neurotoxic and traumatic brain injury. J Neurotrauma. 2007 Mar;24(3):460–72.

137. Yu Y, Jian M-Y, Wang Y-Z, Han R-Q. Propofol ameliorates calpain-induced collapsin response mediator protein-2 proteolysis in traumatic brain injury in rats. Chin Med J (Engl). 2015 Apr 5;128(7):919–27.

138. Reidy K, Tufro A. Semaphorins in kidney development and disease: modulators of ureteric bud branching, vascular morphogenesis, and podocyte-endothelial crosstalk. Pediatr Nephrol Berl Ger. 2011 Sep;26(9):1407–12.

139. Vincent P, Collette Y, Marignier R, Vuaillat C, Rogemond V, Davoust N, et al. A role for the neuronal protein collapsin response mediator protein 2 in T lymphocyte polarization and migration. J Immunol Baltim Md 1950. 2005 Dec 1;175(11):7650–60.

140. Mendes-da-Cruz DA, Linhares-Lacerda L, Smaniotto S, Dardenne M, Savino W. Semaphorins and neuropilins: new players in the neuroendocrine control of the intrathymic T-cell migration in humans. Exp Physiol. 2012 Nov;97(11):1146–50.

141. Li Z, Hao J, Duan X, Wu N, Zhou Z, Yang F, et al. The Role of Semaphorin 3A in Bone Remodeling. Front Cell Neurosci. 2017;11:40.

142. Xu R. Semaphorin 3A: A new player in bone remodeling. Cell Adhes Migr. 2014;8(1):5–10.

143. Ochsenbein AM, Karaman S, Jurisic G, Detmar M. The role of neuropilin-1/semaphorin 3A signaling in lymphatic vessel development and maturation. Adv Anat Embryol Cell Biol. 2014;214:143–52.

144. Schmidt EF, Strittmatter SM. The CRMP family of proteins and their role in Sema3A signaling. Adv Exp Med Biol. 2007;600:1–11.

145. Sharma A, Verhaagen J, Harvey AR. Receptor complexes for each of the Class 3 Semaphorins. Front Cell Neurosci. 2012;6:28.

146. Terman JR, Mao T, Pasterkamp RJ, Yu H-H, Kolodkin AL. MICALs, a Family of Conserved Flavoprotein Oxidoreductases, Function in Plexin-Mediated Axonal Repulsion. Cell. 2002 Jun 28;109(7):887–900.

147. Giridharan SSP, Caplan S. MICAL-Family Proteins: Complex Regulators of the Actin Cytoskeleton. Antioxid Redox Signal. 2014 May 1;20(13):2059–73.

148. Siebold C, Berrow N, Walter TS, Harlos K, Owens RJ, Stuart DI, et al. High-resolution structure of the catalytic region of MICAL (molecule interacting with CasL), a multidomain flavoenzyme-signaling molecule. Proc Natl Acad Sci U S A. 2005 Nov 15;102(46):16836–41.

149. Krueger SK, Williams DE. Mammalian flavin-containing monooxygenases: structure/function, genetic polymorphisms and role in drug metabolism. Pharmacol Ther. 2005 Jun;106(3):357–87.

150. Nadella M, Bianchet MA, Gabelli SB, Barrila J, Amzel LM. Structure and activity of the axon guidance protein MICAL. Proc Natl Acad Sci U S A. 2005 Nov 15;102(46):16830–5.

151. Morinaka A, Yamada M, Itofusa R, Funato Y, Yoshimura Y, Nakamura F, et al. Thioredoxin mediates oxidation-dependent phosphorylation of CRMP2 and growth cone collapse. Sci Signal. 2011;4(170):ra26.

152. Deponte M, Lillig CH. Enzymatic control of cysteinyl thiol switches in proteins. Biol Chem. 2015 Jan 10;

153. Hung R-J, Yazdani U, Yoon J, Wu H, Yang T, Gupta N, et al. Mical links semaphorins to F-actin disassembly. Nature. 2010 Feb 11;463(7282):823–7.

154. Hung R-J, Pak CW, Terman JR. Direct redox regulation of F-actin assembly and disassembly by Mical. Science. 2011 Dec 23;334(6063):1710–3.

155. Lee BC, Péterfi Z, Hoffmann FW, Moore RE, Kaya A, Avanesov A, et al. MsrB1 and MICALs regulate actin assembly and macrophage function via reversible stereoselective methionine oxidation. Mol Cell. 2013 Aug 8;51(3):397–404.

156. Grintsevich EE, Yesilyurt HG, Rich SK, Hung R-J, Terman JR, Reisler E. F-actin dismantling through a Redox-driven synergy between Mical and cofilin. Nat Cell Biol. 2016 Aug;18(8):876–85.

157. Pollard TD, Blanchoin L, Mullins RD. Molecular mechanisms controlling actin filament dynamics in nonmuscle cells. Annu Rev Biophys Biomol Struct. 2000;29:545–76.

158. Omotade OF, Pollitt SL, Zheng JQ. Actin-based growth cone motility and guidance. Mol Cell Neurosci. 2017 Mar 6;

159. Pollard TD. Regulation of actin filament assembly by Arp2/3 complex and formins. Annu Rev Biophys Biomol Struct. 2007;36:451–77.

160. Pollitt AY, Insall RH. WASP and SCAR/WAVE proteins: the drivers of actin assembly. J Cell Sci. 2009 Aug 1;122(Pt 15):2575–8.

161. Kurisu S, Takenawa T. The WASP and WAVE family proteins. Genome Biol. 2009;10(6):226.

162. Miki H, Takenawa T. Regulation of actin dynamics by WASP family proteins. J Biochem (Tokyo). 2003 Sep;134(3):309–13.

163. Hensley K, Venkova K, Christov A, Gunning W, Park J. Collapsin response mediator protein-2: an emerging pathologic feature and therapeutic target for neurodisease indications. Mol Neurobiol. 2011 Jun;43(3):180–91.

164. Ridley AJ. Rho GTPases and actin dynamics in membrane protrusions and vesicle trafficking. Trends Cell Biol. 2006 Oct;16(10):522–9.

165. Cheadle L, Biederer T. Activity-dependent regulation of dendritic complexity by semaphorin 3A through Farp1. J Neurosci Off J Soc Neurosci. 2014 Jun 4;34(23):7999–8009.

166. Kubo T, Yamashita T, Yamaguchi A, Sumimoto H, Hosokawa K, Tohyama M. A novel FERM domain including guanine nucleotide exchange factor is involved in Rac signaling and regulates neurite remodeling. J Neurosci Off J Soc Neurosci. 2002 Oct 1;22(19):8504–13.

167. Toyofuku T, Yoshida J, Sugimoto T, Zhang H, Kumanogoh A, Hori M, et al. FARP2 triggers signals for Sema3A-mediated axonal repulsion. Nat Neurosci. 2005 Dec;8(12):1712–9.

168. Bateman J, Shu H, Van Vactor D. The guanine nucleotide exchange factor trio mediates axonal development in the Drosophila embryo. Neuron. 2000 Apr;26(1):93–106.

169. Hall C, Brown M, Jacobs T, Ferrari G, Cann N, Teo M, et al. Collapsin response mediator protein switches RhoA and Rac1 morphology in N1E-115 neuroblastoma cells and is regulated by Rho kinase. J Biol Chem. 2001 Nov 16;276(46):43482–6.

170. Dent EW. Of microtubules and memory: implications for microtubule dynamics in dendrites and spines. Mol Biol Cell. 2017 Jan 1;28(1):1–8.

171. Lin P-C, Chan PM, Hall C, Manser E. Collapsin response mediator proteins (CRMPs) are a new class of microtubule-associated protein (MAP) that selectively interacts with assembled microtubules via a taxol-sensitive binding interaction. J Biol Chem. 2011 Dec 2;286(48):41466–78.

172. Godoy JR, Funke M, Ackermann W, Haunhorst P, Oesteritz S, Capani F, et al. Redox atlas of the mouse Immunohistochemical detection of glutaredoxin-, peroxiredoxin-, and thioredoxin-family proteins in various tissues of the laboratory mouse. Biochim Biophys Acta [Internet]. 2010 Jun 1 [cited 2010 Sep 13]; Available from: http://www.ncbi.nlm.nih.gov/pubmed/20682242

173. Dexter DT, Holley AE, Flitter WD, Slater TF, Wells FR, Daniel SE, et al. Increased levels of lipid hydroperoxides in the parkinsonian substantia nigra: an HPLC and ESR study. Mov Disord Off J Mov Disord Soc. 1994 Jan;9(1):92–7.

174. Danielson SR, Andersen JK. Oxidative and nitrative protein modifications in Parkinson's disease. Free Radic Biol Med. 2008 May 15;44(10):1787–94.

175. Ortiz GG, Pacheco Moisés FP, Mireles-Ramírez M, Flores-Alvarado LJ, González-Usigli H, Sánchez-González VJ, et al. Oxidative Stress: Love and Hate History in Central Nervous System. Adv Protein Chem Struct Biol. 2017;108:1–31.

176. Multhaup G, Ruppert T, Schlicksupp A, Hesse L, Beher D, Masters CL, et al. Reactive oxygen species and Alzheimer's disease. Biochem Pharmacol. 1997 Sep 1;54(5):533–9.

177. Yoshida H, Watanabe A, Ihara Y. Collapsin response mediator protein-2 is associated with neurofibrillary tangles in Alzheimer's disease. J Biol Chem. 1998 Apr 17;273(16):9761–8.

178. Gu Y, Hamajima N, Ihara Y. Neurofibrillary tangle-associated collapsin response mediator protein-2 (CRMP-2) is highly phosphorylated on Thr-509, Ser-518, and Ser-522. Biochemistry (Mosc). 2000 Apr 18;39(15):4267–75.

179. Good PF, Alapat D, Hsu A, Chu C, Perl D, Wen X, et al. A role for semaphorin 3A signaling in the degeneration of hippocampal neurons during Alzheimer's disease. J Neurochem. 2004 Nov;91(3):716–36.

180. Barber SC, Mead RJ, Shaw PJ. Oxidative stress in ALS: a mechanism of neurodegeneration and a therapeutic target. Biochim Biophys Acta. 2006 Dec;1762(11–12):1051–67.

181. Venkova K, Christov A, Kamaluddin Z, Kobalka P, Siddiqui S, Hensley K. Semaphorin 3A signaling through neuropilin-1 is an early trigger for distal axonopathy in the SOD1G93A

mouse model of amyotrophic lateral sclerosis. J Neuropathol Exp Neurol. 2014 Jul;73(7):702–13.

182. Kadoyama K, Matsuura K, Nakamura-Hirota T, Takano M, Otani M, Matsuyama S. Changes in the expression of collapsin response mediator protein-2 during synaptic plasticity in the mouse hippocampus. J Neurosci Res. 2015 Nov;93(11):1684–92.

183. Hubbard C, Benda E, Hardin T, Baxter T, St John E, O'Brien S, et al. Lanthionine ketimine ethyl ester partially rescues neurodevelopmental defects in unc-33 (DPYSL2/CRMP2) mutants. J Neurosci Res. 2013 Sep;91(9):1183–90.

184. Hensley K, Gabbita SP, Venkova K, Hristov A, Johnson MF, Eslami P, et al. A derivative of the brain metabolite lanthionine ketimine improves cognition and diminishes pathology in the 3 × Tg-AD mouse model of Alzheimer disease. J Neuropathol Exp Neurol. 2013 Oct;72(10):955–69.

185. Dupree JL, Polak PE, Hensley K, Pelligrino D, Feinstein DL. Lanthionine ketimine ester provides benefit in a mouse model of multiple sclerosis. J Neurochem. 2015 Jul;134(2):302–14.

186. Nada SE, Tulsulkar J, Raghavan A, Hensley K, Shah ZA. A derivative of the CRMP2 binding compound lanthionine ketimine provides neuroprotection in a mouse model of cerebral ischemia. Neurochem Int. 2012 Dec;61(8):1357–63.

187. Kotaka K, Nagai J, Hensley K, Ohshima T. Lanthionine ketimine ester promotes locomotor recovery after spinal cord injury by reducing neuroinflammation and promoting axon growth. Biochem Biophys Res Commun. 2017 Jan 29;483(1):759–64.

188. Wilson SM, Khanna R. Specific Binding of Lacosamide to Collapsin Response Mediator Protein 2 (CRMP2) and Direct Impairment of its Canonical Function: Implications for the Therapeutic Potential of Lacosamide. Mol Neurobiol. 2014 Jun 20;

189. Romero JI, Hanschmann E-M, Gellert M, Eitner S, Holubiec MI, Blanco-Calvo E, et al. Thioredoxin 1 and glutaredoxin 2 contribute to maintain the phenotype and integrity of neurons following perinatal asphyxia. Biochim Biophys Acta. 2015 Jun;1850(6):1274–85.

190. Lillig CH, Lonn ME, Enoksson M, Fernandes AP, Holmgren A. Short interfering RNA-mediated silencing of glutaredoxin 2 increases the sensitivity of HeLa cells toward doxorubicin and phenylarsine oxide. Proc Natl Acad Sci. 2004;101(36):13227–32.

191. Fernandes AP, Capitanio A, Selenius M, Brodin O, Rundlöf A-K, Björnstedt M. Expression profiles of thioredoxin family proteins in human lung cancer tissue: correlation with proliferation and differentiation. Histopathology. 2009 Sep;55(3):313–20.

192. Neufeld G, Kessler O. The semaphorins: versatile regulators of tumour progression and tumour angiogenesis. Nat Rev Cancer. 2008 Aug;8(8):632–45.

193. Bachelder RE, Lipscomb EA, Lin X, Wendt MA, Chadborn NH, Eickholt BJ, et al. Competing autocrine pathways involving alternative neuropilin-1 ligands regulate chemotaxis of carcinoma cells. Cancer Res. 2003 Sep 1;63(17):5230–3.

194. Shimada K, Ishikawa T, Nakamura F, Shimizu D, Chishima T, Ichikawa Y, et al. Collapsin response mediator protein 2 is involved in regulating breast cancer progression. Breast Cancer Tokyo Jpn. 2014 Nov;21(6):715–23.

195. Zhou Y, Gunput R-AF, Adolfs Y, Pasterkamp RJ. MICALs in control of the cytoskeleton, exocytosis, and cell death. Cell Mol Life Sci CMLS. 2011 Dec;68(24):4033–44.

5 Abbreviations

Arp2/3	actin-related protein 2/3
ALS	amyotrophic lateral sclerosis
ccRCC	clear cell renal cell carcinoma
CDC42	cell division control protein 42
CDK5	cyclin-dependent kinase 5/p35
CXCL12	chemokine stromal cell-derived factor 1α
CRMP	collapsin response mediator protein
Cyfip1	cytoplasmic FMR1-interactin protein 1
DRP	dihydropyrimidinase-related protein
Etrx	surface-exposed thioredoxin-like lipoprotein
FAD	flavin adenine dinucleotide
FARP	FERM, RhoGEF (ARHGEF), and pleckstrin domain protein)
Fyn	Tyrosin-protein kinase Fyn
GR	Glutathione reductase
Grx	Glutaredoxin
GSH	Glutathione
GSK3β	glycogen synthase kinase-3 beta
LK(E)	lanthionine ketimine (ester)
MAP	microtubule associated protein
MICAL	Molecule interacting with CasL
MICAL-L	MICAL-like protein
Msr	Methionine sulphoxide reductase
NADPH	nicotinamide andenine dinucleotide phosphate
NP	neuropilin
PlexA	class A plexin

PPA2	protein phosphatase 2A
Prx	Peroxiredoxin
Rac	Ras-related C3 botulinum toxin substrate
Ras	rat sarcoma
Rho	Ras homologue family member
RNR	Ribonucleotide reductase
Sema	semaphorin
Sra1	specifically Rac1-associated protein 1
Src	Proto-oncogene tyrosine-protein kinase Src
SUMO	small ubiquitin-like modifier
TOAD	turned on after division
TrxR	Thioredoxin reductase
Trx	Thioredoxin
Ulip	uncoordinated 33-like protein
unc-33	uncoordinated protein 33
WASP	Wiskott-Aldrich syndrome protein
WAVE	WASP-family veropolin homologous protein
Yes	Tyrosine-protein kinase Yes

6 Author contributions

I. **Gellert, M.**, Venz, S., Mitlöhner, J., Cott, C., Hanschmann, E.M., Lillig, C.H. Identification of a dithiol-disulfide switch in collapsin response mediator protein 2 (CRMP2) that is toggled in a model of neuronal differentiation. *J Biol Chem.*;288(49):35117–25. (2013) (DOI: 10.1074/jbc.M113.521443)

MG, SV, and CHL conceived and designed the experiments. MG, SV, JM, CC, and EMH performed the experiments and analysed the results. In particular, MG generated the clones and established the conditions for recombinant expression and purification of CRMP2, she performed the analysis of the quaternary structure of CRMP2 dependent on its redox state (Figure 1), the reduction of the thiol switch by Grx2c (Figure 2), the preparation of the samples for mass spectrometry analysis (Figure 3, performed by SV), the conformational switch induced by the redox switch (Figure 4), and the optimisation of the methods necessary for the analysis of the switch during neuronal development (Figure 5, performed by JM). MG, EMH, and CHL wrote the paper.

II. Saleh, M., Bartual, S.G., Abdullah, M.R., Jensch, I., Asmat, T.M., Petruschka, L., Pribyl, T., **Gellert, M.**, Lillig, C.H., Antelmann, H., Hermoso, J.A., and Hammerschmidt, S. Molecular architecture of Streptococcus pneumoniae surface thioredoxin-fold lipoproteins crucial for extracellular oxidative stress resistance and maintenance of virulence. *EMBO Mol Med.* 2013 Dec;5(12):1852–70. (DOI: 10.1002/emmm.201202435)

MS, JAH, CHL, HA, and SH conceived and designed the experiments. MS, SGB, MRA, IJ, TMA, LP, TP and MG performed the experiments. In particular, MG analysed the reduction and oxidation of MsrAB2 by Etrx1 and Etrx2 and the redox properties of these proteins, see Figure 5. MS, SGB, MRA, TP, JAH, CHL, HA, and SH analysed the data. MS, SGB, HA, JAH and SH wrote the paper.

III. Romero, J.I., Hanschmann, E.M., **Gellert, M.**, Eitner, S., Holubiec, M.I., Blanco-Calvo, E., Lillig, C.H., and Capani, F. Thioredoxin 1 and glutaredoxin 2 contribute to maintain the phenotype and integrity of neurons following perinatal asphyxia. *Biochim Biophys Acta.*; 1850(6):1274–85 (2015) (DOI: 10.1016/j.bbagen.2015.02.015)

CHL and FC conceived and designed the experiments. JJR, EMH, MG, SE, MIH, and EBC performed the experiments and analysed the results. In particular, MG established the gene silencing by RNA interference, and she performed the cell culture experiments, *i.e.* the transfection of the SH-SY5Y cell line and the subsequent analyses by Western-blotting, see Figures 3 and 4. JJR, EMH, and FC wrote the paper.

IV. **Gellert, M.**, Hanschmann, E.M., Lepka, K., Berndt, C., Lillig, C.H. Redox regulation of cytoskeletal dynamics during differentiation and de-differentiation. *Biochim Biophys Acta.*; 1850(8):1575–87 (2015) (DOI: 10.1016/j.bbagen.2014.10.030)

MG, EMH, KL, CB, and CHL, conceived, designed, and wrote this review article. In particular, MG was responsible for chapters 1 and 2.3, including Figures 1, 2, and 5.

V. Möller, D.*, **Gellert, M**.*, Langel, W., Lillig, CH. Molecular dynamics simulations and *in vitro* analysis of the CRMP2 thiol switch. *Mol. BioSyst.* submitted 17.03.2017, Manuscript-ID: MB-ART-03-2017-000160 (https://arxiv.org/abs/1703.10124)
*These authors contributed equally to this work

DM, MG, WL, and CHL conceived and designed this study. DM and MG performed all experimental and computational analyses. In particular, MG performed and analysed all *in vitro* experiments using recombinantly expressed protein, DM performed all in silico analyses. MG, DM, WL, and CHL wrote and reviewed the paper.

VI. **Gellert M.**, Richter, E., Mostertz, J., Kantz, L., Masur, K., Hanschmann, EM., Ribback, S., Kröger, N., Hochgräfe, F., Lillig, CH. The cytosolic isoform of glutaredoxin 2 promotes cell migration and invasion, its expression may contribute to carcinogenesis. *Cancer Res*. submitted 24.04.2017, Manuscript-ID: CAN-17-1219

MG, NK, FH, and CHL conceived and designed this study. MG, ER, JM, LK, KM, EMH, SR, and CHL performed and analysed the experiments. In particular, MG established, performed, and analysed all cell culture experiments, including the expression and gene silencing of the genes investigated, see Figures 1, 2, 3, and suppl. Figures 1 and 5. The microscopic analyses were performed by MG, LK, KM, and CHL. MG prepared the samples for mass spectrometry analysis (Figure 4, suppl. Figure 2-3, performed and analysed by ER, JM, and FH). MG also established and performed the analyses of the clinical samples (see Figure 5, provided by SR and NK, statistical analysis by NK). MG, FH, and CHL wrote and reviewed the paper.

Greifswald, den 04.05.2017

7 Publications

7.1 Publications accepted in peer reviewed journals

I. **Gellert, M.**, Venz, S., Mitlöhner, J., Cott, C., Hanschmann, E.M., Lillig, C.H. Identification of a dithiol-disulfide switch in collapsin response mediator protein 2 (CRMP2) that is toggled in a model of neuronal differentiation. *J Biol Chem.*;288(49):35117–25. (2013) (http://doi.org/10.1074/jbc.M113.521443)

II. Saleh, M., Bartual, S.G., Abdullah, M.R., Jensch, I., Asmat, T.M., Petruschka, L., Pribyl, T., **Gellert, M.**, Lillig, C.H., Antelmann, H., Hermoso, J.A., and Hammerschmidt, S. Molecular architecture of Streptococcus pneumoniae surface thioredoxin-fold lipoproteins crucial for extracellular oxidative stress resistance and maintenance of virulence. *EMBO Mol Med.* 2013 Dec;5(12):1852–70. (http://doi.org/10.1002/emmm.201202435)

III. Romero, J.I., Hanschmann, E.M., **Gellert, M.**, Eitner, S., Holubiec, M.I., Blanco-Calvo, E., Lillig, C.H., and Capani, F. Thioredoxin 1 and glutaredoxin 2 contribute to maintain the phenotype and integrity of neurons following perinatal asphyxia. *Biochim Biophys Acta.*; 1850(6):1274–85 (2015) (http://doi.org/10.1016/j.bbagen.2015.02.015)

IV. **Gellert, M.**, Hanschmann, E.M., Lepka, K., Berndt, C., Lillig, C.H. Redox regulation of cytoskeletal dynamics during differentiation and de-differentiation. *Biochim Biophys Acta.*; 1850(8):1575–87 (2015) (http://doi.org/10.1016/j.bbagen.2014.10.030)

7.2 Manuscripts submitted

V. Möller, D.*, **Gellert, M**.*, Langel, W., Lillig, C.H. Molecular dynamics simulations and *in vitro* analysis of the CRMP2 thiol switch. *Mol. BioSyst.* submitted 17.03.2017, Manuscript-ID: MB-ART-03-2017-000160
*Authors contributed equally to this work

VI. **Gellert M.**, Richter, E., Mostertz, J., Kantz, L., Masur, K., Hanschmann, E.M., Ribback, S., Kröger, N., Hochgräfe, F., Lillig, C.H. The cytosolic isoform of glutaredoxin 2 promotes cell migration and invasion, its expression may contribute to carcinogenesis. *Cancer Res*. submitted 24.04.2017, Manuscript-ID: CAN-17-1219

7.3 Publications not included in this thesis

VII. Bräutigam, L., Schütte, L.D., Godoy, J.R., Prozorovski, T., **Gellert, M.**, Hauptmann, G., Holmgren, A., Lillig, C.H., Berndt, C. Vertebrate-specific glutaredoxin is essential for brain development. *Proc Natl Acad Sci USA* 108(51):20532–7. (2011) (http://doi.org/10.1073/pnas.1110085108)

7.4 Further scientific achievements

7.4.1 Published abstract

VIII. **Gellert, M.**, Berndt, C., Deponte, M., Lillig C.H. Redox control of cytoskeletal dynamics: toggling the thiol switch in CRMP2. *FEBS JOURNAL*. Vol. 282. (2015) pp 115

7.4.2 Invited talks

IX. **Gellert, M.**, Berndt, C., Deponte, M., Kröger, N., Hochgräfe, F., Lillig, C.H.: A thiol-disulphide switch in the regulation of cytoskeletal dynamics
Symposium 'Tumor Immunology meets Oncology XII', April 28th-30th 2016, Halle, Germany

X. **Gellert, M.**, Berndt, C., Deponte, M., Kröger, N., Hochgräfe F., Lillig C.H.: A thiol-disulphide switch in the regulation of cytoskeletal dynamics.
3rd meeting of the study group redox biology of the German Society for Biochemistry and Molecular Biology, July, 4th-5th 2015, Düsseldorf, Germany

XI. **Gellert, M.**, Berndt, C., Deponte, M., Kröger, N., Hochgräfe, F., Lillig C.H.: A thiol-disulphide switch in the regulation of cytoskeletal dynamics.
Frontiers in Redox Biology and Medicine, 5th Young Professionals Workshop on Plasma Medicine, November 28th-December 1st 2016, Rostock, Germany

XII. **Gellert, M.**, Uhlenkamp, D., Möller, D., Berndt, C., Schwarzländer, M., Deponte, M., Kröger, N., Lillig, C.H.: Dissecting a thiol switch in molecular detail.
Symposium 'Redox regulation: Historical background and future developments' March 29th-31st 2017, Nancy, France

7.4.3 Poster presentations

XIII. **Gellert, M.**, Uhlenkamp, D., Masur, K., Kantz, L., Mostertz, J., Hochgräfe, F., Lillig, C.H.: Identification and in depth characterisation of the CRMP2 redox signaling pathway, 7th Young Scientists Meeting of the German Society for Biochemistry and Molecular Biology, Castle Reisensburg, September 12th-13th 2014

XIV. **Gellert, M.**, Uhlenkamp, D., Masur, K., Kantz, L., Mostertz, J., Hochgräfe, F., Lillig, C.H.: Identification and in depth characterisation of the CRMP2 redox signaling pathway. Joint Symposium if the DFG Priority Program 1710 and the study group ‚redox biology‘ of the German Society for Biochemistry and Molecular Biology, Heidelberg, September 22nd-23rd 2014

XV. **Gellert, M.**, Uhlenkamp, D., Masur, K., Kantz, L., Mostertz, J., Hochgräfe, F., Schwarzländer, M., Lillig, C.H.: Identification and in depth characterisation of the CRMP2 redox signaling pathway.
3rd Symposium of the DFG Priority Program 1710, Rauischholzhausen,
March 20th-21st 2015

XVI. **Gellert, M.**, Berndt, C., Deponte, M., Lillig, C.H.: Redox control of cytoskeletal dynamics: toggling the thiol switch in CRMP2
15th FEBS Young Scientists Forum and 40th FEBS Congress, Berlin, July 2nd-4th and 4th-9th 2015

Awarded with the poster price.

XVII. **Gellert, M.**, Berndt, C., Deponte, M., Lillig, C.H.: Redox control of cytoskeletal dynamics: toggling the thiol switch in CRMP2
Symposium of the European Science Foundation and the European Molecular Biology Organization, Sant Feliu, Spain, September 12th-17th 2015

XVIII. **Gellert, M.**, Uhlenkamp, D., Schwarzländer, M., Masur, K., Kantz, L., Berndt, C., Deponte, M., Lillig, C.H.: A thiol-disulfide switch in the regulation of cytoskeletal dynamics.
5th Symposium of the DFG Priority Program 1710, Rauischholzhausen, February 29th-March 1st 2016

XIX. Uhlenkamp, D., Urbainsky, C., Trnka, D., Lillig, C.H., **Gellert, M.**: Identification and in depth characterisation of downstream elements of the CRMP2 redox signalling pathway.
3rd meeting of the study group redox biology of the German Society for Biochemistry and Molecular Biology, July, 4th-5th 2015, Düsseldorf, Germany

XX. **Gellert, M.**, Berndt, C., Deponte, M., Schwarzländer, M., Hochgräfe, F., Lillig, C.H.: Operation of the thiol-disulfide switch in collapsin response mediator protein 2
6th Symposium of the DFG Priority Program 1710, Irsee, September 15th-17th 2016

I. Article

Identification of a dithiol-disulfide switch in collapsin response mediator protein 2 (CRMP2) that is toggled in a model of neuronal differentiation

Manuela Gellert, Simone Venz, Jessica Mitlöhner, Catherine Cott, Eva-Maria Hanschmann, and Christopher Horst Lillig

J. Biol. Chem.

Vol 288 Issue 49 (35117-25)

Published: December 6th, 2013

For supplementary information see DOI: 10.1074/jbc.M113.521443

THE JOURNAL OF BIOLOGICAL CHEMISTRY VOL. 288, NO. 49, pp. 35117–35125, December 6, 2013

Identification of a Dithiol-disulfide Switch in Collapsin Response Mediator Protein 2 (CRMP2) That Is Toggled in a Model of Neuronal Differentiation*[S]

Received for publication, September 24, 2013, and in revised form, October 14, 2013 Published, JBC Papers in Press, October 16, 2013, DOI 10.1074/jbc.M113.521443

Manuela Gellert[‡], Simone Venz[‡], Jessica Mitlöhner[‡], Catherine Cott[§], Eva-Maria Hanschmann[‡], and Christopher Horst Lillig[‡1]

From the [‡]Institute for Medical Biochemistry and Molecular Biology, University Medicine, Ernst-Moritz-Arndt-University Greifswald, 17475 Greifswald, Germany and the [§]Centre For Biological Signalling Studies, Albert-Ludwigs University Freiburg, 79104 Freiburg, Germany

Background: Cytosolic glutaredoxin 2 (Grx2) is essential for neuronal development in zebrafish; collapsin response mediator protein 2 (CRMP2) was identified as Grx2 substrate.
Results: Oxidation of CRMP2 by hydrogen peroxide induces an intermolecular disulfide, changes in α-helical content, and hydrophobicity.
Conclusion: The dithiol-disulfide redox switch defines two conformations of CRMP2.
Significance: This switch may be functional during axonal outgrowth.

Vertebrate-specific glutaredoxin 2 (Grx2) is expressed in at least two isoforms, mitochondrial Grx2a and cytosolic Grx2c. We have previously shown that cytosolic Grx2 is essential for embryonic development of the brain. In particular, we identified collapsin response mediator protein 2 (CRMP2/*DPYSL2*), a mediator of the semaphorin-plexin signaling pathway, as redox-regulated target of Grx2c and demonstrated that this regulation is required for normal axonal outgrowth. In this study, we demonstrate the molecular mechanism of this regulation, a specific and reversible intermolecular Cys-504-Cys-504 dithiol-disulfide switch in homotetrameric CRMP2. This switch determines two conformations of the quaternary CRMP2 complex that controls axonal outgrowth and thus neuronal development.

Glutaredoxins are glutathione-dependent oxidoreductases that catalyze the reduction of protein disulfides first, for instance in ribonucleotide reductase (1) and, second, the reversible formation and reduction of protein-glutathione mixed disulfides (2). The first reaction requires both cysteinyl residues in the *CXXC* active site, the latter only the more N-terminal (see Refs. 3–5 for detailed discussions). Vertebrate-specific glutaredoxin 2 (Grx2)[2] was originally identified as mitochondrial protein (6, 7); however, alternative splicing and transcription initiation give rise to additional isoforms of the protein as demonstrated in human and mouse (8–10). The human *GLRX2* gene gives rise to three transcript variants encoding the mitochondrial Grx2a and the cytosolic Grx2b and Grx2c. The mouse *glrx2* gene gives rise to five transcript variants encoding three protein isoforms. Grx2a and Grx2c are conserved, and Grx2d is unique to mice (10).

The zebrafish genome contains a single gene (*glrx2*) that encodes the equivalent to human and mouse Grx2c. Recently, we demonstrated that embryonic brain development depends on the enzymatic activity of this cytosolic Grx2 (11). Zebrafish with morpholino-silenced expression of the cytosolic Grx2 lost virtually all types of neurons by apoptotic cell death and the ability to develop an axonal scaffold. As early as 18 h post fertilization, the axon scaffold was severely reduced. At 24 h post fertilization, essentially all embryos depleted of cytosolic Grx2 lost HuC-positive (an early neuronal marker) cells in the central nervous system. These severe defects could be rescued by co-injection of morpholino-resistant *glrx2* mRNA but not by co-injection of mRNA encoding redox-inactive mutants. Notably, even a mutant that was still capable of catalyzing the Grx-specific monothiol reaction mechanism, which is sufficient for the catalysis of protein de/glutathionylation, did not rescue the phenotype to any degree. In a cellular model of neuronal differentiation, SH-SY5Y neuroblastoma cells overexpressing Grx2c during differentiation displayed 1.5- to 2-fold longer axons with almost twice as many branching points. Thus, Grx2c is essential for neuronal differentiation through the control of axonal outgrowth in a process that requires the dithiol reaction mechanism, implying the reduction of at least one specific protein disulfide (11).

To uncover the mechanism through which Grx2c acts in axon guidance, we deployed a proteomic approach: enzymatic intermediate trapping. This strategy allowed us to identify proteins that can undergo dithiol-disulfide exchange reactions catalyzed by Grx2 in a dithiol reaction mechanism (12). Among the potential targets, the association of Grx2c with the collapsin response mediator protein 2 (CRMP2/*DPYSL2*/ULIP2), could be confirmed by co-immunoprecipitation. CRMP2 is a part of

* This work was supported by grants from the Deutsche Forschungsgemeinschaft (DFG SFB593-N01) and start-up funding by the Science Networks (Forschungsverbünde) Neuroscience and Molecular Medicine, University Medicine Greifswald.
[S] This article contains supplemental Tables 1 and 2 and Fig. 1.
[1] To whom correspondence should be addressed: University Medicine Greifswald, Institute for Medical Biochemistry and Molecular Biology, J.03 33, Ferdinand-Sauerbruch-Strasse, 17475 Greifswald, Germany. Tel.: 49-3834-865407; Fax: 49-3834-865402; E-mail: horst@lillig.de.
[2] The abbreviations used are: Grx2, glutaredoxin 2; CRMP, collapsin response mediator protein; Grx, glutaredoxin; NEM, *N*-ethylmaleimide; TCEP, Tris(2-chlorethyl)phosphate; Trx, thioredoxin.

the semaphorin-3A-plexin signaling cascade whose critical functions in axon guidance are well documented (13, 14). The protein was reported to be regulated post-translationally by phosphorylation at multiple sites and calpain-catalyzed proteolysis (see, for instance, Refs. 15–17). Phosphorylation was suggested to be facilitated by interaction of CRMP2 with thioredoxin 1 (Trx1), in a redox-dependent mechanism (18).

Using differential labeling of oxidized and reduced thiol groups with *N*-ethylmaleimide (NEM) and 5-maleimido isophthalic acid, the latter compound shifts the isoelectric point of proteins, followed by two-dimensional gel electrophoresis and specific Western blotting, revealed the reduction of cysteinyl residues in CRMP2 in SH-SY5Y and HeLa cells overexpressing Grx2c (11, 12). Corroboratively, CRMP2 in zebrafish embryos depleted of Grx2 was significantly more oxidized (11). Altogether, these results strongly suggest the regulation of CRMP2 through a specific protein dithiol-disulfide switch. Here, we aimed at the identification of this dithiol-disulfide switch, how it controls the function of CRMP2, and whether it could play a role during neuronal differentiation.

EXPERIMENTAL PROCEDURES

Materials—Chemicals and enzymes were purchased from Sigma-Aldrich unless otherwise stated and were of analytical grade or better. The antibodies used in this work were as follows: CRMP2 (Sigma-Aldrich, C2993), CRMP2 P-T514 (Cell Signaling Technologies, catalog no. 9397), neurofilament m (Cell Signaling Technologies, catalog no. 2838), glial fibrillary acidic protein (Thermo Scientific, Waltham, MA; PA3-16727), and GAPDH (Sigma-Aldrich, G9545).

Electrophoresis and Western Blotting—Protein concentrations were determined using Bradford reagent from Bio-Rad. SDS-PAGE and Western blots were run using precasted Precise gels (4–20% (w/v), Thermo Scientific) or mini-Protean TGX Stain-free gels (4–20% (w/v), Bio-Rad), and PVDF membranes (Macherey & Nagel, Düren, Germany) according to the manufacturers' instructions. Horseradish peroxidase-conjugated anti-rabbit and anti-mouse IgGs were obtained from Bio-Rad. Blue native electrophoresis was performed using precasted NativeBlueNovex gels and buffers as suggested by the manufacturer (Life Technologies, Paisley, UK). Western blots were developed by enhanced chemiluminescence staining and documented using a Chemidoc XRS+ documentation system (Bio-Rad).

Cloning of Expression Constructs—CRMP2 was amplified by PCR from human cDNA (Life Technologies) using the oligonucleotides 5′-CACACACATGCTAGCATGTCTTATCAGGGGAAGAAAAATATTCC and 5′-GTGTGTTCTAGACTGCCCAGGCTGGTGATG or 5′-CACACAAGATCTGCCCAGGCTGGTGATGTTG, respectively, ligated into the vector pGEM-T (Promega, Madison, BI), excised with the restriction endonucleases NdeI and BglII, and ligated into the NdeI and BamHI sites of the vectors pET15b and pET24a (Millipore, Darmstadt, Germany), respectively. Correct sequences were confirmed by sequencing at Seqlab (Göttingen, Germany). The plasmids for the recombinant expression and purification of human Grx2c, Grx2c C40S, and thioredoxin 1 have been described previously (19–21).

Quantitative PCR—The cells were treated with trypsin, harvested, and washed once with PBS. RNA isolation was performed according to the manual provided for the NucleoSpin® RNA II kit (Macherey-Nagel, Düren, Germany). RNA concentration was measured photometrically using the NanoDrop 2000c spectrophotometer (Thermo Scientific). First strand cDNA was prepared using the RevertAid First Strand cDNA synthesis kit according to the protocol provided using 1 μg of RNA as template and oligo dT_{18} primer (Thermo Scientific). 1 μl of the cDNA was used as template for quantitative PCR. The SensiMix SYBR HI-ROX contained SYBR Green I dye, dNTPs, stabilizers, and a hot start DNA polymerase was provided as 2× Master Mix (Bioline, London, UK). The primer concentration used for the quantitative PCR was 0.5 μM each (5′-GGAGAGAGATGTCTTATCAGG and 3′-CTGCATAGAACGACTGGTCATC), and the volume was adjusted to 20 μl with double distilled H_2O. All quantitative PCRs were performed using the CFX96 Real Time System from Bio-Rad. For optimization, a gradient quantitative PCR from 55 to 65 °C was performed, and samples were analyzed by agarose gel electrophoresis. At 60 °C annealing temperature, the reaction resulted in a specific product at the expected size. GAPDH was used as a reference (primer pair: 5′-CAAGGTCATCCATGACAACTTTG and 3′-GTCCACCACCCTGTTGCTGTAG) in the ΔΔCq mode.

Recombinant Expression and Purification of CRMP2—For recombinant protein expression, *E. coli* cells were propagated in a 5 liters of Bioreactor (R'ALF; Bioengineering, Wald, Switzerland). The LB medium (5 liters), containing the selective antibiotics, was inoculated at 37 °C with 1% (v/v) of an overnight culture of *E. coli* BL21 (DE3) codon-plus (Life technologies) harboring the pET15b-CRMP2 or pET24a-CRMP2. At OD 0.6, expression was induced by addition of 0.5 mM isopropyl 1-thio-β-D-galactopyranoside and by lowering the temperature to 14 °C. The cells were harvested after 16–20 h by centrifugation. Bacteria were lysed by incubation with 1 mg/ml lysozyme and 0.05 mg/ml Dnase I for 20 min at room temperature and subsequent ultrasonic treatment for 3 min, 80% intensity, 0.5s cycle time (50% cycling) using a UP200S ultrasonic processor (Hielscher; Teltow, Germany). Recombinant His-tagged CRMP2 proteins were purified by the immobilized metal affinity chromatography technique using an Äkta FPLC System as suggested by the manufacturer (GE Healthcare) at 4 °C.

Gel Filtration Chromatography—Gel filtration chromatography was performed using a HiLoad 16/60 Superdex 200 prep grade column and an Äkta System (both GE healthcare) equilibrated with PBS. 85 μM purified CRMP2 were reduced with 5 mM DTT, 5 mM pH-neutralized Tris(2-chlorethyl)phosphate (TCEP), and 0.8 μM human Grx2c and incubated for 30 min at room temperature. To remove all reductants, the protein solution was re-buffered using either NAP-5 or PD10 Sephadex G25 prepacked columns (GE Healthcare). After desalting, 16 nmol of the reduced protein in 200–500 μl were loaded on the column and separated at a flow rate of 1 ml/minute. The remaining protein was oxidized by 200 μM H_2O_2 for 30 min at room temperature. H_2O_2 was removed by rebuffering as described previously, and 16 nmol of oxidized protein were loaded on the column and separated. The remaining protein

was rereduced as before and also separated by gel filtration. The Superdex 200 column was equilibrated with PBS between the runs. Fractions were analyzed by Western blotting. A calibration curve for apparent molecular masses was produced using the manufacturer's calibration standards.

Mass Spectrometry—Recombinant CRMP2 (85 μM) was reduced with 5 mM DTT and 5 mM pH-neutralized TCEP or oxidized with 200 μM H_2O_2 for 30 min at room temperature each. Subsequently, the proteins were denatured, and all thiols were blocked by specific alkylation with 10 mM NEM. A standard SDS-PAGE was performed with the samples considered for mass spectrometry, and the gel was stained with Coomassie staining solution (Thermo Scientific). Excised gel fragments were destained in 100 mM NH_4HCO_3 in 50% (v/v) acetonitrile. Following drying, proteins were digested in 20 μl trypsin (10 ng/μl in 10 mM NH_4HCO_3 solution) at 37 °C overnight. Peptides were collected in 50% (v/v) acetonitrile containing 0.1% (v/v) acetic acid. Next, samples were mixed with 0.7 μl of α-cyano-4-hydroxycinnamic acid matrix in 50% acetonitrile/0.5% TFA on the target and measured by MS using a 4800 MALDI TOF/TOF analyzer (Thermo Scientific). Spectra were aligned manually with data of an *in silico* analysis of the theoretical amino acid sequence, with and without modifications, to confirm the presence of the peptides of interest. Peptide mass fingerprint peak lists were compared with the SwissProt database rel. 57, restricted to human taxonomy, using the Mascot search engine (version 1.9, Matrix Science Ltd, London, UK).

CD Spectroscopy—Circular dichroism spectra were recorded in a Jasco instrument. Freshly purified CRMP2 (80 μM) was reduced with 5 mM DTT, 5 mM pH-neutralized TCEP, and 0.8 μM human Grx2c for 30 min at room temperature. To remove all reductants, the protein solution was rebuffered using NAP-5 columns (GE Healthcare). Next, the protein was oxidized by 200 μM H_2O_2 for 30 min at room temperature. H_2O_2 was removed by rebuffering in 10 mM Hepes, pH 7.3, containing 20 mM $MgCl_2$ as described previously. The oxidized sample (6 μM) was analyzed in a 1-mm cuvette, scanning 0.2-nm steps, averaging 10 iterations. Subsequently, the protein was reduced by addition of 1 mM DTT, 1 mM TCEP, and 0.06 μM Grx2c, incubated for 30 min, and analyzed again. All spectra were corrected by subtraction of the associated baselines.

Differential Scanning Fluorimetry (Thermofluor Assay)—The thermal stability of reduced and oxidized CRMP2 was assayed using the thermofluor assay as outlined in Ref. 22. In brief, 10 μM protein, reduced and oxidized as outlined above and rebuffered in PBS containing 20 mM $MgCl_2$, were mixed with SYPRO Orange (1:100 diluted, Sigma-Aldrich) and heated in a CFX96 Real Time System from Bio-Rad in 0.5 K increments from 20 to 95 °C in 1 h. The increase in fluorescence due to binding of the dye to hydrophobic regions exposed during denaturation was recorded using the FRET settings of the instrument. The curves presented represent the average of five experiments.

Cell Culturing—All media, FCS, antibiotics (penicillin, streptomycin), trypsin, and PBS were purchased from PAA (Cölbe, Germany), disposable plastics from Sarstedt (Nümbrecht, Germany). SH-SY5Y cells were propagated in MEM, low glucose, supplemented with penicillin (100 units/ml)/streptomycin (0.1 mg/ml), 10% (v/v) FCS, and 2 mM L-glutamine. For differentiation into a neuron-like phenotype, cells were treated with 10 μM retinoic acid (solved in dimethyl sulfoxide) up to 7 days (23). SH-SY5Y cells treated with dimethyl sulfoxide served as control. At 6, 24, 48, 72, 120, and 168 h, cells were detached by trypsin treatment, washed with PBS, and lysed by adding 40 mM Hepes, 50 mM NaCl, 1 mM EDTA, 1 mM EGTA, 2% (w/v) CHAPS, 1-fold protease inhibitor mixture (Roche Applied Science), and 1-fold phosphatase inhibitor mixture 3 (Sigma) at pH 7.4 and frozen in liquid nitrogen. Extracts were clarified by centrifugation at 13,000 rpm (21,000 × *g*) for 10 min at 4 °C in a microcentrifuge.

Immunocytochemistry and Confocal Microscopy—Cells were seeded on fibronectin-covered glass slides, cultivated as indicated, washed with PBS, fixated with 4% (w/v) paraformaldehyde at 4 °C for 30 min, washed with PBS, permeabilized for 30 min at room temperature in 0.4% (v/v) Triton X-100 in PBS, and blocked with 3% (w/v) BSA in PBS for another 30 min. The primary antibody (CRMP2, 1:1000) was incubated overnight at 4 °C, the secondary antibody (anti-rabbit Alexa Fluor 488; Life Technologies, 1:400) for 1 h at room temperature. Nuclei were counterstained with 1 μg/ml DAPI. Slides were mounted with Mowiol (Calbiochem, Darmstadt, Germany) and analyzed by confocal microscopy using a Leica TCS SP5 instrument with a 63-fold/1.4 oil lens.

RESULTS

Two isoforms of human CRMP2 have been described, the canonical isoform CRMP2B and CRMP2A with an alternative N-terminal section. Here, we always refer to CRMP2B when addressing CRMP2. Human CRMP2 consists of 572 amino acid residues, it contains eight cysteinyl residues, from which six are conserved from zebrafish to man (see supplemental Fig. 1). The cDNA of human CRMP2 was cloned by PCR from a commercial cDNA library and ligated into the expression vectors pET15b and pET24a for expression as N- and C-terminal His_6 fusion protein, respectively. Expression was optimized in a 5-liter bioreactor; propagation was performed at 14 °C for ~18 h following the induction of expression at an OD of 0.6 typically yielded 5 (pET24a) to 15 mg (pET15b) soluble protein per liter of culture without the appearance of insoluble portions. We could not observe any significant differences between the behavior of the N- and C-terminally tagged proteins in initial gel filtration chromatography and blue native electrophoresis (see below). We have thus chosen the N-terminally tagged protein for in-depth analysis because of the higher yield in expression.

Quaternary State of Reduced and Oxidized CRMP2—CRMP2 was reported to form homotetramers (24). We first hypothesized that redox regulation, *i.e.* oxidation and reduction of CRMP2, could alter this quaternary structure. Freshly purified CRMP2 was reduced by DTT, TCEP, and a catalytic amount of purified human Grx2c (1/100th molar ratio). CRMP2 was efficiently reduced by DTT and TCEP alone; however, the addition of Grx2c significantly increased the velocity of this reaction when followed by CD spectroscopy (see below). Reducing agents were quickly removed by size exclusion chromatography (Sephadex G25), and the quaternary structures of the reduced

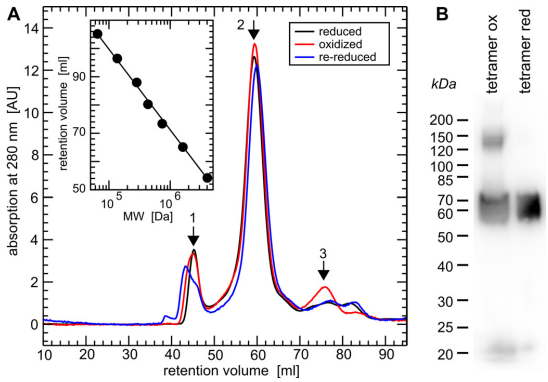

FIGURE 1. **Quaternary structure of reduced, oxidized, and re-reduced CRMP2.** *A*, gel filtration chromatography (HiLoad 16/60 Superdex 200 column, GE Healthcare) of (Grx2c+DTT+TCEP) reduced, H_2O_2-oxidized, and re-reduced recombinant CRMP2 in their native, folded states. Calibration (*inset*) was done using the manufacturer's instructions: *1*, ~800 kDa, *i.e.* dodecamer (theoretical mass, 770.4 kDa); *2*, 256 kDa, *i.e.* (homo)tetramer (theoretical mass, 256.8 kDa); *3*, 65 kDa, *i.e.* monomeric CRMP2 (theoretical mass, 64.2 kDa). *B*, non-reducing SDS-PAGE and Western blot of the tetrameric fractions of oxidized and reduced CRMP2 following the gel-filtration chromatography depicted in *A* and denaturation of the protein complexes.

TABLE 1

Apparent molecular weight and quaternary structure of reduced, oxidized, and re-reduced CRMP2 determined by gel filtration chromatography (see Fig. 1) ($n = 3$)

Fraction	MW	± S.D.	Subunits	MW/subunit
	kDa			*kDa*
1	812.9	4.8	12	67.7
2	256.3	3.3	4	64.1
3	66.0	3.5	1	66.0
4	39.9	2.1		
CRMP2				64.2

and oxidized proteins were analyzed by gel filtration chromatography (Superdex 200, Fig. 1*A*). In parallel, the reduced and rebuffered protein was oxidized by H_2O_2 (5-fold molecular excess) and subsequently analyzed by gel filtration chromatography (Fig. 1*A*). To confirm the reversibility, oxidized CRMP2 was also rebuffered, rereduced as done previously and analyzed by gel filtration chromatography (Fig. 1*A*). As depicted in Fig. 1 and Table 1, reduced, oxidized, and re-reduced CRMP2 fractions with the proteins in their native, folded states were primarily detected in the homotetrameric form, despite a minor fraction of dodecameric protein and the transient appearance of a minor fraction of monomeric CRMP2 in the oxidized form. In conclusion, oxidation and reduction did not change the tetrameric structure of CRMP2 when present in the native state. When analyzed by non-reducing SDS-PAGE (Fig. 1*B*), denatured oxidized CRMP2 migrated in two bands corresponding to dimers, *i.e.* two disulfide-linked monomers and monomeric proteins at a ratio of 1:2. Denatured reduced CRMP2 migrated in a single band at the expected size of monomeric CRMP2. In conclusion, oxidation of CRMP2 did not change the tetrameric quaternary structure of the folded protein, but it led to the formation of up to one intermolecular disulfide in the tetrameric complex.

Grx2c Reduces CRMP2 in a Dithiol Reaction Mechanism—To confirm that the reduction of the CRMP2 disulfide by Grx2c

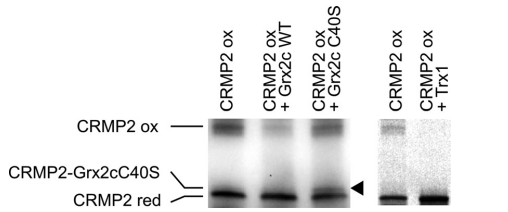

FIGURE 2. **Grx2c reduces CRMP2 in a dithiol reaction mechanism.** Incubation of reduced (*red*) Grx2c with oxidized (*ox*) CRMP2 did not lead to a complex between the proteins when analyzed by non-reducing SDS-PAGE. Only incubation with a Grx2c mutant lacking the second (resolving) cysteinyl residue in the *CXXC* (C40S) active site led to the formation of a mixed disulfide (see *arrowhead*). In addition, wild-type Trx1 was able to reduce the protein *in vitro* and did not form a stable complex with CRMP2.

is catalyzed in a dithiol reaction mechanism, *i.e.* that it requires both thiols in the *CXXC* active site of Grx2c, oxidized CRMP2 was incubated with reduced wild-type and the *CXXS* active site mutant (C40S) Grx2c and analyzed by SDS-PAGE. As predicted for the dithiol reaction mechanism, CRMP2 did not form a complex with wild-type Grx2c, but with the mutant lacking the resolving cysteinyl residue (Fig. 2, see *arrowhead*). Thus, Grx2c reduces CRMP2 by attack of the N-terminal cysteinyl active site thiol on the CRMP2 disulfide; this intermediate mixed disulfide is immediately reduced by the second active site thiol. Noteworthy, also wild-type Trx1 was able to reduce the CRMP2 disulfide *in vitro* and did not form a stable complex with CRMP2.

Oxidation and Reduction of CRMP2 Induce a Significant Conformational Change in the Protein—First information for a switch between two distinct conformations of the CRMP2 tetramer in consequence of oxidation and reduction came from the analysis of zebrafish CRMP2 by CD spectroscopy (11). For human CRMP2, we recorded a reversible decrease in ellipticity upon reduction of CRMP2 at 210–220 nm (Fig. 3*A*), indicative for a reversible decrease in α-helical content of the reduced protein. To confirm and further characterize this switch in conformations, we analyzed the changes induced by reduction and oxidation of tetrameric CRMP2 (in parallel to gel filtration chromatography, see above) in blue native gel electrophoresis (Fig. 3*B*). The mobility of proteins in blue native electrophoresis is determined by the binding of the Coomassie dye to hydrophobic regions of the protein. As shown in Fig. 3, reduced CRMP2 migrates significantly faster in blue native electrophoresis, indicating conformational changes in the reduced tetramer that lead to the exposition of hydrophobic regions. We also tested the influence of the redox switch on the thermal stability of the protein applying differential scanning fluorimetry (Fig. 3*C*) but did not record significant differences between the two species (T_m, 56 *versus* 57 °C).

Identification of Thiol Modifications in CRMP2 upon Oxidation—To identify the cysteinyl residues forming the dithiol-disulfide switch, we labeled the thiol groups of oxidized and reduced CRMP2 with NEM to prevent further redox modifications. Tryptic fragments were analyzed by MALDI-TOF mass spectrometry. Among the peptides containing some of the eight cysteinyl residues, we identified only one difference between the reduced and oxidized protein (see also supplemental Tables 1 and 2). Reduced and NEM-labeled CRMP2 con-

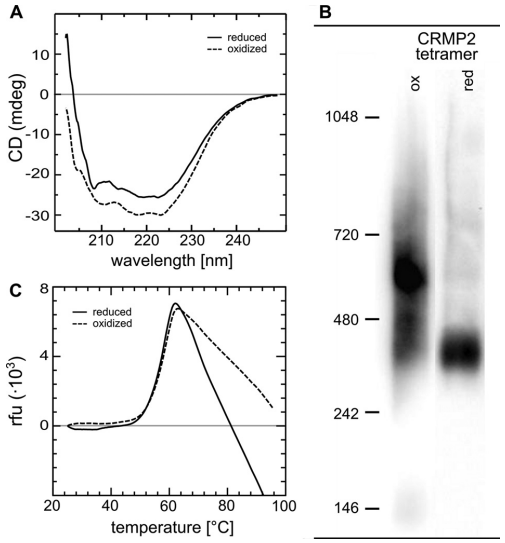

FIGURE 3. **Conformational changes of CRMP2 upon reduction.** *A*, CD spectroscopy of oxidized and subsequently reduced CRMP2. The decrease in ellipticity between 210–220 nm indicates a decrease in α-helical content of reduced CRMP2. *B*, blue native gel electrophoresis of reduced and oxidized tetrameric CRMP2. 1 μg of the protein was reduced by a catalytic amount of Grx2c (1:100, +DTT+TCEP) or oxidized by H_2O_2 treatment. Both fractions were analyzed by blue native gel electrophoresis. The higher migration velocity of reduced CRMP2 indicated binding of more Coomassie dye molecules and thus the exposure of more hydrophobic surfaces compared with the oxidized CRMP2 tetramer. The marks depicted were introduced only for orientation purposes and do not reflect the actual molecular weight of the complexes (see Fig. 1). *C*, differential scanning fluorimetry of reduced and oxidized CRMP2. No significant differences were observed in the thermal stability of reduced and oxidized CRMP2.

tained two peptides corresponding to the masses of a fragment in which Cys-504 was labeled with NEM or NEM/H_2O (Fig. 4, *A.1*, *I* and *II*), which are absent from oxidized CRMP2 (Fig. 4, *A.2*). Oxidized CRMP2 contains one peptide (Fig. 4, *B.2*, *III*) corresponding to the mass of two disulfide-linked Cys-504-containing peptides that was not present in the reduced protein (Fig. 4, *B.1*). Interestingly, we were not able to induce glutathionylation of the protein by treatment with excess GSSG (data not shown). Thus, oxidation specifically induced intermolecular disulfides between the Cys-504 residues of two CRMP2 molecules in the homotetrameric complex.

The Conformational Change Can Be Observed in a Model of Neuronal Differentiation—To confirm the relevance of the redox-induced conformational switch *in vivo*, we have analyzed CRMP2 in a cellular model of neuronal differentiation. The neuroblastoma cell line SH-SY5Y can be transformed into a neuron-like cell culture by treatment with retinoic acid. During this process, the cells display axonal outgrowth, phase out cell division, and express several neuron-specific markers (23). Predominantly, these cells develop a mature dopaminergic-like neurotransmitter phenotype (25). Relative to controls, we did not observe changes in the levels of CRMP2 when analyzed by SDS-PAGE and Western blotting (Fig. 5, *B* and *C*). The phosphorylation of the residue Thr-514 of CRMP2 by cyclin-dependent kinase 5 has been described as a prerequisite for subsequent phosphorylation steps by glycogen synthase kinase 3 that were implied in regulating the function of CRMP2 (26). Using an antibody specific for this modification, we observed a tendency for a decrease in Thr-514 phosphorylation (~50%) at t = 120 and 168 h (Fig. 5*B*); however, the analysis of three independent experiments did not indicate statistical significance. The analysis of CRMP2 by blue native electrophoresis demonstrated an increase of the oxidized conformation of CRMP2 between days three and five (Fig. 5*A*). This is the time frame when the developing protrusions of the cells found their way to other cells and began to establish connections. The success of the differentiation protocol was controlled by analysis of the typical morphological changes, *i.e.* neurite outgrowth and a decrease in the volume of the cell somata (Fig. 5, *D* and *E*) (see Refs. 11 and 23), the presence of neurofilament m, and the loss of the glia marker glial fibrillary acidic protein (Fig. 5, *B* and *C*). Unlike the levels of CRMP2 protein, the levels of the CRMP2 mRNA, analyzed by quantitative PCR, increased continuously during the 7 days (Fig. 5*F*). In case this increased amount of mRNA would lead to an increase in translation, this could indicate a higher turnover of the protein during the process of differentiation.

Together, our results demonstrate the presence of a specific Cys-504-Cys-504 thiol-disulfide switch in recombinant CRMP2 that controls and induces two distinct conformations of the CRMP2 tetramer that can also be observed *in vivo* in a model of neuronal differentiation.

DISCUSSION

Both human and zebrafish CRMP2 contain eight cysteinyl residues, and six of these are conserved between all vertebrate species: Cys-132, -133, -248, -323, -334, and -504 (see supplemental Fig. 1). Here, we demonstrated the oxidation of two adjacent Cys-504 thiols in the homo-tetrameric quaternary complex to a disulfide by treatment with hydrogen peroxide at low levels, *i.e.* 3–5-fold molar excess over CRMP2. Despite rigorous data analysis, we did not find evidence for the oxidation of any of the other seven cysteinyl thiols by treatment, to either disulfides, mixed disulfides with glutathione, sulfenic, sulfinic, or sulfonic acids. Although we cannot exclude that some of the respective peptides could not be ionized and detected by the MALDI-TOF/TOF analysis. The principal product of the reaction between a protein cysteinyl thiol and hydrogen peroxide is a protein sulfenic acid. In some cases, this sulfenic acid is rather stable at physiological conditions; often, however, this sulfenic acid reacts with a second thiol of a protein or with GSH, yielding disulfides. The intermolecular Cys-504-Cys-504 disulfide that resulted from hydrogen peroxide oxidation here most likely formed by oxidation of one Cys-504 residue to a sulfenic acid and the subsequent formation of the intermolecular disulfide. The formation of hydrogen peroxide has been implied in semaphorin signaling before (26), supporting the evidence that such a mechanism may also be relevant *in vivo*.

In this study, we provide clear evidence for a conformational change of tetrameric CRMP2 controlled by the dithiol-disulfide switch. Such conformational switches have been proposed before for CRMP2 and other CRMPs, however, dependent on the phosphorylation state of the proteins (27). At least six phos-

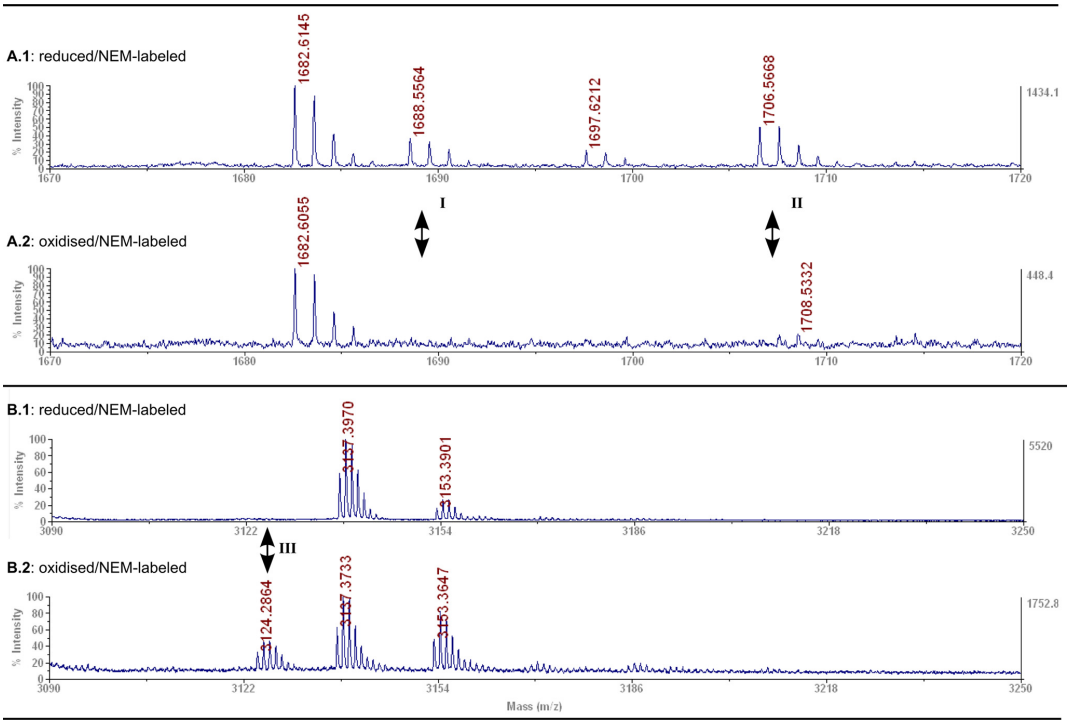

FIGURE 4. **Identification of a specific dithiol-disulfide switch in CRMP2 by MALDI-TOF mass spectrometry.** Mass spectra details of reduced (*A.1*/*B.1*) or oxidized (*A.2*/*B.2*) NEM-labeled CRMP2. *A.1*/*A.2* peptide I, GLYDGPVCEVSVTPK+NEM; peptide II, GLYDGPVCEVSVTPK + NEM/H_2O at Cys-504 (*A.1*, *I* and *II*, theoretical masses, 1688.89/1706.81; observed, 1688.56/1706.57); *B.1*/*B.2* peptide III, 2× GLYDGPVCEVSVTPK in form of disulfide-linked peptides (*B.2*, *III*, theoretical mass, 3124.52; observed, 3124.28) not present in the reduced protein (*B.1*).

phorylation sites for CRMP2 have been characterized in the literature. Following an initial priming phosphorylation of Thr-514 by cyclin-dependent kinase 5 in response to semaphorin signaling, glycogen synthase kinase 3 β was reported to phosphorylate Thr-509, Thr-518, and Ser-522 (28). The Src-type Tyr kinase FYN phosphorylates Tyr-38 (29), Rho kinase and calmodulin-dependent kinase II residue Thr-555 (30, 31). Cys-504 is located in the C terminus of CRMP2, apparently the hotspot for the regulation of the function of the protein through post-translational modifications. Five of the previously characterized phosphorylation sites as well as the putative calpain recognition and cleavage site (17) are located immediately downstream of Cys-504 (supplemental Fig. 1). Note that Cys-504 is conserved in CRMP2s from all available vertebrate genomes but not present in any of the other four CRMPs (1, 3, 4, and 5). Unfortunately, the high resolution structures of CRMP2 and all closely related proteins lack the C-terminal regulatory hot spot (32). Here, we did not record changes in the phosphorylation of Thr-514 during differentiation, however, mechanistically the redox switch and phosphorylation of C-terminal amino acid residues could act in a similar way. The formation of a disulfide in CRMP2 must bring the C-terminal regions of two CRMP2 subunits in close proximity; reduction will lead to a more open conformation of the complex, partial unfolding, and the exposure of hydrophobic regions as demonstrated by CD spectroscopy and blue native electrophoresis (Fig. 3). These newly exposed surface areas could, for instance, function in the interaction with subsequent effector molecules of cytoskeletal dynamics. The addition of negative charge to the C termini in form of phosphate moieties might also lead to a more open conformation through electrostatic repulsion. However, these charged areas might favor interactions with other effector molecules.

It was proposed that the phosphorylation state of CRMP2 may be redox regulated by formation of a mixed disulfide of CRMP2 with the N-terminal active site cysteinyl residue of Trx1, which was supposed to facilitate neuronal growth cone collapse (18). The evidence presented for this hypothesis was primarily deduced from an active site mutant of Trx1 and some faint Western blot bands. Because of the different pK_a values of the active site cysteine residues and the resulting reaction mechanism and kinetics of Trx1 and related oxidoreductases, a stable mixed disulfide complex between wild-type Trx1 and CRMP2 is highly unlikely, if not excluded (33, 34). We did not detect a complex between wild-type Grx2c (or Trx1, data not shown) and CRMP2 *in vivo* or *in vitro*, independent of the experimental conditions and the methods applied (electrophoresis, chromatography, mass spectrometry, or reduced or oxidized species; see also Fig. 2). We did observe, however, a tendency for an inverse correlation between the appearance of the

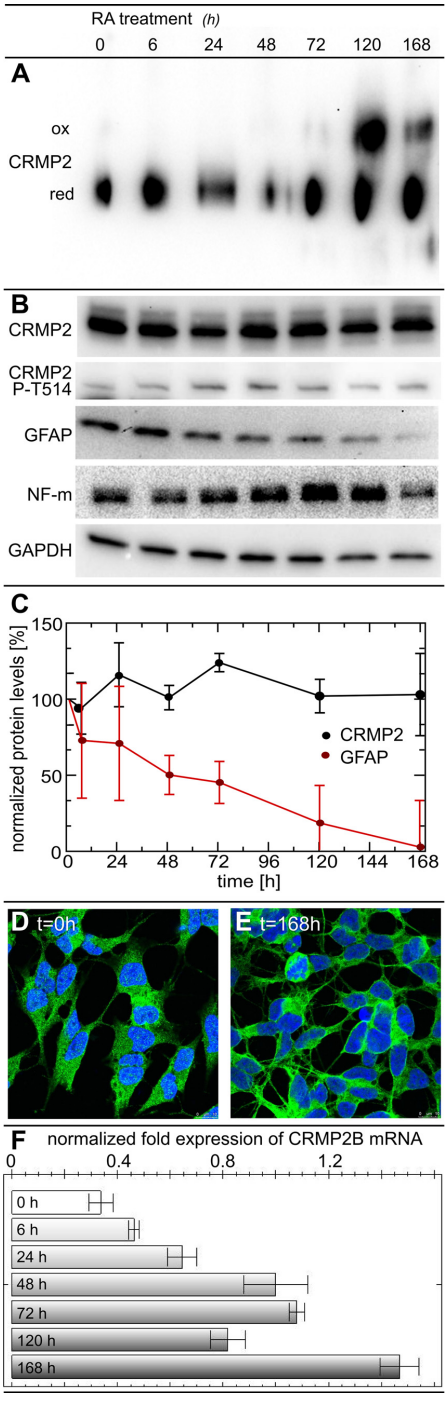

oxidized conformation and the phosphorylation state of the Thr-514 residue of CRMP2 (Fig. 5, *A* and *B*). We can thus not exclude that redox and phosphorylation signaling acting on CRMP2 are functionally connected.

We have previously demonstrated that cytosolic Grx2 is essential for the formation of neuronal networks and the survival of differentiating neurons in zebrafish. Animals with silenced expression of Grx2 lacked virtually all types of neurons investigated, *i.e.* secondary motor neurons, dopaminergic neurons, and glutamatergic excitatory interneurons. Axonal length and number of branching points were significantly reduced in embryos lacking Grx2, neuronal networks did not mature. These functions of cytosolic Grx2 were dependent on the protein disulfide reductase activity of redoxin (11). We thus propose that the redox switch identified here controls CRMP2 function during neuronal development. CRMP2 itself is essential for brain development (16); it is an effector protein of the semaphorin/plexin pathway that controls axon/neurite branching and guidance (35–37). CRMP2 was implied in several neurological disorders. Alzheimer disease is characterized by the presence of neurofibrillary tangles, senile plaques, and loss of axonal networks, and these pathologies have all been attributed to oxidative stress. In a study focused on the identification of oxidized proteins in Alzheimer disease, CRMP2 was identified as significantly more oxidized protein (38). Moreover, hyperphosphorylation of CRMP2 is an early event in Alzheimer disease progression that can be induced by amyloid β (39), and CRMP2 accumulates in the brains of mice that developed neurofibrillary tangles and amyloid β plaques (40). It has been proposed that the manipulation of the biological functions of CRMP2, *e.g.* by the epilepsy drug lacosamide (41), may offer new strategies for therapy against neurological disorders (16, 42).

Axonal outgrowth and thus neuronal connectivity is facilitated by orchestrated dynamics of the cytoskeleton, directed by proteins such as CRMP2 in response to external signals. Redox regulation mechanisms of cytoskeletal dynamics and neuronal development have been suggested previously (*e.g.* Refs. 43–45). For instance, a transcript variant (*TXNRD1*_v3) of the selenoprotein thioredoxin reductase 1 encodes an atypical N-terminal Grx domain. Expression of complete *TXNRD1*_v3 protein or this Grx domain alone induced cell membrane protrusions (46). The Grx domain of *TXNRD1*_v3 localized first in the emerging protrusion and was then accompanied into the protrusions by actin and tubulin. In a subsequent study, *TXNRD1*_v3 was

FIGURE 5. **The CRMP2 conformational switch in a cellular model of neuronal differentiation.** For differentiation into a neuron-like phenotype, SH-SY5Y cells were treated with 10 μM retinoic acid (*RA*). At 6, 24, 48, 72, 120, and 168 h, cells were detached by trypsin treatment, washed with PBS, lysed, separated by blue native gel electrophoresis, and analyzed by anti-CRMP2 Western blotting (*A*). Western blots of CRMP2, CRMP2 phospho-Thr-514, glial fibrillary acidic protein (*GFAP*), neurofilament m (*NF-m*), and the GAPDH loading control following SDS-PAGE (*B*). The presence of the neuronal marker neurofilament m confirmed the neuronal character of the cells. Quantification of CRMP2 and glial fibrillary acidic protein levels by densitometry of Western blots from three independent experiments, normalized to GAPDH levels and the untreated controls (*C*). The phenotype and localization of CRMP2 were analyzed by immunofluorescence and confocal microscopy (*D* and *E*). CRMP2B mRNA was quantified by quantitative PCR and normalized to GAPDH mRNA levels (*F*). *ox*, oxidized; *red*, reduced.

shown to induce dynamic cytoplasmic filaments itself. Actin polymerization was required for filopodia formation triggered by *TXNRD1*_v3 but not for generation of cytoplasmic filaments (47). The authors concluded that the Grx domain of *TXNRD1*_v3 is an atypical regulator of the cytoskeleton (46). Note that targeted deletion of the *TXNRD1* gene leads to severe defects in the development of the brain (48). Grx2 and the Grx domain of *TXNRD1*_v3 share a higher homology to each other than to any other Grx of the mammalian cell. It is thus not unlikely that they act on the same or connected signaling pathways. Importantly, *in vitro*, Trx1 was able to reduce the CRMP2 disulfide (Fig. 2); however, in contrast to Grx2c (11, 12), neither the (over)expression of Trx1 nor Grx1 led to changes in cell morphology or the redox state of CRMP2 in cell cultures.[3]

In this work, we identified a dithiol-disulfide switch in CRMP2, a critical regulator of cytoskeletal dynamics, connecting two Cys-504 residues of neighboring subunits in the tetrameric quaternary complex. This switch controls two distinct conformations of the tetramer, its reduction is controlled specifically by Grx2c in a dithiol reaction mechanism, it is triggered during neuronal differentiation, and it controls axonal outgrowth. The major open questions that remain to be solved in the future are as follows: first, the mechanism of CRMP2 oxidation and, second, how the conformational switch affects subsequent effector proteins of cytoskeletal dynamics.

Acknowledgments—We express our gratitude to Kai Masur and Kristian Wende (INP Greifswald) for providing access to confocal microscopy and Winfried Hinrichs and Gottfried Palm for access to CD spectroscopy.

REFERENCES

1. Holmgren, A. (1979) Glutathione-dependent synthesis of deoxyribonucleotides. Purification and characterization of glutaredoxin from *Escherichia coli*. *J. Biol. Chem.* **254,** 3664–3671
2. Gravina, S. A., and Mieyal, J. J. (1993) Thioltransferase is a specific glutathionyl mixed disulfide oxidoreductase. *Biochemistry* **32,** 3368–3376
3. Mieyal, J. J., Gallogly, M. M., Qanungo, S., Sabens, E. A., and Shelton, M. D. (2008) Molecular mechanisms and clinical implications of reversible protein *S*-glutathionylation. *Antioxid. Redox Signal.* **10,** 1941–1988
4. Lillig, C. H., Berndt, C., and Holmgren, A. (2008) Glutaredoxin systems. *Biochim. Biophys. Acta* **1780,** 1304–1317
5. Lillig, C. H., and Berndt, C. (2013) Glutaredoxins in thiol/disulfide exchange. *Antioxid. Redox Signal.* **18,** 1654–1665
6. Lundberg, M., Johansson, C., Chandra, J., Enoksson, M., Jacobsson, G., Ljung, J., Johansson, M., and Holmgren, A. (2001) Cloning and expression of a novel human glutaredoxin (Grx2) with mitochondrial and nuclear isoforms. *J. Biol. Chem.* **276,** 26269–26275
7. Gladyshev, V. N., Liu, A., Novoselov, S. V., Krysan, K., Sun, Q. A., Kryukov, V. M., Kryukov, G. V., and Lou, M. F. (2001) Identification and characterization of a new mammalian glutaredoxin (thioltransferase), Grx2. *J. Biol. Chem.* **276,** 30374–30380
8. Jurado, J., Prieto-Alamo, M. J., Madrid-Rísquez, J., and Pueyo, C. (2003) Absolute gene expression patterns of thioredoxin and glutaredoxin redox systems in mouse. *J. Biol. Chem.* **278,** 45546–45554
9. Lönn, M. E., Hudemann, C., Berndt, C., Cherkasov, V., Capani, F., Holmgren, A., and Lillig, C. H. (2008) Expression Pattern of Human Glutaredoxin 2 Isoforms: Identification and Characterization of Two Testis/Cancer Cell-Specific Isoforms. *Antioxid. Redox Signal.* **10,** 547–557
10. Hudemann, C., Lönn, M. E., Godoy, J. R., Zahedi Avval, F., Capani, F., Holmgren, A., and Lillig, C. H. (2009) Identification, Expression Pattern, and Characterization of Mouse Glutaredoxin 2 Isoforms. *Antioxid. Redox Signal.* **11,** 1–14
11. Bräutigam, L., Schütte, L. D., Godoy, J. R., Prozorovski, T., Gellert, M., Hauptmann, G., Holmgren, A., Lillig, C. H., and Berndt, C. (2011) Vertebrate-specific glutaredoxin is essential for brain development. *Proc. Natl. Acad. Sci. U.S.A.* **108,** 20532–20537
12. Schütte, L. D., Baumeister, S., Weis, B., Hudemann, C., Hanschmann, E. M., and Lillig, C. H. (2013) Identification of potential protein dithiol-disulfide substrates of mammalian Grx2. *Biochim. Biophys. Acta* **1830,** 4999–5005
13. Arimura, N., Menager, C., Fukata, Y., and Kaibuchi, K. (2004) Role of CRMP-2 in neuronal polarity. *J. Neurobiol.* **58,** 34–47
14. Vincent, P., Collette, Y., Marignier, R., Vuaillat, C., Rogemond, V., Davoust, N., Malcus, C., Cavagna, S., Gessain, A., Machuca-Gayet, I., Belin, M. F., Quach, T., and Giraudon, P. (2005) A role for the neuronal protein collapsin response mediator protein 2 in T lymphocyte polarization and migration. *J. Immunol.* **175,** 7650–7660
15. Arimura, N., Inagaki, N., Chihara, K., Ménager, C., Nakamura, N., Amano, M., Iwamatsu, A., Goshima, Y., and Kaibuchi, K. (2000) Phosphorylation of collapsin response mediator protein-2 by Rho-kinase. Evidence for two separate signaling pathways for growth cone collapse. *J. Biol. Chem.* **275,** 23973–23980
16. Charrier, E., Reibel, S., Rogemond, V., Aguera, M., Thomasset, N., and Honnorat, J. (2003) Collapsin response mediator proteins (CRMPs): involvement in nervous system development and adult neurodegenerative disorders. *Mol. Neurobiol.* **28,** 51–64
17. Bretin, S., Rogemond, V., Marin, P., Maus, M., Torrens, Y., Honnorat, J., Glowinski, J., Prémont, J., and Gauchy, C. (2006) Calpain product of WT-CRMP2 reduces the amount of surface NR2B NMDA receptor subunit. *J. Neurochem.* **98,** 1252–1265
18. Morinaka, A., Yamada, M., Itofusa, R., Funato, Y., Yoshimura, Y., Nakamura, F., Yoshimura, T., Kaibuchi, K., Goshima, Y., Hoshino, M., Kamiguchi, H., and Miki, H. (2011) Thioredoxin mediates oxidation-dependent phosphorylation of CRMP2 and growth cone collapse. *Sci. Signal.* **4,** ra26
19. Lillig, C. H., Berndt, C., Vergnolle, O., Lönn, M. E., Hudemann, C., Bill, E., and Holmgren, A. (2005) Characterization of human glutaredoxin 2 as iron-sulfur protein: A possible role as redox sensor. *Proc. Natl. Acad. Sci. U.S.A.* **102,** 8168–8173
20. Hanschmann, E. M., Lönn, M. E., Schütte, L. D., Funke, M., Godoy, J. R., Eitner, S., Hudemann, C., and Lillig, C. H. (2010) (2010) Both thioredoxin 2 and glutaredoxin 2 contribute to the reduction of the mitochondrial 2-CYS peroxiredoxin PRX3. *J. Biol. Chem.* **285,** 40699–40705
21. Johansson, C., Lillig, C. H., and Holmgren, A. (2004) Human mitochondrial glutaredoxin reduces *S*-glutathionylated proteins with high affinity accepting electrons from either glutathione or thioredoxin reductase. *J. Biol. Chem.* **279,** 7537–7543
22. Ericsson, U. B., Hallberg, B. M., Detitta, G. T., Dekker, N., and Nordlund, P. (2006) Thermofluor-based high-throughput stability optimization of proteins for structural studies. *Anal. Biochem.* **357,** 289–298
23. Påhlman, S., Ruusala, A. I., Abrahamsson, L., Mattsson, M. E., and Esscher, T. (1984) Retinoic acid-induced differentiation of cultured human neuroblastoma cells: a comparison with phorbolester-induced differentiation. *Cell Differ.* **14,** 135–144
24. Wang, L. H., and Strittmatter, S. M. (1997) Brain CRMP forms heterotetramers similar to liver dihydropyrimidinase. *J. Neurochem.* **69,** 2261–2269
25. Korecka, J. A., van Kesteren, R. E., Blaas, E., Spitzer, S. O., Kamstra, J. H., Smit, A. B., Swaab, D. F., Verhaagen, J., and Bossers, K. (2013) Phenotypic characterization of retinoic acid differentiated SH-SY5Y cells by transcriptional profiling. *PLoS One* **8,** e63862
26. Nadella, M., Bianchet, M. A., Gabelli, S. B., Barrila, J., and Amzel, L. M. (2005) Structure and activity of the axon guidance protein MICAL. *Proc. Natl. Acad. Sci. U.S.A.* **102,** 16830–16835
27. Schmidt, E. F., and Strittmatter, S. M. (2007) The CRMP family of proteins and their role in Sema3A signaling. *Adv. Exp. Med. Biol.* **600,** 1–11

[3] M. Gellert, S. Venz, J. Mitlöhner, C. Cott, E.-M. Hanschmann, and C. H. Lillig, unpublished results.

28. Uchida, Y., Ohshima, T., Sasaki, Y., Suzuki, H., Yanai, S., Yamashita, N., Nakamura, F., Takei, K., Ihara, Y., Mikoshiba, K., Kolattukudy, P., Honnorat, J., and Goshima, Y. (2005) Semaphorin3A signalling is mediated via sequential Cdk5 and GSK3β phosphorylation of CRMP2: implication of common phosphorylating mechanism underlying axon guidance and Alzheimer's disease. *Genes Cells* **10,** 165–179
29. Uchida, Y., Ohshima, T., Yamashita, N., Ogawara, M., Sasaki, Y., Nakamura, F., and Goshima, Y. (2009) Semaphorin3A signaling mediated by Fyn-dependent tyrosine phosphorylation of collapsin response mediator protein 2 at tyrosine 32. *J. Biol. Chem.* **284,** 27393–27401
30. Patrakitkomjorn, S., Kobayashi, D., Morikawa, T., Wilson, M. M., Tsubota, N., Irie, A., Ozawa, T., Aoki, M., Arimura, N., Kaibuchi, K., Saya, H., and Araki, N. (2008) Neurofibromatosis type 1 (NF1) tumor suppressor, neurofibromin, regulates the neuronal differentiation of PC12 cells via its associating protein, CRMP-2. *J. Biol. Chem.* **283,** 9399–9413
31. Hou, S. T., Jiang, S. X., Aylsworth, A., Ferguson, G., Slinn, J., Hu, H., Leung, T., Kappler, J., and Kaibuchi, K. (2009) CaMKII phosphorylates collapsin response mediator protein 2 and modulates axonal damage during glutamate excitotoxicity. *J. Neurochem.* **111,** 870–881
32. Deo, R. C., Schmidt, E. F., Elhabazi, A., Togashi, H., Burley, S. K., and Strittmatter, S. M. (2004) Structural bases for CRMP function in plexin-dependent semaphorin3A signaling. *EMBO J.* **23,** 9–22
33. Kallis, G. B., and Holmgren, A. (1980) Differential reactivity of the functional sulfhydryl groups of cysteine-32 and cysteine-35 present in the reduced form of thioredoxin from *Escherichia coli*. *J. Biol. Chem.* **255,** 10261–10265
34. Berndt, C., Lillig, C. H., and Holmgren, A. (2007) Thiol-based mechanisms of the thioredoxin and glutaredoxin systems: implications for diseases in the cardiovascular system. *Am. J. Physiol. Heart. Circ. Physiol.* **292,** H1227–H1236
35. Goshima, Y., Nakamura, F., Strittmatter, P., and Strittmatter, S. M. (1995) Collapsin-induced growth cone collapse mediated by an intracellular protein related to UNC-33. *Nature* **376,** 509–514
36. Inagaki, N., Chihara, K., Arimura, N., Ménager, C., Kawano, Y., Matsuo, N., Nishimura, T., Amano, M., and Kaibuchi, K. (2001) CRMP-2 induces axons in cultured hippocampal neurons. *Nat. Neurosci.* **4,** 781–782
37. Nishimura, T., Fukata, Y., Kato, K., Yamaguchi, T., Matsuura, Y., Kamiguchi, H., and Kaibuchi, K. (2003) CRMP-2 regulates polarized Numb-mediated endocytosis for axon growth. *Nat. Cell Biol.* **5,** 819–826
38. Sultana, R., Boyd-Kimball, D., Poon, H. F., Cai, J., Pierce, W. M., Klein, J. B., Merchant, M., Markesbery, W. R., and Butterfield, D. A. (2006) Redox proteomics identification of oxidized proteins in Alzheimer's disease hippocampus and cerebellum: an approach to understand pathological and biochemical alterations in AD. *Neurobiol. Aging* **27,** 1564–1576
39. Cole, A. R., Noble, W., van Aalten, L., Plattner, F., Meimaridou, R., Hogan, D., Taylor, M., LaFrancois, J., Gunn-Moore, F., Verkhratsky, A., Oddo, S., LaFerla, F., Giese, K. P., Dineley, K. T., Duff, K., Richardson, J. C., Yan, S. D., Hanger, D. P., Allan, S. M., and Sutherland, C. (2007) Collapsin response mediator protein-2 hyperphosphorylation is an early event in Alzheimer's disease progression. *J. Neurochem.* **103,** 1132–1144
40. Takata, K., Kitamura, Y., Nakata, Y., Matsuoka, Y., Tomimoto, H., Taniguchi, T., and Shimohama, S. (2009) Involvement of WAVE accumulation in Aβ/APP pathology-dependent tangle modification in Alzheimer's disease. *Am. J. Pathol.* **175,** 17–24
41. Beydoun, A., D'Souza, J., Hebert, D., and Doty, P. (2009) Lacosamide: pharmacology, mechanisms of action and pooled efficacy and safety data in partial-onset seizures. *Expert Rev. Neurother.* **9,** 33–42
42. Hensley, K., Venkova, K., Christov, A., Gunning, W., and Park, J. (2011) Collapsin response mediator protein-2: an emerging pathologic feature and therapeutic target for neurodisease indications. *Mol. Neurobiol.* **43,** 180–191
43. Giles, G. I. (2006) The redox regulation of thiol dependent signaling pathways in cancer. *Curr. Pharm. Des.* **12,** 4427–4443
44. Giridharan, S. S., Rohn, J. L., Naslavsky, N., and Caplan, S. (2012) Differential regulation of actin microfilaments by human MICAL proteins. *J. Cell Sci.* **125,** 614–624
45. Wang, J., Boja, E. S., Tan, W., Tekle, E., Fales, H. M., English, S., Mieyal, J. J., and Chock, P. B. (2001) Reversible glutathionylation regulates actin polymerization in A431 cells. *J. Biol. Chem.* **276,** 47763–47766
46. Dammeyer, P., Damdimopoulos, A. E., Nordman, T., Jiménez, A., Miranda-Vizuete, A., and Arnér, E. S. (2008) Induction of cell membrane protrusions by the N-terminal glutaredoxin domain of a rare splice variant of human thioredoxin reductase 1. *J. Biol. Chem.* **283,** 2814–2821
47. Damdimopoulou, P. E., Miranda-Vizuete, A., Arnér, E. S., Gustafsson, J. A., and Damdimopoulos, A. E. (2009) The human thioredoxin reductase-1 splice variant TXNRD1_v3 is an atypical inducer of cytoplasmic filaments and cell membrane filopodia. *Biochim. Biophys. Acta* **1793,** 1588–1596
48. Soerensen, J., Jakupoglu, C., Beck, H., Förster, H., Schmidt, J., Schmahl, W., Schweizer, U., Conrad, M., and Brielmeier, M. (2008) The role of thioredoxin reductases in brain development. *PLoS One* **3,** e1813

II. Article

Molecular architecture of *Streptococcus pneumoniae* surface thioredoxin-fold lipoproteins crucial for extracellular oxidative stress resistance and maintanance of virulence

Malek Saleh*, Sergio G. Bartual*, Mohammed R. Abdullah*, Inga Jensch, Tauseef M. Asmat, Lothar Petruschka, Thomas Pribyl, **Manuela Gellert**, Christopher H. Lillig, Haike Antelmann, Juan A. Hermoso, Sven Hammerschmidt

EMBO Mol. Med.

Vol 5 Issue 12 (1852-70)

Published: December 2nd, 2013

* These authors contributed equally to this work.

For supplementary information see DOI: 10.1002/emmm.201202435

EMBO Molecular Medicine
OPEN ACCESS TRANSPARENT PROCESS SOURCE DATA

Research Article
Pneumococcal surface oxidative resistance system

Molecular architecture of *Streptococcus pneumoniae* surface thioredoxin-fold lipoproteins crucial for extracellular oxidative stress resistance and maintenance of virulence

*Malek Saleh[1†], Sergio G. Bartual[2†], Mohammed R. Abdullah[1†], Inga Jensch[1], Tauseef M. Asmat[1], Lothar Petruschka[1], Thomas Pribyl[1], Manuela Gellert[3], Christopher H. Lillig[3], Haike Antelmann[4], Juan A. Hermoso[2**], Sven Hammerschmidt[1*]*

Keywords: lipoproteins; meningitis; oxidative stress; pneumococci; pneumonia

DOI 10.1002/emmm.201202435

Received December 29, 2012
Revised August 15, 2013
Accepted September 10, 2013

→See accompanying article
http://dx.doi.org/10.1002/emmm.201303482

The respiratory pathogen *Streptococcus pneumoniae* has evolved efficient mechanisms to resist oxidative stress conditions and to displace other bacteria in the nasopharynx. Here we characterize at physiological, functional and structural levels two novel surface-exposed thioredoxin-family lipoproteins, Etrx1 and Etrx2. The impact of both Etrx proteins and their redox partner methionine sulfoxide reductase *Sp*MsrAB2 on pneumococcal pathogenesis was assessed in mouse virulence studies and phagocytosis assays. The results demonstrate that loss of function of either both Etrx proteins or *Sp*MsrAB2 dramatically attenuated pneumococcal virulence in the acute mouse pneumonia model and that Etrx proteins compensate each other. The deficiency of Etrx proteins or *Sp*MsrAB2 further enhanced bacterial uptake by macrophages, and accelerated pneumococcal killing by H_2O_2 or free methionine sulfoxides (MetSO). Moreover, the absence of both Etrx redox pathways provokes an accumulation of oxidized *Sp*MsrAB2 *in vivo*. Taken together our results reveal insights into the role of two extracellular electron pathways required for reduction of *Sp*MsrAB2 and surface-exposed MetSO. Identification of this system and its target proteins paves the way for the design of novel antimicrobials.

INTRODUCTION

Streptococcus pneumoniae (pneumococci) are Gram-positive human commensals but also pathogens with high virulence potential. Pneumococci are dreaded as the etiologic agent of respiratory and life-threatening invasive diseases, such as pneumonia, meningitis and septicemia. The disease burden is high in developed and developing countries and, *e.g.* one million children under the age of 5 years are killed every year (Gamez & Hammerschmidt, 2012; Kadioglu et al, 2008). Its location in the human respiratory tract forces the bacterial cell to develop mechanisms to resist the host defenses like the oxidative burst produced by the innate immune system (West et al, 2011).

Reactive oxygen species (ROS) are also produced during one-electron transfer reactions to O_2 that include hydrogen peroxide

(1) Department Genetics of Microorganisms, Interfaculty Institute for Genetics and Functional Genomics, Ernst Moritz Arndt University of Greifswald, Greifswald, Germany
(2) Departamento de Cristalografía y Biología Estructural, Instituto de Química-Física "Rocasolano", CSIC, Madrid, Spain
(3) Institute for Medical Biochemistry and Molecular Biology, University Medicine, Ernst Moritz Arndt University of Greifswald, Greifswald, Germany
(4) Institute for Microbiology, Ernst Moritz Arndt University of Greifswald, Greifswald, Germany
***Corresponding author:** Tel: +49 3834 864161; Fax: +49 3834 86 4172; E-mail: sven.hammerschmidt@uni-greifswald.de
****Corresponding author:**Tel: +34 917459538; Fax: +34 915642431; E-mail: xjuan@iqfr.csic.es
†These authors contributed equally to this work.

(H_2O_2), hydroxyl radical ($HO^•$) and superoxide anions (O_2^-). ROS are able to react with all cellular macromolecules, such as proteins, lipids, carbohydrates and nucleotides (Gutteridge & Halliwell, 2000; Johansson et al, 2004). Cysteine and methionine (Met) residues are the most susceptible targets for oxidation by ROS. The oxidation of Met residues in proteins generates methionine sulfoxides (MetSO) that can induce conformational changes leading either to activation or inactivation of proteins (Zeller & Klug, 2006). In eukaryotic cells, Met oxidation has been shown to inactivate calmodulin and activate calmodulin kinase (Bigelow & Squier, 2011; Erickson et al, 2008) or in *Escherichia coli* the transcription factor HypT is activated specifically by MetSO formation (Drazic et al, 2013). This reaction is reversible and MetSO modifications can be reduced to Met by methionine sulfoxide reductases (Msr). Depending on the stereospecific orientation two distinct classes of Msr enzymes have been described. MsrA is specific for the reduction of the S-form and MsrB reduces the R-form of MetSO (Brot et al, 1981; Grimaud et al, 2001; Sharov & Schoneich, 2000; Weissbach et al, 2005). MsrA and MsrB occur typically as separate enzymes, but in some bacteria like *S. pneumoniae*, *Neisseria gonorrhoeae* and *Haemophilus influenzae* they are translationally fused as MsrAB (Delaye et al, 2007; Kim et al, 2009; Tarrago & Gladyshev, 2012; Wizemann et al, 1996). The reduction of MetSO by Msr involves the formation of an intramolecular disulphide in MsrA and MsrB, which is reduced by thioredoxins (Trx) that transfer electrons from their CXXC active site to the MsrA and MsrB disulphides (Hoshi & Heinemann, 2001; Lowther et al, 2000; Ranaivoson et al, 2009). The reduction of MsrA and MsrB by Trx leads to oxidation of Trx, which is reduced by the thioredoxin reductase (TrxB) on expense of NADPH. The Trx/TrxB system together with the glutaredoxin/glutathione (GSH)/GSH reductase system maintain the cellular reducing environment (Fernandes & Holmgren, 2004; Paget & Buttner, 2003). Trx proteins also function as electron donors to regenerate peroxiredoxins and other antioxidant enzymes in their detoxification cycle (Collet & Messens, 2010; Das & Das, 2000; Hanschmann et al, 2013; Kang et al, 1998; Zander et al, 1998).

Pneumococci are able to produce millimolar H_2O_2 by the pyruvate oxidase SpxB as a chemical weapon against bacterial competitors and hence this pathogen can tolerate high H_2O_2 concentrations (Pericone et al, 2002, 2003). By H_2O_2 production *S. pneumoniae* can displace *H. influenzae*, *N. meningitidis* and *Staphylococcus aureus*, which also involves the induction of resident prophages in *S. aureus* (Margolis, 2009; Pericone et al, 2000; Selva et al, 2009).

Despite their peroxide resistance, pneumococci lack the major peroxide scavenging enzyme catalase. However, other ROS scavenging enzymes, like the superoxide dismutase (SodA) (Yesilkaya et al, 2000), NADH oxidase (Auzat et al, 1999) and alkyl hydroperoxidase (Paterson et al, 2006) limit ROS mediated killing in the cytoplasm. In addition, the thiol peroxidase (TpxD) functions in H_2O_2 detoxification and survival under aerobic conditions and is responsible for enhanced survival of pneumococci in mice virulence assays after intranasal infections (Hajaj et al, 2012; Hiller et al, 2007; Yesilkaya et al, 2013). Recently, the roles of the cellular redox buffer GSH, its GshT importer and the glutathione reductase (Gor) in protection against oxidative stress and during pneumococcal colonization have been demonstrated (Potter et al, 2012). Such cytoplasmic antioxidant and protein reducing systems are well studied in many bacteria (Kim et al, 2009; Wizemann et al, 1996). In contrast, the extracellular compartment of Gram-positive bacteria and the periplasm of Gram-negatives are considered as an oxidizing environment where disulphide bond oxidases and isomerases, such as the DsbA/DsbB and DsbC/DsbD pathways catalyse oxidative protein folding (Cho & Collet, 2013; Denoncin & Collet, 2013). However, also periplasmic reducing redox pathways have been described in few pathogenic Gram-negative bacteria, such as in *N. gonorrhoeae* and *N. meningitidis* (Brot et al, 2006; Ranaivoson et al, 2006; Wu et al, 2005). In these periplasmic reducing redox pathways of Gram-negative bacteria, the membrane-bound DsbD protein provides the electrons for reduction of sulfenic acids, for cytochrome maturation and to reduce periplasmic antioxidant enzymes, such as peroxidases and Msr (Cho & Collet, 2013; Denoncin & Collet, 2013). In pneumococci, the extracellular thioredoxin-like protein TlpA was suggested to be involved in the extracellular oxidative stress resistance, but DsbD-like reducing redox pathways that are associated with TlpA were not explored (Andisi et al, 2012). In addition, the molecular interplay of the surface-exposed TlpA (renamed Etrx1) with its extracellular paralogue Etrx2 on oxidative stress resistance and virulence are unknown. This study discovers the unique molecular architecture of two surface-exposed thioredoxin-systems, Etrx1 and Etrx2 and their redox partners CcdA1, CcdA2 and *Sp*MsrAB2 as important pneumococcal extracellular reducing systems essential for pneumococcal pathogenesis and oxidative stress resistance. We further provide evidence that both CcdA-Etrx pathways function in *Sp*MsrAB2 reduction *in vivo*. Thus, Etrx1, Etrx2 and *Sp*MsrAB2 are attractive targets for the design of novel anti-infectives to block the initial states of pneumococcal infection.

RESULTS

Identification and genetic organization of the *etrx1* and *etrx2* operons in pneumococci

The bioinformatic analysis of pneumococcal genomes identified two genes encoding surface-exposed thioredoxin-like lipoproteins, renamed here Etrx1 and Etrx2. Production of the Etrx proteins in *S. pneumoniae* D39 and other strains was demonstrated by immunoblot analysis (Fig 1). Etrx1 consists of 188 amino acids (20.8 kDa) and shows 39.4% sequence identity with Etrx2 (Supporting Information Fig S1) that consists of 185 amino acids (20.7 kDa). The two potential redox partners encoded by the conserved pneumococcal three-gene *etrx1* operon are the methionine sulfoxide reductase AB2 (*Sp*MsrAB2) and cytochrome C-type biogenesis protein, renamed here CcdA1 (Fig 1 and Supporting Information Figs S2–S5). *Sp*MsrAB2 shows 77% of sequence homology with the intracellular pneumococcal *Sp*MsrAB1 (Kim et al, 2009; Supporting Information Fig S6). The *etrx2* gene is located together with a second *ccdA*-like gene (renamed *ccdA2*) in a bicistronic operon, but without a second

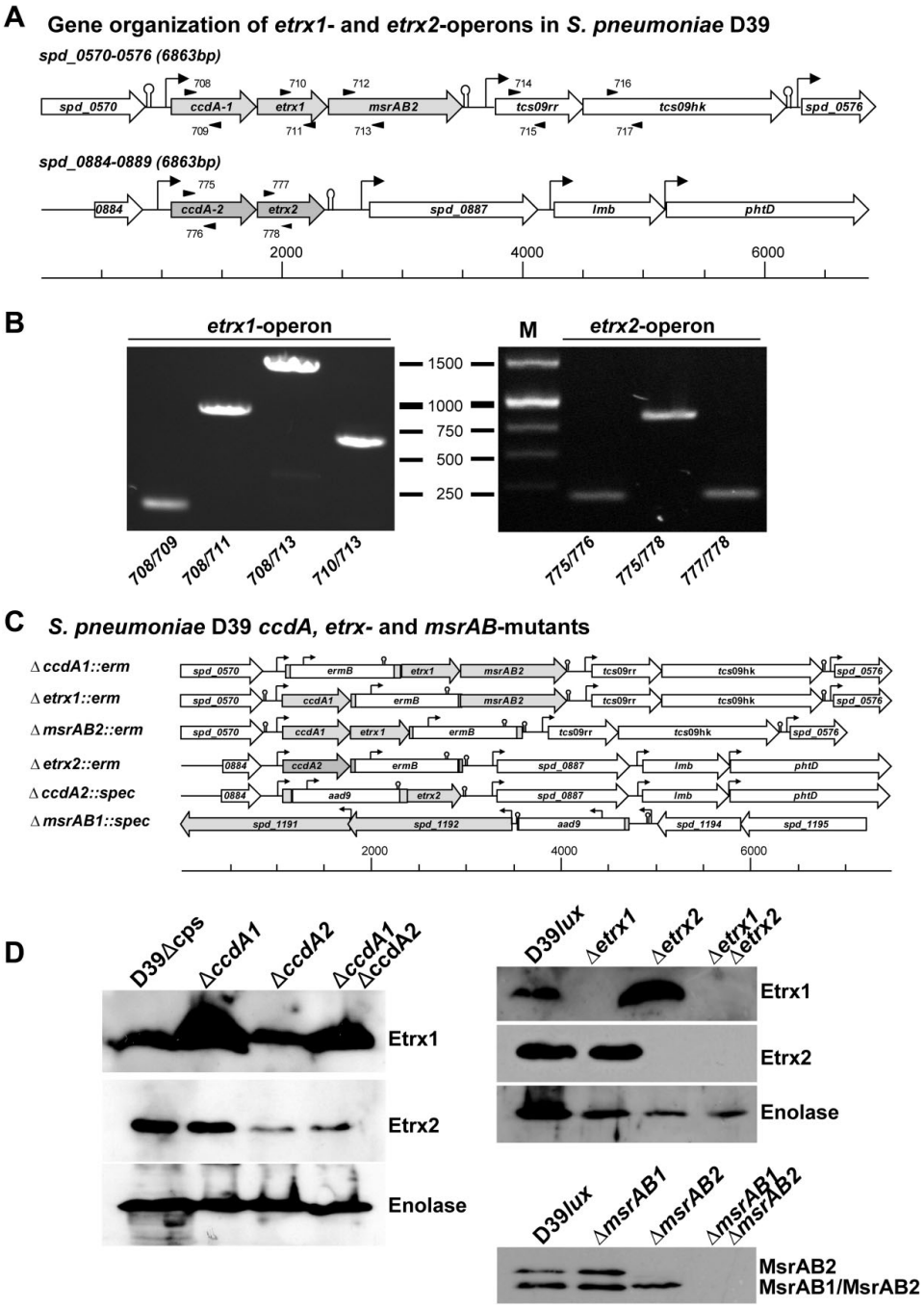

Figure 1.

msrAB-like gene (Fig 1A and B and Supporting Information Figs S7 and S8). CcdA1 and CcdA2 share 58.8% sequence identity (Supporting Information Fig S9) and possess 18 and 21% sequence identity, respectively, with the transmembrane domain of the *Neisseria* periplasmic DsbD protein (Krupp et al, 2001; Supporting Information Fig S10).

Etrx1, Etrx2 and *Sp*MsrAB2 are displayed on the pneumococcal surface and are essential for resistance against oxidative stress

Both Etrx proteins possess a typical lipoprotein-specific signal peptide containing a lipobox suggesting covalent binding of the putative lipoproteins to the outer leaflet of the phospholipid bilayer. The anchoring of lipoproteins is catalysed by a diacylglyceryl transferase (Lgt), which adds a diacylglyceryl residue to the thiol group of the conserved cysteine in the lipobox, while the signal peptide is cleaved after translocation and lipid-modification by the lipoprotein-specific signal peptidase Lsp. The lipid-modified cysteine residue remains at the mature lipoprotein as the new N-terminus (Kovacs-Simon et al, 2011). *Sp*MsrAB2 contains one transmembrane segment and is probably anchored via this segment to the pneumococcal membrane. To analyse the surface localization of the putative lipoproteins Etrx1 and Etrx2 and of the membrane anchored protein *Sp*MsrAB2, isogenic mutants D39Δ*etrx1*, D39Δ*etrx2* and D39Δ*msrAB2* were constructed by allelic replacement and verified by immunoblot analysis (Fig 1C and D). Flow cytometric analysis of wild-type and mutants demonstrated that Etrx1, Etrx2, and also *Sp*MsrAB2 are displayed on the pneumococcal surface of wild-type bacteria, while no surface association of Etrx1, Etrx2 and *Sp*MsrAB2 was found in the Δ*etrx1*, Δ*etrx2* and Δ*msrAB2* mutants, respectively (Fig 2A). Proteolytic treatment of pneumococci with trypsin and pronase E, respectively, followed by immunoblot analysis confirmed these results (Supporting Information Fig S11). Immunoblot analysis was further conducted for the cytoplasmic and surface-displayed protein fractions of the wild-type and an *lgt*-mutant that is unable to anchor lipoproteins in the membrane (Voss et al, 2013). This subcellular analysis indicated that Etrx1 and Etrx2 are indeed lipoproteins and surface-exposed. They are released into the medium fraction of the *lgt*-mutant because of their inefficient anchoring to the membrane (Fig 2B). *Sp*MsrAB2 is also displayed on the cell surface but has no lipid-anchor characteristic for lipoproteins and thus, is retained in the *lgt*-mutant membrane fraction (Fig 2B). However, we noticed that the *Sp*MsrAB2 antibodies cross-reacted with the intracellular MsrAB1 that was detected in the cytoplasm of pneumococci (Figs 1D and 2B). Interestingly, the amount of *Sp*MsrAB2 was enhanced in the *ccdA1*- and *etrx1*-mutants, which was not caused by the strategy of the mutant construction (Fig 1C and Supporting Information Fig S12).

To test the effect of Etrx lipoproteins and *Sp*MsrAB2 on resistance against oxidative stress, D39 and its isogenic *etrx*-mutants were exposed for 30 min to 10, 15 and 20 mM H_2O_2 or for 90 min to 0.25, 0.5 and 0.75 mM paraquat (Fig 2C and D). The exposure to 10–20 mM H_2O_2 reduced the survival of the wild-type to about 50%. However, the *etrx1*/*etrx2* double mutant was more affected and showed only 20–30% survival after exposure to 10 mM H_2O_2, and less than 2% survival in the presence of 20 mM H_2O_2. The survival of the *etrx1* or *etrx2* single mutants was also decreased by H_2O_2, but to a lower degree as determined for the double mutant (Fig 2C). Similar to the *etrx*-mutants, the survival of the *msrAB2*-mutant was affected by H_2O_2. Remarkably, the *msrAB1*-mutant was much more sensitive to H_2O_2 compared to the *msrAB2* single or *etrx* double mutants (Fig 2C). This peroxide sensitive phenotype of the *msrAB2*-mutant is in agreement with a previous study (Andisi et al, 2012). The superoxide-generating compound paraquat showed a weaker effect on the survival of the *etrx* single mutants (Fig 2D). Surprisingly, the *etrx* double and *msrAB2* mutants were resistant to 0.25–0.5 mM paraquat, but the reasons are not known. The most dramatic effect on survival was determined for the *msrAB1*-mutant suggesting that *Sp*MsrAB1 is more important for paraquat resistance than *Sp*MsrAB2. These results suggest that both Etrx1 and Etrx2 can function as redox partners for *Sp*MsrAB2 since the inactivation of both Etrx proteins or *Sp*MsrAB2 renders pneumococci, to varying degrees, sensitive to extracellular peroxide stress.

Crystal structures of Etrx1 and Etrx2

The crystal structures of oxidized Etrx1 and Etrx2 have been solved in this study using the untagged-recombinant lipoproteins (Supporting Information Fig S13; details of the expression cloning and protein purification are described in the Supporting Information). Crystallographic data collection and model statistics are summarized in Table 1. The Etrx1 model comprises amino acid residues from Ala53 to Leu187. Etrx1

Figure 1. Molecular organization of the *etrx* operons in *Streptococcus pneumoniae* and schematic molecular model of isogenic *etrx*-mutants. Source data is available for this figure in the Supporting Information.

A. Genetic organization of operons encoding the *etrx1* and *etrx2* genes in *S. pneumoniae* D39. Putative promoters (arrows) were predicted by the Neural Network Promoter Prediction program (http://www.fruitfly.org/seq_tools/promoter.html) and potential rho-independent termination sequences were extracted from the TransTermHP Terminator Prediction list of *S. pneumoniae* D39 (http://transterm.cbcb.umd.edu/tt/Streptococcus_pneumoniae_D39.tt). Black arrowheads indicate primers used for RT-PCR analysis.

B. Transcript length analysis of the putative *etrx1* and *etrx2* operons by RT-PCR. PCR-fragments, generated from cDNA of strain *S. pneumoniae* D39 using the indicated primer combinations, are shown.

C. Schematic models of constructed mutants in the *etrx1*-, e*trx2*-operon and the *msrAB1* gene. Shown are the genetic organization of the operons and insertion sites of the *ermB*- or *aad9*-gene cassette in *ccdA*, *etrx* or *msrAB* genes.

D. Immunoblot analysis of Etrx and MsrAB production in wild-type and mutant pneumococci. Left panel and upper right panel: production of Etrx1 and Etrx2 in *S. pneumoniae* D39 and its isogenic *ccdA1*-, *ccdA2*-, *etrx1*- and *etrx2*-mutants using Etrx specific polyclonal antibodies. Enolase was used as a control and detected with anti-enolase antibodies (Hermans et al, 2006). Lower right panel: production of MsrAB2 in pneumococcal *msrAB1*- and *msrAB2*-mutants using MsrAB2 specific polyclonal antibodies recognizing also the intracellular MsrAB1.

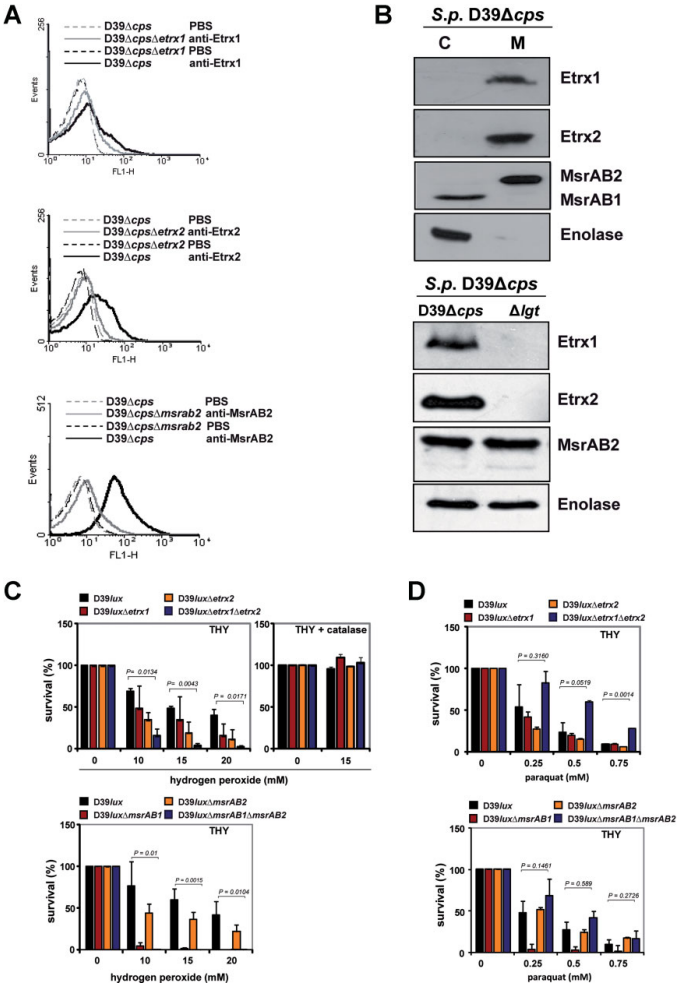

Figure 2. Etrx proteins are displayed on the pneumococcal surface and essential for oxidative stress resistance. Source data is available for this figure in the Supporting Information.

A. The surface localization of Etrx1, Etrx2 and MsrAB2 was analysed by flow cytometry. Wild-type pneumococci and isogenic mutants were incubated with anti-Etrx antibodies or PBS followed by detection using a goat anti-mouse IgG coupled Alexa-Fluor-488. The increase of fluorescence intensity (FL1-H) in the histograms indicates the presence of the Etrx and MsrAB2 proteins on the surface of non-encapsulated D39 bacteria, while the mutants and control treated pneumococci do not show an increase in fluorescence intensity.

B. Immunoblot analysis showing the surface localization of Etrx proteins and MsrAB2. Upper panel: pneumococci were fractionated and cytoplasmic (C) and cell membrane (M) fractions were separated by SDS–PAGE. Anti-Etrx or anti-MsrAB polyclonal antibodies were used to detect the proteins. Enolase was used as loading control and detected with anti-enolase antibodies (Hermans et al, 2006). Lower panel: Etrx1 and Etrx2 are lipoproteins as indicated by the absence of the protein in the isogenic *lgt*-mutant of D39Δ*cps* (Δ*lgt*) (Kovacs-Simon et al, 2011; Voss et al, 2013), while *Sp*MsrAB2 is anchored in the membrane via one transmembrane domain (see also Fig 8 and Supporting Information S6).

C,D. Oxidative stress response. Encapsulated bioluminescent D39 and isogenic pneumococcal *etrx*-mutants were treated for 30 min with various concentrations of H_2O_2 (C) or 90 min with paraquat (D). Survival was determined by plating and determination of the CFU. Data are represented as mean ± SEM of three independent experiments.

presents a globular structure (38 × 28 × 29 Å) displaying a thioredoxin-like fold that contains seven β-strands and five α-helices (Fig 3A). Besides the canonical Trx fold, Etrx1 has two insertions (Supporting Information Fig S14). The first insertion (residues 53–72) results in β1, β2 and α1 elements, and the second insertion (residues 112–144) gives rise to an additional β-strand (β5) and α-helix (α3). The loop connecting β3 with α2 contains the CXXC motif (^{84}CSIC^{87}) defining the nucleophilic active site Cys84 and the resolving Cys87 (Fig 3D). These cysteine residues form a disulphide bridge reflecting the oxidized state of the protein. The structural data clearly show that only the active site Cys84 is solvent-exposed and accessible for electron transfer reactions. At the beginning of the second insertion and near the active site there is an additional loop connecting β4 with α3 (residues 112–120) that is not present in the closely related family of cytochrome maturation proteins. A search for proteins structurally related to Etrx1 performed with DALI server (Holm & Rosenstrom, 2010) identified the N-terminal domain of PilB protein (NterPilB) from *N. gonorrhoeae* (PDB code 2H30, *Z* score of 21.1 and rmsd of 1.5 Å for 133 Cα atoms), and *N. meningitidis* (PDB code 2FY6, *Z* score of 21.1 and rmsd of 2.1 Å for 136 Cα atoms) as the most closely related 3D structures. PilB is secreted to the periplasm and involved in the pathogen survival strategies against the oxidative burst as encountered in the host (Quinternet et al, 2008).

The three-dimensional structure of Etrx2 in complex with Cyclofos-3™ comprises the sequence from Ile43 to Asn185. Four molecules were found in the asymmetric unit presenting a similar structure (rmsd value of 0.184 Å for all Cα atoms) (Fig 3B). Etrx2 presents also a modified thioredoxin-like fold that

Table 1. Data collection and refinement statistics

Data collection	Etrx1	Etrx2:Cyclofos 3™	Etrx2:HED
Space group	$P4_32_12$	$P2_12_12_1$	$P1$
a, b, c (Å)	62.85, 62.85, 89.60	61.46, 116.31, 116,42	32.10, 36.08, 58.64
α, β, γ (°)	90, 90, 90	90, 90, 90	101.13, 100.26, 101.59
T (K)	100	100	100
X-ray source	Synchrotron	Synchrotron	Synchrotron
Wavelength (Å)	1.0053	0.93340	1.00000
Resolution (Å)	29.87–1.48 (1.56–1.48)	32.81–1.77 (1.86–1.77)	23.89–1.22 (1.24–1.22)
Total no. reflections	810807 (118971)	467968 (66226)	243076 (69159)
No. unique reflections	30641(4393)	82391 (11813)	67595 (3219)
Redundancy	26.5 (27.1)	5.7 (5.6)	3.2 (3.2)
Completeness (%)	99.9 (100)	99.9 (99.4)	92.1 (89.0)
Average $I/\sigma(I)$	24.2 (7.1)	37.1 (4.2)	13.3 (5.5)
R_{merge}	0.088 (0.51)	0.041 (0.48)	0.043 (0.16)
Refinement statistics			
Resolution (Å)	28.11 (1.48)	32.81 (1.77)	23.87 (1.22)
R_{work}/R_{free}	0.18/0.20	0.16/0.19	0.15/0.18
Non-hydrogen atoms	1435	5649	2957
Protein	1173	4990	2531
Ligands	39	236	23
Solvent	223	423	403
B-factor values (Å)^2			
Protein	17.80	18.71	16.88
Ligands	33.48	64.53	44.43
Solvent	31.39	34.14	28.43
Rmsd bond length (Å)	0.058	0.012	0.009
Rmsd bond angles (°)	1.373	1.302	1.256
PDB code	4HQS	2YP6	4HQZ

is highly reminiscent of Etrx1 (rmsd value of 1.5 Å for 130 Cα atoms), where the classical thioredoxin-like motif of Etrx2 is embellished by a central αβ insertion and an N-terminal β-hairpin (Fig 3C). The CXXC motif (^{81}CGPC^{84}) defines the active site (Fig 3D). The main differences between Etrx1 and Etrx2 structures are the presence of eight extra residues forming a coil at the C-terminus of Etrx2, the conformation of β4–α3 loop, the disposition of α3 helix and the more extended conformation of the β7 strand in Etrx2 (Fig 3C and D). ResA, a thiol-disulfide oxidoreductase involved in cytochrome c biosynthesis in *Bacillus subtilis* and accepting electrons from CcdA, is the closest reported homologue of Etrx2 (rmsd of 1.5 Å for 132 Cα atoms and Z score of 20.7). The Cyclofos-3™ is located in close proximity to the Etrx2 active site. The ligand, found in the four monomers of the asymmetric unit, is stabilized in a pocket (Fig 4A) formed by the β4–α3 loop, the α4 helix, the α4–β3 loop and the CXXC region (Fig 3B). This pocket presents a strong hydrophobic character (Ala78, Trp80, Ala109, Pro110, Ile112, Ala141, Phe144, Ile149, Ile 122) *versus* the more polar character of the equivalent region in Etrx1 (Fig 4A–C). Cyclofos-3™ is stabilized by an H-bond with Gln113, by cation–π interaction of the polar face of the detergent with Trp80 and by pi–pi stacking interaction between phenyl ring of the detergent and Phe144 (Fig 4C). Attempts to obtain the reduced form of Etrx2 by co-crystallization with β-mercaptoethanol resulted in a new oxidized structure in which Etrx2 forms a complex with a 2-hydroxyethyl disulfide (HED) molecule (Fig 4D). A different conformation of the β4–α3 loop was observed coupled with the presence of the HED molecule at the hydrophobic cavity.

Both Etrx proteins share a conserved *cis*-proline residue (Pro156 in Etrx1 and Pro153 in Etrx2), placed in front of the catalytic cysteine residue, which is conserved in all thioredoxin-like proteins. As already mentioned above, the hydrophobic binding site, which is observed for Etrx2 but not for Etrx1, is of special interest. This hydrophobic binding site has not been observed in any extra-cytoplasmic thiol-disulfide oxidoreductases (TDORs) reported so far. Remarkably, both pockets differ in their amino acid composition and also in their conformation. Etrx2 presents a deep groove, while the Etrx1 site is filled by Tyr155 and covered by the α4–β3 loop. The electrostatic potential on the molecular surface is also quite different in both proteins. The Etrx2 binding site presents a hydrophobic character while Etrx1 presents a highly basic character in this region (Fig 4A). These differences point to a differential specificity of each Etrx protein for its redox partner.

Functional analysis of the extracellular thioredoxin proteins Etrx1 and Etrx2 of *S. pneumoniae*

To decipher the function of Etrx1 and Etrx2 as thioredoxin proteins reducing the potential redox partner protein *Sp*MsrAB2,

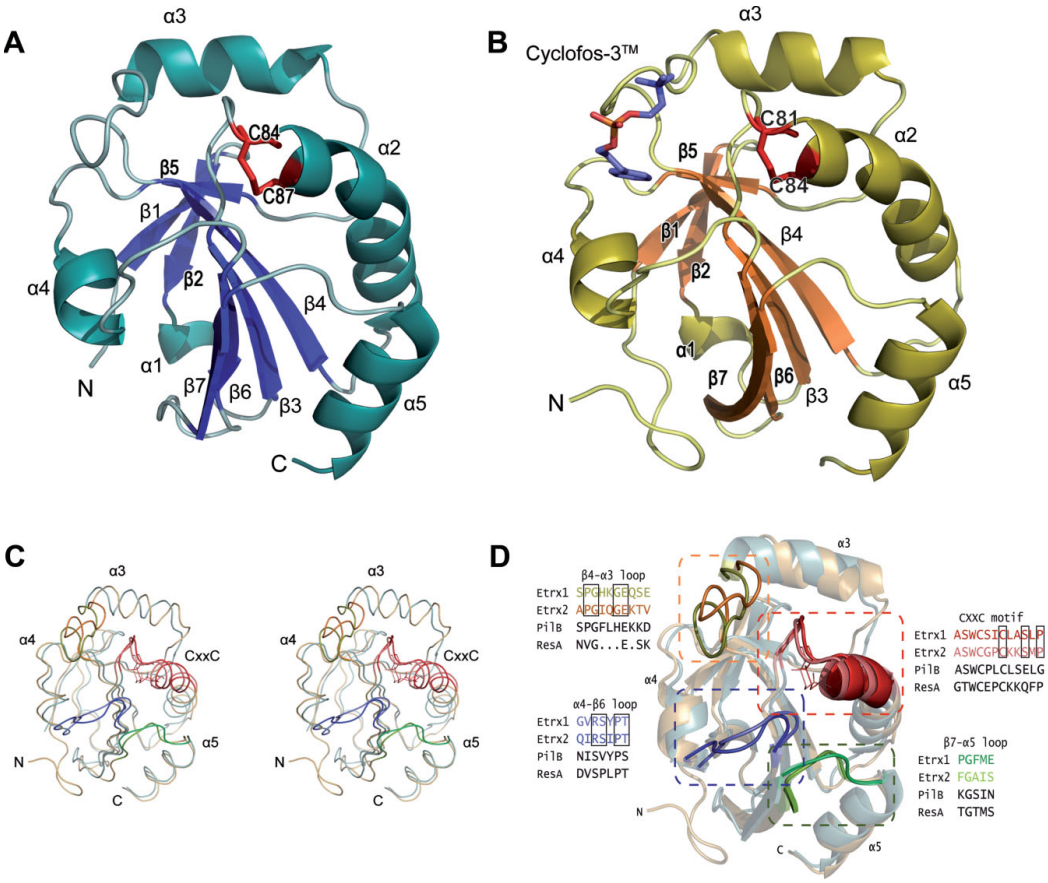

Figure 3. Three-dimensional structures of pneumococcal surface-exposed thioredoxins.

A. Overall Etrx1 structure showing β-strands as blue arrows and α-helices as light blue helices. Catalytic Cys84 and Cys87 residues are labelled in red.

B. Overall Etrx2 structure representation showing β-strands as orange arrows and α-helices in green. Cyclofos-3 is shown as sticks. Catalytic Cys81 and Cys84 residues are labelled in red.

C. Stereo view of the superimposition of Etrx1 (cyan) and Etrx2 (light brown). Loops around the active site are highlighted: the CXXC region in red, the β4–α3 loop in yellow (Etrx1) and orange (Etrx2), the α4–β6 loop in blue and the β7–α5 in green.

D. Structural comparison between Etrx1 and Etrx2. Loops around the active site are highlighted: the CXXC region in red, the β4–α3 loop in yellow (Etrx1) and orange (Etrx2), the α4–β6 loop in blue and the β7–α5 in green. Sequence alignment of Etrx1, Etrx2 and equivalent regions in NterPilB and ResA loop regions are shown for comparison. Composition and colours were chosen according to Quinternet et al (2009).

the redox states and potentials of purified Etrx proteins and *Sp*MsrAB2 subunits (MsrA2 and MsrB2; Supporting Information Fig S13) were determined. Different ratios of GSH and glutathione disulfide (GSSG) were used to determine the redox potentials. The reduced thiols of Etrx1, Etrx2 MsrA2 and MsrB2 were alkylated with AMS in an anaerobic nitrogen environment, causing a mass shift after separation by SDS–PAGE. The redox potentials were calculated from densitometric analysis and the results revealed redox potentials of -191 ± 6 mV for Etrx1, -282 ± 16.5 mV for Etrx2, -132.8 ± 5.9 mV for MsrA2 and -120.9 ± 0.6 mV for MsrB2 (Fig 5A). The apparent redox potential of purified MsrAB2 has also been analysed and was determined between the redox potential of the individual MsrA2 and MsrB2 domains, confirming the previous results. Thus, thermodynamically, the transfer of electrons from both Etrx proteins to the Msr subunits of *Sp*MsrAB2 would be possible. In order to elucidate whether both Etrx proteins can transfer electrons to *Sp*MsrAB2 kinetically, the NADPH-dependent methionine sulfoxide reductase activity of rMsrA2 and rMsrB2, respectively, was measured in kinetic experiments with Etrx1 or

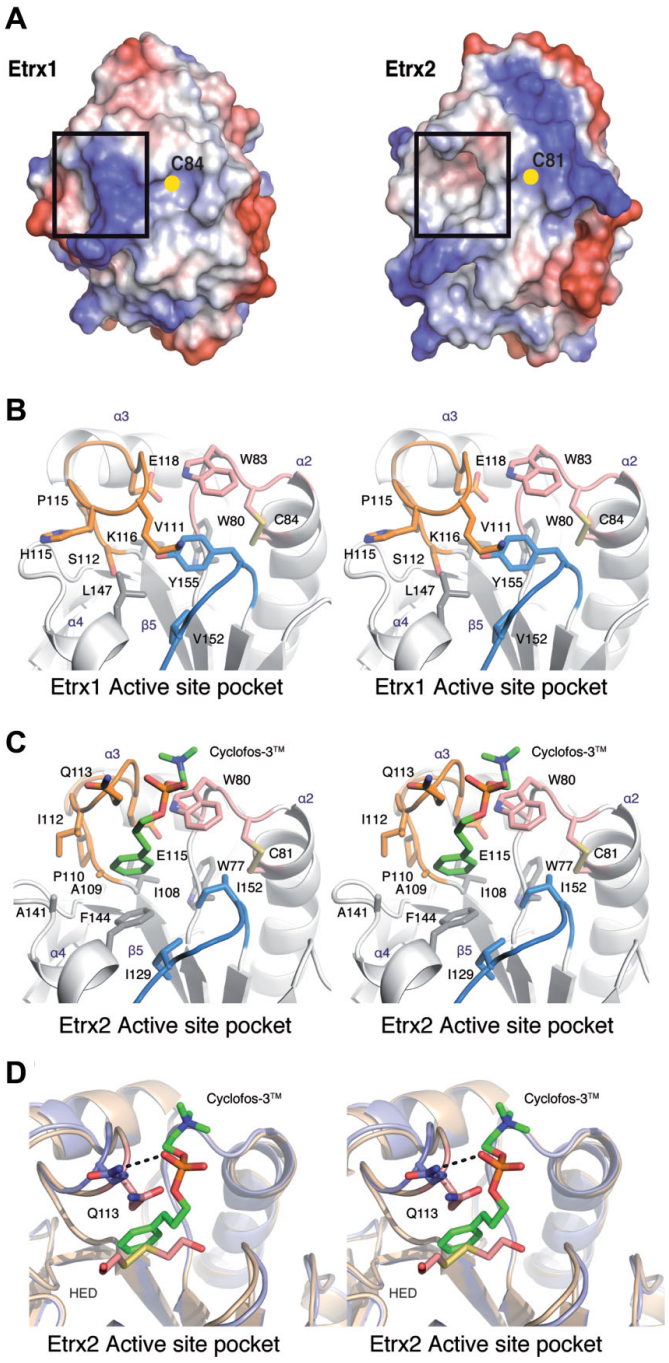

Figure 4. Structural differences between Etrx1 and Etrx2 active sites.

A. Electrostatic potential on the Etrx1 and Etrx2 molecular surface. The exposed active sites are marked with a black box. Catalytic cysteines are labelled. Acidic regions are coloured in red and basic regions in blue.

B. Stereo view of Etrx1 active site. Colour code as in Fig 3C.

C. Stereo view of Etrx2 active site. Relevant residues and Cyclofos-3 ligand are drawn as capped sticks. Carbon atoms of the ligand are shown in green, while those in the protein are colour coded as in Fig 3C. Hydrogen bonds are shown as dashed lines.

D. Stereo view of the Etrx2 catalytic core in complex with ligands. Shown is the superimposition of the reduced (light blue) and oxidized (light brown) forms. Relevant residues are labelled and shown as capped sticks. Polar interactions are shown as dashed lines.

Etrx2 as electron donor. Calculation of the specific activities indicated that Etrx1 efficiently regenerates oxidized MsrA2 but not MsrB2. In contrast, Etrx2 can reduce MsrB2 but has a 3.6-fold lower activity for the reduction of MsrA2 compared to Etrx1 (Fig 5B and Table 2).

The redox state of *Sp*MsrAB2 was analysed *in vivo* for the *ccdA* single mutants as well as the *ccdA1/2* and *etrx1/2* double mutants using diagonal non-reducing/reducing SDS–PAGE assays followed by immunoblot analysis with anti-*Sp*MsrAB2 and anti-pneumococcal antisera (Fig 5C). This diagonal assay distinguishes intramolecular and intermolecular disulphides in proteins (Leichert & Jakob, 2006). Bacterial extracts of non-encapsulated pneumococci were harvested under non-stress control conditions and proteins with reduced thiol-groups were irreversibly alkylated with NEM (*N*-ethylmaleimide), while disulphide bonds within the same protein and between different proteins are maintained. In this diagonal assay pneumococcal protein extracts were separated in the first dimension by non-reducing SDS–PAGE, the lane was cut and separated horizontally by a second reducing SDS-PAGE. Proteins with no disulphides run along the diagonal, while intramolecular disulphides migrate slightly above the diagonal. The diagonal immunoblot analysis revealed several *Sp*MsrAB2 isoforms in the reduced form that were detected along the diagonal with

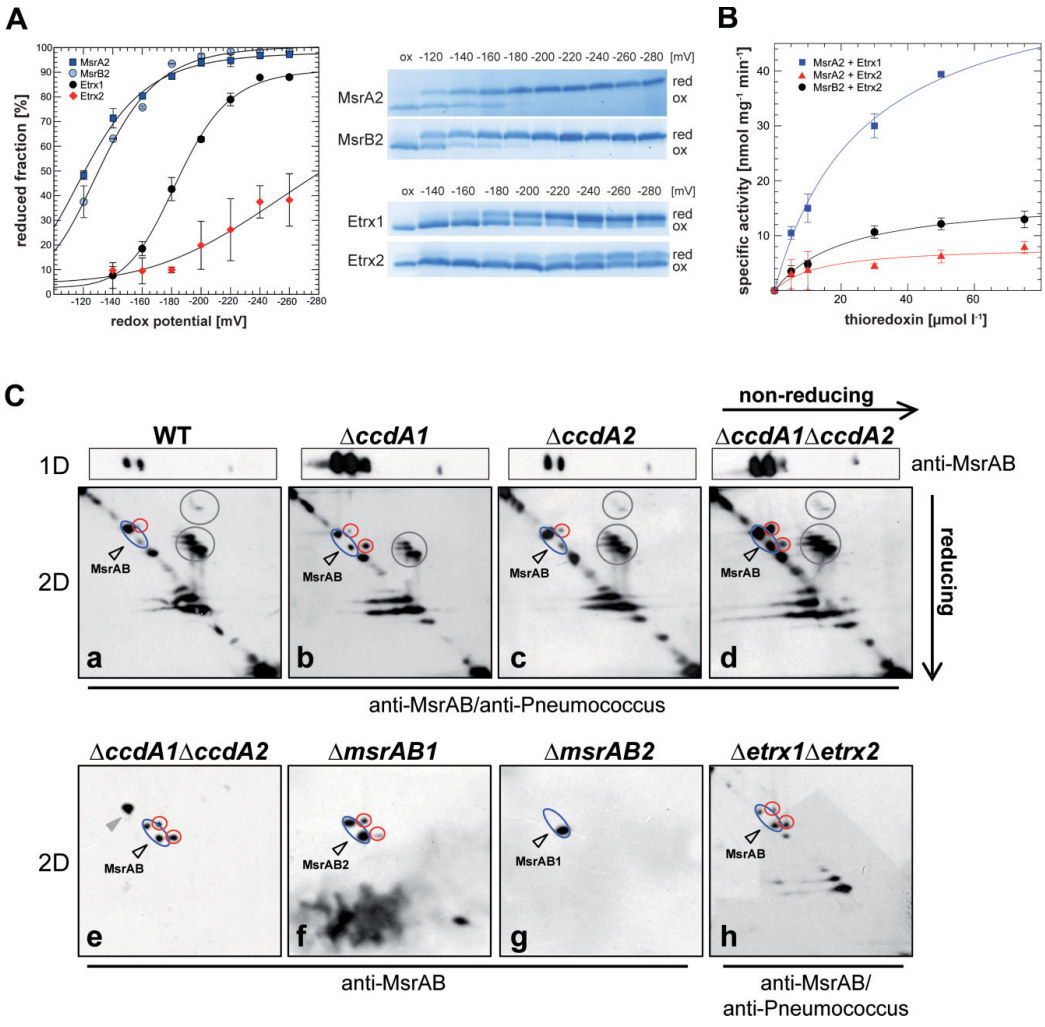

Figure 5.

Table 2. Kinetic parameters of methionine sulfoxide reductase activity of MsrA2 or MsrB2

Enzyme–substrate	V_{max} nmol/mg min	K_m μmol/L	Efficiency (V_{max}/K_m) AU
MsrA2 + Etrx1	59.0	26.5	2.22
MsrA2 + Etrx2	8.2	13.3	0.61
MsrB2 + Etrx1	(No activity)	(No activity)	(No activity)
MsrB2 + Etrx2	17.1	21.0	0.81

The methionine sulfoxide reductase activity was measured in the presence of Etrx1 and Etrx2 protein, respectively. The reaction was performed at pH 7.4 in a mixture containing the Etrx protein, NADPH, human thioredoxin reductase and the reaction was started by the addition of MsrAB2 subunits.
AU, arbitrary units.

the anti-*Sp*MsrAB2 antiserum (Fig 5C). The lower *Sp*MsrAB2 isoform probably is mixed with *Sp*MsrAB1 as shown by *msrAB1*- and *msrAB2*-mutant blots (Fig 5C; see also Fig 1D). Importantly, the oxidized intramolecular disulphide of the upper *Sp*MsrAB2 isoform accumulates strongly above the diagonal in the D39Δ*cps*Δ*ccdA1*Δ*ccdA2* and D39Δ*cps*Δ*etrx1*Δ*etrx2* mutants (Fig 5C), but is only weakly detected in the single *ccdA* mutants. The results suggest that *Sp*MsrAB2 is more oxidized in the *ccdA1/2* and *etrx1/2* double mutants compared to the single mutants. The functions of Etrx1 and Etrx2 as electron partners for *Sp*MsrAB2 were further demonstrated by growth experiments in the presence of 6 mM free MetSO as physiological Msr substrate. Growth in the presence of free MetSO was significantly impaired in the *msrAB2* single or *etrx1/2* and *ccdA1/2* double mutants compared to the *etrx* or *ccdA* single mutants (Supporting Information Fig S15). This MetSO-sensitive phenotype is indicative for the deficiency of methionine sulfoxide reductase activity in the absence of both functional CcdA-Etrx electron pathways *in vivo* (Supporting Information Fig S15).

Etrx1 and Etrx2 are required for full virulence of pneumococci in an acute pneumonia mouse infection model

The acute experimental pneumonia and sepsis infection models were applied to assess the role of thioredoxin-like lipoproteins Etrx1 and Etrx2 on pneumococcal colonization and virulence in CD-1 outbred mice. In the acute pneumonia model mice ($n = 12$) were challenged intranasally with 1.0×10^7 bioluminescent wild-type D39*lux* or its isogenic mutants D39*lux*Δ*etrx1*, D39*lux*Δ*etrx2* and D39*lux*Δ*etrx1*Δ*etrx2*, respectively. Mice infected with wild-type pneumococci or single *etrx* mutants showed the first weak signs of pneumococcal spread into the lungs at 30 h post-infection. In contrast, the D39*lux*Δ*etrx1*Δ*etrx2* double mutant showed earliest at 72 h post-infection a strong increase in bioluminescence in the lungs as monitored by real-time bioimaging, which could be correlated with a strong increase in bacterial load in the lungs (Fig 6). This delay of pneumococcal pneumonia and septicemia after intranasal infection suggested an attenuation of virulence for the double mutant D39*lux*Δ*etrx1*Δ*etrx2*. In contrast, the single knockout mutants D39*lux*Δ*etrx1* and D39*lux*Δ*etrx2* showed no significant differences in bioluminescent flux compared to D39*lux* and had mostly developed severe lung infections or succumbed to sepsis 72 h post-infection (Fig 6D). The results of the real-time monitoring correlated with the survival rates of mice. The intranasal infection with the double mutant D39*lux*Δ*etrx1*Δ*etrx2* prolonged significantly the survival time of mice ($p < 0.0001$), whereas survival of mice infected with the Etrx1- or Etrx2-deficient single mutants was not significantly altered compared to the wild-type

Figure 5. Reduction of SpMsrAB2 by thioredoxin lipoproteins Etrx1 and Etrx2. Source data is available for this figure in the Supporting Information.

A. Redox potential of Etrx proteins and methionine sulfoxide reductases. The redox potential was determined in the presence of different ratios of glutathione (GSH) and glutathione disulfide (GSSG) by specific alkylation using AMS in an anaerobic nitrogen environment. Free thiols were alkylated which resulted in a shift of 536 Da per alkylated thiol. The redox potential was calculated and the CBB staining shows at this point similar ratios of the oxidized and reduced protein forms.

B. The kinetic parameters of Etrx proteins for the methionine sulfoxide reductase subunits MsrA2 and MsrB2 were determined in the presence of NADPH as described in the Supporting Information. Activity was determined in an optical assay from the decrease in $A_{340\,nm}$. Each data point represents the mean value of two/three independent experiments.

C. Diagonal non-reducing/reducing SDS–PAGE combined with *Sp*MsrAB-specific immunoblot analysis showed accumulation of *Sp*MsrAB2 intramolecular disulphides (marked in red) particularly in the D39Δ*cps*Δ*ccdA1*Δ*ccdA2* and D39Δ*cps*Δ*etrx1*Δ*etrx2* double mutants *in vivo*. The diagonal non-reducing/reducing immunoblot analyses were performed using whole cell protein extracts of parental strain D39Δ*cps* (a) and isogenic mutants D39Δ*cps*Δ*ccdA1* (b), D39Δ*cps*Δ*ccdA2* (c), D39Δ*cps*Δ*ccdA1*Δ*ccdA2* (d and e), D39Δ*cps*Δ*msrAB1* (f), D39Δ*cps*Δ*msrAB2* (g) and D39Δ*cps*Δ*etrx1*Δ*etrx2* (h), respectively, as described previously (Pother et al, 2009). Pneumococcal protein extracts were harvested from bacteria cultured under non-stress conditions and proteins with reduced thiol-groups were alkylated with 20 mM NEM. Proteins were first separated using a non-reducing SDS–PAGE without DTT (1D) and the lane was cut and separated horizontally by a second reducing SDS–PAGE with DTT (2D). The reducing diagonal SDS-gel (2D) was subjected to *Sp*MsrAB-and pneumococcus-specific immunoblot analysis. The non-reducing one-dimensional gel (1D) was subjected to *Sp*MsrAB immunoblot analysis and is shown on top of the corresponding diagonal immunoblot (a–d). In the diagonal immunoblots the *Sp*MsrAB intramolecular disulphides were detected using the anti-MsrAB antiserum alone as shown for D39Δ*cps*Δ*msrAB1* (f), D39Δ*cps*Δ*msrAB2* (g) and the double mutant D39Δ*cps*Δ*ccdA1*Δ*ccdA2* (e), or with anti-MsrAB2 antiserum in combination with the anti-pneumococcus antiserum (a–d, h) to visualize the reduced proteins migrating along the diagonal. *Sp*MsrAB2 appeared in two isoforms as indicated in the diagonal assay by the blue circles. The lower isoform of *Sp*MsrAB2 overlapped with *Sp*MsrAB1 as revealed by the immunoblots of the *msrAB1*- and *msrAB2*-mutants (f and g) and as shown by the immunoblot in Fig 1D. The *Sp*MsrAB intramolecular disulphides migrate slightly above the diagonal (red circles) and accumulate especially in the *ccdA1/2* and *etrx1/2* double mutants suggesting that *Sp*MsrAB2 is more oxidized in the double knockouts compared to the single *ccdA*-mutants. Grey circles show proteins with intramolecular disulphides detected by anti-pneumococcal antibodies. The grey arrowhead in (e) indicates a non-specific signal.

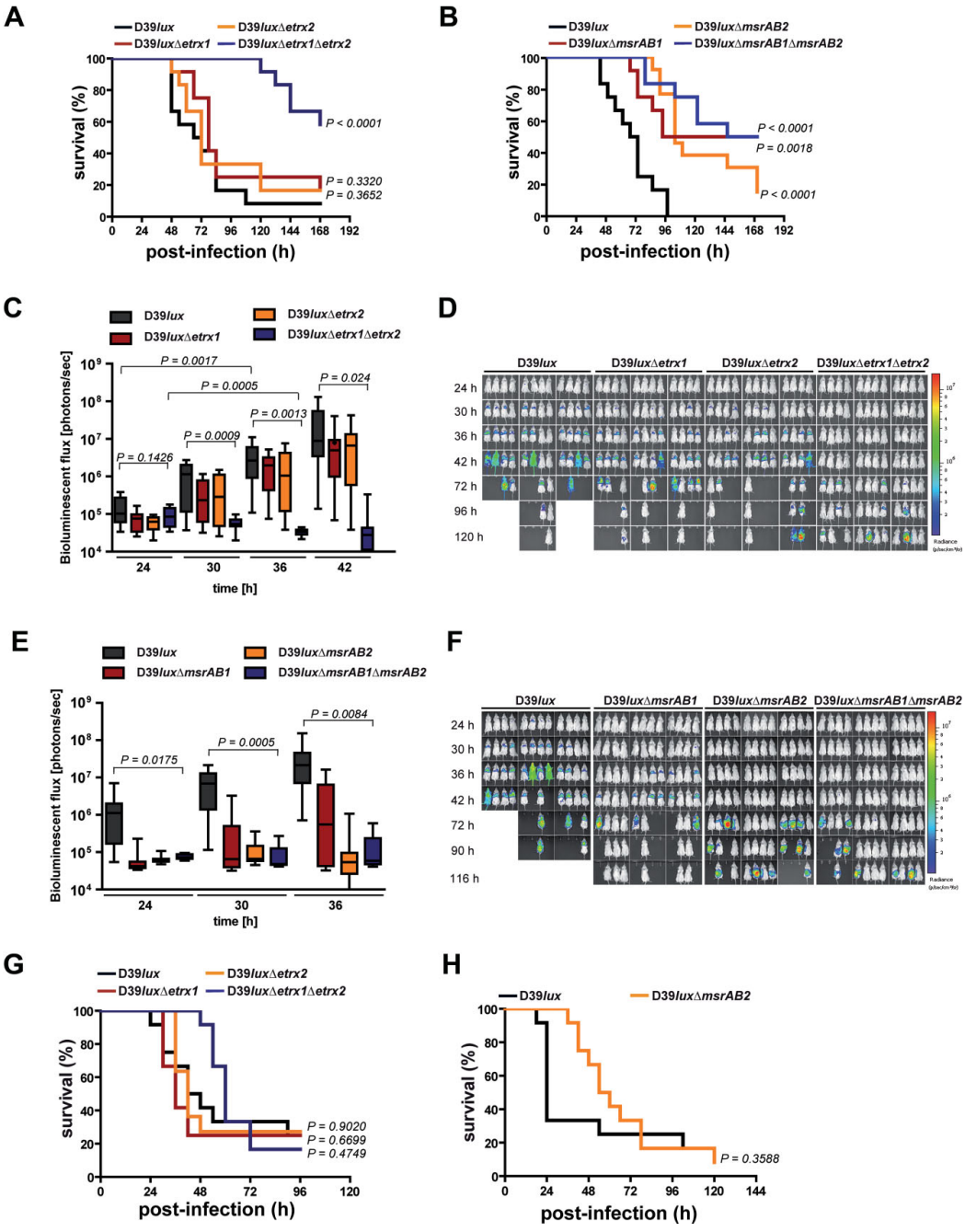

Figure 6.

infected mice (Fig 6A). Similar to the H_2O_2 resistance only the *etrx* double mutant is affected in virulence during *in vivo* infection, while in the study of Andisi et al the attenuation of the mutant is due to the deficiency of Etrx1 (TlpA) and *Sp*MsrAB (Andisi et al, 2012). To investigate whether the deficiency of *Sp*MsrAB2 results in a phenotype similar to the double mutant D39*lux*Δ*etrx1*Δ*etrx2*, mice were also infected intranasally with the *msrAB*-mutants. Indeed, the results revealed significant attenuation of the *msrAB2*-mutant ($p < 0.0001$) compared to the wild-type D39*lux* (Fig 6B, E and F). Importantly, the *etrx*-mutants and the *msrAB2*-mutant showed no growth defects under *in vitro* conditions (Supporting Information Fig S16). In contrast, the deficiency of *Sp*MsrAB1 impaired growth in a chemically defined medium (Supporting Information Fig S16) and pneumococcal virulence was also significantly reduced (Fig 6B) as has been shown previously (Wizemann et al, 1996). The real-time monitoring correlates with the survival rates of the mice (Fig 6E and F) and the lack of *Sp*MsrAB1 and *Sp*MsrAB2 had no additive effect. Furthermore, CD-1 mice ($n = 9$) were infected with a lower infection dose (1×10^6) to explore the effect of Etrx proteins or *Sp*MsrAB2 on nasopharyngeal colonization in the carriage model. Pneumococci were recovered after 1, 3 and 5 days from the nasopharynx and the lung by a bronchioalveolar lavage. These results showed at all time points a significant reduction of nasopharyngeal carriage for the double mutant D39*lux*Δ*etrx1*Δ*etrx2* compared to the wild-type (Supporting Information Fig S17). The other *etrx*- or *msrAB2*-mutants did not significantly differ in nasopharyngeal carriage from the isogenic wild-type (Supporting Information Fig S17). However, the *msrAB2*-mutant showed immediately at 24 h post-infection a significantly reduced number of CFU in the lung (Supporting Information Fig S17B).

To analyse the impact of the Etrx and *Sp*MsrAB2 proteins on pneumococcal survival during sepsis, mice were infected via the intraperitoneal route. The survival rates of mice ($n = 12$) were similar for groups infected with wild-type or single *etrx* mutants, although there was a moderate but not significant attenuation for the double mutant D39*lux*Δ*etrx1*Δ*etrx2* (Fig 6G). Similarly, the *msrAB2*-mutant showed no significant attenuation during invasive disease (Fig 6H).

Taken together, these *in vivo* infection experiments suggest that loss of one of the Etrx lipoproteins does not affect virulence. In contrast, loss of function of either surface-exposed Etrx lipoproteins or the *Sp*MsrAB2 protein does significantly reduce virulence and spread of pneumococci from the nasopharynx into the lungs and blood.

Pneumococcal resistance against killing phagocytosis relies on Etrx and *Sp*MsrAB2

To investigate the role of the Etrx and *Sp*MsrAB2 proteins on uptake by professional phagocytes and to allow significant phagocytosis non-encapsulated pneumococci were incubated with macrophages. The results showed significantly higher numbers of internalized and recovered D39Δ*cps*Δ*etrx1*Δ*etrx2* pneumococci deficient in both Etrx proteins compared to the isogenic D39Δ*cps* and individual *etrx*-mutants (Fig 7A). The number of recovered pneumococci was also significantly increased for the *msrAB2*-mutant (Fig 7A). The increased number of phagocytosed *etrx* double mutants or *msrAB2*-mutants was also confirmed by immunofluorescence microscopy (Fig 7B). Remarkably, the lack of Etrx1 in D39Δ*cps* also accelerated phagocytosis (Fig 7A). In addition, the intracellular fate of wild-type and *etrx*-mutants was assessed. Regarding the intracellular survival, all strains showed a time-dependent decrease in the number of recovered and viable pneumococci. However, the relative decline of recovered D39Δ*cps*Δ*etrx1*Δ*etrx2* mutants did not show significant differences compared to the non-encapsulated *S. pneumoniae* D39Δ*cps*. Similar to the non-encapsulated pneumococci, phagocytosis of the encapsulated strains showed a higher number of phagocytosed and recovered mutants deficient in both Etrx proteins. These data suggest that the total loss of Etrx lipoprotein or *Sp*MsrAB2 activity accelerates phagocytosis and hence, killing of pneumococci.

DISCUSSION

Thioredoxin lipoproteins are required for resistance to extracellular oxidative stress

In this study, we performed a comprehensive functional and structural analysis of the extracellular oxidative stress resistance system of *S. pneumoniae* mediated by two CcdA-Etrx pathways and their redox partner *Sp*MsrAB2. Our results demonstrated that single *etrx*-mutants expressing *Sp*MsrAB2 showed lower susceptibility to killing by H_2O_2, compared to the *etrx* double mutant that had a similar peroxide sensitive phenotype like the *Sp*MsrAB2 mutant. Thus, only the deficiency of both Etrx1 and Etrx2 proteins or *Sp*MsrAB2 significantly accelerated pneumococcal killing by H_2O_2 and diminished growth in the presence of MetSO, respectively. Similarly, only the deficiency of both, Etrx1 and Etrx2, or their electron acceptor *Sp*MsrAB2 attenuates significantly pneumococcal virulence in the acute pneumonia model but not in the sepsis model. The importance of the Etrx proteins and *Sp*MsrAB2 for virulence functions is supported by our phagocytosis assays, which showed that only

Figure 6. Impact of the Etrx proteins on pneumococcal virulence in mice.

A,B. Survival of CD-1 mice after intranasal infection with pneumococci. Groups of mice ($n = 12$) were intranasally infected with 10^7 CFU of bioluminescent *S. pneumoniae* D39 wild-type (D39*lux*) or its isogenic mutants deficient for Etrx (A) or MsrAB proteins (B).

C–F. Bioluminescent optical imaging of pneumococcal dissemination after intranasal infection of CD-1 mice ($n = 12$). Dissemination of bioluminescent D39*lux*, and isogenic mutants deficient for Etrx1, Etrx2, Etrx1 and 2 (D), MsrAB1, MsrAB2 or MsrAB1 and 2 (F) were analysed at indicated time points by determination of the luminescence intensity (photons/s) measured with the IVIS Spectrum system. The bioluminescent flux of grouped mice is shown for indicated time points in the box whisker graph (C and E).

G,H. Survival of CD-1 mice in a systemic infection model. A CFU of 5×10^3 pneumococci was used for intraperitoneal infection of mice ($n = 12$).

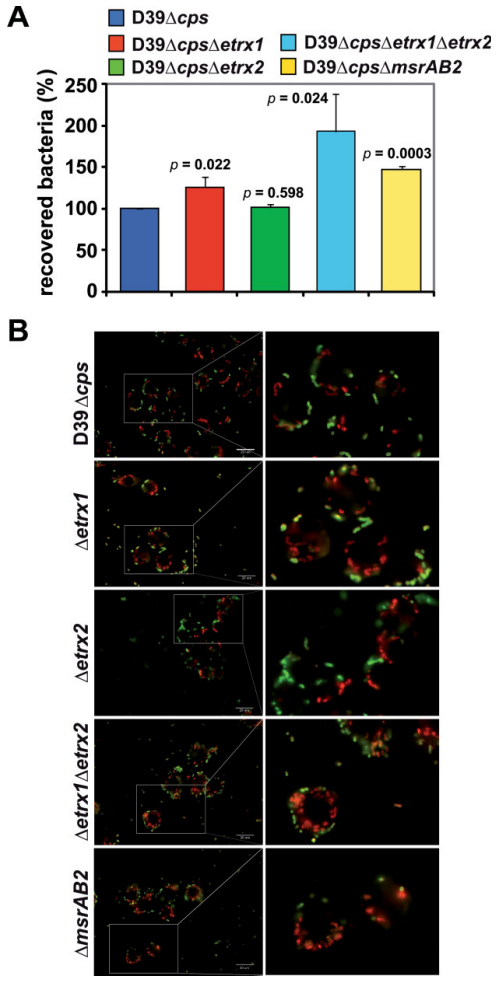

Figure 7. Influence of extracellular thioredoxin lipoproteins and MsrAB2 deficiency on uptake of *S. pneumoniae* D39Δ*cps* by macrophages.

A. J774 cells were infected with a multiplicity of infection of 50 non-encapsulated D39Δ*cps* and isogenic *etrx*-mutants per cell. The internalization of the bacteria was determined by applying antibiotic protection and quantitative plating 30 min post-infection. Experiments were done at least three times in triplicate and data represent the mean ± SEM.

B. Immunofluorescence microscopy of pneumococci attached (green) to J774 macrophages and phagocytosed, intracellular pneumococci (red) 30 min post-infection. Attached bacteria are stained green (Alexa Fluor 488), while intracellular bacteria are stained red (Alexa Fluor 568).

the uptake of the *etrx* double or *msrAB2* mutant is massively enhanced, whereas only a minor effect was observed for the single *etrx*-mutants. These data suggest that the Etrx proteins can functionally replace each other, which ensures proper function of surface-exposed pneumococcal proteins. The determination of the redox potentials for the Etrx and *Sp*MsrAB2 proteins together with our structural and kinetic data further demonstrate that *Sp*MsrAB2 can be reduced by both Etrx proteins. Interestingly, Etrx1 seems to reduce preferentially the MsrA2 subunit of *Sp*MsrAB2 while Etrx2 is able to reduce both MsrA2 and MsrB2 domains *in vitro* (Fig 5). Importantly, diagonal non-reducing/reducing SDS–PAGE analysis combined with *Sp*MsrAB2 specific immunoblots further verified the *in vivo* accumulation of oxidized *Sp*MsrAB2 protein especially in the *ccdA1/2* and *etrx1/2* double mutants. This indicates that both thioredoxin systems are required for efficient regeneration of *Sp*MsrAB2. Interestingly, we detected strong growth sensitivities of the *etrx1/2* double mutant in the presence of H_2O_2 and free MetSO as physiological MsrAB2 substrate. Hence, we postulate that both extracellular CcdA-Etrx-*Sp*MsrAB2 electron pathways are involved in reduction of oxidized Met residues present in surface-exposed virulence proteins or as free MetSO on the bacterial surface that has to be further explored in future studies.

Structural determinants of Etrx1 and Etrx2 proteins and evidence for two CcdA-Etrx-*Sp*MsrAB2 pathways

Thiol-disulfide oxidoreductases (TDORs) comprise a large superfamily of proteins that are present in all kingdoms of life where they control the redox state of Cys containing proteins. Cytoplasmic TDORs like the thioredoxin system are usually involved in maintaining protein cysteines in a reduced state (Fernandes & Holmgren, 2004). In contrast, periplasmic TDORs of Gram-negative bacteria like the Dsb family proteins or extracellular TDORs of Gram-positive bacteria catalyse disulphide bond formation or isomerization in the oxidizing periplasm or extracellular space (Cho & Collet, 2013; Denoncin & Collet, 2013). These extra-cytoplasmic or periplasmic TDORs are involved in a wide range of processes, including cytochrome maturation, *e.g. B. subtilis* ResA (Lewin et al, 2006), cell motility, *e.g. E. coli* DsbB (Dailey & Berg, 1993), natural competence development, *e.g. B. subtilis* BdbD (Meima et al, 2002), toxin biosynthesis, *e.g. E. coli* DsbA (Yamanaka et al, 1994) and synthesis of the endospore peptidoglycan cortex protective layer, *e.g. B. subtilis* StoA (Crow et al, 2009). Periplasmic reducing systems are present in this oxidizing compartment of Gram-negative bacteria to reduce sulfenic acids in the periplasm (*e.g.* DsbDG) or to deliver electrons for MetSO reduction (*e.g.* PilB) (Cho & Collet, 2013). Both Etrx1 and Etrx2 share sequence homology (30.48 and 21.83%, respectively) with the C-terminal periplasmic domain of DsbD. CcdA1 and CcdA2 are homolog to the membrane-embedded domain of DsbD (Supporting Information Fig S10). Hence, we postulate that the CcdA-Etrx-MsrAB2 pathways also function in the extracellular compartment of the Gram-positive pneumococci in MetSO reduction.

According to the accepted catalytic mechanism of thioredoxin-like proteins (Crow et al, 2004), Etrx1/Etrx2 would bind their redox partner *Sp*MsrAB2 by means of a hydrophobic surface and subsequently perform a nucleophilic attack on the target disulphide bond via the N-terminal nucleophilic thiolate of the CXXC motif (Cys84 in Etrx1, Cys81 in Etrx2). This process would lead to the formation of a mixed intermolecular disulphide between Etrx and its redox partner proteins, which

is resolved by the second C-terminal resolving Cys residue (Cys87 in Etrx1, Cys84 in Etrx2). The N-terminal active-site Cys residue is present in the reactive thiolate anion form, which is stabilized by an interaction with the dipole of helix α2. In several thiol-disulphide oxidoreductases this interaction reduces the pK_a of the nucleophilic active-site Cys by at least two pH units (Roos et al, 2013).

In the CXXC motif of both Etrx proteins, only the active-site Cys is solvent-exposed and accessible to the redox partner (Cys84 in Etrx1 and Cys81 in Etrx2). Many thioredoxin-like proteins share also a proline residue within the CXXC motif. This proline residue is also present in the CXXC motif of Etrx2 (Fig 3D), but not in Etrx1. The presence of proline residues at the cap of the active site helix has been reported to have important consequences for the distribution of the electrostatic field near the cysteines as proline does not possess a standard peptide group (Crow et al, 2009). The absence of proline in Etrx1 would affect the macrodipole arising from α2 helix that is often invoked as primary cause of the lowered pK_a values associated with the active-site cysteine residue of the CXXC motif in most TDORs (Kortemme & Creighton, 1995). Furthermore, the limited conformational freedom of proline (in comparison with other residues) has been reported to be an important factor in maintaining rigidity of the CXXC motif and relevant for the structural changes from the reduced to its oxidized forms. Etrx1, representing one of the rare cases without proline in the CXXC motif, is therefore expected to have more structural variations between reduced and oxidized forms than Etrx2. Another relevant difference between both Etrx proteins and other extra-cytoplasmic TDORs concern a glutamate residue that is placed three positions after the C-terminal cysteine residue of the CXXC motif. Substitution of this glutamate has been shown to have a significant effect on the active site properties of ResA and StoA of *B. subtilis* (Crow et al, 2009; Hodson et al, 2008; Lewin et al, 2006). Etrx1 and Etrx2 do not have a glutamate at this position, but possess instead a serine residue (Ser90 in Etrx1 and Ser87 in Etrx2; Supporting Information Fig S18).

Etrx2 has an unprecedented hydrophobic cavity close to the active site. The presence of a hydrophobic patch near the active site has been associated with substrate recognition in other TDORs (Crow et al, 2009). In the structure of the oxidized forms of Etrx2, a detergent molecule (Cyclofos-3™) or a HED molecule is bound to this hydrophobic pocket, very likely mimicking the redox partner interaction. Etrx1 lacks this cavity and this region shows differences in both the nature of the amino acids and in the conformation of the β4–α3 loop (Fig 3). In agreement with these results, soaking experiments with Etrx1 crystals did not yield a complex with Cyclofos-3™ even at high concentrations of the detergent.

In conclusion, some of the structural determinants of the CXXC motif observed in other extra-cytoplasmic thioredoxins, such as the presence of proline or glutamate residues are not observed in pneumococcal Etrx proteins (except for the proline in Etrx1). Despite strong similarities in the overall fold of both, Etrx1 and Etrx2, relevant differences are observed between their active sites (presence of hydrophobic cavity in Etrx2, different electrostatic potential, different CXXC motifs). These differences provide a structural basis for the specific interaction of Etrx with the MsrA or the MsrB domains of the *Sp*MsrAB2 redox partner observed in the redox potential determination and kinetics.

Model for the two CcdA-Etrx-*Sp*MsrAB2 electron pathways

The mechanism for the protection against oxidative stress via both CcdA-Etrx-*Sp*MsrAB2 electron pathways is modeled in Fig 8 and Supplementary Information Movie 1. The pneumococcal cell wall is an oxidizing environment in which the sulphur-containing amino acids Met and cysteine are highly susceptible to oxidation by endogenously produced peroxide. Electrons are transported from the cytoplasmic NADPH pool to the cell wall to keep pneumococcal surface proteins in a reduced state. The first proteins of this extracellular electron transport system are the integral membrane proteins CcdA1 and CcdA2. Electrons from the cytoplasmic Trx are shuttled between CcdA1 and CcdA2 to Etrx1 and Etrx2, respectively, similarly to that observed between the transmembrane and the periplasmic domains of DsbD. Surface-exposed Etrx1 and Etrx2 deliver electrons to the *Sp*MsrAB2 protein for the reduction of MsrA2 (by Etrx1 or Etrx2) and MsrB2 (by Etrx2) domains (Fig 8). Oxidation of Met results in a mixture of the two diastereomers methionine-*S*-sulfoxide and methionine-*R*-sulfoxide, which are reduced by MsrA and MsrB, respectively. Besides the catalytic domains, *Sp*MsrAB2 also carries a transmembrane segment that anchors the protein to the membrane. It has also a long and flexible coiled coil region allowing the enzyme to reach damaged virulence proteins and to reduce MetSO (Fig 8 and Supporting Information movie). Thioredoxin-like lipoproteins Etrx1/Etrx2 are critical in the turnover of the system by reducing the methionine sulfoxide reductase *Sp*MsrAB2. Since this seems to be the sole extracellular thioredoxin system of pneumococci, the lack of functional Etrx proteins or *Sp*MsrAB2 protein has direct consequences to resist oxidative stress and host immune defense mechanisms. In this sense, the pneumococcal surface-exposed thioredoxin systems reported here provide an important framework for the development of new antibacterial therapies.

MATERIALS AND METHODS

Bacterial strains, culture conditions and transformation techniques

E. coli strains and *S. pneumoniae* genotypes and strains used in this study are listed in Supporting Information Table S1. *E. coli* and *S. pneumoniae* strains were cultured and transformed as described recently (Jensch et al, 2010).

Primers, construction of pneumococcal mutants and protein purification

Primers that were used in this study and plasmids used for the mutagenesis and recombinant protein expression are listed in Supporting Information Table S2. For the generation of the pneumococcal mutants in D39*lux* (Jensch et al, 2010) and D39Δ*cps* the insertion–deletion mutagenesis strategy was used as described (Rennemeier et al, 2007). Mutagenesis, expression cloning and protein

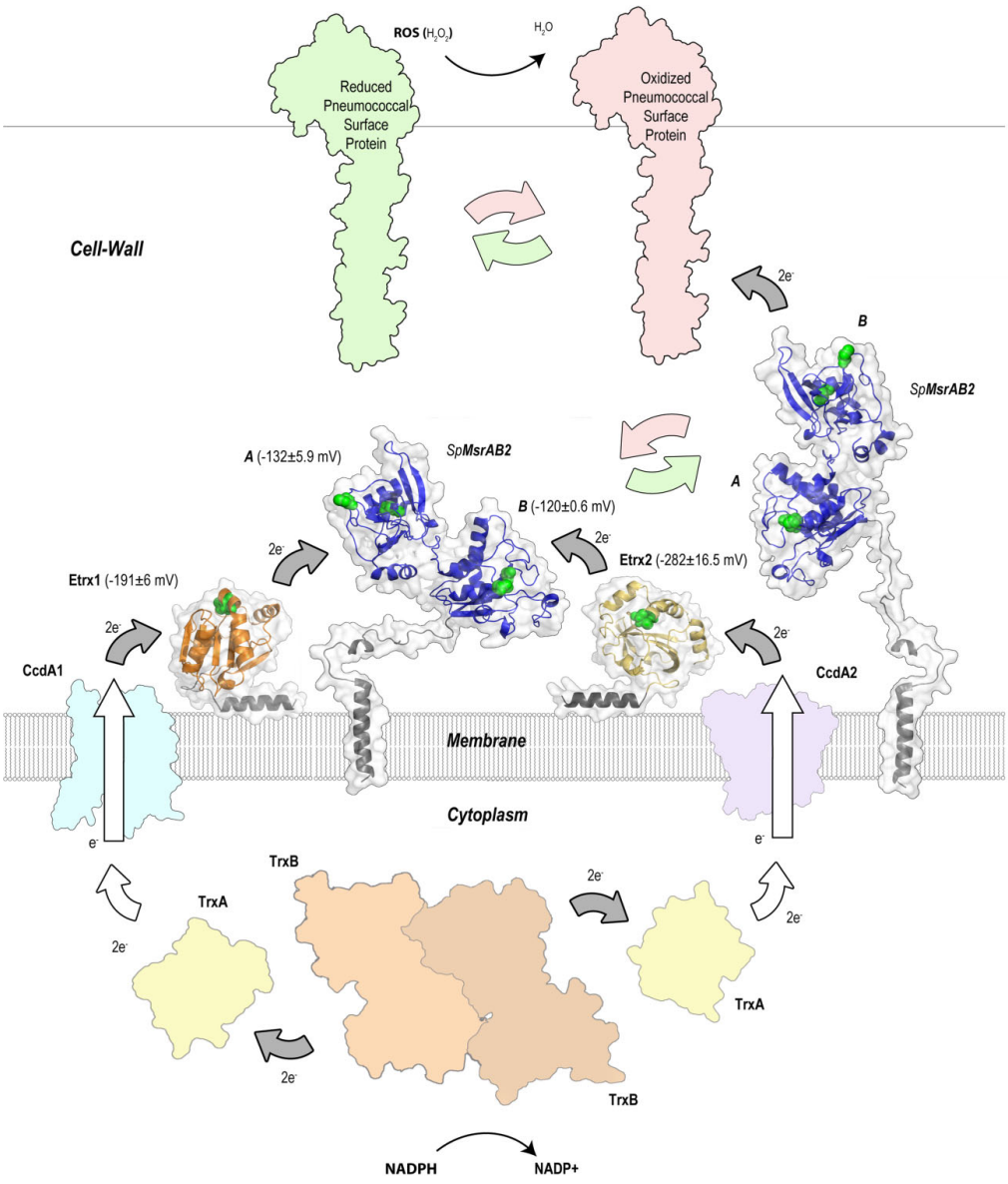

Figure 8. Proposed mechanism of oxidative stress defense mediated by the CcdA1-Etrx1 and CcdA2-Etrx2 electron pathways and their redox partner *Sp*MsrAB2 on the pneumococcal surface. Electrons provided from NADPH by the cytoplasmic TrxB (SPD_1287) are transferred to the cytoplasmic TrxA (SPD_1567) and shuttled between the integral membrane protein CcdA1 (SPD_0571) to the surface-exposed thioredoxin-like Etrx1 (SPD_0572), and between the integral membrane protein CcdA2 (SPD_0885) to surface-exposed thioredoxin-like Etrx2 (SPD_0886) following the same mechanism. Both thioredoxin-like proteins provide reducing equivalents to *Sp*MsrAB2 (SPD_0573) for the reduction of the MsrA (by Etrx1 or Etrx2) and MsrB (by Etrx2) domains. *Sp*MsrAB2 remains anchored to the membrane and presents a long and flexible coiled coil region allowing *Sp*MsrAB2 to reach and repair ROS damaged surface proteins. Catalytic cysteine residues in Etrx1, Etrx2 and *Sp*MsrAB2 are represented as green spheres. Experimentally determined redox potentials for each protein are labelled. White arrows indicate presumed interactions and grey arrows indicate those demonstrated experimentally. All accession numbers refer to the *S. pneumoniae* D39 annotation.

The paper explained

PROBLEM:

The respiratory pathogen *Streptococcus pneumoniae* (the pneumococcus) is a serious pathogen causing life-threatening community-acquired pneumonia and invasive diseases. The high morbidity and mortality caused by pneumococcal diseases (more than 1.5 million every year, particularly in infants, elderly and immunocompromised patients), is exacerbated by the increasing prevalence of antibiotic-resistant strains and the suboptimal efficacy of available vaccines. Pneumococci have evolved efficient mechanisms to resist protein damage under oxidative stress conditions and to displace other bacteria in the nasopharynx. While oxidative stress-resistance mechanisms in the cytoplasm are well studied, the extracellular mechanism required to resist attack from the host is less investigated.

RESULTS:

We have identified a two-operon system responsible for the extracellular oxidative stress resistance. This system is composed of two integral membrane proteins (CcdA1 and CcdA2), two thioredoxin-like lipoproteins (Etrx1 and Etrx2) and a single methionine sulfoxide reductase (*Sp*MsrAB2). We have solved the crystal structures of both Etrx proteins and analysed the functions of both Etrx and *Sp*MsrAB2 proteins on oxidative stress resistance and virulence. We further observed in phagocytosis experiments with macrophages that both thioredoxin lipoproteins and *Sp*MsrAB2 play a crucial role in pneumococcal pathogenesis. We can finally conclude that both Etrx proteins function as electron donors for the *Sp*MsrAB2 redox partner and are therefore crucial for the extracellular reducing redox pathways of pneumococci.

IMPACT:

The data highlight the crucial role of thioredoxin lipoproteins Etrx1 and Etrx2 and *Sp*MsrAB2 for virulence and the redox-reactions of the extracellular oxidative stress resistance mechanism of pneumococci. Suppression of that system severely reduces pneumococcal virulence and lethality. In this sense, the combined effect of antibiotics with new ligands blocking this crucial pneumococcal system could be intended. Therefore, our data provide a new framework for the development of novel bactericidals against this important human pathogen.

purification of His_6-tagged proteins are described in detail in the Supporting Information.

Pneumococcal survival under oxidative conditions

The survival experiments under oxidative condition with hydrogen peroxide (H_2O_2), paraquat (stimulating superoxide production in cells; kindly provided by A. Littmann, Julius Kühn Institute (JKI), Braunschweig, Germany) or MetSO (Sigma–Aldrich, Taufkirchen, Germany) were conducted as described previously (Johnston et al, 2004). Briefly, wild-type pneumococci and Etrx-deficient mutants were cultured in THY broth at 37°C to mid-log phase and treated for 30 min with 10, 15 or 20 mM H_2O_2 and 90 min with 0.25, 0.5 or 0.75 mM paraquat, respectively. Untreated pneumococci were used as a control. To determine the percentage of survival, serial dilutions were plated onto blood agar plates and CFU were counted after overnight incubation at 37°C and 5% CO_2. In control experiments catalase (5000 U/ml) was added simultaneously with H_2O_2 to the bacterial cultures.

Protein crystallization

Etrx1 crystals were obtained with 30% v/v PEG 4000; 0.1 M tris pH 8.5; 0.2 M $MgCl_2$ 18°C. Etrx2:Cyclofos 3™ complex crystal was obtained with 3.4 M sodium malonate pH 6.0 18°C, while the Etrx2:HED Complex crystal was obtained in 30% PEG 1500 supplemented with 14 mM β-mercaptoethanol. Details in Supporting Information.

Data collection, phasing and model refinement

Native data sets of Etrx1 and Etrx2: Cyclofos-3™ crystals were collected on ESRF ID14-4 beamline in Grenoble, France. Native data set of Etrx2:HED crystal was collected on SLS PXIII beamline in Villigen, Switzerland (Table 1). Details in Supporting Information.

*Sp*MsrAB2 homology model

The 3D model for the catalytic domains of pneumococcal *Sp*MsrAB2 (residues 60–312) was obtained by comparative homology via modeler and energy minimization.

Ethics statement

Animal experiments were performed in strict accordance with the German regulations of the Society for Laboratory Animal Science (GV-SOLAS) and the European Health Law of the Federation of Laboratory Animal Science Associations (FELASA). All experiments were approved by the ethical board and Landesamt für Landwirtschaft, Lebensmittelsicherheit und Fischerei Mecklenburg-Vorpommern (LALLFV MV), Rostock in Germany (permit no. 7221.3-1.1-006/09 and 7221.3-1.1-019/11).

Mouse models of infection and bioluminescent optical imaging

Eight weeks old female outbred CD1 mice (Charles River, Sulzfeld, Germany) were infected intranasally or intraperitoneally with bioluminescent pneumococci as described recently (Hartel et al, 2011; Jensch et al, 2010). Briefly, pneumococci were cultured to $A_{600} = 0.35$ in THY supplemented with 10% foetal bovine serum and the infection dose was adjusted to 1.0×10^7 CFU in 25 µl for the intranasal route ($n = 12$) and 5×10^3 CFU in 100 µl for the intraperitoneal route ($n = 12$). Before intranasal infection, mice were anaesthetized by intraperitoneal injection of ketamine (Ketanest S; Pfizer Pharma, Karslruhe, Germany) and xylazine (Rompun®; Provet AG, Lyssach, Germany). Once anesthetized the animals were scuffed, with the nose held upright, and the bacterial suspension of 25 µl was administered intranasally by adding a series of small droplets into the nostrils for the mice to involuntarily inhale. The infection dose was confirmed by determination of the CFU after plating serial dilutions

of the infection dose on blood agar plates. Bioluminescent optical imaging using the IVIS® Spectrum Imaging System (Caliper Life Sciences, Hopkinton, US) allowed monitoring of pneumococcal dissemination after intranasal infection (Hartel et al, 2011; Jensch et al, 2010). At prechosen time intervals post-infection mice were imaged for 1 min to monitor dissemination of pneumococci into the lungs. A time series of the images was generated and the bioluminescent intensity (BLI) was determined by quantification of the total photon emission using the LivingImage® 4.1 software package (Caliper Life Sciences).

Phagocytosis experiments

To determine the rate of phagocytosed wild-type and mutant pneumococci and their intracellular survival in macrophages, phagocytosis experiments with J774A.1 murine macrophages (DSMZ, Braunschweig, Germany) were carried out as described (Hartel et al, 2011; Jensch et al, 2010).

Statistical analysis

All data are reported as mean ± SD unless otherwise noted. Results were statistically analysed using the unpaired two-tailed Student's test. Kaplan–Meier survival curves were compared by the log rank test. *p* Values for bioluminescence measurements were calculated using the unpaired, one-tailed *t*-test for differences between groups, while differences of one group between days were analysed by the paired *t*-test. Statistical significance was confirmed by ANOVA analysis with Bonferroni's multiple comparison *post hoc* test. A p-value <0.05 was considered to be statistically significant.

For more detailed materials and methods see the Supporting Information.

Accession numbers

Sequence data for the *etrx* genes 1 and 2 of D39 or TIGR4 are deposited in the EMBL/GenBank databases under accessions numbers ABJ55360 and ABJ55355 or AAK74804 and AAK75117. Sequence data for the *ccdA1* and *ccdA2* of D39 or TIGR4 are deposited in the EMBL/GenBank databases under accession numbers ABJ54003 and ABJ54567 or AAK74803 and AAK75116. Sequence data for the *msrAB2* gene of D39 or TIGR4 are available from the EMBL/GenBank databases under accessions numbers ABJ53896 or AAK74805. The atomic coordinates and structure factors for Etrx1, Etrx2:Cyclofos-3™ complex and Etrx2:HED complex (codes 4HQS, 2YP6 and 4HQZ, respectively) have been deposited in the Protein Data Bank, Research Collaboratory for Structural Bioinformatics, Rutgers University, New Brunswick, US (http://www.rcsb.org/).

Author contributions

MS, JAH, CHL, HA and SH conceived and designed the experiments. MS, SGB, MRA, IJ, TMA, LP, TP and MG performed the experiments. MS, SGB, MRA, TP, JAH, CHL, HA and SH analysed the data. MS, SGB, HA, JAH and SH wrote and reviewed the paper.

Acknowledgements

The authors thank the PXIII beamline at SLS and the ESRF beamline ID14-1 for access to synchrotron radiation. We are also grateful to Kristine Sievert-Giermann, Nadine Gotzmann and Melanie Skibbe (Department of Genetics, University of Greifswald, Germany) for technical assistance. This work was supported by grants from the Deutsche Forschungsgemeinschaft DFG HA3125/4-2 (to S.H.), DFG AN746/3-1 (to H.A.), BFU2011-25326 and S2010/BMD-2457 (to J.A.H.) and EU FP7 *CAREPNEUMO* Grant EU-CP223111 from the European Union (to J.A.H. and S.H.).

Supporting Information is available at EMBO Molecular Medicine Online.

The authors declare that they have no conflict of interest.

References

Andisi VF, Hinojosa CA, de Jong A, Kuipers OP, Orihuela CJ, Bijlsma JJ (2012) Pneumococcal gene complex involved in resistance to extracellular oxidative stress. Infect Immun 80: 1037-1049

Auzat I, Chapuy-Regaud S, Le Bras G, Dos Santos D, Ogunniyi AD, Le Thomas I, Garel JR, Paton JC, Trombe MC (1999) The NADH oxidase of *Streptococcus pneumoniae*: its involvement in competence and virulence. Mol Microbiol 34: 1018-1028

Bigelow DJ, Squier TC (2011) Thioredoxin-dependent redox regulation of cellular signaling and stress response through reversible oxidation of methionines. Mol Biosyst 7: 2101-2109

Brot N, Collet J-F, Johnson LC, Jönsson TJ, Weissbach H, Lowther WT (2006) The thioredoxin domain of *Neisseria gonorrhoeae* PilB can use electrons from DsbD to reduce downstream methionine sulfoxide reductases. J Biol Chem 281: 32668-32675

Brot N, Weissbach L, Werth J, Weissbach H (1981) Enzymatic reduction of protein-bound methionine sulfoxide. Proc Natl Acad Sci USA 78: 2155-2158

Cho SH, Collet JF (2013) Many roles of the bacterial envelope reducing pathways. Antioxid Redox Signal 18: 1690-1698

Collet JF, Messens J (2010) Structure, function, and mechanism of thioredoxin proteins. Antioxid Redox Signal 13: 1205-1216

Crow A, Acheson RM, Le Brun NE, Oubrie A (2004) Structural basis of redox-coupled protein substrate selection by the cytochrome c biosynthesis protein ResA. J Biol Chem 279: 23654-23660

Crow A, Liu Y, Möller MC, Le Brun NE, Hederstedt L (2009) Structure and functional properties of *Bacillus subtilis* endospore biogenesis factor StoA. J Biol Chem 284: 10056-10066

Dailey FE, Berg HC (1993) Mutants in disulfide bond formation that disrupt flagellar assembly in *Escherichia coli*. Proc Natl Acad Sci USA 90: 1043-1047

Das KC, Das CK (2000) Thioredoxin, a singlet oxygen quencher and hydroxyl radical scavenger: redox independent functions. Biochem Biophys Res Commun 277: 443-447

Delaye L, Becerra A, Orgel L, Lazcano A (2007) Molecular evolution of peptide methionine sulfoxide reductases (MsrA and MsrB): on the early development of a mechanism that protects against oxidative damage. J Mol Evol 64: 15-32

Denoncin K, Collet JF (2013) Disulfide bond formation in the bacterial periplasm: major achievements and challenges ahead. Antioxid Redox Signal 119: 63-71

Drazic A, Miura H, Peschek J, Le Y, Bach NC, Kriehuber T, Winter J (2013) Methionine oxidation activates a transcription factor in response to oxidative stress. Proc Natl Acad Sci USA 110: 9493-9498

Erickson JR, Joiner ML, Guan X, Kutschke W, Yang J, Oddis CV, Bartlett RK, Lowe JS, O'Donnell SE, Aykin-Burns N *et al* (2008) A dynamic pathway for calcium-independent activation of CaMKII by methionine oxidation. Cell 133: 462-474

Fernandes AP, Holmgren A (2004) Glutaredoxins: glutathione-dependent redox enzymes with functions far beyond a simple thioredoxin backup system. Antioxid Redox Signal 6: 63-74

Gamez G, Hammerschmidt S (2012) Combat pneumococcal infections: adhesins as candidates for protein-based vaccine development. Curr Drug Targets 13: 323-337

Grimaud R, Ezraty B, Mitchell JK, Lafitte D, Briand C, Derrick PJ, Barras F (2001) Repair of oxidized proteins. Identification of a new methionine sulfoxide reductase. J Biol Chem 276: 48915-48920

Gutteridge JM, Halliwell B (2000) Free radicals and antioxidants in the year 2000. A historical look to the future. Ann N Y Acad Sci 899: 136-147

Hajaj B, Yesilkaya H, Benisty R, David M, Andrew PW, Porat N (2012) Thiol peroxidase is an important component of *Streptococcus pneumoniae* in oxygenated environments. Infect Immun 80: 4333-4343

Hanschmann EM, Godoy JR, Berndt C, Hudemann C, Lillig CH (2013) Thioredoxins, glutaredoxins, and peroxiredoxins-molecular mechanisms and health significance: from cofactors to antioxidants to redox signaling. Antioxid Redox Signal, DOI: 10.1089/ars.2012.4599

Hartel T, Klein M, Koedel U, Rohde M, Petruschka L, Hammerschmidt S (2011) Impact of glutamine transporters on pneumococcal fitness under infection-related conditions. Infect Immun 79: 44-58

Hermans PW, Adrian PV, Albert C, Estevao S, Hoogenboezem T, Luijendijk IH, Kamphausen T, Hammerschmidt S (2006) The streptococcal lipoprotein rotamase A (SlrA) is a functional peptidyl-prolyl isomerase involved in pneumococcal colonization. J Biol Chem 281: 968-976

Hiller NL, Janto B, Hogg JS, Boissy R, Yu S, Powell E, Keefe R, Ehrlich NE, Shen K, Hayes J *et al* (2007) Comparative genomic analyses of seventeen *Streptococcus pneumoniae* strains: insights into the pneumococcal supragenome. J Bacteriol 189: 8186-8195

Hodson CT, Lewin A, Hederstedt L, Le Brun NE (2008) The active-site cysteinyls and hydrophobic cavity residues of ResA are important for cytochrome c maturation in *Bacillus subtilis*. J Bacteriol 190: 4697-4705

Holm L, Rosenstrom P (2010) Dali server: conservation mapping in 3D. Nucleic Acids Res 38: W545-W549

Hoshi T, Heinemann S (2001) Regulation of cell function by methionine oxidation and reduction. J Physiol 531: 1-11

Jensch I, Gamez G, Rothe M, Ebert S, Fulde M, Somplatzki D, Bergmann S, Petruschka L, Rohde M, Nau R *et al* (2010) PavB is a surface-exposed adhesin of *Streptococcus pneumoniae* contributing to nasopharyngeal colonization and airways infections. Mol Microbiol 77: 22-43

Johansson C, Lillig CH, Holmgren A (2004) Human mitochondrial glutaredoxin reduces S-glutathionylated proteins with high affinity accepting electrons from either glutathione or thioredoxin reductase. J Biol Chem 279: 7537-7543

Johnston JW, Myers LE, Ochs MM, Benjamin WH, Jr, Briles DE, Hollingshead SK (2004) Lipoprotein PsaA in virulence of *Streptococcus pneumoniae*: surface accessibility and role in protection from superoxide. Infect Immun 72: 5858-5867

Kadioglu A, Weiser JN, Paton JC, Andrew PW (2008) The role of *Streptococcus pneumoniae* virulence factors in host respiratory colonization and disease. Nat Rev Microbiol 6: 288-301

Kang SW, Chae HZ, Seo MS, Kim K, Baines IC, Rhee SG (1998) Mammalian peroxiredoxin isoforms can reduce hydrogen peroxide generated in response to growth factors and tumor necrosis factor-alpha. J Biol Chem 273: 6297-6302

Kim YK, Shin YJ, Lee W-H, Kim H-Y, Hwang KY (2009) Structural and kinetic analysis of an MsrA-MsrB fusion protein from *Streptococcus pneumoniae*. Mol Microbiol 72: 699-709

Kortemme T, Creighton TE (1995) Ionisation of cysteine residues at the termini of model alpha-helical peptides. Relevance to unusual thiol pKa values in proteins of the thioredoxin family. J Mol Biol 253: 799-812

Kovacs-Simon A, Titball RW, Michell SL (2011) Lipoproteins of bacterial pathogens. Infect Immun 79: 548-561

Krupp R, Chan C, Missiakas D (2001) DsbD-catalyzed transport of electrons across the membrane of *Escherichia coli*. J Biol Chem 276: 3696-3701

Leichert LI, Jakob U (2006) Global methods to monitor the thiol-disulfide state of proteins in vivo. Antioxid Redox Signal 8: 763-772

Lewin A, Crow A, Oubrie A, Le Brun NE (2006) Molecular basis for specificity of the extracytoplasmic thioredoxin ResA. J Biol Chem 281: 35467-35477

Lowther WT, Brot N, Weissbach H, Honek JF, Matthews BW (2000) Thiol-disulfide exchange is involved in the catalytic mechanism of peptide methionine sulfoxide reductase. Proc Natl Acad Sci USA 97: 6463-6468

Margolis E (2009) Hydrogen peroxide-mediated interference competition by *Streptococcus pneumoniae* has no significant effect on *Staphylococcus aureus* nasal colonization of neonatal rats. J Bacteriol 191: 571-575

Meima R, Eschevins C, Fillinger S, Bolhuis A, Hamoen LW, Dorenbos R, Quax WJ, van Dijl JM, Provvedi R, Chen I *et al* (2002) The bdbDC operon of *Bacillus subtilis* encodes thiol-disulfide oxidoreductases required for competence development. J Biol Chem 277: 6994-7001

Paget MS, Buttner MJ (2003) Thiol-based regulatory switches. Annu Rev Genet 37: 91-121

Paterson GK, Blue CE, Mitchell TJ (2006) An operon in *Streptococcus pneumoniae* containing a putative alkylhydroperoxidase D homologue contributes to virulence and the response to oxidative stress. Microb Pathog 40: 152-160

Pericone CD, Bae D, Shchepetov M, McCool T, Weiser JN (2002) Short-sequence tandem and nontandem DNA repeats and endogenous hydrogen peroxide production contribute to genetic instability of *Streptococcus pneumoniae*. J Bacteriol 184: 4392-4399

Pericone CD, Overweg K, Hermans PW, Weiser JN (2000) Inhibitory and bactericidal effects of hydrogen peroxide production by *Streptococcus pneumoniae* on other inhabitants of the upper respiratory tract. Infect Immun 68: 3990-3997

Pericone CD, Park S, Imlay JA, Weiser JN (2003) Factors contributing to hydrogen peroxide resistance in *Streptococcus pneumoniae* include pyruvate oxidase (SpxB) and avoidance of the toxic effects of the fenton reaction. J Bacteriol 185: 6815-6825

Pother DC, Liebeke M, Hochgrafe F, Antelmann H, Becher D, Lalk M, Lindequist U, Borovok I, Cohen G, Aharonowitz Y *et al* (2009) Diamide triggers mainly S thiolations in the cytoplasmic proteomes of *Bacillus subtilis* and *Staphylococcus aureus*. J Bacteriol 191: 7520-7530

Potter AJ, Trappetti C, Paton JC (2012) *Streptococcus pneumoniae* uses glutathione to defend against oxidative stress and metal ion toxicity. J Bacteriol 194: 6248-6254

Quinternet M, Tsan P, Neiers F, Beaufils C, Boschi-Muller S, Averlant-Petit M-C, Branlant G, Cung M-T (2008) Solution structure and dynamics of the reduced and oxidized forms of the N-terminal domain of PilB from *Neisseria meningitidis*. Biochemistry 47: 8577-8589

Quinternet M, Tsan P, Selme-Roussel L, Jacob C, Boschi-Muller S, Branlant G, Cung M-T (2009) Formation of the complex between DsbD and PilB N-terminal domains from *Neisseria meningitidis* necessitates an adaptability of nDsbD. Structure (London, England: 1993) 17: 1024-1033

Ranaivoson FM, Kauffmann B, Neiers F, Wu J, Boschi-Muller S, Panjikar S, Aubry A, Branlant G, Favier F (2006) The X-ray structure of the N-terminal domain of PILB from *Neisseria meningitidis* reveals a thioredoxin-fold. J Mol Biol 358: 443-454

Ranaivoson FM, Neiers F, Kauffmann B, Boschi-Muller S, Branlant G, Favier F (2009) Methionine sulfoxide reductase B displays a high level of flexibility. J Mol Biol 394: 83-93

Rennemeier C, Hammerschmidt S, Niemann S, Inamura S, Zahringer U, Kehrel BE (2007) Thrombospondin-1 promotes cellular adherence of gram-positive pathogens via recognition of peptidoglycan. FASEB J 21: 3118-3132

Roos G, Foloppe N, Messens J (2013) Understanding the pK(a) of redox cysteines: the key role of hydrogen bonding. Antioxid Redox Signal 18: 94-127

Selva L, Viana D, Regev-Yochay G, Trzcinski K, Corpa JM, Lasa I, Novick RP, Penadés JR (2009) Killing niche competitors by remote-control bacteriophage induction. Proc Natl Acad Sci USA 106: 1234-1238

Sharov VS, Schoneich C (2000) Diastereoselective protein methionine oxidation by reactive oxygen species and diastereoselective repair by methionine sulfoxide reductase. Free Radic Biol Med 29: 986-994

Tarrago L, Gladyshev VN (2012) Recharging oxidative protein repair: catalysis by methionine sulfoxide reductases towards their amino acid, protein, and model substrates. Biochemistry (Mosc) 77: 1097-1107

Voss S, Hallstroem T, Saleh M, Burchhardt G, Pribyl T, Singh B, Riesbeck K, Zipfel PF, Hammerschmidt S (2013) The choline-binding protein PspC of *Streptococcus pneumoniae* interacts with the C-terminal heparin-binding domain of vitronectin. J Biol Chem 288: 15614-15627

Weissbach H, Resnick L, Brot N (2005) Methionine sulfoxide reductases: history and cellular role in protecting against oxidative damage. Biochim Biophys Acta 1703: 203-212

West AP, Brodsky IE, Rahner C, Woo DK, Erdjument-Bromage H, Tempst P, Walsh MC, Choi Y, Shadel GS, Ghosh S (2011) TLR signalling augments macrophage bactericidal activity through mitochondrial ROS. Nature 472: 476-480

Wizemann TM, Moskovitz J, Pearce BJ, Cundell D, Arvidson CG, So M, Weissbach H, Brot N, Masure HR (1996) Peptide methionine sulfoxide reductase contributes to the maintenance of adhesins in three major pathogens. Proc Natl Acad Sci USA 93: 7985-7990

Wu J, Neiers F, Boschi-Muller S, Branlant G (2005) The N-terminal domain of PILB from *Neisseria meningitidis* is a disulfide reductase that can recycle methionine sulfoxide reductases. J Biol Chem 280: 12344-12350

Yamanaka H, Kameyama M, Baba T, Fujii Y, Okamoto K (1994) Maturation pathway of *Escherichia coli* heat-stable enterotoxin I: requirement of DsbA for disulfide bond formation. J Bacteriol 176: 2906-2913

Yesilkaya H, Andisi VF, Andrew PW, Bijlsma JJ (2013) *Streptococcus pneumoniae* and reactive oxygen species: an unusual approach to living with radicals. Trends Microbiol 21: 187-195

Yesilkaya H, Kadioglu A, Gingles N, Alexander JE, Mitchell TJ, Andrew PW (2000) Role of manganese-containing superoxide dismutase in oxidative stress and virulence of *Streptococcus pneumoniae*. Infect Immun 68: 2819-2826

Zander T, Phadke ND, Bardwell JC (1998) Disulfide bond catalysts in *Escherichia coli*. Methods Enzymol 290: 59-74

Zeller T, Klug G (2006) Thioredoxins in bacteria: functions in oxidative stress response and regulation of thioredoxin genes. Naturwissenschaften 93: 259-266

III. Article

Thioredoxin 1 and Glutaredoxin 2 contribute to maintain the phenotype and integrity of neurons following perinatal asphyxia

Juan Ignacio Romero, Eva-Maria Hanschmann, **Manuela Gellert**, Susanne Eitner, Mariana Inés Holubiec, Eduardo Blanco-Calvo, Christopher Horst Lillig, Francisco Capani

Biochim. Biophys. Acta

Vol 1850 Issue 6 (1274-85)

Published: May 30th, 2015

Biochimica et Biophysica Acta 1850 (2015) 1274–1285

Contents lists available at ScienceDirect

Biochimica et Biophysica Acta

journal homepage: www.elsevier.com/locate/bbagen

Thioredoxin 1 and glutaredoxin 2 contribute to maintain the phenotype and integrity of neurons following perinatal asphyxia

Juan Ignacio Romero [a], Eva-Maria Hanschmann [b], Manuela Gellert [b], Susanne Eitner [b], Mariana Inés Holubiec [a], Eduardo Blanco-Calvo [a,c], Christopher Horst Lillig [b], Francisco Capani [a,d,*]

[a] Instituto de Investigaciones Cardiológicas "Prof. Dr. Alberto C. Taquini" (ININCA), Facultad de Medicina, UBA-CONICET, Marcelo T. de Alvear 2270, C1122AAJ, Ciudad de Buenos Aires, Argentina
[b] Institute for Medical Biochemistry and Molecular Biology, Universitätsmedizin Greifswald, Ernst-Moritz-Arndt-Universität Greifswald, 17475 Greifswald, Germany
[c] Facultat d'Educació, Psicologia i Treball Social Universitat de Lleida Av. de l'Estudi General, 4, 25001 Lleida, Spain
[d] Departamento de Biología, UAJFK, C1197AAR, Ciudad de Buenos Aires, Argentina

ARTICLE INFO

Article history:
Received 11 August 2014
Received in revised form 14 February 2015
Accepted 24 February 2015
Available online 28 February 2015

Keywords:
Common carotid artery occlusion
Thioredoxin family of proteins
Hypoxia
Reoxygenation
Perinatal asphyxia

ABSTRACT

Background: Thioredoxin (Trx) family proteins are crucial mediators of cell functions via regulation of the thiol redox state of various key proteins and the levels of the intracellular second messenger hydrogen peroxide. Their expression, localization and functions are altered in various pathologies. Here, we have analyzed the impact of Trx family proteins in neuronal development and recovery, following hypoxia/ischemia and reperfusion.
Methods: We have analyzed the regulation and potential functions of Trx family proteins during hypoxia/ischemia and reoxygenation of the developing brain in both an animal and a cellular model of perinatal asphyxia. We have analyzed the distribution of 14 Trx family and related proteins in the cerebellum, striatum, and hippocampus, three areas of the rat brain that are especially susceptible to hypoxia. Using SH-SY5Y cells subjected to hypoxia and reoxygenation, we have analyzed the functions of some redoxins suggested by the animal experiment.
Results and conclusions: We have described/discovered a complex, cell-type and tissue-specific expression pattern following the hypoxia/ischemia and reoxygenation. Particularly, Grx2 and Trx1 showed distinct changes during tissue recovery following hypoxia/ischemia and reoxygenation. Silencing of these proteins in SH-SY5Y cells subjected to hypoxia-reoxygenation confirmed that these proteins are required to maintain the normal neuronal phenotype.
General significance: These findings demonstrate the significance of redox signaling in cellular pathways. Grx2 and Trx1 contribute significantly to neuronal integrity and could be clinically relevant in neuronal damage following perinatal asphyxia and other neuronal disorders.

1. Introduction

Brain damage resulting from an ischemic event in the fetus or newborn infant (also known as perinatal asphyxia, PA) remains a major cause of neonatal death and neurological deficits in children. Cerebral palsy, mental retardation, and epilepsy are among the most common complications of PA [1–4]. The incidence of severe PA is estimated to be about 1/1000 live births in developed countries, and 5–10/1000 live births in developing countries [5]. This clinical picture has been extensively reproduced in murine models of PA consisting of the ligation of the right common carotid artery followed by an exposure to an oxygen deprived environment at postnatal day 7 [3,6–10]. The model for common carotid artery ligation used in the present study has been previously developed and validated by Lopez-Aguilera et al., 2012 [7]. It has been extensively investigated and is generally accepted that the rat brain at the age of 7 days is histologically similar to that of a 32–34 week gestation human fetus or newborn infant, i.e., the cerebral cortical neuronal layering is complete, the germinal matrix is involuting, and white matter has undergone some myelination [11–13].

Damage caused by the effects of reactive oxygen species (ROS) has been proposed as an important cause of neuronal death and consequently brain damage after hypoxia-ischemia [14,15]. In aerobic cells, ROS are produced within the cytoplasm and mitochondria [16]. Under physiological conditions, they are part of

Abbreviations: CCA, Common carotid artery; cer, Cerebellum; CNS, Central nervous system; ELISA, Enzyme-linked immunosorbent assay; Grx, Glutaredoxins; hip, Hippocampus; P7, Postnatal day 7; PA, Perinatal asphyxia; PBS, Phosphate buffer saline; Prx, Peroxiredoxins; ROS, Reactive oxygen species; SEM, Standard error of the mean; str, Striatum; Trx, Thioredoxins; TrxR, Thioredoxin reductase

* Corresponding author at: Instituto de Investigaciones Cardiológicas "Prof. Dr. Alberto C. Taquini" (ININCA), UBA-CONICET, Marcelo T. de Alvear 2270, C1122AAJ, Buenos Aires, Argentina. Tel./fax: +54 11 4508 3880/8.
E-mail addresses: franciscocapani@hotmail.com, fcapani@fmed.uba.ar (F. Capani).

http://dx.doi.org/10.1016/j.bbagen.2015.02.015
0304-4165/

specific signaling processes, regulating for instance developmental processes, cell proliferation, differentiation and apoptosis [16–18]. They are locally produced by specific enzymes and are rapidly degraded by others, affecting specific target molecules and signaling pathways [16,18]. However, excessive production of specific ROS, e.g. hydroxyl radicals, can lead to oxidative and irreversible damage to macromolecules and has been linked to various pathological conditions, including hypoxia/ischemia and reoxygenation [14,19,20]. Several therapeutic approaches to counteract the effects induced by ROS during hypoxia/ischemia and especially reoxygenation have been proposed. However, no neuroprotective agent has been proven safe and effective in the protection of neonates from neurological sequels following an ischemic insult beside hypothermia in some specific cases [21]. Therefore, it is essential to gain more insights into biochemical and cellular mechanisms of neuronal injury induced by PA to identify potential therapeutic targets, compounds and strategies [22].

The members of the thioredoxin (Trx) family are small proteins that present the characteristic Trx fold, and the cysteine(s)-containing active site motif, which is crucial for the transfer of electrons and the general oxidoreductase activity [23,24]. The Trx superfamily of proteins includes thioredoxins (Trxs) glutaredoxins (Grxs) and peroxiredoxins (Prxs) [25]. These proteins share a common structural motif, the Trx fold, consisting of a central core of four-stranded β-sheets surrounded by three or more α-helices. The thiol-disulfide oxidoreductases Trx and Grx also share the conserved active site Cys-X-X-Cys that enables them to catalyze thiol-disulfide exchange reactions [25]. Peroxiredoxins are thiol-dependent peroxidases [23,24]. Trx was first described as a hydrogen donor for ribonucleotide reductase from *Escherichia coli* [26]. Later on, these proteins were recognized as key regulators in the cell response to redox signals [24]. Mammals possess two principal Trx isoforms, the cytosolic Trx1 and the mitochondrial Trx2. These proteins are reduced by thioredoxin reductases [27,28], the cytosolic TrxR1 and the mitochondrial TrxR2, respectively. TrxRs are homodimeric flavo- and seleno-enzymes which are able to reduce Trxs, as well as peroxides and other compounds [29–31]. Mammalian genomes encode various Grxs, among them the cytosolic Grx1 and Grx3, the mitochondrial Grx5 and Grx2a, and the least frequent nuclear/cytosolic isoforms of Grx2 (Grx2b and Grx2c, respectively) [24,32]. Grxs are reduced by glutathione, with electrons from glutathione reductase and NADPH [32]. Peroxiredoxins (Prxs) reduce different peroxides and peroxynitrite [33]. Prx1 to Prx4 belong to the typical 2-Cys Prx class, Prx5 is an atypical 2-Cys Prx, Prx6 is a 1-Cys Prx [34,35]. Prx1, Prx2 and Prx5 can be found in the nucleus and cytoplasm, whereas Prx3 and Prx5 are localized in mitochondria. Prx4 and Prx6 can be found in the cytoplasm. In addition, Prx1, Prx2 and Prx4 were shown to be secreted from the cell [34,36].

Here, we have analyzed the regulation and potential functions of Trx family proteins on the effects of hypoxia/ischemia and reoxygenation on the developing brain both *in vivo* and in a neurological cell culture model.

2. Experimental procedures

2.1. Animals

All experiments were conducted according to the principles of the Guide for the Care and Use of Laboratory Animals (NIH Publications No. 80-23, revised 1996), and approved by the Institutional Animal Care and Use Committee at the University of Buenos Aires (School of Medicine). All efforts were made to reduce the number of animals used and to minimize suffering. Pregnant rats were obtained from the School of Veterinary Sciences' central *vivarium* at the University of Buenos Aires. All animals were kept in a temperature (21 ± 2 °C) and humidity (65 ± 5%) controlled environment on a 12 h light/dark cycle. Animals had *ad libitum* access to food (Purina chow) and tap water.

2.2. Model for common carotid artery ligation

The model for common carotid artery ligation used in this study, has been previously developed and validated by Lopez-Aguilera et al. [7]. Seven days of age (P7) male Sprague–Dawley rats were anesthetized with a combination of ketamine (40 mg/kg) and xylazine (4 mg/kg). The animals were placed on a heat plate ensuring a constant body temperature of 37 °C. An incision on the right side of the neck was performed exposing the right common carotid artery (CCA), which was then isolated from nerve and vein and permanently ligated with a 6–0 surgical silk (carotid group n = 14). The wound was then sutured and the animals were returned to their dams for recovery for 4–5 h. Subsequently, pups were placed in a stoppered 1 L glass jar and exposed to 100% nitrogen (delivered at 3 L per minute) for 3 min to induce anoxia. The jar was partially submerged in a 37 °C water bath to maintain a constant thermal environment. In sham operated rats (sham group n = 12) the right CCA was exposed but not ligated and no nitrogen was supplied. At 21 days of age (14 days post-surgery), when the synaptic connections are well established in the rat [37], animals were sacrificed.

2.3. Brain dissection

Brains were dissected as previously described in Chiu et al. [38]. After the animals were sacrificed at 21 days of age, brains were isolated and dissected at 4 °C. Brains were cut in half into right and left hemisphere. Three cuts were performed in each hemisphere. The first cut was situated at the *Genu* of the *Corpus callosum* (~Bregma +1.0 mm based on the rat brain atlas by Paxinos and Watson [39]), the second cut was situated at the anterior tip of the *Fornix* (approx. Bregma −1.0 mm based on the rat brain atlas by Paxinos and Watson [39]). The third cut was situated at the 4th ventricle (~Bregma −8.0 mm based on the rat brain atlas by Paxinos and Watson [39]). The striatum was dissected between the first and second cut with the help of two Miltex Iris Tissue Forceps, and stored at −80 °C. The hippocampus was dissected after the second cut. The midbrain was removed to expose the hippocampus, which was then dissected from the cortex using two tissue forceps, and stored at −80 °C. Finally, the cerebellum was dissected after the third cut, that was separated from the ponds and medulla oblongata with the help of two tissue forceps, and stored at −80 °C.

2.4. Cell culture

SH-SY5Y cells were cultivated in MEM (PAA), supplemented with 10% FCS good (PAN), 2 mM L-glutamine, 100 units/ml penicillin and 0.1 mg/ml streptomycin at 37 °C in a 90% humidified atmosphere containing 5% CO_2. SH-SY5Y cells were transiently transfected with 15 μg specific, custom-made siRNA (Eurogentech) for Trx1 (sense: GUA GAU GUG GAU GAC UGU C, antisense: GAC AGU CAU CCA CAU CUA C) and Grx2 (sense: GGU GCA ACU GAC ACU CAU; antisense: UAU GAG UGU CAG UUG CAC). Unspecific control (scr)bled siRNA (sense: CAU UCA CUC AGG UCA UCA, antisense: CUG AUG ACC UGA GUG AAU) was used as control. Five million SH-SY5Y cells were resuspended in electroporation buffer (21 mM HEPES, 137 mM NaCl, 5 mM KCl, 0.7 mM Na_2HPO_4, 6 mM D-glucose, pH 7.15), mixed with siRNA and were electroporated in a total volume of 550 μl at 230 V, 1050 microfarads and 500 ohm. FCS was immediately added to the transfected cells and they were seeded out in 1:5 conditioned medium (1 part old and 4 parts fresh medium). To sufficiently knock-down Trx1 and Grx2, cells were transfected a second time after 3 days.

Twenty-four hours following the second transfection, cells were incubated under 1% O_2 and 5% CO_2 at 37 °C (hypoxia) in a CO_2 incubator (binder) for 24 h followed by a reoxygenation period of 24 or 48 h in an atmosphere containing 20% O_2 and 5% CO_2 at 37 °C. Cells were detached by trypsin treatment, washed with PBS, lysed in lysis buffer (10 mM

Tris/HCl, pH 7.4, 10 mM NaCl, 3 mM $MgCl_2$, 0.1% NP-40, protease inhibitors) and were frozen at −80 °C.

2.5. Western blotting and ELISA

Western blot analysis was performed essentially as previously described in Godoy et al. [40]. Animals were euthanized by decapitation, brains were dissected, homogenized in ice-cold lysis buffer (10 mM Tris/HCl, pH 7.4, 10 mM NaCl, 3 mM $MgCl_2$, 0.1% NP-40, protease inhibitors) and were fast frozen in liquid nitrogen. Tissue and cell lysates were thawed on ice and centrifuged at 13,000 rpm for 15 min at 4 °C. The supernatants were analyzed for total protein concentration using Bradford solution (Bio-Rad, Munich, Germany) in 96-well plates using bovine serum albumin (BSA) as standard. 10–20 μg of total protein were diluted in sample buffer (0.3 M Tris/HCl, pH 7, 50% glycerol, 5% SDS, 1 mM EDTA, 0.1% bromphenol blue). In the case of tissue homogenates, the samples were subjected to SDS-PAGE using the Novex mini-cell (Invitrogen, Carlsbad, CA, USA) with precast 4–20% Precise gels (Pierce-Thermo Fisher). Proteins were transferred to PVDF membranes (Schleicher & Schuell, Germany) according to the manufacturer's instructions. In the case of cell lysates, the samples were subjected to SDS-PAGE using the Mini-Protean TGX stain-free 4–20% precast gels (Biorad) and were transferred to PVDF membranes using the Trans-Blot Turbo Transfer System (Biorad).

Membranes were blocked with 5% nonfat milk powder and 1% BSA in Tris-buffered saline containing 0.05% Tween 20 and incubated with specific primary antibodies at 4 °C overnight. Antigen–antibody complexes were stained using horseradish peroxidase (HRP)-coupled antibodies (Bio-Rad, Richmond CA, USA) and the enhanced chemiluminescence method. Luminescence was recorded using a gel documentation system from Intas (Göttingen, Germany) or the ChemiDoc™ XRS + System, respectively. Anti-GAPDH antibody (Sigma-Aldrich, St. Louis, MO, USA) was used as a loading control for the tissue sample. For cell lysates, total protein in each lane of a blot was quantified based on the stain-free technology of Biorad and used for normalization of the blotting data obtained from densitometric analysis [41,42]. The generation and validation for Western blot analysis of the antibodies against the Trx family of proteins (Grx1, Grx2, Grx3, Grx5, Prx1, Prx2, Prx3, Prx4, Prx5, Prx6, Trx1, Trx2, TrxR1 and TrxR2) used in this study were described in Aon-Bertolino et al. [43] and Godoy et al. [44]. Antibodies detecting GAPDH (G9545), HSP70 (4873S), GFAP (PA3-16727), neurofilament M (2838S), NeuroD1 (sc-1084) were purchased from Sigma Aldrich (Steinheim, Germany), Santa Cruz Biotechnology Inc. (Santa Cruz, USA), Cell Signaling Technology (Danvers, USA) and Thermo Fisher Scientific Inc. (Rockford, USA). To analyze the levels of ubiquitin, polyubiquitin and ubiquitinylated proteins a specific antibody against ubiquitin (sc-9133) was used.

The more sensitive sandwich ELISA was used to quantify the levels of glutaredoxin 2 as described in Hanschmann et al. [45]; the antibodies for Grx2 were not validated for Western blot analysis.

2.6. Quantitative PCR

Cells were harvested by trypsinization, were washed once with PBS and RNA isolation was performed according to the manual provided for the NucleoSpin® RNA II kit (Macherey-Nagel, Düren, Germany). The RNA concentration was determined from the absorbance at 260 nm, analyzed with a NanoDrop 2000c spectrophotometer (Thermo Scientific). First strand cDNA was prepared using the RevertAid First Strand cDNA Synthesis Kit according to the protocol provided using 1 μg RNA as template and Oligo dT_{18} primer (Thermo Scientific). 1 μl of cDNA was used as template for quantitative PCR (qPCR). The SensiMix SYBR HI-ROX contained SYBR® Green I dye, dNTPs, stabilizers, and a hot start DNA polymerase (Bioline, London, UK). The primer concentration used for the qPCR was 0.25 μM each (Grx2: 5′-CTGGTTTGGAGCAGGAGCGGCTC; 3′-GCCTATGAGTGTCAGTTGCACC; Trx1: 5′-GGTGAAGCAGATCGAGAGCAAG; 3′-CACACTCTGAAGCAACATCCTG) and the volume was adjusted to 20 μl with ddH_2O. All qPCRs were performed using the CFX96 Real Time System from BioRad. For optimization, a gradient qPCR from 55 °C to 65 °C was performed and samples were analyzed by agarose gel electrophoresis. At 58 °C annealing temperature, the reaction resulted in a specific product at the expected size. GAPDH was used as a reference (primer pair: 5′-CAAGGTCATCCATGACAACTTTG; 3′-GTCCACCACCCTGTTGCTGTAG) in the ΔΔCq mode. Calculations were performed with the Biorad software.

2.7. Immunohistochemistry

Immunohistochemistry analysis was performed as previously described in Aon-Bertolino et al. [43] and Godoy et al. [44] with slight modifications. Animals were anesthetized with 28% (w/v) chloral hydrate, 0.1 ml/100 g of body weight, and intracardially perfused with 4% paraformaldehyde (Sigma-Aldrich, St. Louis, MO, USA) freshly prepared in 0.1 M phosphate buffer, pH 7.4. Brains were dissected and post-fixed in the same solution for 2 h. Coronal brain sections (40 μm thick) were cut on an Oxford vibratome and then recovered for light microscopic studies. Prior to staining, sections were incubated in 3% hydrogen peroxide for 10 min to quench endogenous peroxidases. After three washing steps in PBS, nonspecific antibody binding sites were blocked with 10% normal goat serum (Invitrogen Corporation, Camarillo, CA, USA) in PBS and sections were incubated overnight with the primary antibodies at 4 °C. The generation and validation for IHC of the antibodies against the Trx family of proteins (Grx1, Grx2, Grx3, Grx5, Prx1, Prx2, Prx3, Prx4, Prx5, Prx6, Trx1, Trx2, TrxR1 and TrxR2) used in this study were described in Aon-Bertolino et al. [43] and Godoy et al. [44]. Sections were washed three times with PBS and subsequently incubated with a biotinylated secondary antibody (Vector Laboratories Inc., Burlingame, CA, USA) for 60 min at room temperature. The Extravidin-Peroxidase detection system (Sigma-Aldrich, St. Louis, MO, USA) was used for antigen staining according to the manufacturer's recommendations. Sections were incubated with the substrate Diaminobenzidine (Sigma-Aldrich, St. Louis, MO, USA) for 5 min at room temperature. Samples were counterstained for 1 min at RT with hematoxilin and were mounted with Canada balsam (Sigma-Aldrich, St. Louis, MO, USA). Sections without incubation with the primary antibody were used as control to verify the specificity of the secondary antibody. Sections were examined by light microscopy using a Leitz Laborlux S microscope (Heidelberg, Germany) equipped with a CCD video camera (Canon). Images were analyzed and compiled using Adobe Photoshop 11.0 CS4. Note that for each protein staining all samples (both sham and carotid groups) were processed together in the same batch, using the same antibody dilutions and the same time for DAB development. Intensity assessment was carried out as a blind test with a 0 to +++ score used as a qualitative measurement.

2.8. Immunocytochemistry

Transiently transfected SH-SY5Y cells were seeded on 100 μg/ml fibronectin-coated coverslips in 24-well plates. After induction of hypoxia-reoxygenation, the cells were fixed with 4% paraformaldehyde for 20 min and permeabilized and blocked (0.3% Triton X-100, 3% (w/v) BSA, 10 mM HEPES in PBS). Cells were incubated overnight with the primary antibody, diluted in 3% (w/v) BSA in PBS at 4 °C and with Alexa-488 labeled secondary antibody (Invitrogen) for 1 h at RT. In addition, F-actin was stained for 1 h at RT using Phalloidin (Invitrogen) and nuclei for 10 min at RT using 100 ng/ml DAPI (Sigma). Coverslips were mounted with Mowiol and processed for confocal microscopy. Cells were analyzed using a Leica TCS SP5 microscope with a 63-fold/1.4 oil lens.

2.9. Cell proliferation and viability (MTT assay)

Cell proliferation and viability were analyzed using the tetrazolium dye MTT (thiazolyl blue tetrazolium bromide, Roth) in a colorimetric assay. 20,000–35,000 cells per well were seeded in a 96 well plate. Following 24 h incubation at 20% oxygen, cells were cultured for 24 h at 1% oxygen with or without subsequent reoxygenation for 24 h or 48 h. For these three different conditions, control cells were seeded out at the same density and were grown for the same duration at 20% oxygen. Cells were washed once with PBS and were incubated with 500 μg/ml of the yellow MTT dye solved in cell culture medium for up to 4 h at 37 °C. The formation of the insoluble, purple formazan via the reduction of MTT was determined by light microscopy. The MTT dye was removed and the plate was stored at −80 °C over night. Cells were lysed in lysis reagent (346 mM SDS, 0.2% HCl in DMSO) for up to 30 min at RT. The absorbance was measured at 550 nm in the Tecan plate reader against a blank without any cells.

2.10. Statistical analysis

At 21 days of age, animals were prepared for the sham-operated group (n = 12) as well as the carotid-ligated group (n = 14). Band intensities of Western blots were quantified using GelPro 3.1 or ImageJ and were expressed as percentage of the control levels (sham operated rats or control SH-SY5Y cells). Total protein amount, visualized using the stain-free technology of Biorad was quantified using the ImageLab 5.0 software (Biorad). Bar diagrams depict the mean of four independent quantifications of each sample of sham-operated (sham, n = 6) and ischemic (carotid, n = 8) animals ± SEM, correlated to total protein. A two way ANOVA with the factors of condition (sham, carotid) and region (hippocampus, striatum, cerebellum) or culture condition (20% O_2, 1% O_2, 24 h reox, 48 h reox) and treatment (control (scr), siGrx2, siTrx1) followed by Tukey HSD post hoc tests for pair-wise multiple comparisons were employed to analyze the statistical significance of changes in biochemical parameters and protein levels. The level of significance was set up at 5%. All analyses were performed using SPSS 15.0 (Chicago, IL, USA).

3. Results

3.1. Changes in Trx family protein expression and localisation following hypoxia/ischemia and reoxygenation induced by common carotid artery ligation

The expression pattern of the 14 Trx family proteins in carotid and sham operated animals was analyzed in cerebellum, striatum and hippocampus homogenates by Western blot or in the case of Grx2 by

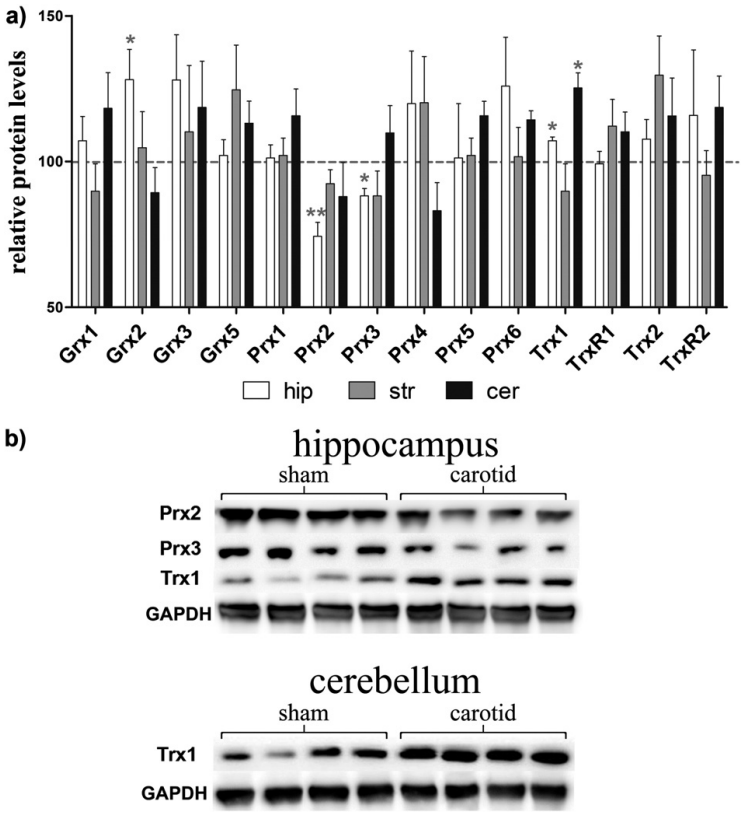

Fig. 1. Relative protein levels of Trx family and related proteins in carotid-ligated asphyxic and sham-operated control rats. Hippocampus (hip), striatum (str), and cerebellum (cer) were isolated and analyzed for protein levels by Western blot or in the case of Grx2 by a specific sandwich ELISA. a) The diagram depicts the relative protein levels of asphyxic animals stated in percent compared to sham-operated rats. b) Representative Western blots are illustrated for the groups showing a significant change. Bars represent the mean ± SEM of eight carotid and six sham rats. *$p \leq 0.05$, **$p \leq 0.01$ in respect to sham animals. Two way ANOVA [condition (sham, carotid) × brain region (hippocampus, striatum, cerebellum)] followed by Tukey HSD post hoc tests for pair-wise multiple comparisons were employed to analyze the statistical significance.

a specific sandwich ELISA (Fig. 1). All antibodies were evaluated thoroughly beforehand [43,44].

At 21 days of age (14 days post-surgery), the Western blot analysis showed increased levels of Grx2 and Trx1 and decreased levels of Prx2 and Prx3 in the hippocampus of carotid-clamped rats (Fig. 1). An increase in the protein amount of Trx1 was also observed in the cerebellum (Fig. 1). The immunohistochemical analysis of Grx2 resulted in a more intense staining throughout the entire hippocampus compared to the control group (Fig. 2a). In particular, the nuclei of the neurons displayed an increased Grx2 immunostaining. Staining for Prx2 was markedly decreased in the somata of the neurons of carotid-clamped animals in comparison to the sham group; this tendency was most pronounced in the CA1 area of the brain (Fig. 2b). Similar to Grx2, Trx1 immunostaining was increased in the extracellular matrix and possibly in the nuclei of the neurons in all areas of the hippocampus (Fig. 2c). The increased immunostaining of Grx2 and Trx1 suggested important functions in the protection and preservation of the neuronal phenotype and integrity.

3.2. The importance and effects of Trx1 and Grx2 in a cellular model of hypoxia-reoxygenation

To confirm this hypothesis and to analyze the role and effects of Trx1 and Grx2, we used a cellular model. In order to mimic hypoxic conditions, human neuroblastoma SH-SY5Y cells were cultivated for 24 h in an atmosphere containing 1% oxygen. In addition, cells were reoxygenated for 24 h or 48 h at 20% oxygen. Cells were harvested, lysed, and analyzed for Grx2 and Trx1 mRNA and protein levels by quantitative RT-PCR and Western blotting, respectively. Moreover, the levels of Hsp70 were assessed as a neuronal damage marker [46,47]. Hypoxia and reperfusion did not significantly affect the protein amounts of Grx2 or Trx1 at the analyzed time points (Fig. 3). The protein levels of HSP70, on the other hand, decreased continuously during the treatment to approx. 55% after 48 h of reoxygenation (Fig. 3).

To analyze the function of Grx2 and Trx1 during hypoxia/reoxygenation, we specifically silenced the expression of the redoxins using the RNA-interference technique (Fig. 4). We aimed at analyzing cell morphology, differentiation, proliferation and viability (Figs. 5 and 6). siRNA-silencing of Grx2c was originally developed in Hanschmann et al. [45], siRNA silencing of Trx1 was newly established here. Transfected SH-SY5Y cells were cultivated for 24 h at 1% oxygen, followed by up to 48 h of reoxygenation at 20% oxygen. The efficiency of the knock-down was assessed by quantitative RT-PCR, Western blot and ELISA. siRNA mediated silencing decreased the levels of both Trx1 and Grx2 mRNA to below 10% (Fig. 4a), Trx1 protein levels were down to below 6% (Fig. 4b) and the levels of Grx2 below 5% (quantified by ELISA as described in Hanschmann et al. [45]). In order to evaluate the differentiation state of the neuroblastoma cell line, we analyzed the protein levels of neurogenic differentiation 1 (NeuroD1), neurofilament M, and glial fibrillary acidic protein (GFAP) (Fig. 5a, b, c). NeuroD1 is a transcription factor that plays a key role in the moment in which cells acquire a specific neuronal subtype, and is essential for the differentiation and survival of neurons in the hippocampus [48]. Neurofilaments are proteins specifically expressed in neurons, where they stabilize the axon [49]. Neurofilaments M are intermediate filament proteins that play a key role in the maintenance of the neuronal phenotype [50]. GFAP is an intermediate filament protein specifically expressed in astroglia, the dominant and functionally most dynamic glial cell type [51,52]. In addition, we also analyzed the levels of HSP70 [46,47] and poly-ubiquitinylation of proteins [53–55] as markers for neuronal and protein damage, respectively (Fig. 5d, e). The knock-down cells were also analyzed for changes in their general phenotype by immunocytochemistry, staining microtubuli and F-actin (Fig. 6a). Cells transfected with an unspecific control (scrambled, scr) siRNA showed a normal SH-SY5Y phenotype. These cells appeared to increase in volume and length during the hypoxic period and maintained this phenotype during the reoxygenation phase (Fig. 6a). In parallel, viability and proliferation were analyzed using the MTT assay (Fig. 6b). After 24 h of reoxygenation, mitochondrial activity/proliferation increased and dropped again

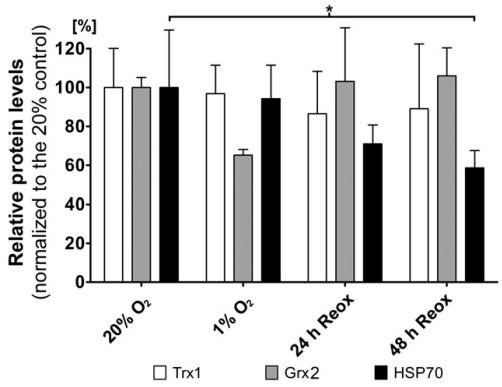

Fig. 3. Effect of hypoxia and reoxygenation on the levels of Grx2, Trx1, and HSP70 in SH-SY5Y cells. SH-SY5Y cells were cultured for 24 h in an atmosphere containing 20% O_2 or 1% O_2, respectively. Thereafter, both the normoxic and hypoxic cells were incubated for another 24 or 48 h at 20% O_2. The levels of Trx1, Grx2, and HSP70 were quantified by Western blotting and densitometric analysis. Three independent experiments were averaged, the SD is included.

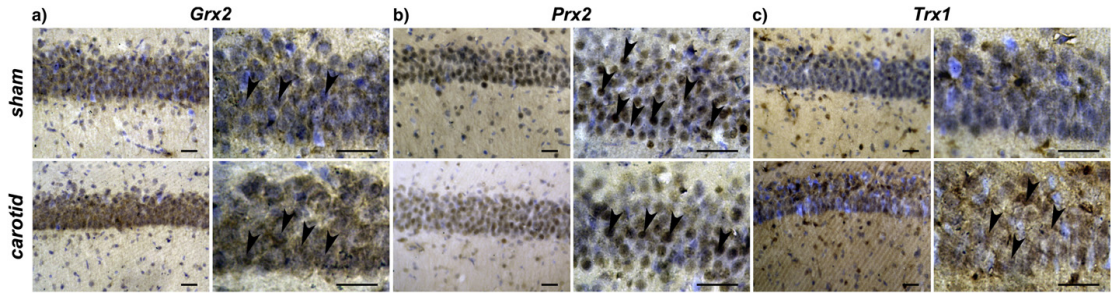

Fig. 2. Immunohistochemical analysis of the expression pattern of Trx family proteins in sham and carotid-ligated animals, 21 days after the ischemic insult. a) Representative immunostainings of Grx2 in the CA1 area of the hippocampus, arrowheads illustrate the differences in the nuclear staining following the induction of hypoxia/ischemia and reoxygenation. b) Representative pictures of Prx2 staining of the CA1 area of the hippocampus, arrowheads indicate the reduction seen in the labeling for Prx2-positive cellular bodies. c) Representative stainings for Trx1 in the CA1 area of the hippocampus, arrowheads show the faint labeling for Trx1-positive cellular bodies. Hematoxylin was used for nuclear staining. n = 6 sham and 6 carotid animals. Scale bars = 50 μm.

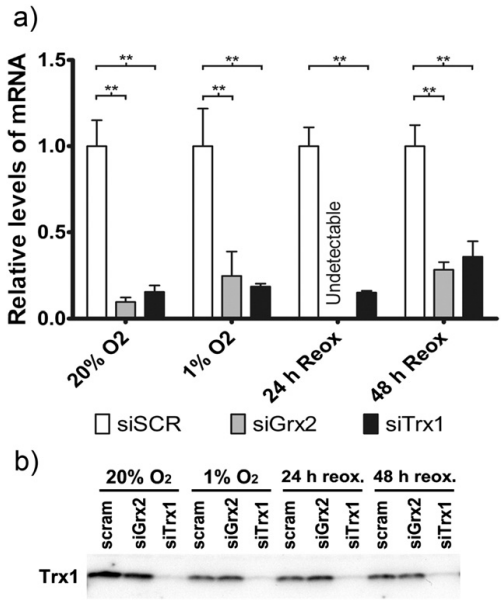

Fig. 4. Knock-down efficiency of Grx2 and Trx1 silencing. The efficiency of the knock-down of Grx2 and Trx1 was assessed by measuring of mRNA levels by means of quantitative RT-PCR (a), western Blot (b), and ELISA. Bars represent the mean ± SD. **$p \leq 0.01$. Two way ANOVA [condition (20% O_2, 1% O_2, 24 h reox, 48 h reox) × treatment (control (scr), siGrx2, siTrx1)] followed by Tukey HSD post hoc tests for pair-wise multiple comparisons were employed to analyze the statistical significance.

during the extended reoxygenation phase, compared to controls that did not undergo the hypoxic treatment, but were grown for the same time lapses. NeuroD1 levels were significantly increased after 48 h of reoxygenation (Fig. 5a, f), whereas the levels of neurofilament M were slightly decreased during the reoxygenation period (Fig. 5b, f). The protein levels (see 20% O_2, siGrx2) were strongly decreased during hypoxia and reoxygenation (Fig. 5c, f). The protein amount of HSP70 was decreased by 20-30% following reoxygenation (Fig. 5d, f). Poly-ubiquitination was quantified densiometrically from Western-blots. Noteworthy, even under basal conditions, silencing of Trx1 led to an increase in poly-ubiquitinated proteins (Fig. 5e).

Grx2 silencing led to an increase in cell soma (Fig. 6a) and induced the formation of F-actin in filopodia like structures, both in the hypoxic group and the reoxygenation groups. (Fig. 6a) [55]. The lack of Grx2 increased mitochondrial activity/proliferation by approx. 25% under generally all conditions (Fig. 6b). NeuroD1 expression was increased under normal conditions as well as following reoxygenation (Fig. 5 a, f). The levels of neurofilament M were decreased under all conditions in the absence of Grx2 in comparison to the control (scr) siRNA group cultured in an atmosphere containing 20% oxygen (Fig. 5b, f). GFAP levels were decreased during hypoxia and following 48 h reoxygenation under normal cultivation conditions (control (scr) group). Grx2 silencing led to a decrease in GFAP levels both after silencing under normal conditions (see 20% O_2, siGrx2) and following reoxygenation in comparison to the 20% O_2 control (scr) group. During the hypoxic period siGrx2 cells displayed similar levels of GFAP compared to the 20% O_2 control (scr) group (Fig. 5c, f). Surprisingly, silencing of the Grx2 expression decreased HSP70 levels under all conditions analyzed for Grx2 silencing in comparison to the 20% O_2 control (scr) group (Fig. 5d, f). Moreover, the lack of Grx2 led to an increase in poly-ubiquitinated proteins, compared to the controls that were cultured under the same conditions. Interestingly, the strongest relative increase was seen at 48 h of reoxygenation (Fig. 5e).

Trx1 silencing showed some morphological alterations, most of all elongated neurites—even under normoxic conditions (Fig. 6a). Using the MTT assay, we could show that the lack of Trx1 led to a slight decrease in mitochondrial activity/proliferation of about 15% under essentially all conditions (Fig. 6b). Silencing of Trx1 did not significantly influence the levels of NeuroD1 following hypoxia and reoxygenation in comparison to the 20% O_2 control (scr) group (Fig. 5a, f), meaning that the levels of NeuroD1 increased after 48 h of reoxygenation regardless of the presence of Trx1. However, the levels of neurofilament M were clearly decreased both after Trx1 silencing in the 20% oxygen group compared to the 20% O_2 control (scr) (Fig. 5b,f), as well as after 48 h reoxygenation in both the control (scr) and the siTrx1 group in comparison with their respective 20% oxygen group. On the contrary, the levels of GFAP were more than three-fold increased following reoxygenation after Trx1 silencing (Fig. 5c, f). Trx1 silencing, by itself, had no significant effect on the levels of HSP70 in the 20% oxygen group in comparison to the 20% O_2 control (scr) group. Nonetheless, after reoxygenation Trx1 silencing led to an increase in the protein levels of HSP70 (Fig. 5d, f). In addition, the lack of Trx1 led to a general increase in poly-ubiquitinated proteins, compared to the control (scr) groups (Fig. 5e).

4. Discussion

Reperfusion after an ischemic event leads to an increased production of ROS [56,57], that have been proposed as causative agent for the death and degeneration of neurons following the insult [14,15, 57,58]. We have previously shown that Trx family (and related) proteins are distributed in a highly region and cell-type specific manner in the rat and mouse CNS [43,44], implying specific functions and a complex crosstalk between the Trx family members. Trx1 immunohistochemistry in gerbil brains during reperfusion following transient ischemia demonstrated an induction of Trx in hippocampal glial cells not seen in control animals [59]. Brain ischemia in rats, as a consequence of middle cerebral artery occlusion, leads to a decrease in Trx staining in ischemic areas, while immunoreaction and mRNA for Trx was increased in the penumbra regions [60]. Transgenic mice overexpressing human Trx1 and submitted to focal cerebral ischemia showed smaller infarct areas and fewer neuronal deficits than wild type mice [24]. In a similar manner, the loss of Grx1 correlated with neuronal damage following middle cerebral artery occlusion [61]. Trx2 overexpression protects from an oxidative insult-induced NF-κB activation and apoptosis [62]. In the present study, we examined the regulation and potential functions of 14 proteins of this family in an animal model and analyzed the function of particular redoxins in a cellular model of perinatal asphyxia, with the aim to better understand the regulation and potential roles of the proteins in the cellular pathways triggered by the hypoxic insult.

Hypoxic insults induce molecular and cellular changes, affecting cell morphology, cell polarity, osmoregulation, protein synthesis and the release of neurotransmitters [63,64]. The reoxygenation phase causes rapid changes in the redox properties of the affected tissue and an increase in the cytokine and chemokine levels, as well as the infiltration of immune cells [65]. Not surprisingly, members of the Trx family have been described to protect against ischemic injuries. Overexpression of Trx1, Grx1, Grx2, and Prx2 were shown to attenuate ischemic damage of neurons [66–68]. Moreover, Trx family proteins could function in a systemic inflammatory response, due to their versatile extra- and intracellular functions [18].

In the murine animal model, we detected complex and tissue-specific changes in the expression and distribution of distinct proteins following the hypoxic insult. Notably, the analyzed protein levels did not change uniformly, but highly specific for the region and cell type. Although no studies on Trx family proteins in PA have been published, both the release of ROS and RNS have been demonstrated under this

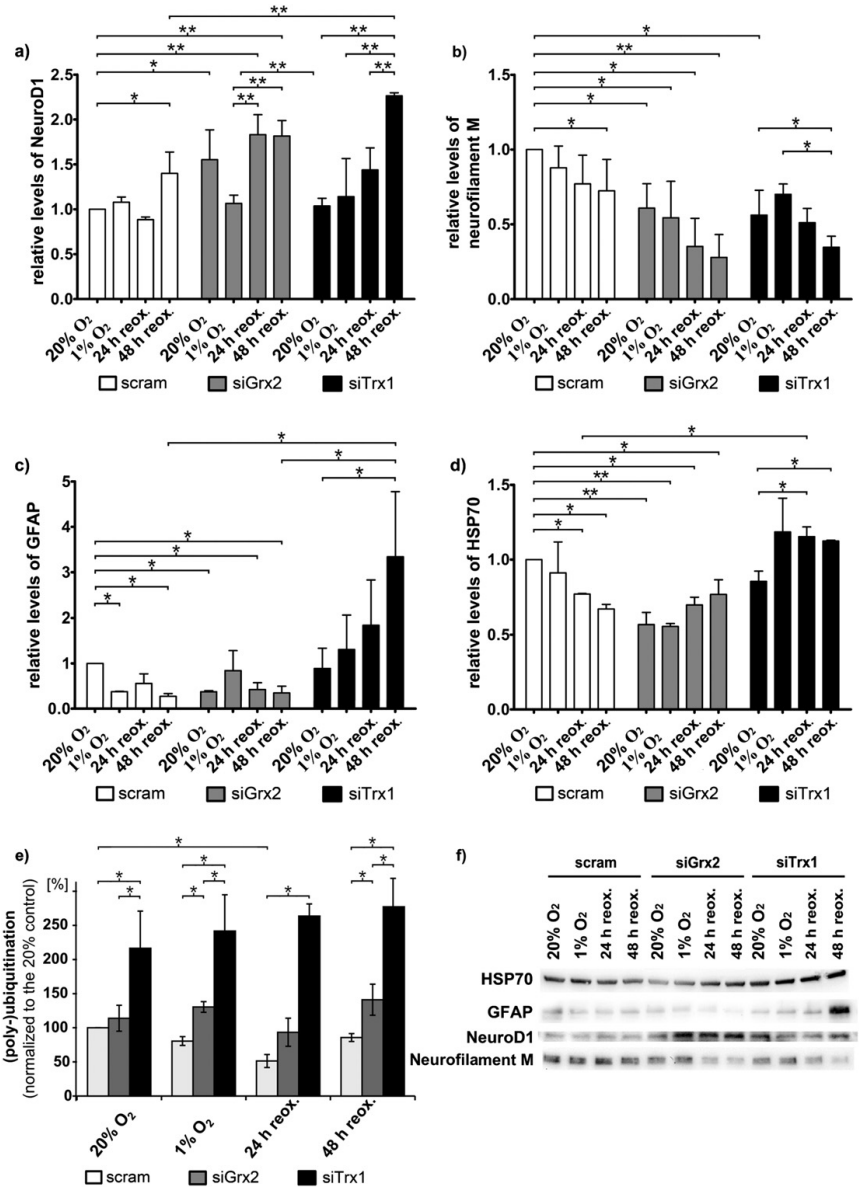

Fig. 5. Modulation of Trx1 and Grx2 expression in SH-SY5Y cells submitted to hypoxia and reoxygenation. Following transient knock-down of hTrx1 (siTrx1) and hGrx2 (siGrx2) using specific siRNAs, SH-SY5Y cells were cultured for 24 h in an atmosphere containing 20% O_2 or 1% O_2, respectively. The latter were reoxygenated at 20% O_2 for 24 h and 48 h. Cells transfected with an unspecific control siRNA (control (scr)) were used as control. The protein levels of neurogenic differentiation 1 (NeuroD1) (a, f), neurofilament M (b, f), glial fibrillary acidic protein (GFAP) (c, f), heat shock protein 70 (HSP70) (d, f), and poly-ubiquitinylation (e), were analyzed by Western Blot showing the hypoxia/reoxygenation-induced cellular damage and the state of differentiation. Densitometric quantification against total protein amount using the stain-free technology (Biorad) from three independent experiments are depicted. Relative protein levels are illustrated, comparing all treatments to control (scr) cells cultured at 20% O_2. Bars represent the mean ± SEM. *$p \leq 0.05$, **$p \leq 0.01$. Two way ANOVA [condition (20% O_2, 1% O_2, 24 h reox, 48 h reox) × treatment (control (scr), siGrx2, siTrx1)] followed by Tukey HSD post hoc tests for pair-wise multiple comparisons were employed to analyze the statistical significance.

condition [14], potentially leading to the dysregulation of redox signaling, which could be responsible for the induction of apoptosis and de-differentiation in the CNS and thus the long-term neurological deficits. The disruption of redox control or generally the generation of ROS by uncoupling of the mitochondrial chain [69] and inflammation [70,71] were described as the most destructive causes of hypoxia/ischemia and reoxygenation injury.

The thioredoxin system is a key regulator of cellular redox responses and was shown to be altered in different models of ischemia. Trx1 was shown to be up-regulated in the hippocampus of gerbil after transient

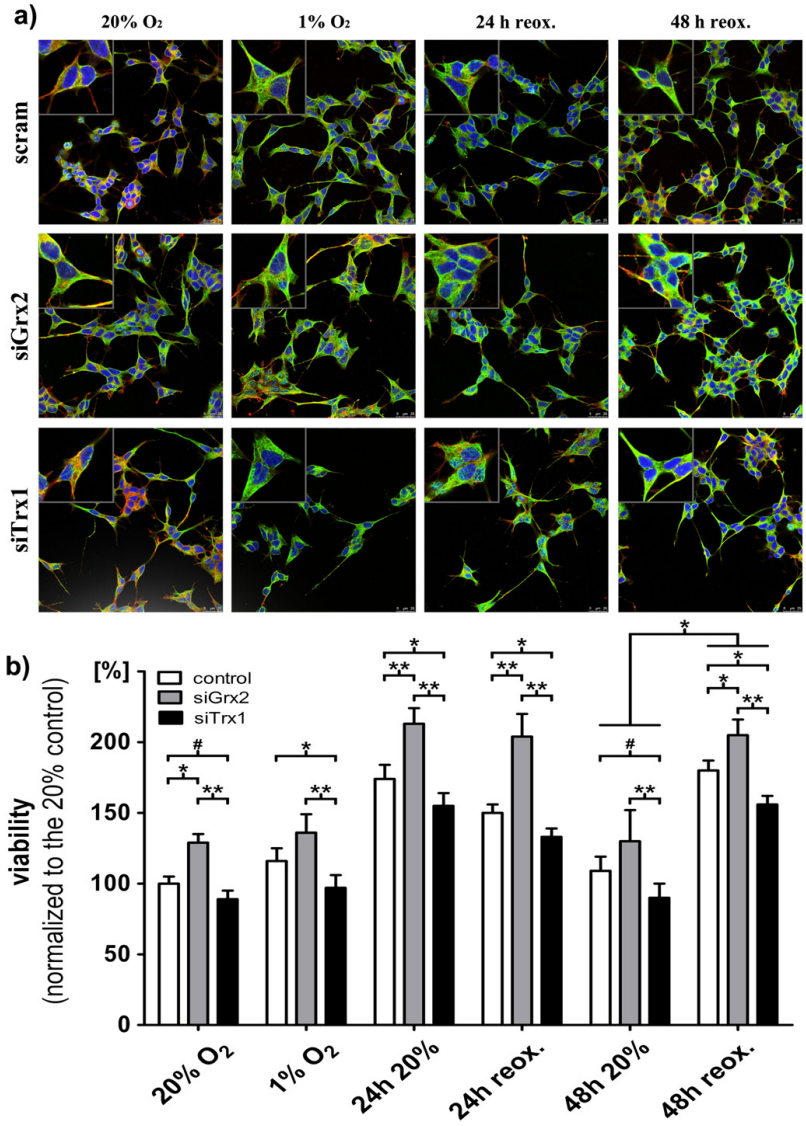

Fig. 6. Morphological evaluation of SH-SY5Y cells after modulation of Trx1 and Grx2 expression. Following transient knock-down of hTrx1 (siTrx1) and hGrx2 (siGrx2) using specific siRNAs, SH-SY5Y cells were cultured for 24 h in an atmosphere containing 20% O_2 or 1% O_2, respectively. The latter were reoxygenated at 20% O_2 for 24 h and 48 h. Cells transfected with an unspecific control (scr) siRNA were used as control. (a) Cells were fixed and analyzed for cytoskeleton changes by immunofluorescence using an antibody against tubulin and phalloidin staining for F-Actin. Five layers in the volume $z = 0.5$ μm were scanned by confocal microscopy. Red: phalloidin, green: tubulin, blue: DAPI. Representative pictures from $n = 4$ independent experiments are shown. Scale bars: 25 μm. (b) The cell number as a measure of viability and proliferation was analyzed using the MTT assay with cell cultured in 96 well plates. Three independent experiments were performed with six replicates each. The data were normalized to the 20% oxygen control at time point zero. Bars represent the mean ± SD. #$p \leq 0.06$, *$p \leq 0.05$, **$p \leq 0.01$. Two way ANOVA [condition (20% O_2, 1% O_2, 24 h 20%, 24 h reox, 48 h 20%, 48 h reox) × treatment (control (scr), siGrx2, siTrx1)] followed by Tukey HSD post hoc tests for pair-wise multiple comparisons were employed to analyze the statistical significance.

cerebral ischemia [59]. After occlusion of the middle cerebral artery, rats displayed an increased expression of Trx1 in the perifocal regions of ischemia [60]. Moreover, transgenic mice overexpressing human Trx1 that suffered a focal cerebral ischemia showed a reduction in the damage as well as lower neuronal deficits than wild type mice [24]. The MDA-MB-231 breast cancer cell line grown in hypoxia showed an increase in Trx1 expression after reoxygenation. When these cells were subjected to hypoxic cyclic preconditioning pre-treatment, the Trx1 expression levels were even higher [72]. Trx2 overexpression was shown to reduce TNF-L, normally induced by ROS, which in turn leads to NF-κB activation and apoptosis [62]. In a model for renal ischemia-reperfusion, Grx2, Prx3 and Prx6 were highly expressed in the proximal tubule cells of the kidney, which can regenerate following an ischemic insult. Interestingly, the overexpression of these proteins in

HeLa and HEK293 cells protected them from hypoxia/reoxygenation-induced oxidative damage and increased the total cell number following the ischemia [40]. Both Prx1 and Prx5 were induced after treatment with hydrogen peroxide or hypoxia. Silencing of Prx1, and Prx5 expression sensitized cells to oxidative insults [73]. All these data indicate that modulation of the Trx family of proteins is an important target for the protection of cells from an oxidative insult, but might also reveal new insights in the regenerative capacities and underlying mechanisms of specific cell types.

In our study, the immunostaining of Trx1 was increased following hypoxia/ischemia and reoxygenation in the areas of the hippocampus and cerebellum of the brain (see Fig. 1). Although the effect of severe hypoxia on the expression of the cytosolic Trx1 in the brain has been shown in preconditioned rats at 24 h and 72 h after reperfusion [61, 74], no study has been performed at extended periods after reperfusion. The expression of Grx2 also increased significantly after hypoxia/ischemia and reoxygenation in the carotid-clamped group (see Fig. 1). As mentioned above, the induction of the expression of the oxidoreductase was also shown in a model for renal ischemia reperfusion injury [40]. Besides the anti-apoptotic function of mitochondrial Grx2a [75,76], cytosolic Grx2c was recently shown to be essential for embryonic brain development. Zebrafish with silenced expression of the oxidoreductase were characterized by the loss of basically all types of neurons due to apoptosis and a developed axonal scaffold [77]. Moreover, the cytosolic isoform Grx2c, has been shown to be involved in axonal outgrowth and neuronal differentiation [77,78]. We believe that Grx2 expression might be induced in an attempt to recover the system from the hypoxic-ischemic insult. Grx2 could be crucial for the long term regeneration of physiological redox signaling and the recovery of the affected tissues.

Surprisingly, Grx2 silencing had no such effect in the SH-SY5Y cells. After having been subjected to hypoxia, SH-SY5Y cells showed a reduction of the HSP70 levels under all conditions relative to the 20% O_2 control (scr) group (see Fig. 5d). Upon different stimuli, cells activate the so called unfolded protein response (UPR), allowing an initial response that leads to the restoration of the normal functions of the ER by the induction of heat shock proteins. However, this response needs to be tightly controlled; otherwise it can lead to the induction of cell death through the activation of the apoptotic pathway associated to the ER [47,79]. Therefore, high levels of the marker HSP70 (an ER chaperone), can be used as indicator of ER stress and are also generally used as neuronal damage marker [46]. In this manner, the reduction of HSP70 levels due to Grx2 silencing was unexpected and seemed like an unusual behavior considering that Grx2 has been implicated in anti-apoptotic signaling before [48,51]. However, when analyzed for poly-ubiquitination (Fig. 5 e), a marker for protein damage, the lack of Grx2 led to an increase in ubiquitination under all conditions. In comparison, Trx1 silencing had no significant effect on the levels of HSP70 under normoxic conditions. However, following reoxygenation Trx1 silencing induced an increase in the cellular HSP70 levels (Fig. 5d, f). Also, silencing of Trx1 led to an increase in poly-ubiquitinated proteins, compared to the controls (Fig. 5e). Taking all this together, the expression of Grx2 and Trx1 seems to contribute to protect neuronal cells from hypoxia-induced protein and cellular damage. Interestingly, the knock-down of Trx1 also affects cellular proliferation and viability as analyzed by the MTT assay. Following the hypoxia and reoxygenation, a decrease of approximately 15% in mitochondrial activity/proliferation was detected in Trx1 knock-down cells (Fig. 6b), indicating a reduction in cell number and/or a decreased viability which could be due to elevated levels of cellular damage. Surprisingly, Grx2 knock-down, which was shown before to sensitize cells towards distinct oxidative stimuli [76], led to an overall elevated mitochondrial activity/proliferation following the hypoxia and reoxygenation. Thus, the lower extent of cellular damage is reflected in the overall higher mitochondrial activity/proliferation of Grx2 depleted cells following the ischemic insult, compared to control cells but also compared to Trx1 depleted cells.

In our SH-SY5Y cell model we could not detect any significant changes in the protein levels of Trx1 and Grx2 when exposing the cells to hypoxia and reoxygenation (see Fig. 3). Nonetheless, when the protein levels were manipulated by RNA interference it was possible to observe functional consequences (see Figs. 5 and 6), supporting the hypothesis that both *in vivo* and *in vitro* these redoxins could have an important role in the recovery after a hypoxia and reoxygenation event.

Oxygen concentrations and ROS levels are not only known to affect cell viability, but also to affect and regulate embryonic development and cellular differentiation. NeuroD1 is a transcription factor that regulates several cells differentiation pathways, for instance, the differentiation of neuronal cells that contribute to the formation and maintenance of the cerebellum or the hippocampus [80]. While its levels were unaffected by hypoxia in our cellular model, they were increased in all samples following reoxygenation, slightly more pronounced in the absence of Trx1. Neurofilament M is an intermediate filament protein that contributes to the maintenance of the neuronal phenotype [50]; GFAP is an intermediary filament protein that is specifically expressed in astrocytes [52]. Both the lack of Grx2 and Trx1 led to a significant reduction in neurofilament M levels compared to the control siRNA 20% O_2 group as well as the siGrx2 and siTrx1 20% O_2 groups. Grx2 silencing also led to a reduction in GFAP both following silencing under normal conditions as well as following reoxygenation in comparison to the 20% O_2 control. However, silencing of the Trx1 expression led to a strong, highly significant increase in the protein levels of GFAP. SH-SY5Y cells are derived from a neuroblastoma patient and frequently used as a model for neuronal differentiation and function. These cells can be maintained in a rather undifferentiated state but can also develop a neuron-like adrenergic and dopamine-sensitive phenotype [81]. Our results suggest that in the absence of Grx2 or Trx1 the cells undergo differentiation into what appears to be a more glial-like cell type, following hypoxia and reoxygenation, as shown by the decreased neurofilament M and GFAP levels (particularly in the absence of Trx1). Grx2, for instance, was shown to be expressed in both, neurons and glia cells of the mouse brain [82]. It is tempting to speculate that both redoxins have distinct function in both neurons and glia cells and that they can also function in the development of distinct cell types within the brain. Changes in the protein levels might affect the differentiation state of a cell, and thereby also the susceptibility towards the ischemic insult.

Prx2 immunostaining was consistently reduced in the carotid-clamped animals. Depletion of Prx2 had exhibited potent pro-survival effects in ischemic neurons by indirectly maintaining Trx in its reduced state [83]. In this respect, the low levels of Prx2 found in the present study could be related to high amounts of active Trx1.

The role of Trx family proteins in hypoxia is not well understood. Previous studies have shown that the Trx family of proteins contributes to mechanisms of brain tolerance in early periods after exposure to stress [74,84]. Cells have developed response mechanisms to cope with these low oxygen concentrations. Hypoxia-inducible factors 1 and 2 constitute transcription factors that regulate the expression of more than 180 genes under hypoxic conditions [85]. The HIF-1 target ATIA (anti-TNFa-induced-apoptosis) was shown to protect cells against hypoxia-induced apoptosis via Trx2 and the generation of ROS [86]. Moreover, hypoxia-induced mitochondrial ROS are essential for HIF activation [87,88], regulate inflammatory responses via interleukin (IL)-6 [89], and apoptosis via p38 phosphorylation [90]. Other studies suggested that overexpression of Trx1 leads to elevated HIF-1α levels in cells cultured under both normoxic and hypoxic conditions, whereas inhibition of TrxR1 activity blocked the activation of HIF-1α [91]. Trx1 leads to an induction of HIF-1α, possibly by activating Akt [92]. Trx1 might also be involved in depleting HIF-1α levels upon reoxygenation [93].

Not all areas of the brain are equally vulnerable to hypoxia-ischemia. Among the most vulnerable areas are the superior brainstem, cerebellum, white matter and subcortical structures supplied by the distal

branches of deep and superficial penetrating blood vessels, cerebral white matter at the zones between the major cerebral artery territories, CA1 region of the hippocampus, and neocortical layers 3, 5, and 6 [94–96]. The expression pattern of the Trx family proteins changed in the most vulnerable areas of the brain, particularly in the hippocampus and cerebellum. Interestingly, by IHC we were able to observe an overall stronger immunostaining for Trx1 in the hippocampus, not only in the cytosol but also what appears to be a nuclear staining. Moreover, it is tempting to speculate that the overall higher background in the tissue of the asphyxic animals, compared to sham control rats, is due to Trx1 secretion into the extracellular space (see Fig. 2c). This is particularly interesting considering that Trx1 secretion [24,97–101], as well as its nuclear translocation [24,102–107] have been implicated in regulating cell proliferation, differentiation, and apoptosis. These findings imply that these proteins could be clinically applied as a therapeutic strategy to counteract the hypoxia/ischemia and reoxygenation damage. Beneficial effects of the administration of the Trx family of protein after a hypoxia-reperfusion injury in an adult model of stroke have been demonstrated already [108,109].

Transparency document

The Transparency document associated with this article can be found, in the online version.

Acknowledgments

This work was supported by the Deutsche Forschungsgemeinschaft (SFB593-N01, LI984/3-1, and GRK1947-A1) to CHL, the Federal Ministry for Science and Education (BMBF: 01DN13023-PAREDOX) and MINCYT to CHL and FC, the German Academic Exchange Service DAAD and MINCYT (PROALAR program) to CHL and FC, the 5 (PIP 1142010010019, CONICET, Argentina) to FC, and the University of Buenos Aires (UBACYT 20020090100118) to FC. JIR and MIH are fellowship holders from the National Scientific and Technical Research Council (CONICET, Argentina). None of the authors have any conflict of interest to report related to this manuscript.

References

[1] K.B. Nelson, J.K. Grether, Potentially asphyxiating conditions and spastic cerebral palsy in infants of normal birth weight, Am. J. Obstet. Gynecol. 179 (1998) 507–513.
[2] N. Paneth, The causes of cerebral palsy. Recent evidence, Clinical and investigative medicine, Med. Clin. Exp. 16 (1993) 95–102.
[3] J.E. Rice III, R.C. Vannucci, J.B. Brierley, The influence of immaturity on hypoxic-ischemic brain damage in the rat, Ann. Neurol. 9 (1981) 131–141.
[4] L. Titomanlio, A. Kavelaars, J. Dalous, S. Mani, V. El Ghouzzi, C. Heijnen, O. Baud, P. Gressens, Stem cell therapy for neonatal brain injury: perspectives and challenges, Ann. Neurol. 70 (2011) 698–712.
[5] W. McGuire, Perinatal asphyxia, Clin. Evid. (2006) 511–519.
[6] S. Levine, Anoxic-ischemic encephalopathy in rats, Am. J. Pathol. 36 (1960) 1–17.
[7] F. Lopez-Aguilera, M.G. Plateo-Pignatari, V. Biaggio, C. Ayala, A.M. Seltzer, Hypoxic preconditioning induces an AT2-R/VEGFR-2(Flk-1) interaction in the neonatal brain microvasculature for neuroprotection, Neuroscience 216 (2012) 1–9.
[8] H. Taniguchi, K. Andreasson, The hypoxic-ischemic encephalopathy model of perinatal ischemia, J. Vis. Exp. 19 (21) (2008) http://dx.doi.org/10.3791/955 (Nov 19) pii: 955.
[9] Y. Wang, P.T. Cheung, G.X. Shen, E.X. Wu, G. Cao, I. Bart, W.H. Wong, P.L. Khong, Hypoxic-ischemic brain injury in the neonatal rat model: relationship between lesion size at early MR imaging and irreversible infarction, AJNR, Am. J. Neuroradiol. 27 (2006) 51–54.
[10] S.G. Benitez, A.E. Castro, S.I. Patterson, E.M. Munoz, A.M. Seltzer, Hypoxic preconditioning differentially affects GABAergic and glutamatergic neuronal cells in the injured cerebellum of the neonatal rat, PLoS One 9 (2014) e102056.
[11] J.W. Calvert, W. Yin, M. Patel, A. Badr, G. Mychaskiw, A.D. Parent, J.H. Zhang, Hyperbaric oxygenation prevented brain injury induced by hypoxia-ischemia in a neonatal rat model, Brain Res. 951 (2002) 1–8.
[12] H. Hagberg, R. Ichord, C. Palmer, J.Y. Yager, S.J. Vannucci, Animal models of developmental brain injury: relevance to human disease. A summary of the panel discussion from the Third Hershey Conference on Developmental Cerebral Blood Flow and Metabolism, Dev. Neurosci. 24 (2002) 364–366.
[13] R.C. Vannucci, S.J. Vannucci, Perinatal hypoxic-ischemic brain damage: evolution of an animal model, Dev. Neurosci. 27 (2005) 81–86.
[14] F. Capani, C.F. Loidl, F. Aguirre, L. Piehl, G. Facorro, A. Hager, T. De Paoli, H. Farach, J. Pecci-Saavedra, Changes in reactive oxygen species (ROS) production in rat brain during global perinatal asphyxia: an ESR study, Brain Res. 914 (2001) 204–207.
[15] G. Buonocore, S. Perrone, R. Bracci, Free radicals and brain damage in the newborn, Biol. Neonate 79 (2001) 180–186.
[16] L. Shalak, J.M. Perlman, Hypoxic-ischemic brain injury in the term infant-current concepts, Early Hum. Dev. 80 (2004) 125–141.
[17] A.D. Edwards, H. Mehmet, Apoptosis in perinatal hypoxic-ischaemic cerebral damage, Neuropathol. Appl. Neurobiol. 22 (1996) 494–498.
[18] E.M. Hanschmann, J.R. Godoy, C. Berndt, C. Hudemann, C.H. Lillig, Thioredoxins, glutaredoxins, and peroxiredoxins–molecular mechanisms and health significance: from cofactors to antioxidants to redox signaling, Antioxid. Redox Signal. 19 (2013) 1539–1605.
[19] J.V. Bonventre, J.M. Weinberg, Recent advances in the pathophysiology of ischemic acute renal failure, J. Am. Soc. Nephrol. 14 (2003) 2199–2210.
[20] E.N. Wardle, Cellular oxidative processes in relation to renal disease, Am. J. Nephrol. 25 (2005) 13–22.
[21] R.D. Higgins, S. Shankaran, Hypothermia: novel approaches for premature infants, Early Hum. Dev. 87 (Suppl. 1) (2011) S17–S18.
[22] M.C. Lai, S.N. Yang, Perinatal hypoxic-ischemic encephalopathy, J. Biomed. Biotechnol. 2011 (2011) 609813.
[23] A. Holmgren, Thioredoxin and glutaredoxin systems, J. Biol. Chem. 264 (1989) 13963–13966.
[24] C.H. Lillig, A. Holmgren, Thioredoxin and related molecules–from biology to health and disease, Antioxid. Redox Signal. 9 (2007) 25–47.
[25] J.L. Martin, Thioredoxin–a fold for all reasons, Structure 3 (1995) 245–250.
[26] T.C. Laurent, E.C. Moore, P. Reichard, Enzymatic synthesis of deoxyribonucleotides. IV. Isolation and characterization of thioredoxin, the hydrogen donor from *Escherichia coli* B, J. Biol. Chem. 239 (1964) 3436–3444.
[27] E.S. Arner, Focus on mammalian thioredoxin reductases–important selenoproteins with versatile functions, Biochim. Biophys. Acta 1790 (2009) 495–526.
[28] E.S. Arner, A. Holmgren, Physiological functions of thioredoxin and thioredoxin reductase, Eur. J. Biochem. 267 (2000) 6102–6109.
[29] L. Zhong, A. Holmgren, Essential role of selenium in the catalytic activities of mammalian thioredoxin reductase revealed by characterization of recombinant enzymes with selenocysteine mutations, J. Biol. Chem. 275 (2000) 18121–18128.
[30] A. Nishiyama, M. Matsui, S. Iwata, K. Hirota, H. Masutani, H. Nakamura, Y. Takagi, H. Sono, Y. Gon, J. Yodoi, Identification of thioredoxin-binding protein-2/vitamin D(3) up-regulated protein 1 as a negative regulator of thioredoxin function and expression, J. Biol. Chem. 274 (1999) 21645–21650.
[31] S. Watabe, Y. Makino, K. Ogawa, T. Hiroi, Y. Yamamoto, S.Y. Takahashi, Mitochondrial thioredoxin reductase in bovine adrenal cortex its purification, properties, nucleotide/amino acid sequences, and identification of selenocysteine, Eur. J. Biochem. 264 (1999) 74–84.
[32] C.H. Lillig, C. Berndt, A. Holmgren, Glutaredoxin systems, Biochim. Biophys. Acta 1780 (2008) 1304–1317.
[33] A. Rubartelli, A. Bajetto, G. Allavena, E. Wollman, R. Sitia, Secretion of thioredoxin by normal and neoplastic cells through a leaderless secretory pathway, J. Biol. Chem. 267 (1992) 24161–24164.
[34] S.G. Rhee, S.W. Kang, T.S. Chang, W. Jeong, K. Kim, Peroxiredoxin, a novel family of peroxidases, IUBMB Life 52 (2001) 35–41.
[35] B. Hofmann, H.J. Hecht, L. Flohe, Peroxiredoxins, Biol. Chem. 383 (2002) 347–364.
[36] Z.A. Wood, E. Schroder, J. Robin Harris, L.B. Poole, Structure, mechanism and regulation of peroxiredoxins, Trends Biochem. Sci. 28 (2003) 32–40.
[37] K.M. Harris, F.E. Jensen, B. Tsao, Three-dimensional structure of dendritic spines and synapses in rat hippocampus (CA1) at postnatal day 15 and adult ages: implications for the maturation of synaptic physiology and long-term potentiation, J. Neurosci. 12 (1992) 2685–2705.
[38] K. Chiu, W.M. Lau, H.T. Lau, K.F. So, R.C. Chang, Micro-dissection of rat brain for RNA or protein extraction from specific brain region, J.Vis. Exp. (2007) 269.
[39] G. Paxinos, C. Watson, The Rat Brain: In Stereotaxic Coordinates, Academic Press, Incorporated, 1998.
[40] J.R. Godoy, S. Oesteritz, E.M. Hanschmann, W. Ockenga, W. Ackermann, C.H. Lillig, Segment-specific overexpression of redoxins after renal ischemia and reperfusion: protective roles of glutaredoxin 2, peroxiredoxin 3, and peroxiredoxin 6, Free Radic. Biol. Med. 51 (2011) 552–561.
[41] A. Gurtler, N. Kunz, M. Gomolka, S. Hornhardt, A.A. Friedl, K. McDonald, J.E. Kohn, A. Posch, Stain-Free technology as a normalization tool in Western blot analysis, Anal. Biochem. 433 (2013) 105–111.
[42] J.E. Gilda, A.V. Gomes, Stain-Free total protein staining is a superior loading control to beta-actin for Western blots, Anal. Biochem. 440 (2013) 186–188.
[43] M.L. Aon-Bertolino, J.I. Romero, P. Galeano, M. Holubiec, M.S. Badorrey, G.E. Saraceno, E.M. Hanschmann, C.H. Lillig, F. Capani, Thioredoxin and glutaredoxin system proteins-immunolocalization in the rat central nervous system, Biochim. Biophys. Acta 1810 (2011) 93–110.
[44] J.R. Godoy, M. Funke, W. Ackermann, P. Haunhorst, S. Oesteritz, F. Capani, H.P. Elsasser, C.H. Lillig, Redox atlas of the mouse. Immunohistochemical detection of glutaredoxin-, peroxiredoxin-, and thioredoxin-family proteins in various tissues of the laboratory mouse, Biochim. Biophys. Acta 1810 (2011) 2–92.
[45] E.M. Hanschmann, M.E. Lonn, L.D. Schutte, M. Funke, J.R. Godoy, S. Eitner, C. Hudemann, C.H. Lillig, Both thioredoxin 2 and glutaredoxin 2 contribute to the reduction of the mitochondrial 2-Cys peroxiredoxin Prx3, J. Biol. Chem. 285 (2010) 40699–40705.

[46] S. Carloni, M.C. Albertini, L. Galluzzi, G. Buonocore, F. Proietti, W. Balduini, Increased autophagy reduces endoplasmic reticulum stress after neonatal hypoxia-ischemia: role of protein synthesis and autophagic pathways, Exp. Neurol. 255 (2014) 103–112.

[47] S. Oyadomari, M. Mori, Roles of CHOP/GADD153 in endoplasmic reticulum stress, Cell Death Differ. 11 (2004) 381–389.

[48] T. Miyata, T. Maeda, J.E. Lee, NeuroD is required for differentiation of the granule cells in the cerebellum and hippocampus, Genes Dev. 13 (1999) 1647–1652.

[49] P.N. Hoffman, D.W. Cleveland, J.W. Griffin, P.W. Landes, N.J. Cowan, D.L. Price, Neurofilament gene expression: a major determinant of axonal caliber, Proc. Natl. Acad. Sci. U. S. A. 84 (1987) 3472–3476.

[50] J.M. Dale, M.L. Garcia, Neurofilament phosphorylation during development and disease: which came first, the phosphorylation or the accumulation? J. Amino Acids 2012 (2012) 382107.

[51] H. Sun, Q. Su, H. Zhang, W. Liu, H. Zhang, D. Ding, Z. Zhu, H. Li, Alterations of proliferation and differentiation of hippocampal cells in prenatally stressed rats, Brain Dev. (2014)http://dx.doi.org/10.1016/j.braindev.2014.09.007 (Oct 7) pii: S0387-7604(14)00219-8. [Epub ahead of print].

[52] J. Middeldorp, E.M. Hol, GFAP in health and disease, Prog. Neurobiol. 93 (2011) 421–443.

[53] T. Mengesdorf, P.H. Jensen, G. Mies, C. Aufenberg, W. Paschen, Down-regulation of parkin protein in transient focal cerebral ischemia: a link between stroke and degenerative disease? Proc. Natl. Acad. Sci. U. S. A. 99 (2002) 15042–15047.

[54] J.J. Liu, H. Zhao, J.H. Sung, G.H. Sun, G.K. Steinberg, Hypothermia blocks ischemic changes in ubiquitin distribution and levels following stroke, Neuroreport 17 (2006) 1691–1695.

[55] F. Capani, G.E. Saraceno, V. Botti, L. Aon-Bertolino, D.M. de Oliveira, G. Barreto, P. Galeano, L.D. Giraldez-Alvarez, H. Coirini, Protein ubiquitination in postsynaptic densities after hypoxia in rat neostriatum is blocked by hypothermia, Exp. Neurol. 219 (2009) 404–413.

[56] E.S. Flamm, H.B. Demopoulos, M.L. Seligman, R.G. Poser, J. Ransohoff, Free radicals in cerebral ischemia, Stroke 9 (1978) 445–447.

[57] J.W. Phillis, A "radical" view of cerebral ischemic injury, Prog. Neurobiol. 42 (1994) 441–448.

[58] D. Alonso-Alconada, E. Hilario, F.J. Alvarez, A. Alvarez, Apoptotic cell death correlates with ROS overproduction and early cytokine expression after hypoxia-ischemia in fetal lambs, Reprod. Sci. 19 (2012) 754–763.

[59] H. Tomimoto, I. Akiguchi, H. Wakita, J. Kimura, K. Hori, J. Yodoi, Astroglial expression of ATL-derived factor, a human thioredoxin homologue, in the gerbil brain after transient global ischemia, Brain Res. 625 (1993) 1–8.

[60] Y. Takagi, T. Tokime, K. Nozaki, Y. Gon, H. Kikuchi, J. Yodoi, Redox control of neuronal damage during brain ischemia after middle cerebral artery occlusion in the rat: immunohistochemical and hybridization studies of thioredoxin, J. Cereb. Blood Flow Metab. 18 (1998) 206–214.

[61] S.A. Stroev, T.S. Gluschenko, E.I. Tjulkova, G. Spyrou, E.A. Rybnikova, M.O. Samoilov, M. Pelto-Huikko, Preconditioning enhances the expression of mitochondrial antioxidant thioredoxin-2 in the forebrain of rats exposed to severe hypobaric hypoxia, J. Neurosci. Res. 78 (2004) 563–569.

[62] J.M. Hansen, H. Zhang, D.P. Jones, Mitochondrial thioredoxin-2 has a key role in determining tumor necrosis factor-alpha-induced reactive oxygen species generation, NF-kappaB activation, and apoptosis, Toxicol. Sci. 91 (2006) 643–650.

[63] U. Dirnagl, C. Iadecola, M.A. Moskowitz, Pathobiology of ischaemic stroke: an integrated view, Trends Neurosci. 22 (1999) 391–397.

[64] M.V. Johnston, W.H. Trescher, A. Ishida, W. Nakajima, Neurobiology of hypoxic-ischemic injury in the developing brain, Pediatr. Res. 49 (2001) 735–741.

[65] C. Fan, R.M. Zwacka, J.F. Engelhardt, Therapeutic approaches for ischemia/reperfusion injury in the liver, J. Mol. Med. 77 (1999) 577–592.

[66] S. Boulos, B.P. Meloni, P.G. Arthur, C. Bojarski, N.W. Knuckey, Peroxiredoxin 2 overexpression protects cortical neuronal cultures from ischemic and oxidative injury but not glutamate excitotoxicity, whereas Cu/Zn superoxide dismutase 1 overexpression protects only against oxidative injury, J. Neurosci. Res. 85 (2007) 3089–3097.

[67] Y. Takagi, A. Mitsui, A. Nishiyama, K. Nozaki, H. Sono, Y. Gon, N. Hashimoto, J. Yodoi, Overexpression of thioredoxin in transgenic mice attenuates focal ischemic brain damage, Proc. Natl. Acad. Sci. U. S. A. 96 (1999) 4131–4136.

[68] B. Zhang, Y. Wang, Y. Su, Peroxiredoxins, a novel target in cancer radiotherapy, Cancer Lett. 286 (2009) 154–160.

[69] C.P. Baines, The mitochondrial permeability transition pore and ischemia-reperfusion injury, Basic Res. Cardiol. 104 (2009) 181–188.

[70] M.P. Hutchens, J. Dunlap, P.D. Hurn, P.O. Jarnberg, Renal ischemia: does sex matter? Anesth. Analg. 107 (2008) 239–249.

[71] S.C. Weight, P.R. Bell, M.L. Nicholson, Renal ischaemia–reperfusion injury, Br. J. Surg. 83 (1996) 162–170.

[72] T.C. Karlenius, F. Shah, G. Di Trapani, F.M. Clarke, K.F. Tonissen, Cycling hypoxia upregulates thioredoxin levels in human MDA-MB-231 breast cancer cells, Biochem. Biophys. Res. Commun. 419 (2012) 350–355.

[73] M. Shiota, H. Izumi, N. Miyamoto, T. Onitsuka, E. Kashiwagi, A. Kidani, G. Hirano, M. Takahashi, M. Ono, M. Kuwano, S. Naito, Y. Sasaguri, K. Kohno, Ets regulates peroxiredoxin1 and 5 expressions through their interaction with the high-mobility group protein B1, Cancer Sci. 99 (2008) 1950–1959.

[74] S.A. Stroev, E.I. Tyul'kova, T.S. Glushchenko, I.A. Tugoi, M.O. Samoilov, M. Pelto-Huikko, Thioredoxin-1 expression levels in rat hippocampal neurons in moderate hypobaric hypoxia, Neurosci. Behav. Physiol. 39 (2009) 1–5.

[75] M. Enoksson, A.P. Fernandes, S. Prast, C.H. Lillig, A. Holmgren, S. Orrenius, Overexpression of glutaredoxin 2 attenuates apoptosis by preventing cytochrome c release, Biochem. Biophys. Res. Commun. 327 (2005) 774–779.

[76] C.H. Lillig, M.E. Lonn, M. Enoksson, A.P. Fernandes, A. Holmgren, Short interfering RNA-mediated silencing of glutaredoxin 2 increases the sensitivity of HeLa cells toward doxorubicin and phenylarsine oxide, Proc. Natl. Acad. Sci. U. S. A. 101 (2004) 13227–13232.

[77] L. Brautigam, L.D. Schutte, J.R. Godoy, T. Prozorovski, M. Gellert, G. Hauptmann, A. Holmgren, C.H. Lillig, C. Berndt, Vertebrate-specific glutaredoxin is essential for brain development, Proc. Natl. Acad. Sci. U. S. A. 108 (2011) 20532–20537.

[78] M. Shiota, T. Horiuchi, No difference found between cognitive processing of self-face (self-name) and other's face (other's name) using a priming task, Shinrigaku kenkyu 79 (2008) 432–438.

[79] R. Jager, M.J. Bertrand, A.M. Gorman, P. Vandenabeele, A. Samali, The unfolded protein response at the crossroads of cellular life and death during endoplasmic reticulum stress, Biol. Cell 104 (2012) 259–270.

[80] L. Roybon, T. Hjalt, S. Stott, F. Guillemot, J.Y. Li, P. Brundin, Neurogenin2 directs granule neuroblast production and amplification while NeuroD1 specifies neuronal fate during hippocampal neurogenesis, PLoS One 4 (2009) e4779.

[81] M. Encinas, M. Iglesias, Y. Liu, H. Wang, A. Muhaisen, V. Cena, C. Gallego, J.X. Comella, Sequential treatment of SH-SY5Y cells with retinoic acid and brain-derived neurotrophic factor gives rise to fully differentiated, neurotrophic factor-dependent, human neuron-like cells, J. Neurochem. 75 (2000) 991–1003.

[82] S. Karunakaran, U. Saeed, S. Ramakrishnan, R.C. Koumar, V. Ravindranath, Constitutive expression and functional characterization of mitochondrial glutaredoxin (Grx2) in mouse and human brain, Brain Res. 1185 (2007) 8–17.

[83] Y. Gan, X. Ji, X. Hu, Y. Luo, L. Zhang, P. Li, X. Liu, F. Yan, P. Vosler, Y. Gao, R.A. Stetler, J. Chen, Transgenic overexpression of peroxiredoxin-2 attenuates ischemic neuronal injury via suppression of a redox-sensitive pro-death signaling pathway, Antioxid. Redox Signal. 17 (2012) 719–732.

[84] X. Hu, Z. Weng, C.T. Chu, L. Zhang, G. Cao, Y. Gao, A. Signore, J. Zhu, T. Hastings, J.T. Greenamyre, J. Chen, Peroxiredoxin-2 protects against 6-hydroxydopamine-induced dopaminergic neurodegeneration via attenuation of the apoptosis signal-regulating kinase (ASK1) signaling cascade, J. Neurosci. 31 (2011) 247–261.

[85] R. Trollmann, M. Gassmann, The role of hypoxia-inducible transcription factors in the hypoxic neonatal brain, Brain Dev. 31 (2009) 503–509.

[86] S. Choksi, Y. Lin, Y. Pobezinskaya, L. Chen, C. Park, M. Morgan, T. Li, S. Jitkaew, X. Cao, Y.S. Kim, H.S. Kim, P. Levitt, G. Shih, M. Birre, C.X. Deng, Z.G. Liu, A HIF-1 target, ATIA, protects cells from apoptosis by modulating the mitochondrial thioredoxin, TRX2, Mol. Cell 42 (2011) 597–609.

[87] K.D. Mansfield, R.D. Guzy, Y. Pan, R.M. Young, T.P. Cash, P.T. Schumacker, M.C. Simon, Mitochondrial dysfunction resulting from loss of cytochrome c impairs cellular oxygen sensing and hypoxic HIF-alpha activation, Cell Metab. 1 (2005) 393–399.

[88] A. Sanjuan-Pla, A.M. Cervera, N. Apostolova, R. Garcia-Bou, V.M. Victor, M.P. Murphy, K.J. McCreath, A targeted antioxidant reveals the importance of mitochondrial reactive oxygen species in the hypoxic signaling of HIF-1alpha, FEBS Lett. 579 (2005) 2669–2674.

[89] D.P. Pearlstein, M.H. Ali, P.T. Mungai, K.L. Hynes, B.L. Gewertz, P.T. Schumacker, Role of mitochondrial oxidant generation in endothelial cell responses to hypoxia, Arterioscler. Thromb. Vasc. Biol. 22 (2002) 566–573.

[90] A. Kulisz, N. Chen, N.S. Chandel, Z. Shao, P.T. Schumacker, Mitochondrial ROS initiate phosphorylation of p38 MAP kinase during hypoxia in cardiomyocytes, Am. J. Physiol. Lung Cell. Mol. Physiol. 282 (2002) L1324–L1329.

[91] P.J. Moos, K. Edes, P. Cassidy, E. Massuda, F.A. Fitzpatrick, Electrophilic prostaglandins and lipid aldehydes repress redox-sensitive transcription factors p53 and hypoxia-inducible factor by impairing the selenoprotein thioredoxin reductase, J. Biol. Chem. 278 (2003) 745–750.

[92] J. Zhou, A.E. Damdimopoulos, G. Spyrou, B. Brune, Thioredoxin 1 and thioredoxin 2 have opposed regulatory functions on hypoxia-inducible factor-1alpha, J. Biol. Chem. 282 (2007) 7482–7490.

[93] U.R. Jewell, I. Kvietikova, A. Scheid, C. Bauer, R.H. Wenger, M. Gassmann, Induction of HIF-1alpha in response to hypoxia is instantaneous, FASEB J. 15 (2001) 1312–1314.

[94] A. Arbelaez, M. Castillo, S.K. Mukherji, Diffusion-weighted MR imaging of global cerebral anoxia, AJNR, Am. J. Neuroradiol. 20 (1999) 999–1007.

[95] K.M. Busl, D.M. Greer, Hypoxic-ischemic brain injury: pathophysiology, neuropathology and mechanisms, NeuroRehabilitation 26 (2010) 5–13.

[96] J.A. Chalela, R.L. Wolf, J.A. Maldjian, S.E. Kasner, MRI identification of early white matter injury in anoxic-ischemic encephalopathy, Neurology 56 (2001) 481–485.

[97] M. Lundberg, S. Curbo, K. Reiser, T. Masterman, S. Braesch-Andersen, I. Arestrom, N. Ahlborg, Methodological aspects of ELISA analysis of thioredoxin 1 in human plasma and cerebrospinal fluid, PLoS One 9 (2014) e103554.

[98] B. Owe-Larsson, K. Ekdahl, T. Edbom, U. Osby, H. Karlsson, C. Lundberg, M. Lundberg, Increased plasma levels of thioredoxin-1 in patients with first episode psychosis and long-term schizophrenia, Prog. Neuro-Psychopharmacol. Biol. Psychiatry 35 (2011) 1117–1121.

[99] T. Ito, M. Yamakuchi, C.J. Lowenstein, Thioredoxin increases exocytosis by denitrosylating N-ethylmaleimide-sensitive factor, J. Biol. Chem. 286 (2011) 11179–11184.

[100] H. Nakamura, Thioredoxin and its related molecules: update 2005, Antioxid. Redox Signal. 7 (2005) 823–828.

[101] B.J. Park, M.K. Cha, I.H. Kim, Thioredoxin 1 as a serum marker for ovarian cancer and its use in combination with CA125 for improving the sensitivity of ovarian cancer diagnoses, Biomarkers 19 (2014) 604–610.

[102] T. Hayashi, Y. Ueno, T. Okamoto, Oxidoreductive regulation of nuclear factor kappa B. Involvement of a cellular reducing catalyst thioredoxin, J. Biol. Chem. 268 (1993) 11380–11388.
[103] K. Hirota, M. Matsui, S. Iwata, A. Nishiyama, K. Mori, J. Yodoi, AP-1 transcriptional activity is regulated by a direct association between thioredoxin and Ref-1, Proc. Natl. Acad. Sci. U. S. A. 94 (1997) 3633–3638.
[104] J.R. Matthews, N. Wakasugi, J.L. Virelizier, J. Yodoi, R.T. Hay, Thioredoxin regulates the DNA binding activity of NF-kappa B by reduction of a disulphide bond involving cysteine 62, Nucleic Acids Res. 20 (1992) 3821–3830.
[105] M. Saitoh, H. Nishitoh, M. Fujii, K. Takeda, K. Tobiume, Y. Sawada, M. Kawabata, K. Miyazono, H. Ichijo, Mammalian thioredoxin is a direct inhibitor of apoptosis signal-regulating kinase (ASK) 1, EMBO J. 17 (1998) 2596–2606.
[106] M. Ueno, H. Masutani, R.J. Arai, A. Yamauchi, K. Hirota, T. Sakai, T. Inamoto, Y. Yamaoka, J. Yodoi, T. Nikaido, Thioredoxin-dependent redox regulation of p53-mediated p21 activation, J. Biol. Chem. 274 (1999) 35809–35815.
[107] S.J. Welsh, W.T. Bellamy, M.M. Briehl, G. Powis, The redox protein thioredoxin-1 (Trx-1) increases hypoxia-inducible factor 1alpha protein expression: Trx-1 overexpression results in increased vascular endothelial growth factor production and enhanced tumor angiogenesis, Cancer Res. 62 (2002) 5089–5095.
[108] I. Hattori, Y. Takagi, H. Nakamura, K. Nozaki, J. Bai, N. Kondo, T. Sugino, M. Nishimura, N. Hashimoto, J. Yodoi, Intravenous administration of thioredoxin decreases brain damage following transient focal cerebral ischemia in mice, Antioxid. Redox Signal. 6 (2004) 81–87.
[109] Y.H. Ma, N. Su, X.D. Chao, Y.Q. Zhang, L. Zhang, F. Han, P. Luo, Z. Fei, Y. Qu, Thioredoxin-1 attenuates post-ischemic neuronal apoptosis via reducing oxidative/nitrative stress, Neurochem. Int. 60 (2012) 475–483.

IV. Article

Redox regulation of cytoskeletal dynamics during differentiation and de-differentiation

Manuela Gellert, Eva-Maria Hanschmann, Klaudia Lepka, Carsten Berndt, Christopher Horst Lillig

Biochim. Biophys. Acta

Vol 1850 Issue 8 (1575-87)

Published: August 31st, 2015

This research was originally published in the Journal Biochimica et Biophysica acta General Subjects, Gellert M, Hanschmann E-M, Lepka K, Berndt C, Lillig CH. Redox regulation of cytoskeletal dynamics during differentiation and de-differentiation. *Biochim Biophys Acta.*; 1850(8):1575–87, DOI: 10.1016/j.bbagen.2014.10.030 (2015)

Link to the publication on ScienceDirect: http://doi.org/10.1016/j.bbagen.2014.10.030

Biochimica et Biophysica Acta 1850 (2015) 1575–1587

Contents lists available at ScienceDirect

Biochimica et Biophysica Acta

journal homepage: www.elsevier.com/locate/bbagen

Review

Redox regulation of cytoskeletal dynamics during differentiation and de-differentiation☆

Manuela Gellert [a], Eva-Maria Hanschmann [a], Klaudia Lepka [b], Carsten Berndt [b], Christopher Horst Lillig [a,*]

[a] Institut für Biochemie und Molekularbiologie, Universitätsmedizin Greifswald, Ernst-Moritz-Arndt-Universität, Greifswald, Germany
[b] Klinik für Neurologie, Medizinische Fakultät, Heinrich-Heine-Universität, Düsseldorf, Germany

ARTICLE INFO

Article history:
Received 9 September 2014
Received in revised form 24 October 2014
Accepted 27 October 2014
Available online 8 November 2014

Keywords:
Cytoskeleton remodeling
Redox switch
Redox signaling
Thioredoxin
Glutaredoxin
Methionine sulfoxide reductase

ABSTRACT

Background: The cytoskeleton, unlike the bony vertebrate skeleton or the exoskeleton of invertebrates, is a highly dynamic meshwork of protein filaments that spans through the cytosol of eukaryotic cells. Especially actin filaments and microtubuli do not only provide structure and points of attachments, but they also shape cells, they are the basis for intracellular transport and distribution, all types of cell movement, and – through specific junctions and points of adhesion – join cells together to form tissues, organs, and organisms.
Scope of review: The fine tuned regulation of cytoskeletal dynamics is thus indispensible for cell differentiation and all developmental processes. Here, we discussed redox signalling mechanisms that control this dynamic remodeling. Foremost, we emphasised recent discoveries that demonstrated reversible thiol and methionyl switches in the regulation of actin dynamics.
Major conclusions: Thiol and methionyl switches play an essential role in the regulation of cytoskeletal dynamics.
General significance: The dynamic remodeling of the cytoskeleton is controlled by various redox switches. These mechanisms are indispensible during development and organogenesis and might contribute to numerous pathological conditions. This article is part of a Special Issue entitled Redox regulation of differentiation and de-differentiation.

1. Redox signalling

Cells constantly receive and process signals from their environment. The coordinated and specific response to these signals is the basis of essentially all cell functions. Errors, misinterpretations, or displacements in these signal transduction events are responsible for numerous diseases such as malignant or degenerative disorders. Signalling molecules are sensed by an extra- or intracellular receptor molecule; the activated receptor promotes the activation of transducer proteins, such as protein kinases, often through the conversion, production, release, or elimination of second messenger molecules such as calcium ions, cyclic adenosine monophosphate, or nitric oxide. Transducer proteins regulate further messenger molecules or act directly on effector molecules that trigger the biological response. These complex pathways and networks allow for the amplification, modulation, and adaptation of signal and response. In recent years, the reversible redox modifications of protein side chains emerged as a key mechanism that affects essentially all signalling pathways, in a rapid, compartmentalised, reversible, and highly specific manner [1–4]. Most notably, these post-translational redox modifications do not occur randomly, they need to be catalysed by specific enzymes [5].

1.1. Redox modifications of cysteinyl side chains

The major targets of redox signalling are cysteinyl side chains (Fig. 1). Two protein thiols can be oxidised to an intra- or intermolecular disulfide. Disulfides may also form with small molecular weight thiols, such as the most abundant cellular thiol compound, glutathione (GSH). This modification is known as S-glutathionylation [6]. S-nitrosylation of protein thiols can be induced, for instance, by metal catalysed reaction of endogenously produced nitric oxide with thiols, or by the subsequent transfer of S-nitroso groups to other thiols, i.e.

Abbreviations: ARP, actin-related protein; CDC42, cell division control protein 42; CRMP2, collapsin response mediator protein2; DPYL2, dihydropyrimidinase like protein 2; EAE, experimental autoimmune encephalomyelitis; GR, glutathione reductase; Grx, glutaredoxin; GSH, glutathione; GSSG, glutathione disulfide; Hif, hypoxia-inducible factor; MICAL, molecule interacting with CasL; MS, multiple sclerosis; Msr, methionine sulfoxide reductase; NDPK, nucleoside diphosphate kinase; NP1, neuropilin-1; OPC, ooligodendroglial progenitor cells; PlexA, class A plexin; Rac, RAS-related C3 botulinum toxin substrate; Rho, Ras homolog gene family member; Sema, semaphorin; SIRT1, sirtuin 1; Trx, thioredoxin, TrxR, thioredoxin reductase; VEGF-C, vascular endothelial growth factor-C; WASP, Wiskott–Aldrich syndrome protein; WAVE, WASP-family verprolin-homologous protein

☆ This article is part of a Special Issue entitled Redox regulation of differentiation and de-differentiation.

* Corresponding author at: Universitätsmedizin Greifswald KdöR, Institut für Medizinische Biochemie und Molekularbiologie DZ7 J03 33, Ferdinand-Sauerbruch-Strasse, 17475 Greifswald, Germany. Tel.: +49 3834 865407; fax: +49 3834 865402.
E-mail address: horst@lillig.de (C.H. Lillig).

http://dx.doi.org/10.1016/j.bbagen.2014.10.030
0304-4165/

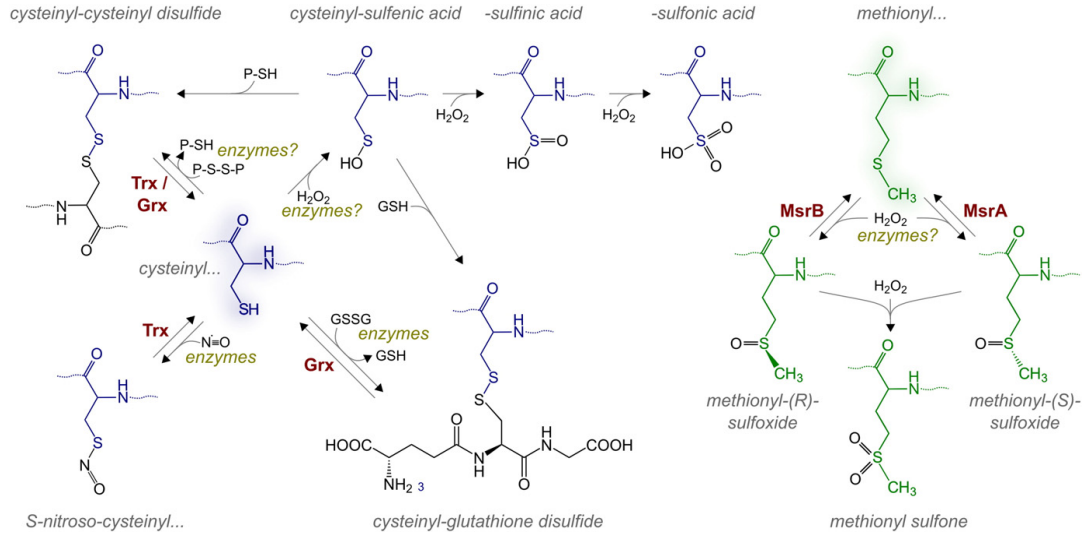

Fig. 1. Redox modifications of protein cysteinyl and methionyl residues. In the presence of another thiol (SH), the cysteinyl residue (left site, blue) can be modified to a protein (cysteinyl–cysteinyl) disulfide, that can be reduced by Trxs and Grxs, or cysteinyl–glutathione mixed disulfides. Protein cysteinyl residues can be oxidised to sulfenic acid (R-SOH) by peroxides or (at least in some cases) specific enzymes. In the presence of excessive peroxides this may be irreversibly 'over'-oxidised to sulfinic ($R\text{-}SO_2H$) and sulfonic acid ($R\text{-}SO_3H$). Cysteinyl–glutathione disulfides may also be formed through thiol–disulfide exchange reactions with glutathione disulfide or by specific enzymes, e.g. Grxs that also specifically catalyse the reduction of these disulfides. Nitric oxide (·NO) in general can only lead to the nitrosylation of cysteinyl residues through the catalysis during which one electron is transferred from the ·NO to a recipient, e.g. a metal cofactor. S-nitrosylation can be reversed by trans-nitrosylation to another protein thiol, e.g. to the active site of Trxs. Methionyl residues (right site) are oxidised stero-selective to R- or S-methionyl sulfoxides. These are specific substrates for methionine sulfoxide reductases (Msr) B and A, respectively. Further oxidation of methionyl sulfoxides results in methionyl sulfone, a step that has to be considered irreversible.

trans-nitrosylation [7,8]. Via the reaction with hydrogen peroxide or peroxy nitrite, cysteinyl thiols may be oxidised to sulfenic acids or further to sulfinic and sulfonic acids [9], the latter two have to be considered irreversible, although they do occur at specific target sites as well [10]. These modifications are specific for both the redox active compound, i.e. the second messenger, and the cysteinyl side chain of the transducer and effector proteins, respectively [11]. This specificity is determined by the molecular environment of the thiol group and the modifying enzymes potentially involved.

The key enzymes that catalyse post-translational redox modifications of protein thiol groups, for instance disulfide reduction, S-glutathionylation, and trans-nitrosylation, are part of the thioredoxin family of proteins, namely thioredoxins (Trxs) and glutaredoxins (Grxs) [12–15]. Isoforms of these proteins are ubiquitously expressed in all organisms, tissues, cells, and targeted to all subcellular compartments, including the extracellular space. The members of this protein family are characterised by a common structural motif of approximately 12 kDa, the thioredoxin fold, and the highly conserved dithiol active site motif, Cys-X-X-Cys, that facilitates thiol–disulfide exchange reactions (Fig. 2A). Both Trxs and dithiol Grxs utilise these two cysteinyl side chains for the reduction of protein disulfides in the so called dithiol mechanism (Fig. 2B). The N-terminal active site thiol easily deprotonates due to a low pK_a value, thus allowing a nucleophilic attack on one of the substrate's disulfide sulphur atoms. This reaction leads to the formation of a transient mixed disulfide intermediate between the Trx or Grx and the substrate (Fig. 2A and B, reactions 1 and 1a, respectively). In the second step the C-terminal active site thiol reduces the mixed disulfide, resulting in a reduced substrate and a disulfide in the active site of the Trx or Grx (Fig. 2, reaction 2). The protein disulfide in the active site of Trx is reduced by NADPH-dependent thioredoxin reductase (TrxR) [16]. Grx is reduced by two molecules of glutathione [17] that are kept reduced by NADPH-dependent glutathione reductase (GR) (Fig. 2A, reactions 3 and 4). Protein de-glutathionylation requires only the N-terminal active site cysteinyl residue and was thus named the monothiol reaction mechanism (Fig. 2B, reactions 1b and 4) [18–20]. The reaction sequence is initiated by a nucleophilic attack of the N-terminal active site thiolate on the sulphur atom of GSH in the glutathionylated protein. Thereby, the protein is reduced, and a mixed disulfide between glutathione and Grx is formed (Fig. 2B, reaction 1b), which is subsequently reduced by a second molecule of GSH yielding glutathione disulfide (GSSG) (Fig. 2B, reaction 4).

1.2. Methionine sulfoxidation

Methionine contains a thioether group that can be reversibly oxidised to methionine sulfoxide (Fig. 1). Similar to the variety of thiol redox modifications, reversible methionine oxidation is now being recognised as a redox signalling mechanism [21]. The methionyl thioether group can be oxidised to a mixture of two diastereomers, methionine-S-sulfoxide and methionine-R-sulfoxide. Methionine-S-sulfoxide is stereospecifically reduced by methionine sulfoxide reductase (Msr) A, the reduction of methionine-R-sulfoxide is specifically catalysed by MsrB. In general, the reaction mechanism of MsrA requires three cysteinyl residues in its catalytic centre, MsrB's activity requires two cysteinyl residues [22].

Human MsrA is expressed in various isoforms, encoded by a single gene, that are localised in different cellular compartments, i.e. mitochondria, cytosol, and nucleus [23–25]. The first catalytic sulfenic cysteinyl residue of MsrA reacts with methionine-S-sulfoxide leading to a sulfenic acid intermediate (Fig. 2C, reaction 1a or 1b). This is reduced by the second cysteinyl residue leading to a disulfide with the catalytic cysteinyl residue (Fig. 2C, reaction 2). This disulfide is attacked by the third cysteinyl residue leading to a disulfide between the second and third cysteinyl residues (Fig. 2C, reaction 8). This disulfide is a substrate for Trxs or Grxs that regenerates the fully reduced enzymes (Fig. 2C, reactions 9 and 10) [22,26]. Most mammalian genomes possess three MsrB genes. MsrB1 is characterised by one selenocysteinyl residue in its active site instead of the sulfenic catalytic cysteinyl residue and

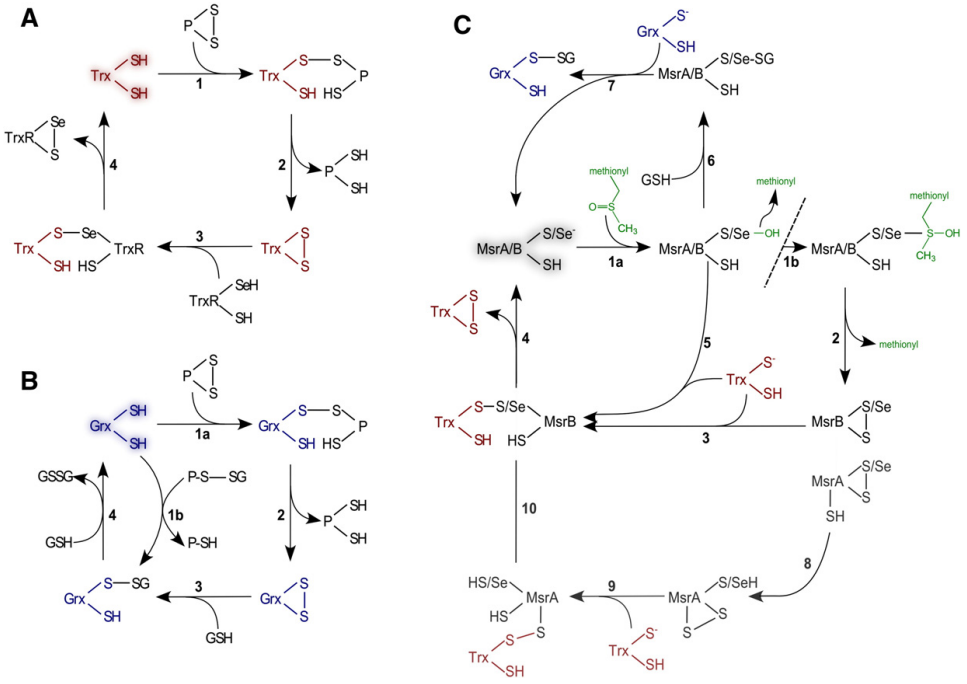

Fig. 2. Reaction mechanisms of thioredoxins, glutaredoxins, and methionine sulfoxide reductases. (A) Trxs (red) reduce protein disulfides in the dithiol mechanism using both active site thiols (SH). The N-terminal active site cysteinyl residue forms a covalent mixed disulfide intermediate with the oxidised substrate protein (A 1), which is reduced in the second step by the C-terminal active site cysteinyl residue, releasing the reduced protein (A 2). The disulfide in the active site of oxidised Trx is reduced by NADPH-dependent TrxR in a similar reaction sequence (A 3 and 4). (B) Grxs (blue) also reduce protein disulfides, similar to Trxs, but their active site disulfide is reduced by two molecules of glutathione (GSH) (B 1–4). In addition, Grxs reduce protein–cysteinyl–glutathione mixed disulfides in the so called monothiol mechanism (B 5–4), that only depends on the N-terminal active site cysteinyl residue. This thiolate attacks the GSH moiety and forms a GSH-mixed disulfide intermediate itself (B 5), that is subsequently reduced by another GSH molecule (B 4). (C) The catalytic active site sulfenic cysteinyl residue of MsrAs and Bs (black/grey) react with methionine-R/S-sulfoxide yielding a sulfenic acid intermediate (C 1a) or a methionyl-bound intermediate (C 1b). Both are attacked by the second cysteinyl residue leading to the formation of a disulfide with the catalytic cysteinyl residue (C 2). In case of the MsrBs, this disulfide is attacked by a third cysteinyl residue leading to a disulfide between the second and third cysteinyl residues (C 8). In either case, the disulfide in the active sites of the MsrA and MsrB is a substrate for Trxs or Grxs (C 3–4 or 8–10). Alternatively, the sulfenic/selenenic intermediate may react with GSH yielding a glutathione-mixed disulfide (C 6), that is reduced by Grxs (C 7).

exhibits the highest activity; MsrB2 and 3 contain cysteinyl residues only and are catalytically less efficient [27,28]. Reaction of MsrB with methionine-R-sulfoxide results in a sulfenic or selenenic acid intermediate, that is reduced by the second cysteinyl residue to a disulfide or selenosulfide bond (Fig. 2C, reactions 1 and 2). This disulfide is directly reduced by Trxs, regenerating the reduced active form of MsrB (Fig. 2C, reaction 3) [27,22]. Alternatively, the sulfenic/selenenic intermediate might be directly or via a glutathione-mixed disulfide reduced by Trxs or Grxs, respectively (Fig. 2C, reactions 6 and 7) [26].

While previously an unspecific oxidation of methionyl residues, for instance by hydrogen peroxide, leading to an inactivation of protein function was the prevalent concept, kinetic constrains and the discovery of enzymes that specifically catalyse methionine oxidation (see Sections 2.1 and 2.3) suggest a fine tuned, enzymatically catalysed activation and inactivation of protein functions by methionine sulfoxide formation [21].

1.3. Redox modifications of non-sulphur containing amino acid side chains

Various redox modifications of non-sulphur containing amino acid side chains have been reported. These have to be considered irreversible, however, they may serve as signals that are recognised by specific receptor molecules, or they may compromise distinct signalling pathways.

Aromatic and heterocyclic amino acid side chains, for instance, are highly susceptible to a broad range of modifications, e.g. mono- and dihydroxy derivatives, dityrosine, and various others [29,30], often by reaction with the most reactive oxygen species, the hydroxy radical. Tyrosine residues are susceptible to reaction with reactive nitrogen species, such as peroxynitrite and nitrogen dioxide, that may react with tyrosyl residues, leading to 3-nitrotyrosine [31–33], a reaction that, at least in some cases, may also require catalysis [34].

One of the most common oxidative modifications of proteins is the unspecific generation of carbonyl groups, termed protein carbonylation. It is so common that it has been widely analysed as a biomarker of "oxidative stress", aging, and various pathologies [29,30,35]. Protein carbonyl modifications are predominantly the product of hydroxy radicals that are metal-dependent generated in the Fenton reaction from hydrogen peroxide. Despite of the rather unspecific nature of this reaction, it could even be signal regulated. As an example, the endothelin-1-mediated carbonylation and subsequent degradation of annexin A1 was shown to promote cell growth of smooth muscle cells [36]. Due to their high reactivity, any given hydroxy radical likely abstracts the first hydrogen atom of a biomolecule it hits. Hence, they also abstract α-hydrogen atoms of peptide-bonded amino acids. This reaction leaves a carbon-centered radical that reacts further and ultimately leads to the cleavage of the peptide bond, another irreversible oxidative protein modification [37,38].

Prolyl and lysyl hydroxylases are enzymes that catalyse the introduction of hydroxyl groups into prolyl and lysyl amino acid side chains using molecular oxygen and α-ketoglutarate as substrates. These modifications are required for the quaternary structures of matrix proteins

such as collagen and elastin. In the case of the hypoxia-inducible factors (Hifs), this enzymatically catalysed modification is also used for sensing and signalling the presence of molecular oxygen. In the presence of oxygen, the α-subunits of the Hif proteins are hydroxylated at two specific prolyl residues targeting them for degradation. During hypoxia, when the proteins cannot be hydroxylated and degraded, Hifs act as transcription factors promoting the transcription of several specific genes [39–41].

2. Redox signalling in actin dynamics and cell movements

Actin filaments are assumably the most dynamic cytoskeletal structures. The dynamics of filamentous actin is controlled by numerous actin-binding proteins that stabilise filaments, promote elongation, severing, or nucleation of new or daughter-filaments [42]. Cell movements are controlled by numerous signalling pathways, including phosphorylation cascades, calcium signalling, and phospholipid signalling. These signals allow the spatio-temporal control of actin dynamics in specific regions of the cytosol, for instance the lamellipodia at the leading edge of the moving cell. One of the nucleation factors of filamentous actin is the ARP (actin-related protein) 2/3 complex. It is active at the leading edge of motile cells and in neuronal growth cones, where it initiates branches on the sides of existing filaments. The growing filaments produce force that induces membrane protrusion, for an overview see [43]. The unbound ARP2/3 complex is inactive in the nucleation of new daughter-filaments and requires an activation step facilitated by nucleation promoting factors. These factors belong to the Wiskott–Aldrich syndrome protein (WASP) and WASP-family verprolin-homologous protein (WAVE) families of proteins [44,45]. The WASP/WAVE complexes are recruited to the membrane and activated by the action of the Ras (rat sarcoma) family GTPases Rho (Ras homolog gene family, member), Rac (Ras-related C3 botulinum toxin substrate), and CDC42 (cell division control protein 42) in response to various signalling pathways [46]. These small GTPases are probably the key signal integrators and mediators controlling the coordinated dynamic changes that move cells.

2.1. Redox modifications and regulation of actin

B.F. Straub (1914–1996) is credited for the discovery of actin in 1942 [47,48], however, most likely actin was isolated for the first time by W. D. Halliburton (1860–1931) in 1887 [49]. Interestingly, Straub was affiliated in the laboratory of A. Szent-Györgyi working also on aspects related to redox regulation. Szent-Györgyi (1893–1986) was awarded with the Nobel Prize in Physiology and Medicine in 1937 for his discovery and general findings of vitamin C. Actin is one of the most abundant eukaryotic proteins and is present as monomeric, globular (G)-actin or as filamentous (F)-actin. The latter forms microfilaments, an essential part of the cytoskeleton in all eukaryotic cells, and is thereby essential for apoptosis, cell division, cellular adhesion, cell polarity, connectivity, and migration.

Actin is susceptible to a number of post-translational modifications including for instance acetylation, phosphorylation, methylation, and thiol redox modifications [50]. More or less all cysteinyl residues (except for a single cysteine in α-actin) and almost half of the methionyl residues are susceptible to redox modifications (Fig. 3A). Cysteines 10 (only in α-actin), 217, 257, and 374 can be reversibly S-glutathionylated [51–53]; cysteines 217, 257, 285, and 374 can be S-nitrosylated [54–56]; cysteines 217, 257, 272 (only in β-actin), 285, and 374 can be oxidised to sulfenic, sulfinic, and sulfonic acids [57–59]. Methionines 44, 47, 178 (only in α-actin), 190, 227, 269, 325, and 355 can be oxidised to sulfoxides, whereas methionine 82 can be further oxidised to the sulfone [60,59,61]. These redox modified sulphur containing amino acids are distributed all over the primary structure of the actins (Fig. 3B). In addition, histidyl (40, 87, 173), as well as tryptophyl residues (79, 86, 340, 356) can be irreversibly oxidised [62,59,63].

Most of the redox modifications have been connected to conformational changes (e.g. oxidation of Cys272, Fig. 3C, D) affecting polymerisation/de-polymerisation as well as the interaction with binding partners. The majority of oxidative post-translational modifications lead to a generally decreased polymerisation rate of G-actin and depolymerisation of F-actin, effects which have been already observed by Straub using an oxidising agent [64]. Intra- and intermolecular disulfide formation enhances the flexibility of the actin network [65]. Actin S-nitrosylated at Cys374, glutathionylated at Cys374, or (sulf)oxidised at Cys374 and methionyl residues 44, 47, or 355 showed a moderate inhibition of polymerisation of G-actin and stability of F-actin [66,54,67,60]. In contrast, sulfoxidation of methionyl residues 178 and 190 completely inhibits polymerisation and induces rapid disassembly of F-actin [60] indicating specific effects of different redox modifications. Some reports speculate that S-glutathionylation might protect actin sulfhydryl groups against irreversible oxidation during conditions of "oxidative stress" and preserve microfilament organisation [68,52].

As mentioned above, actin dynamics depend on the interaction with many actin-binding proteins. The best known interaction of actin is the formation of the actomyosin S1 ATPase complex together with myosin which is essential for muscle contractility. Already 1947, Bailey and Perry noted that the thiol state of actin does not affect actomyosin formation [69]. Although post-translational redox modifications of actin, especially S-glutathionylation, do not alter the binding efficiency of myosin, ATPase activity of actomyosin and thereby muscle functionality were significantly deceased via inhibition of disassembly of the inactive ADP-bound complex [70,71]. Fiaschi et al. demonstrated the involvement of Cys374 glutathionylation in this process by the expression of a Cys374Arg mutant, however, here actin S-glutathionylation seems to promote the disassembly of this complex [72]. The binding efficiency to tropomyosin, another interaction partner important for muscle contractility, is decreased upon actin S-glutathionylation [73]. Actin harboring a Cys374Ser mutation lacks its binding ability to profilin, a protein important for polymerisation of actin monomers, indicating that thiol redox modifications regulate the formation of the actin–profilin complex [74].

Several reports connect redox modifications of actin with a variety of diseases (see also Section 4). Elevated levels of carbonylated actin have been observed in ischemia–reperfusion [75] and diabetes mellitus [76] among other pathological conditions [77]; S-nitrosylated actin accumulates in the spinal cord of inflammatory pain model mice [78]; in fibroblasts isolated from Friedreich's ataxia patients glutathionylated actin is connected to an abnormal pattern of actin filaments [79] and failed actin de-glutathionylation attenuates neutrophil recruitment to sites of inflammation [80].

However, actin is not only redox regulated under pathological conditions or treatments inducing "oxidative stress". Redox-regulated actin dynamics are also important in physiological conditions, e.g. axonal outgrowth. Therefore, redox modifications of actin need to be regulated by specific enzymes (see Section 1). Grxs 1 and 2 are able to deglutathionylate actin in vitro and in vivo increasing the polymerisation rate of G-actin and thus affecting cellular migration [67,81–83,53]. The Trx system enhances actin polymerisation via reduction of oxidised cysteinyl residues [58,84]. Surprisingly, not the active site cysteines, but Cys62 of Trx1 is essential for regulation of actin polymerisation [84]. Thiol–disulfide exchange between actin Cys374 and protein disulfide isomerase regulates cell migration [85]. De-nitrosylation of actin is facilitated by TrxR, which is linked to actin filaments via the focal adhesion kinase [86]. Methionine R-sulfoxide reductases – SelR in *Drosophila*, MsrB1 and 2 in mammals – specifically reduce Met44- and Met47-R-sulfoxides [87,88], modifications introduced by direct interaction between actin and the flavo-mono-oxygenase molecule interacting with CasL (MICAL) [89,87]. In mammals two of the three MICAL isoforms, 1 and 2, oxidise actin [87,90]. The antagonistic effect of Msr and MICAL on the oxidation state of actin methionine and thereby on F-actin (de)-polymerisation was demonstrated by transgenic flies. Overexpression of SelR resembled MICAL mutant actin phenotypes,

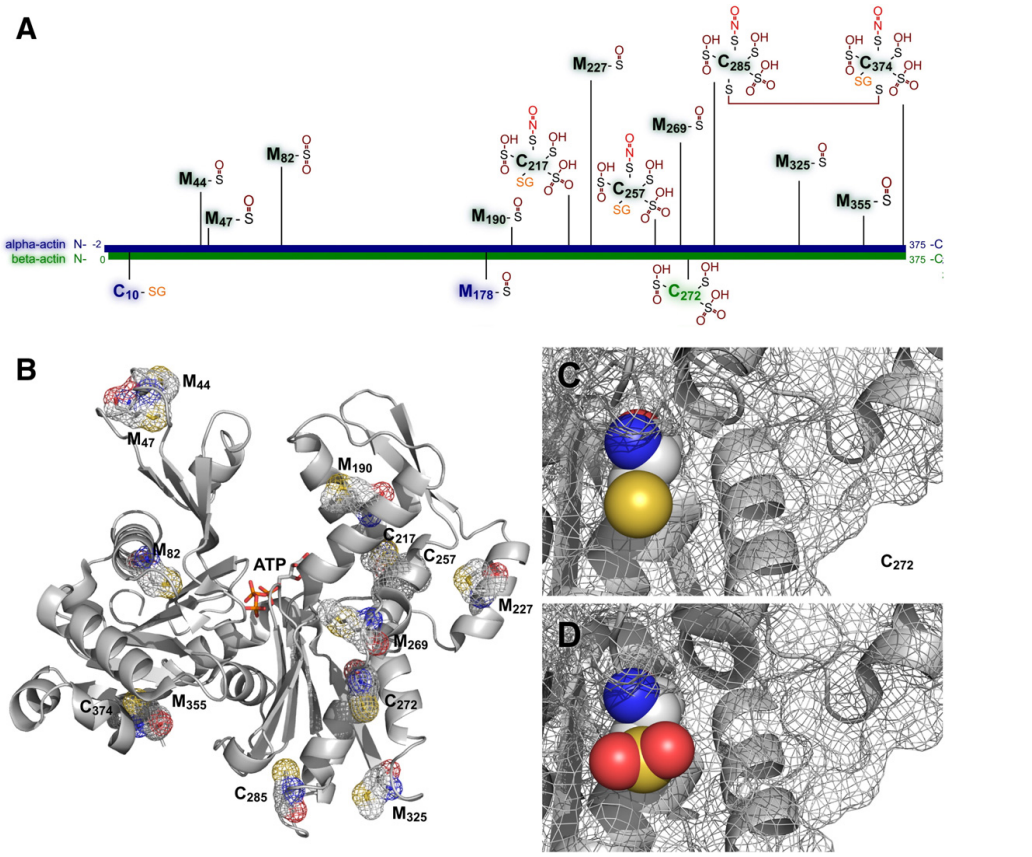

Fig. 3. Post-translational redox modifications of actin. (A) Schematic representation of the cysteinyl and methionyl residues of alpha- (blue) or beta-actin (green) that are susceptible to S-glutathionylation (orange/– SG), S-nitrosylation (red/– NO), and oxidation (dark red/disulfide: S – S, sulfenic acid: – SOH, sulfinic acid: – SO_2H, sulfonic acid: – SO_3H, sulfoxide: – SO, sulfone: – SO_2). (B) Structure of human beta-actin (PDB entry: 2BTF, [198]) in cartoon representation with all redox susceptible cysteinyl and methionyl residues in stick and mesh surface representation. ATP is highlighted in its central binding pocket. (D) Cysteinyl residue 272 in its reduced form (PDB entry: 2BTF), and (E) in the sulfinic form (PDB entry: 2OAN, [58]).

whereas SelR mutants phenocopied MICAL overexpression phenotypes [88]. MICAL links actin dynamics to semaphorin 3A signalling, which is important for axonal outgrowth and guidance (see Section 2.3).

Actin dynamics are also indirectly modulated by redox regulation via redox modification of binding proteins. As described above, redox modulation of actin is not interfering with myosin binding. In contrast, oxidised myosin does not react with actin [69]. Moreover, myosin cysteins are susceptible to S-glutathionylation modulating its ATPase activity [91]. Cofilin controls stability of F-actin and, depending on its oxidation state, actin dynamics are impaired [92].

Cytosolic Trx1 also functions in the regulation of nuclear proteins, e.g. transcription factors such as NF-κB. Recently, Go et al. demonstrated that cadmium treatment that also induces the oxidation of Cys39 and 139 of β-actin [93], stimulates the nuclear translocation of Trx1 and p65 of NF-κB. This translocation depended on actin polymerisation [94], suggesting that actin polymerisation itself contributes to specific redox signalling.

2.2. Redox regulation of cofilin activity

Cofilins are small (15–20 kDa), abundant proteins of the actin-binding protein family, found in all eukaryotic species. They bind to monomeric as well as filamentous actin and control cytoskeletal dynamics mostly by actin de-polymerisation, but can also induce the dissociation of phosphate from ADP-Pi filaments and exhibit to a lower extent actin-filament severing activity, thereby promoting actin polymerisation. The activity of cofilins is regulated by phosphorylation, phosphoinositides, pH and interactions with other proteins [95]. Post-translational phosphorylation of the conserved N-terminal serine (Ser3), regulated by LIM and TESK kinases and slingshot and chronophin phosphatases (for an overview see [96]), was shown to act as a switch of cofilin function. De-phosphorylated cofilin can bind to actin and functions in actin de-polymerisation, whereas phosphorylated cofilin cannot bind to actin and therefore promotes actin polymerisation [97]. Cofilin activity can be regulated via reactive oxygen species through redox-sensitive proteins and signalling cascades, including the activities of RhoA [98], PKD1 [99], and 14-3-3 zeta [100]. Moreover, redox regulation of specific cysteine residues of cofilin is emerging as another form of post-translational regulation, also assuring rapid and spatial control of protein function and cytoskeleton action towards distinct stimuli [92]. The human, non-muscle isoform cofilin-1 contains four cysteine residues at the positions 39, 80, 139 and 147; with 39 and 80 being located inside the protein and 139 and 147 being located on the surface of the protein [101]. The muscle-specific isoform, cofilin-2, only contains the two conserved Cys39 and Cys80 (Fig. 4).

In vitro studies showed that cofilin-1 exists in different redox states and that treatment with hydrogen peroxide leads to the formation of an intramolecular disulfide between the conserved Cys39 and Cys80 residues, inducing a conformational change that prevents phosphorylation by LIM kinase and thereby actin polymerisation, even though actin binding is not altered. Treating unstimulated and stimulated T cells with 50 μM of hydrogen peroxide also led to de-phosphorylation of cofilin and increased levels of F-actin independent of Ras, MEK and PI3K activity. It is worth mentioning that concentrations of 1–10 μM H_2O_2 did not affect the phosphorylation state of cofilin. H_2O_2 endogenously produced by activated granulocytes led to reduced levels of phosphorylated cofilin in unstimulated T cells, which could be prevented by the addition of catalase [102]. 30 min incubation with 500 μM H_2O_2 also induced the de-phosphorylation of cofilin in vascular smooth muscle [103]. Taurine chloramine, the main oxidant produced by activated neutrophils, oxidised all four Cys residues of cofilin-1 in B-lymphoma and COS cells and induced the formation of two intramolecular disulfides, presumably Cys39–Cys80 and Cys139–Cys147. The authors stated that Cys39 can generally also form a disulfide bridge with Cys139, however Cys80 only crosslinks with Cys39. Interestingly, the oxidation of all four Cys residues, as well as the de-phosphorylation at Ser3, was necessary for cofilin to lose its affinity for actin, translocate from the cytosol into mitochondria and induce apoptosis by opening the permeability transition pore and cytochrome c release [104,105].

Moreover, all four Cys residues seem to be crucial for the disulfide isomerisation process during protein folding (self-chaperoning). Following protein expression cofilin-1 contains at least one disulfide bridge in vivo, possibly involving Cys39 and Cys80, that is susceptible to reduction [106]. The authors furthermore claimed, that the surfaces Cys139 and Cys147 are most likely essential for protein oligomerization, a process that has been described for cofilin-1 before [107–109]. Mutating these Cys residues to Ala renders the protein more stable than the WT and prevents oligomerization and protein aggregation [106]. A different study indicated Cys39 and Cys147 to be involved in the formation of intermolecular disulfides and oligomers that constitute different redox states of the protein with distinct biological functions. Using in vivo disulfide cross-linking experiments and gel filtration, the different fractions were analysed. While the main, monomeric form exhibited severing activity, the dimeric and oligomeric forms exhibited actin bundling activity [107]. Interestingly, only the monomeric cofilin was phosphorylated, whereas the dimeric and oligomeric forms were not phosphorylated. The authors postulated that de-/phosphorylation influences the equilibrium of monomer/oligomer cofilin and thereby regulates actin dynamics [109].

It was shown that cofilin self-association was significantly increased by PIP_2, which is known to inhibit the binding of cofilin towards actin and thereby de-polymerisation activity [107]. Schulte and coworkers showed that reduction of WT cofilin and Cys/Ser mutants with dithiothreitol did not change the actin binding or de-polymerisation activity, but counteracted the inhibitory effect of PIP_2 on cofilin function. This redox regulatory mechanism modulates cofilin function in a spatial way, because the cofilin–PIP_2 complex is anchored in the plasma membrane. Upon specific stimuli, including a so far unknown cellular reductase, the reduction of cofilin prevents the inhibition by PIP_2, resulting in

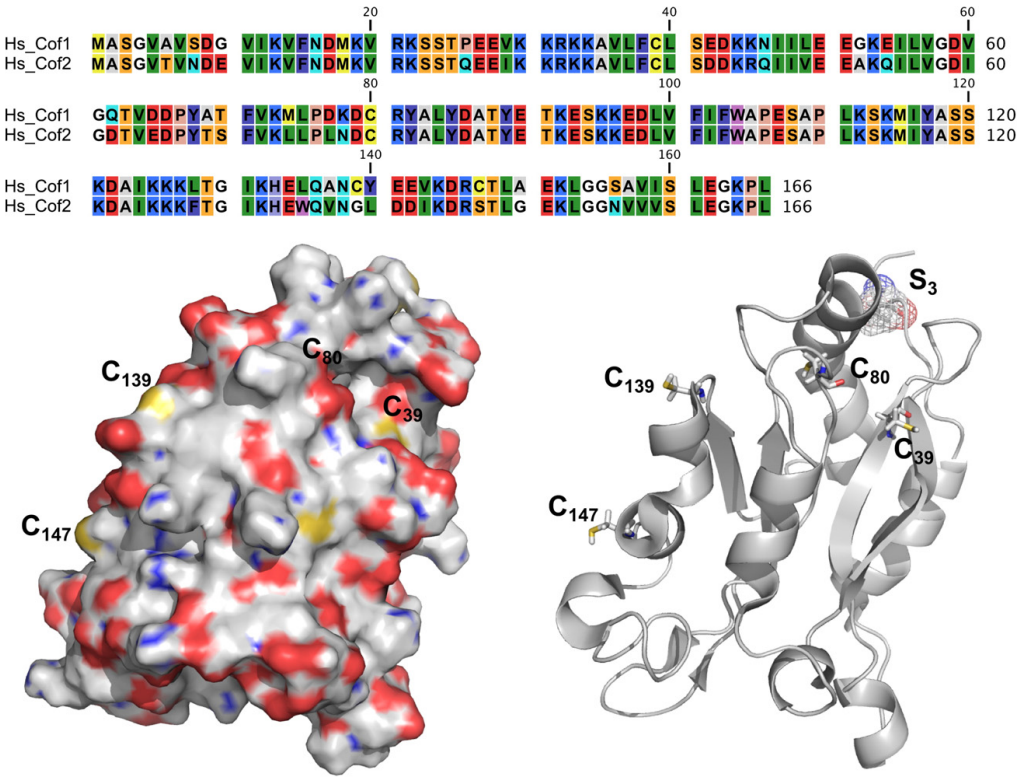

Fig. 4. Primary and tertiary structure of human cofilin. Upper panel: Alignment of the primary structures of human cofilin 1 and 2. Below: tertiary structure of human cofilin 1 (PDB entry: 1Q8G, [101]) with all four cysteins highlighted. Left site: surface representation coloured by the nature of the atoms (grey, carbon; blue, nitrogen; red, oxygen; yellow, sulphur). Right site: cartoon representation with the cysteinyl residues in stick representation. The regulatory seryl residue 3 is shown in stick representation with mesh surface.

increased actin dynamics, e.g. in the immune synapse of untransformed T cells [106]. The Cys39–Cys147 intermolecular disulfide was confirmed in vivo and was shown to be important for the cofilin–actin rod formation in neurons [108].

Besides the formation of disulfides, single Cys modifications were described for cofilin. The thiol group of Cys139 can be oxidised to sulfenic, sulfinic or sulfonic acid [102]. In addition, cofilin and other cytoskeletal proteins including actin, myosin, profilin, tropomyosin, and vimentin were shown to be glutathionylated in PBMCs treated with either 1 mM diamide or 1 mM hydrogen peroxide for 5 min. So far, no physiological function for the S-glutathionylation of cofilin has been demonstrated, however it might be a protective mechanism against irreversible over-oxidation or a regulatory function inhibiting actin polymerisation [110].

2.3. Semaphorin signalling, CRMP2, and MICALs

Semaphorins (Semas) are secreted and membrane-bound signalling proteins that control cellular differentiation and organogenesis such as axonal guidance during neuronal differentiation [111]. Semaphorins are grouped into eight major classes, each of these classes contains many subgroups and each of these subgroups various individual proteins [112]. Class 3 Sema's are secreted signalling molecules. In the kidney, for instance, Sema3A modulates ureteric bud branching, vascular patterning, and podocyte-endothelial crosstalk [113]. In neuronal development, Sema3A induces the collapse of axonal growth cones, thereby controlling axon guidance [114]. Moreover, Sema3A controls migration of developing thymocytes within the thymic lobules [115] and adult T-cell polarisation and migration [116]. Higher expression levels of a Sema3A mutant in smooth muscle cell segments lacking ganglion cells of patients suffering from Hirschsprung's disease indicate a correlation with this disease [117]. The Sema3A receptor is a heterodimeric transmembrane protein build up from neuropilin-1 (NP1) and a class A plexin (PlexA) (see Fig. 5). NP1 was characterised as the high-affinity ligand binding partner, and PlexA as the part transducing the signal into the cell [114]. Receptor binding of Sema3A to NP1 and PlexA leads to the inactivation of RhoA and therefore diminishes stress fibre formation by promoting F-actin de-polymerisation, e.g. through cofilin activation (Fig. 5) [118]. Prolonged inflammatory stress (e.g. IL-1β) as well as hypoxia induce Sema3A expression and secretion in neuronal cells and therefore prevent vascular regeneration. The role of Sema3A during development is elucidated by high mortality rates and confounding neuronal deficits in transgenic mice [119]. Galectin-1, an endogenous glycan-binding protein, promotes functional recovery of spinal lesions by binding to the NP1/PlexA4 receptor and therefore interfering with inhibitory signals triggered by Sema3A binding to NP1/PlexA4 [120]. In response to Sema3A signalling, Rac1 function changes from promoting actin polymerisation associated with axon growth to driving endocytosis of the plasma membrane, leading to growth cone collapse [121]. Lacking a defined signalling domain, NP1 still has a specific function in this signalling pathway presumably via its C-terminal domain and interaction with intracellular binding partners. NP1 appears to be essential for neuronal and cardiovascular development [122].

Collapsin response mediator protein 2 or dihydropyrimidinase like protein 2 (CRMP2/DPYL2) is a mediator of the semaphorin signalling cascade. The protein is subject to various post-translational modifications, including alternative splicing and phosphorylation by other mediators of Sema signalling, namely CdK5 and GSK3β, [123,124]. CRMP2 is essential for mediating the repulsive effect of Sema3A on axons [125], but the molecular interactions of CRMP2 are not well defined. CRMP2 binds tubulin-heterodimers and promotes microtubuli assembly during neuronal differentiation, axonal outgrowth and branching [126], however, the function of the protein controls the dynamics of the actin cytoskeleton in a dramatic way as well, e.g. [127,128], see also (Fig. 5). CRMP2 forms homo-tetramers as well as hetero-tetramers with other CRMPs, quaternary structures that were suggested to be important in regulating CRMP2 function as well [129]. Recently, also redox modifications of CRMP2 were reported that are essential for at least some of the protein functions. CRMP2 can form an intermolecular disulfide through two Cys504 residues in the tetrameric complex [130,131]. This disulfide may be a target for Trx. In fact, Morinaka et al. reported a mixed

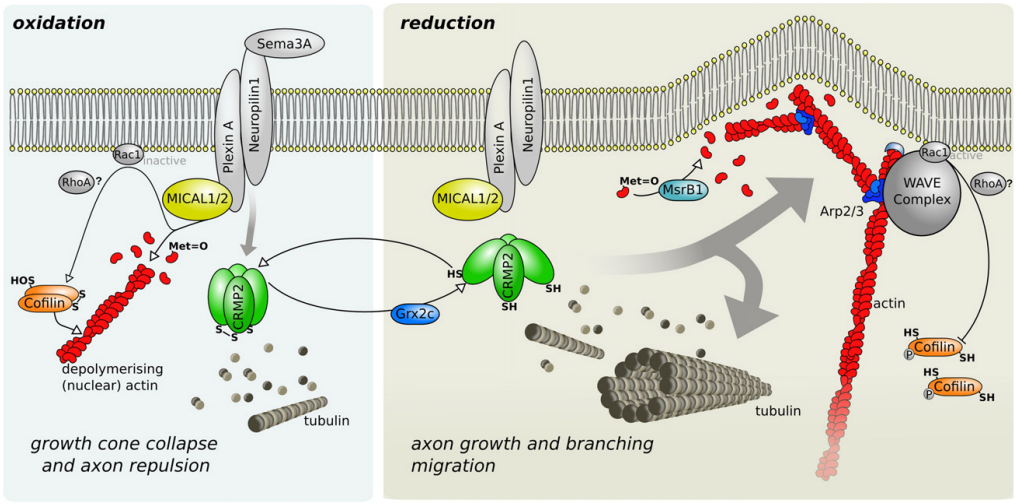

Fig. 5. Redox switches in semaphorin signalling, cofilin, and actin dynamics. Sema3A binding to NP1 activates PlexA and the semaphorin signalling cascade. Activated PlexA interacts with MICAL1/2 that then leads to actin de-polymerisation, through cofilin activation or the proposed sulfoxidation of methionyl residues of β-actin. CRMP2 is another mediator of the Sema3A signalling cascade that induces growth cone collapse and axon repulsion (left side: 'oxidation'). Without ligand binding, MICALs are not activated by the NP1/PlexA receptor. The reduction of CRMP2 by cytosolic Grx2 leads to a conformational change of the homo-tetramer. This conformational change causes (directly or indirectly) the polymerisation of actin and tubulin. MsrB1 is able to reduce the sulfoxides of methionyl residues of β-actin, allowing polymerisation. The WAVE complex is activated close to the membrane by active Rac1 and binds Arp2/3 which leads to actin polymerisation and branching. Activated Rac1 also leads to the phosphorylation and therefore inactivation of cofilin. The absence of Sema3A and the resulting changes of the cytoskeletal dynamics lead to axon outgrowth and branching as well as enabling active migration (right side: 'reduction').

disulfide of Cys504 with Trx that shall stimulates CRMP2 phosphorylation through GSK3β [130]. This mechanism, however, is unlikely, since the transient mixed disulfide of Trx with its substrate cannot be stable enough to serve as signal. The rate limiting step of the reaction is the nucleophilic attack that leads to the transient mixed disulfide, the second step takes place instantly, see [13,15] for in depth discussions. Cytosolic vertebrate-specific Grx2c is essential for embryonic brain development [128] and is specifically induced in many cancer cells [132]. We identified CRMP2 as redox regulated target of Grx2c [133] and demonstrated that this regulation is required for normal axonal outgrowth [128,131]. We identified a specific and reversible intermolecular thiol–disulfide switch in homo-tetrameric CRMP2 that determines two conformations of the complex and is efficiently reduced by Grx2c in vivo and in vitro [131]. Cysteine residues in CRMP2 are not modified by S-nitrosylation in vivo in experimental autoimmune encephalomyelitis (EAE), a murine model for multiple sclerosis (MS), even though S-nitrosylation could be induced in vitro by incubation with NO donors [134].

MICALs are another family of transducer/effector proteins of the Sema3A–PlexA signalling cascade, directly interact with PlexA. As CRMP2, MICALs are required for axon repulsion and guidance [135]. Noteworthy, MICALs were also reported to interact with CRMP2 [136]. MICAL1 interacts with PlexA1 and A3 of the semaphorin receptor (Fig. 5), MICAL2 with PlexA4 but neither directly interact with B, C or D class plexins [135]. MICALs and other FAD-dependent monooxygenases catalyse the NADPH-dependent oxygenation of nucleophilic nitrogen, sulphur, selenium, or phosphorus atoms. The reduced flavin ($FADH_2$) reacts with molecular oxygen yielding peroxyflavin. One of these oxygen molecules is transferred to a nucleophilic substrate. Peroxyflavin may also dissociate and lead to the production of H_2O_2 [137]. MICALs supposedly act through the local production of H_2O_2 in response to receptor activation [138,139], however, also the direct sulfoxidation of amino acid side chains, for instance a methionyl residue in β-actin, has been suggested [89], see also Fig. 5. Recently, the control of actin assembly by MICAL1/2 and MsrB1 was suggested via site-specific stereo-selective methionine oxidation and reduction. This regulatory redox couple may be important in macrophages during cellular activation [87]. In addition, the redox-dependent de-polymerisation of nuclear actin is induced by MICAL2, which therefore also influences gene transcription of certain targets [140].

3. Redox regulation of microtubuli dynamics

Microtubuli are polymers of small globular proteins, mostly α- and β-tubulin family members. α/β-Tubulin heterodimers assemble, generally with the help of numerous chaperones and scaffolds, into polarised microtubuli of variable length that often reach from the microtubuli organisation centre/centrosome somewhere near the nucleus to the periphery of the cells. This railway network enables both transport and organisation of cellular contents such as organelles and vesicles. The dynamics of microtubuli are controlled by β-tubulin's intrinsic GTPase activity as well as numerous tubulin-binding proteins, for recent summaries see, for instance, [141–144]. Dynamics of microtubuli are, among many other functions, essential for chromosome alignment and segregation during mitosis [145,146] and the formation of dendritic spines and axons during neuronal differentiation [147,148]. Human α-tubulins contain twelve conserved cysteinyl and eight conserved methionyl residues; human β-tubulin's seven conserved cysteinyl and 17 conserved methionyl residues. Even between these two subfamilies that make up the majority of microtubuli, three cysteinyl and four methionyl residues were conserved during evolution.

Protein disulfides i.e. intermolecular disulfides between the α- and β-tubulin subunits could be induced in porcine brain extracts by peroxynitrite, likely through a sulfenic intermediate. In vitro, these disulfides were a substrate for Grxs, similar to cysteinyl–glutathione disulfides formed under the same conditions [149], or the Trx system [150]. The reduction of the disulfide bonds restored tubulin polymerisation activity that was lost following peroxynitrite addition [151,149]. Both α- and β-tubulin isoforms were identified as potential protein disulfide substrates of the cytosolic Grx2c [133], whose crucial functions during development have been demonstrated before [128,131,152,53].

S-glutathionylation of tubulin family proteins has been demonstrated in response to peroxynitrite treatment [149] and treatment with the antimitotic agent 2-acetylamino-3-[4-(2-acetylamino-2-carboxyethylsulfanylcarbonylamino)phenyl carbamoylsulfanyl]propionic acid, leading to the de-polymerisation of microtubuli [153]. Interleukin 22 treatment of vascular smooth muscle cells leads to the activation of the NADPH oxidase and, specifically to the S-glutathionylation of α-tubulin [154]. In Friedreich's ataxia, an iron overload disorder, microtubuli abnormalities co-localised with an increase in overall protein S-glutathionylation in the affected areas [155].

S-nitrosylation of both α- and β-tubulin cysteinyl residues were identified by proteomic techniques in the hippocampus, substantia nigra and cortex of Alzheimer's disease patients [156], during the differentiation of spermatogenic cells [157], and in EAE [134]. The treatment of cultured vertebrate neurons with nitric oxide led to the collapse of axonal growth cones, and thus axon retraction, along with the reconfiguration of axonal microtubuli. The microtubule-associated protein MAP1B was identified as being regulated by S-nitrosylation leading to enhanced interactions with microtubuli and the inhibition of neuronal differentiation [158].

4. Disturbed redox-regulated migration under pathological conditions — therapeutic implications

Cytoskeletal dynamics, especially cell migration, is the underlying scaffold of fundamental biological processes. During embryonic development migration of different cell types is essential for the precise and accurate development of the organism. Formation of all organs, bones, and other tissues depends on the appearance of specialised cells at defined places at certain time points. In adults, the regulation of migratory processes is essential for regeneration, tissue repair and inflammatory immune response. Altered migration contributes to cancer metastasis as well as age related disorders like atherosclerosis. This chapter focuses on redox-regulated mechanisms modifying cell migration of differentiating and de-differentiating cells under pathological and age-related conditions.

Surprisingly little is known about redox regulation of cytoskeletal rearrangements and migration during embryonic development. The cytosolic isoform of Grx2, Grx2c [132,159], has been identified as essential for vertebrate development. Regulation of reversible thiol redox modifications of sirtuin 1 (SIRT1) [152], actin [53], and CRMP2 [128,131] (see Section 2.3) controls axon formation, vessel outgrowth as well as migration of cardiac neural crest cells and thereby formation of both the cardiovascular system and the brain.

Due to its tightly regulated and restricted regeneration potential, the central nervous system is a well-studied and therefore suitable model to investigate the role of migratory defects in failed regeneration. Here, impaired regeneration is a common pitfall in the chronic phase of degenerative disorders, e.g. succeeding a stroke, or in Alzheimer's disease, or MS [160–162]. In chronic MS, de-myelination by oligodendroglial cell death and disturbed re-myelination lead to lesion areas and subsequently to neuronal cell loss responsible for neurological dysfunctions [163]. Re-myelination is thought to ameliorate disease symptoms and to delay progression. Recent findings highlight the importance of altered migration capacities of oligodendroglial progenitor cells (OPCs) into de-myelinated lesion areas as the major cause for disturbed myelin regeneration [164]. Changes in the chemotactic milieu in chronic lesion areas inhibit OPC migration and subsequently their differentiation into myelinating mature oligodendrocytes and have the potential to reduce protective effects of drugs like IFN-β [165]. Among others, semaphorin guidance molecules are responsible for these effects

[165–167], see also Section 2.3. In addition, Bizzozero et al. demonstrated increased S-nitrosylation and carbonylation of cytoskeletal proteins, e.g. α/β-tubulin and β-actin in diseased animals of EAE [134,168], the animal model for MS. Among others, these findings manifest the importance of a functioning redox regulated OPC migration in MS disease progression [169]. Beyond MS, migration of progenitor cells is of importance for several other diseases comprising neuro-inflammation and their regeneration capacity like traumatic brain injury, stroke and other oligo- and neurodegenerative diseases [170,171].

In Alzheimer's as well as Parkinson's disease redox based cytoskeletal modifications were found to play a major role in axonal de- and regeneration [172,173]. Elevated carbonylation of β-actin as well as cysteine oxidation of microtubule-associated proteins directly influence both degeneration rates and the regeneration capacity of axonal loss [35,174]. Carbonylation of β-tubulin, however, was not enhanced in Alzheimer's disease brain extracts [173]. Moreover, migratory processes play an essential role in the origin of age-related diseases aside from the CNS, for instance atherosclerosis [175] and impaired wound healing. There are several cell types known to have an altered migration potential upon aging for example dermal fibroblasts, endothelial cells, smooth muscle cells and CD4 T cells [176–179]. Age-related impaired migration in dermal fibroblasts is based on disorganized β-actin and a decreased function of collagen-binding protein integrin α1β2, for instance [180]. The structure of β-actin depends on redox regulation of Cys374 during integrin-mediated cell adhesion [72], pointing towards a considerable role of specific redox switches in cytoskeletal dynamics upon aging. Furthermore, beneficial effects of hypoxia on wound healing via increased TGFβ1-mediated migration of dermal fibroblast are lost during aging [177]. The relaying signalling pathway was sshown to generally depend on the amount of free thiols even though the exact type and site of redox modification remain elusive [181,182].

Cancer cell spreading is connected to pathological cell migration. Metastasis is linked to expression of both SIRT1 [183,184] and cellular nucleoside diphosphate kinase (NDPK) [185]. SIRT1 was found to be highly expressed in brain metastatic tissue of non-small cell lung cancers [186]. Both SIRT1 and NDPK activities are regulated by redox modification of a single cysteine. NDPK loses its ability to suppress tumor metastasis depending on the redox state of Cys109 which is reduced by the Trx system [187], whereas SIRT1 activity is modulated via Grx2(c)-dependent reversible S-glutathionylation of Cys204 [152]. NDPK as well as SIRT1 regulate the activation of the transcription factor FOXO-1 and thereby the release of vascular endothelial growth factor-C (VEGF-C). Subsequently, an enhanced release of VEGF-C positively regulates cell migration and metastasis [188]. These findings connect redox-modulated pathways with cancer cell migration and might represent a possible target in cancer therapy.

In summary, redox regulated migration is essential not only during embryonic development but also under pathological conditions and in age-related diseases, affecting the fate of differentiating and de-differentiating cells (Fig. 6). Within this section, we presented some examples of specific thiol redox switches in proteins forming or controlling the cytoskeleton that play a defined role in the onset and progression of distinct diseases. To our knowledge, at present only two pharmacological substances are being evaluated that potentially affect the redox control of cytoskeletal dynamics in these pathologies. First, U-83836E which attenuates cytoskeletal damage after traumatic brain injury via scavenging lipid peroxyl radicals [189]. Second, nitroxyl (HNO) or rather HNO donors. HNO can react as both nucleophile and electrophile depending on the nature of its interaction partner and targets predominantly iron heme proteins and protein thiols [190]. Although known for quite a long time, just recently HNO emerged as a potential pharmacological agent not only in cardiovascular diseases but also in cancer [191]. By specifically inducing disulfides between actin Cys257 and tropomyosin Cys190 as well as Cys81 and Cys37 in myosin light and heavy chain, HNO increases cardiac contractility [192].

Microtubule dynamics (see Section 3) are essential for cell division and microtubule-targeting drugs have been used in anti-cancer treatment for almost 50 years. These drugs either destabilise or stabilise microtubules subsequently leading to inhibition of mitosis and cancer cell proliferation. Moreover, the targeting of microtubule dynamics may become of importance in neurodegenerative diseases [193,194]. All these drugs bind to tubulin within the microtubule structure. In contrast, pharmacological inhibitors of actin assembly and nucleation are so far not implemented in the clinics, however, some may be used to combat cancer development and metastasis in the future [195]. CRMP2 has a strong influence on both microtubule and actin filament dynamics (see Section 2.3). CRMP2 is inhibited by the compound lacosamide, also known as the anti-epileptic drug VIMPAT. The mode of action of the drug is not understood on a molecular level, but it was suggested that lacosamide-mediated inactivation of CRMP2 leads to inhibition of the aberrant neurite outgrowth during epilepsy [196]. Moreover, CRMP2 is also considered as a promising target in several other neurological diseases including Alzheimer's disease [197].

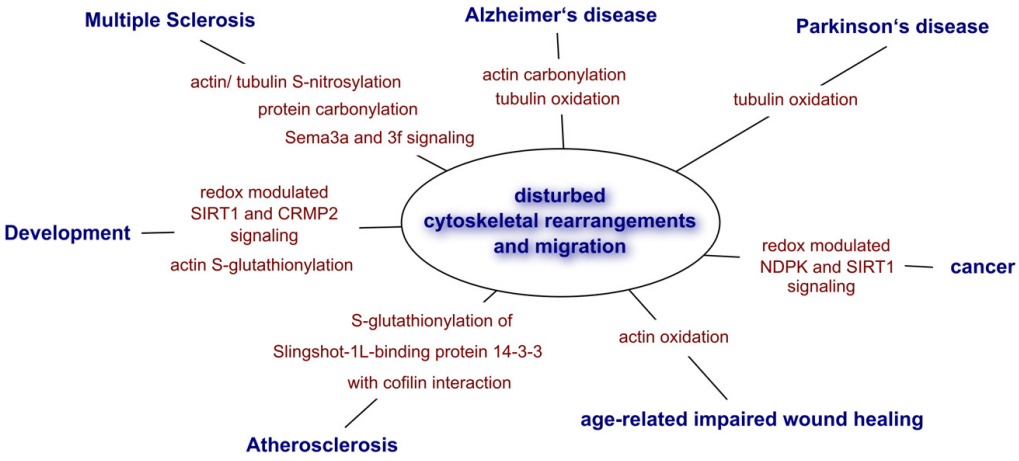

Fig. 6. Disturbed redox regulation of cytoskeletal rearrangements connected to selected physiological and pathophysiological conditions. CRMP2: collapsin response mediator protein 2, NDPK: nucleoside diphosphate kinase, Sema: semaphorin, SIRT1: sirtuin1.

The understanding and modulation of the particular redox mechanisms and signalling pathways mentioned above, might lead to the development of new therapeutic strategies which are urgently needed in diseases connected to failed migration/cytoskeletal rearrangements, e.g. metastatic cancer and neurological disorders such as MS or spinal cord injury.

5. Conclusion

The dynamic remodeling of the cytoskeleton can be spatio-temporally controlled by various redox signalling mechanisms, as exemplified in the thiol/disulfide switch in CRMP2 and the methionyl/methionyl sulfoxide switches in β-actin (Fig. 5). These mechanisms are indispensible during development and organogenesis, and they might also contribute to numerous pathological conditions. We currently witness a shift in paradigms. The redox switches that control these cellular functions might not be the result of random modifications by unspecified oxidants. More and more appear to be controlled by specific enzymes that specifically catalyse the oxidation and reduction of these distinct redox modifications in a manner similar to the kinases and phosphatases in phosphorylation signalling.

Acknowledgements

Among other sources, CHL and CB gratefully acknowledge the financial support by the priority program (SPP) 1710 which was recently founded by the German Research Foundation (DFG) to investigate thiol switches in cellular physiology (DFG grants Li 984/3-1 and Be 3259/5-1).

References

[1] P. Ghezzi, V. Bonetto, M. Fratelli, Thiol Disulfide Balance: From the Concept of Oxidative Stress to that of Redox Regulation, Antioxid. Redox Signal. 7 (2005) 964–972.
[2] D.P. Jones, Redefining oxidative stress, Antioxid. Redox Signal. 8 (2006) 1865–1879, http://dx.doi.org/10.1089/ars.2006.8.1865.
[3] P.J. Halvey, W.H. Watson, J.M. Hansen, Y.-M. Go, A. Samali, D.P. Jones, Compartmental oxidation of thiol-disulphide redox couples during epidermal growth factor signalling, Biochem. J. 386 (2005) 215–219 (doi:BJ20041829).
[4] Y.-M. Go, D.P. Jones, Redox compartmentalization in eukaryotic cells, Biochim. Biophys. Acta, Gen. Subj. 1780 (2008) 1273–1290.
[5] C. Berndt, C.H. Lillig, L. Flohé, Redox regulation by glutathione needs enzymes, Front. Pharmacol. 5 (2014), http://dx.doi.org/10.3389/fphar.2014.00168.
[6] M.M. Gallogly, J.J. Mieyal, Mechanisms of reversible protein glutathionylation in redox signaling and oxidative stress, Curr. Opin. Pharmacol. 7 (2007) 381–391 (doi:S1471-4892(07)00103-8.).
[7] D.T. Hess, A. Matsumoto, S.-O. Kim, H.E. Marshall, J.S. Stamler, Protein S-nitrosylation: purview and parameters, Nat. Rev. Mol. Cell Biol. 6 (2005) 150–166, http://dx.doi.org/10.1038/nrm1569.
[8] M.W. Foster, D.T. Hess, J.S. Stamler, Protein S-nitrosylation in health and disease: a current perspective, Trends Mol. Med. 15 (2009) 391–404, http://dx.doi.org/10.1016/j.molmed.2009.06.007.
[9] L.B. Poole, Formation and functions of protein sulfenic acids, Curr. Protoc. Toxicol. Editor. Board Mahin Maines Ed.–Chief Al. Chapter 17 (2004) Unit17.1. http://dx.doi.org/10.1002/0471140856.tx1701s18.
[10] Y.-C. Chang, C.-N. Huang, C.-H. Lin, H.-C. Chang, C.-C. Wu, Mapping protein cysteine sulfonic acid modifications with specific enrichment and mass spectrometry: an integrated approach to explore the cysteine oxidation, Proteomics 10 (2010) 2961–2971, http://dx.doi.org/10.1002/pmic.200900850.
[11] S.E. Leonard, K.G. Reddie, K.S. Carroll, Mining the thiol proteome for sulfenic acid modifications reveals new targets for oxidation in cells, ACS Chem. Biol. 4 (2009) 783–799, http://dx.doi.org/10.1021/cb900105q.
[12] M.D. Shelton, P.B. Chock, J.J. Mieyal, Glutaredoxin: Role in Reversible Protein S-Glutathionylation and Regulation of Redox Signal Transduction and Protein Translocation, Antioxid. Redox Signal. 7 (2005) 348–366.
[13] C.H. Lillig, A. Holmgren, Thioredoxin and Related Molecules From Biology to Health and Disease, Antioxid. Redox Signal. 9 (2007) 25–47.
[14] C.H. Lillig, C. Berndt, A. Holmgren, Glutaredoxin systems, Biochim. Biophys. Acta, Gen. Subj. 1780 (2008) 1304–1317, http://dx.doi.org/10.1016/j.bbagen.2008.06.003.
[15] E.-M. Hanschmann, J.R. Godoy, C. Berndt, C. Hudemann, C.H. Lillig, Thioredoxins, glutaredoxins, and peroxiredoxins–molecular mechanisms and health significance: from cofactors to antioxidants to redox signaling, Antioxid. Redox Signal. 19 (2013) 1539–1605, http://dx.doi.org/10.1089/ars.2012.4599.
[16] A. Holmgren, M. Björnstedt, Thioredoxin and thioredoxin reductase, Methods Enzymol. 252 (1995) 199–208.
[17] A. Holmgren, F. Aslund, Glutaredoxin, Methods Enzymol. 252 (1995) 283–292 (doi:7476363).
[18] A. Holmgren, Glutathione-dependent enzyme reactions of the phage T4 ribonucleotide reductase system, J. Biol. Chem. 253 (1978) 7424–7430.
[19] J.H. Bushweller, F. Aslund, K. Wüthrich, A. Holmgren, Structural and functional characterization of the mutant Escherichia coli glutaredoxin (C14–S) and its mixed disulfide with glutathione, Biochemistry (Mosc) 31 (1992) 9288–9293.
[20] S.A. Gravina, J.J. Mieyal, Thioltransferase is a specific glutathionyl mixed disulfide oxidoreductase, Biochemistry (Mosc) 32 (1993) 3368–3376.
[21] A. Drazic, J. Winter, The physiological role of reversible methionine oxidation, Biochim. Biophys. Acta 1844 (2014) 1367–1382, http://dx.doi.org/10.1016/j.bbapap.2014.01.001.
[22] S. Boschi-Muller, A. Gand, G. Branlant, The methionine sulfoxide reductases: Catalysis and substrate specificities, Arch. Biochem. Biophys. 474 (2008) 266–273, http://dx.doi.org/10.1016/j.abb.2008.02.007.
[23] A. Hansel, L. Kuschel, S. Hehl, C. Lemke, H.-J. Agricola, T. Hoshi, et al., Mitochondrial targeting of the human peptide methionine sulfoxide reductase (MSRA), an enzyme involved in the repair of oxidized proteins, FASEB J. Off. Publ. Fed. Am. Soc. Exp. Biol. 16 (2002) 911–913, http://dx.doi.org/10.1096/fj.01-0737fje.
[24] A. Hansel, S.H. Heinemann, T. Hoshi, Heterogeneity and function of mammalian MSRs: enzymes for repair, protection and regulation, Biochim. Biophys. Acta 1703 (2005) 239–247, http://dx.doi.org/10.1016/j.bbapap.2004.09.010.
[25] J.W. Lee, N.V. Gordiyenko, M. Marchetti, N. Tserentsoodol, D. Sagher, S. Alam, et al., Gene structure, localization and role in oxidative stress of methionine sulfoxide reductase A (MSRA) in the monkey retina, Exp. Eye Res. 82 (2006) 816–827, http://dx.doi.org/10.1016/j.exer.2005.10.003.
[26] H.-Y. Kim, Glutaredoxin serves as a reductant for methionine sulfoxide reductases with or without resolving cysteine, Acta Biochim. Biophys. Sin. 44 (2012) 623–627, http://dx.doi.org/10.1093/abbs/gms038.
[27] H.-Y. Kim, V.N. Gladyshev, Methionine sulfoxide reduction in mammals: characterization of methionine-R-sulfoxide reductases, Mol. Biol. Cell 15 (2004) 1055–1064, http://dx.doi.org/10.1091/mbc.E03-08-0629.
[28] B.C. Lee, A. Dikiy, H.-Y. Kim, V.N. Gladyshev, Functions and evolution of selenoprotein methionine sulfoxide reductases, Biochim. Biophys. Acta 1790 (2009) 1471–1477, http://dx.doi.org/10.1016/j.bbagen.2009.04.014.
[29] R.T. Dean, S. Fu, R. Stocker, M.J. Davies, Biochemistry and pathology of radical-mediated protein oxidation, Biochem. J. 324 (Pt 1) (1997) 1–18.
[30] E. Stadtman, Free Radical Mediated Oxidation of Proteins, in: T. Özben (Ed.), Free Radic. Oxidative Stress Antioxid, Springer US, 1998, pp. 51–64, http://dx.doi.org/10.1007/978-1-4757-2907-8_5.
[31] J.S. Beckman, Oxidative damage and tyrosine nitration from peroxynitrite, Chem. Res. Toxicol. 9 (1996) 836–844, http://dx.doi.org/10.1021/tx9501445.
[32] O. Augusto, M.G. Bonini, A.M. Amanso, E. Linares, C.C.X. Santos, S.L. De Menezes, Nitrogen dioxide and carbonate radical anion: two emerging radicals in biology, Free Radic. Biol. Med. 32 (2002) 841–859.
[33] R. Radi, Peroxynitrite, a stealthy biological oxidant, J. Biol. Chem. 288 (2013) 26464–26472, http://dx.doi.org/10.1074/jbc.R113.472936.
[34] M. Zou, A. Yesilkaya, V. Ullrich, Peroxynitrite inactivates prostacyclin synthase by heme-thiolate-catalyzed tyrosine nitration, Drug Metab. Rev. 31 (1999) 343–349, http://dx.doi.org/10.1081/DMR-100101922.
[35] I. Dalle-Donne, G. Aldini, M. Carini, R. Colombo, R. Rossi, A. Milzani, Protein carbonylation, cellular dysfunction, and disease progression, J. Cell. Mol. Med. 10 (2006) 389–406.
[36] C.M. Wong, L. Marcocci, L. Liu, Y.J. Suzuki, Cell signaling by protein carbonylation and decarbonylation, Antioxid. Redox Signal. 12 (2010) 393–404, http://dx.doi.org/10.1089/ars.2009.2805.
[37] W.M. Garrison, Reaction mechanisms in the radiolysis of peptides, polypeptides, and proteins, Chem. Rev. 87 (1987) 381–398, http://dx.doi.org/10.1021/cr00078a006.
[38] E.R. Stadtman, Metal ion-catalyzed oxidation of proteins: biochemical mechanism and biological consequences, Free Radic. Biol. Med. 9 (1990) 315–325.
[39] D.R. Mole, P.H. Maxwell, C.W. Pugh, P.J. Ratcliffe, Regulation of HIF by the von Hippel–Lindau tumour suppressor: implications for cellular oxygen sensing, IUBMB Life 52 (2001) 43–47, http://dx.doi.org/10.1080/15216540252774757.
[40] M. Safran, W.G. Kaelin, HIF hydroxylation and the mammalian oxygen-sensing pathway, J. Clin. Invest. 111 (2003) 779–783, http://dx.doi.org/10.1172/JCI18181.
[41] P.J. Ratcliffe, Oxygen sensing and hypoxia signalling pathways in animals: the implications of physiology for cancer, J. Physiol. 591 (2013) 2027–2042, http://dx.doi.org/10.1113/jphysiol.2013.251470.
[42] T.D. Pollard, L. Blanchoin, R.D. Mullins, Molecular mechanisms controlling actin filament dynamics in nonmuscle cells, Annu. Rev. Biophys. Biomol. Struct. 29 (2000) 545–576, http://dx.doi.org/10.1146/annurev.biophys.29.1.545.
[43] T.D. Pollard, Regulation of actin filament assembly by Arp2/3 complex and formins, Annu. Rev. Biophys. Biomol. Struct. 36 (2007) 451–477, http://dx.doi.org/10.1146/annurev.biophys.35.040405.101936.
[44] S. Kurisu, T. Takenawa, WASP and WAVE family proteins: friends or foes in cancer invasion? Cancer Sci. 101 (2010) 2093–2104, http://dx.doi.org/10.1111/j.1349-7006.2010.01654.x.
[45] A.Y. Pollitt, R.H. Insall, WASP and SCAR/WAVE proteins: the drivers of actin assembly, J. Cell Sci. 122 (2009) 2575–2578, http://dx.doi.org/10.1242/jcs.023879.
[46] H. Miki, T. Takenawa, Regulation of actin dynamics by WASP family proteins, J. Biochem. (Tokyo) 134 (2003) 309–313.
[47] F. Straub, Actin, Stud Inst Med Chem Univ Szeged. II, 1942. 1–15.
[48] A. Szent-Györgyi, Studies on muscle, Acta Physiol. Scand. 9 (Suppl. 25) (1945).

[49] W.D. Halliburton, On Muscle-Plasma, J. Physiol. 8 (1887) 133–202.
[50] J.R. Terman, A. Kashina, Post-translational modification and regulation of actin, Curr. Opin. Cell Biol. 25 (2013) 30–38, http://dx.doi.org/10.1016/j.ceb.2012.10.009.
[51] Y. Hamnell-Pamment, C. Lind, C. Palmberg, T. Bergman, I.A. Cotgreave, Determination of site-specificity of S-glutathionylated cellular proteins, Biochem. Biophys. Res. Commun. 332 (2005) 362–369, http://dx.doi.org/10.1016/j.bbrc.2005.04.130.
[52] C. Stournaras, G. Drewes, H. Blackholm, I. Merkler, H. Faulstich, Glutathionyl(cysteine-374) actin forms filaments of low mechanical stability, Biochim. Biophys. Acta 1037 (1990) 86–91.
[53] C. Berndt, G. Poschmann, K. Stühler, A. Holmgren, L. Bräutigam, Zebrafish heart development is regulated via glutaredoxin 2 dependent migration and survival of neural crest cells, Redox Biol. 2 (2014) 673–678, http://dx.doi.org/10.1016/j.redox.2014.04.012.
[54] I. Dalle-Donne, A. Milzani, D. Giustarini, P. Di Simplicio, R. Colombo, R. Rossi, S-NO-actin: S-nitrosylation kinetics and the effect on isolated vascular smooth muscle, J. Muscle Res. Cell Motil. 21 (2000) 171–181.
[55] S.R. Thom, V.M. Bhopale, D.J. Mancini, T.N. Milovanova, Actin S-nitrosylation inhibits neutrophil beta2 integrin function, J. Biol. Chem. 283 (2008) 10822–10834, http://dx.doi.org/10.1074/jbc.M709200200.
[56] S.C. Chen, B. Huang, Y.C. Liu, K.G. Shyu, P.Y. Lin, D.L. Wang, Acute hypoxia enhances proteins' S-nitrosylation in endothelial cells, Biochem. Biophys. Res. Commun. 377 (2008) 1274–1278, http://dx.doi.org/10.1016/j.bbrc.2008.10.144.
[57] S. Ishiwata, Freezing of actin. Reversible oxidation of a sulfhydryl group and structural change, J. Biochem. (Tokyo) 80 (1976) 595–609.
[58] I. Lassing, F. Schmitzberger, M. Björnstedt, A. Holmgren, P. Nordlund, C.E. Schutt, et al., Molecular and structural basis for redox regulation of beta-actin, J. Mol. Biol. 370 (2007) 331–348 (doi:S0022-2836(07)00555-4).
[59] M. Fedorova, N. Kuleva, R. Hoffmann, Identification of cysteine, methionine and tryptophan residues of actin oxidized in vivo during oxidative stress, J. Proteome Res. 9 (2010) 1598–1609, http://dx.doi.org/10.1021/pr901099e.
[60] I. Dalle-Donne, R. Rossi, D. Giustarini, N. Gagliano, P. Di Simplicio, R. Colombo, et al., Methionine oxidation as a major cause of the functional impairment of oxidized actin, Free Radic. Biol. Med. 32 (2002) 927–937.
[61] B. Ghesquière, V. Jonckheere, N. Colaert, J. Van Durme, E. Timmerman, M. Goethals, et al., Redox proteomics of protein-bound methionine oxidation, Mol. Cell. Proteomics MCP. 10 (2011), http://dx.doi.org/10.1074/mcp.M110.006866 (M110.006866).
[62] I. Dalle-Donne, M. Carini, G. Vistoli, L. Gamberoni, D. Giustarini, R. Colombo, et al., Actin Cys374 as a nucleophilic target of alpha, beta-unsaturated aldehydes, Free Radic. Biol. Med. 42 (2007) 583–598, http://dx.doi.org/10.1016/j.freeradbiomed.2006.11.026.
[63] M. Fedorova, T. Todorovsky, N. Kuleva, R. Hoffmann, Quantitative evaluation of tryptophan oxidation in actin and troponin I from skeletal muscles using a rat model of acute oxidative stress, Proteomics 10 (2010) 2692–2700, http://dx.doi.org/10.1002/pmic.201000147.
[64] G. Feuer, F. Molnár, E. Pettkó, F. Straub, Studies on the composition and polymerization of actin, Hung. Acta Physiol. 1 (1948) 150.
[65] J.X. Tang, P.A. Janmey, T.P. Stossel, T. Ito, Thiol oxidation of actin produces dimers that enhance the elasticity of the F-actin network, Biophys. J. 76 (1999) 2208–2215, http://dx.doi.org/10.1016/S0006-3495(99)77376-5.
[66] I. DalleDonne, A. Milzani, R. Colombo, The tert-butyl hydroperoxide-induced oxidation of actin Cys-374 is coupled with structural changes in distant regions of the protein, Biochemistry (Mosc) 38 (1999) 12471–12480.
[67] J. Wang, E.S. Boja, W. Tan, E. Tekle, H.M. Fales, S. English, et al., Reversible glutathionylation regulates actin polymerization in A431 cells, J. Biol. Chem. 276 (2001) 47763–47766 (doi:11684673).
[68] K. Rokutan, R.B. Johnston, K. Kawai, Oxidative stress induces S-thiolation of specific proteins in cultured gastric mucosal cells, Am. J. Physiol. 266 (1994) G247–G254.
[69] K. Bailey, S.V. Perry, The role of SH groups in the myosin–actin interaction, Biochem. J. 41 (1947) xxii.
[70] G.O. Pizarro, O. Ogut, Impact of actin glutathionylation on the actomyosin-S1 ATPase, Biochemistry (Mosc) 48 (2009) 7533–7538, http://dx.doi.org/10.1021/bi900669m.
[71] C. Passarelli, A. Di Venere, N. Piroddi, A. Pastore, B. Scellini, C. Tesi, et al., Susceptibility of isolated myofibrils to in vitro glutathionylation: Potential relevance to muscle functions, Cytoskelet. Hoboken NJ. 67 (2010) 81–89, http://dx.doi.org/10.1002/cm.20425.
[72] T. Fiaschi, G. Cozzi, G. Raugei, L. Formigli, G. Ramponi, P. Chiarugi, Redox regulation of beta-actin during integrin-mediated cell adhesion, J. Biol. Chem. 281 (2006) 22983–22991, http://dx.doi.org/10.1074/jbc.M603040200.
[73] F.C. Chen, O. Ogut, Decline of contractility during ischemia–reperfusion injury: actin glutathionylation and its effect on allosteric interaction with tropomyosin, Am. J. Physiol. Cell Physiol. 290 (2006) C719–C727, http://dx.doi.org/10.1152/ajpcell.00419.2005.
[74] P. Aspenström, C.E. Schutt, U. Lindberg, R. Karlsson, Mutations in beta-actin: influence on polymer formation and on interactions with myosin and profilin, FEBS Lett. 329 (1993) 163–170.
[75] S. Oikawa, T. Yamada, T. Minohata, H. Kobayashi, A. Furukawa, S. Tada-Oikawa, et al., Proteomic identification of carbonylated proteins in the monkey hippocampus after ischemia–reperfusion, Free Radic. Biol. Med. 46 (2009) 1472–1477, http://dx.doi.org/10.1016/j.freeradbiomed.2009.02.029.
[76] M. Oh-Ishi, T. Ueno, T. Maeda, Proteomic method detects oxidatively induced protein carbonyls in muscles of a diabetes model Otsuka Long-Evans Tokushima Fatty (OLETF) rat, Free Radic. Biol. Med. 34 (2003) 11–22.
[77] J.P. Castro, T. Jung, T. Grune, H. Almeida, Actin carbonylation: from cell dysfunction to organism disorder, J. Proteomics. 92 (2013) 171–180, http://dx.doi.org/10.1016/j.jprot.2013.05.006.
[78] J. Lu, T. Katano, D. Uta, H. Furue, S. Ito, Rapid S-nitrosylation of actin by NO-generating donors and in inflammatory pain model mice, Mol. Pain 7 (2011) 101, http://dx.doi.org/10.1186/1744-8069-7-101.
[79] A. Pastore, G. Tozzi, L.M. Gaeta, E. Bertini, V. Serafini, S. Di Cesare, et al., Actin glutathionylation increases in fibroblasts of patients with Friedreich's ataxia: a potential role in the pathogenesis of the disease, J. Biol. Chem. 278 (2003) 42588–42595, http://dx.doi.org/10.1074/jbc.M301872200.
[80] K. Sakai, K. Matsumoto, T. Nishikawa, M. Suefuji, K. Nakamaru, Y. Hirashima, et al., Mitochondrial reactive oxygen species reduce insulin secretion by pancreatic beta-cells, Biochem. Biophys. Res. Commun. 300 (2003) 216–222.
[81] J. Wang, E. Tekle, H. Oubrahim, J.J. Mieyal, E.R. Stadtman, P.B. Chock, Stable and controllable RNA interference: Investigating the physiological function of glutathionylated actin, Proc. Natl. Acad. Sci. U. S. A. 100 (2003) 5103–5106 (doi:12697895).
[82] M. Johansson, M. Lundberg, Glutathionylation of beta-actin via a cysteinyl sulfenic acid intermediary, BMC Biochem. 8 (2007) 26, http://dx.doi.org/10.1186/1471-2091-8-26.
[83] J. Sakai, J. Li, K.K. Subramanian, S. Mondal, B. Bajrami, H. Hattori, et al., Reactive oxygen species-induced actin glutathionylation controls actin dynamics in neutrophils, Immunity 37 (2012) 1037–1049, http://dx.doi.org/10.1016/j.immuni.2012.08.017.
[84] X. Wang, S. Ling, D. Zhao, Q. Sun, Q. Li, F. Wu, et al., Redox regulation of actin by thioredoxin-1 is mediated by the interaction of the proteins via cysteine 62, Antioxid. Redox Signal. 13 (2010) 565–573, http://dx.doi.org/10.1089/ars.2009.2833.
[85] K. Sobierajska, S. Skurzynski, M. Stasiak, J. Kryczka, C.S. Cierniewski, M. Swiatkowska, Protein disulfide isomerase directly interacts with β-actin Cys374 and regulates cytoskeleton reorganization, J. Biol. Chem. 289 (2014) 5758–5773, http://dx.doi.org/10.1074/jbc.M113.479477.
[86] S.R. Thom, V.M. Bhopale, T.N. Milovanova, M. Yang, M. Bogush, Thioredoxin reductase linked to cytoskeleton by focal adhesion kinase reverses actin S-nitrosylation and restores neutrophil β(2) integrin function, J. Biol. Chem. 287 (2012) 30346–30357, http://dx.doi.org/10.1074/jbc.M112.355875.
[87] B.C. Lee, Z. Péterfi, F.W. Hoffmann, R.E. Moore, A. Kaya, A. Avanesov, et al., MsrB1 and MICALs regulate actin assembly and macrophage function via reversible stereoselective methionine oxidation, Mol. Cell 51 (2013) 397–404, http://dx.doi.org/10.1016/j.molcel.2013.06.019.
[88] R.-J. Hung, C.S. Spaeth, H.G. Yesilyurt, J.R. Terman, SelR reverses Mical-mediated oxidation of actin to regulate F-actin dynamics, Nat. Cell Biol. 15 (2013) 1445–1454, http://dx.doi.org/10.1038/ncb2871.
[89] R.-J. Hung, U. Yazdani, J. Yoon, H. Wu, T. Yang, N. Gupta, et al., Mical links semaphorins to F-actin disassembly, Nature 463 (2010) 823–827, http://dx.doi.org/10.1038/nature08724.
[90] C.A. McDonald, Y.Y. Liu, B.A. Palfey, Actin stimulates reduction of the MICAL-2 monooxygenase domain, Biochemistry (Mosc) 52 (2013) 6076–6084, http://dx.doi.org/10.1021/bi4008462.
[91] C. Passarelli, S. Petrini, A. Pastore, V. Bonetto, P. Sale, L.M. Gaeta, et al., Myosin as a potential redox-sensor: an in vitro study, J. Muscle Res. Cell Motil. 29 (2008) 119–126, http://dx.doi.org/10.1007/s10974-008-9145-x.
[92] Y. Samstag, I. John, G.H. Wabnitz, Cofilin: a redox sensitive mediator of actin dynamics during T-cell activation and migration, Immunol. Rev. 256 (2013) 30–47, http://dx.doi.org/10.1111/imr.12115.
[93] Y.-M. Go, M. Orr, D.P. Jones, Actin cytoskeleton redox proteome oxidation by cadmium, Am. J. Physiol. Lung Cell. Mol. Physiol. 305 (2013) L831–L843, http://dx.doi.org/10.1152/ajplung.00203.2013.
[94] Y.-M. Go, M. Orr, D.P. Jones, Increased nuclear thioredoxin-1 potentiates cadmium-induced cytotoxicity, Toxicol. Sci. Off. J. Soc. Toxicol. 131 (2013) 84–94, http://dx.doi.org/10.1093/toxsci/kfs271.
[95] V.O. Paavilainen, E. Bertling, S. Falck, P. Lappalainen, Regulation of cytoskeletal dynamics by actin-monomer-binding proteins, Trends Cell Biol. 14 (2004) 386–394, http://dx.doi.org/10.1016/j.tcb.2004.05.002.
[96] K. Mizuno, Signaling mechanisms and functional roles of cofilin phosphorylation and dephosphorylation, Cell. Signal. 25 (2013) 457–469, http://dx.doi.org/10.1016/j.cellsig.2012.11.001.
[97] B.J. Agnew, L.S. Minamide, J.R. Bamburg, Reactivation of phosphorylated actin depolymerizing factor and identification of the regulatory site, J. Biol. Chem. 270 (1995) 17582–17587.
[98] A.S. Nimnual, L.J. Taylor, D. Bar-Sagi, Redox-dependent downregulation of Rho by Rac, Nat. Cell Biol. 5 (2003) 236–241, http://dx.doi.org/10.1038/ncb938.
[99] T. Eiseler, H. Döppler, I.K. Yan, K. Kitatani, K. Mizuno, P. Storz, Protein kinase D1 regulates cofilin-mediated F-actin reorganization and cell motility through slingshot, Nat. Cell Biol. 11 (2009) 545–556, http://dx.doi.org/10.1038/ncb1861.
[100] J.-S. Kim, T.Y. Huang, G.M. Bokoch, Reactive oxygen species regulate a slingshot-cofilin activation pathway, Mol. Biol. Cell 20 (2009) 2650–2660, http://dx.doi.org/10.1091/mbc.E09-02-0131.
[101] B.J. Pope, K.M. Zierler-Gould, R. Kühne, A.G. Weeds, L.J. Ball, Solution structure of human cofilin: actin binding, pH sensitivity, and relationship to actin-depolymerizing factor, J. Biol. Chem. 279 (2004) 4840–4848, http://dx.doi.org/10.1074/jbc.M310148200.
[102] M. Klemke, G.H. Wabnitz, F. Funke, B. Funk, H. Kirchgessner, Y. Samstag, Oxidation of cofilin mediates T cell hyporesponsiveness under oxidative stress conditions, Immunity 29 (2008) 404–413, http://dx.doi.org/10.1016/j.immuni.2008.06.016.

[103] C.-K. Lee, H.-J. Park, H.H. So, H.J. Kim, K.S. Lee, W.S. Choi, et al., Proteomic profiling and identification of cofilin responding to oxidative stress in vascular smooth muscle, Proteomics 6 (2006) 6455–6475, http://dx.doi.org/10.1002/pmic.200600124.

[104] F. Klamt, S. Zdanov, R.L. Levine, A. Pariser, Y. Zhang, B. Zhang, et al., Oxidant-induced apoptosis is mediated by oxidation of the actin-regulatory protein cofilin, Nat. Cell Biol. 11 (2009) 1241–1246, http://dx.doi.org/10.1038/ncb1968.

[105] B.T. Chua, C. Volbracht, K.O. Tan, R. Li, V.C. Yu, P. Li, Mitochondrial translocation of cofilin is an early step in apoptosis induction, Nat. Cell Biol. 5 (2003) 1083–1089, http://dx.doi.org/10.1038/ncb1070.

[106] B. Schulte, I. John, B. Simon, C. Brockmann, S.A. Oelmeier, B. Jahraus, et al., A reducing milieu renders cofilin insensitive to phosphatidylinositol 4,5-bisphosphate (PIP2) inhibition, J. Biol. Chem. 288 (2013) 29430–29439, http://dx.doi.org/10.1074/jbc.M113.479766.

[107] J. Pfannstiel, M. Cyrklaff, A. Habermann, S. Stoeva, G. Griffiths, R. Shoeman, et al., Human cofilin forms oligomers exhibiting actin bundling activity, J. Biol. Chem. 276 (2001) 49476–49484, http://dx.doi.org/10.1074/jbc.M104760200.

[108] B.W. Bernstein, A.E. Shaw, L.S. Minamide, C.W. Pak, J.R. Bamburg, Incorporation of cofilin into rods depends on disulfide intermolecular bonds: implications for actin regulation and neurodegenerative disease, J. Neurosci. Off. J. Soc. Neurosci. 32 (2012) 6670–6681, http://dx.doi.org/10.1523/JNEUROSCI. 6020-11.2012.

[109] P. Goyal, D. Pandey, D. Brünnert, E. Hammer, M. Zygmunt, W. Siess, Cofilin oligomer formation occurs in vivo and is regulated by cofilin phosphorylation, PLoS One 8 (2013) e71769, http://dx.doi.org/10.1371/journal.pone.0071769.

[110] M. Fratelli, H. Demol, M. Puype, S. Casagrande, I. Eberini, M. Salmona, et al., Identification by redox proteomics of glutathionylated proteins in oxidatively stressed human T lymphocytes, Proc. Natl. Acad. Sci. U. S. A. 99 (2002) 3505–3510, http://dx.doi.org/10.1073/pnas.052592699.

[111] R. Fiore, A.W. Püschel, The function of semaphorins during nervous system development, Front. Biosci. J. Virtual Libr. 8 (2003) s484–s499.

[112] Unified nomenclature for the semaphorins/collapsins. Semaphorin Nomenclature Committee, Cell 97 (1999) 551–552.

[113] K. Reidy, A. Tufro, Semaphorins in kidney development and disease: modulators of ureteric bud branching, vascular morphogenesis, and podocyte-endothelial crosstalk, Pediatr. Nephrol. Berl. Ger. 26 (2011) 1407–1412, http://dx.doi.org/10.1007/s00467-011-1769-1.

[114] E.F. Schmidt, S.M. Strittmatter, The CRMP family of proteins and their role in Sema3A signaling, Adv. Exp. Med. Biol. 600 (2007) 1–11, http://dx.doi.org/10.1007/978-0-387-70956-7_1.

[115] D.A. Mendes-da-Cruz, L. Linhares-Lacerda, S. Smaniotto, M. Dardenne, W. Savino, Semaphorins and neuropilins: new players in the neuroendocrine control of the intrathymic T-cell migration in humans, Exp. Physiol. 97 (2012) 1146–1150, http://dx.doi.org/10.1113/expphysiol.2011.061515.

[116] Y. Collette, R. Marignier, C. Vuaillat, V. Rogemond, N. Davoust, C. Malcus, et al., A role for the neuronal protein collapsin response mediator protein 2 in T lymphocyte polarization and migration, J. Immunol. Baltim. Md 1950 (175) (2005) 7650–7660.

[117] B. Luzón-Toro, R.M. Fernández, A. Torroglosa, J.C. de Agustín, C. Méndez-Vidal, D.I. Segura, et al., Mutational spectrum of semaphorin 3A and semaphorin 3D genes in Spanish Hirschsprung patients, PLoS One 8 (2013) e54800, http://dx.doi.org/10.1371/journal.pone.0054800.

[118] V. Procaccia, H. Nakayama, A. Shimizu, M. Klagsbrun, Gleevec/imatinib, an ABL2 kinase inhibitor, protects tumor and endothelial cells from semaphorin-induced cytoskeleton collapse and loss of cell motility, Biochem. Biophys. Res. Commun. 448 (2014) 134–138, http://dx.doi.org/10.1016/j.bbrc.2014.04.063.

[119] J.-S. Joyal, N. Sitaras, F. Binet, J.C. Rivera, A. Stahl, K. Zaniolo, et al., Ischemic neurons prevent vascular regeneration of neural tissue by secreting semaphorin 3A, Blood 117 (2011) 6024–6035, http://dx.doi.org/10.1182/blood-2010-10-311589.

[120] H.R. Quintá, J.M. Pasquini, G.A. Rabinovich, L.A. Pasquini, Glycan-dependent binding of galectin-1 to neuropilin-1 promotes axonal regeneration after spinal cord injury, Cell Death Differ. 21 (2014) 941–955, http://dx.doi.org/10.1038/cdd.2014.14.

[121] W.M. Jurney, G. Gallo, P.C. Letourneau, S.C. McLoon, Rac1-mediated endocytosis during ephrin-A2- and semaphorin 3A-induced growth cone collapse, J. Neurosci. Off. J. Soc. Neurosci. 22 (2002) 6019–6028 (doi:20026594).

[122] I.C. Zachary, P. Frankel, I.M. Evans, C. Pellet-Many, The role of neuropilins in cell signalling, Biochem. Soc. Trans. 37 (2009) 1171–1178, http://dx.doi.org/10.1042/BST0371171.

[123] Y. Sasaki, C. Cheng, Y. Uchida, O. Nakajima, T. Ohshima, T. Yagi, et al., Fyn and Cdk5 mediate semaphorin-3A signaling, which is involved in regulation of dendrite orientation in cerebral cortex, Neuron 35 (2002) 907–920.

[124] B.J. Eickholt, F.S. Walsh, P. Doherty, An inactive pool of GSK-3 at the leading edge of growth cones is implicated in Semaphorin 3A signaling, J. Cell Biol. 157 (2002) 211–217, http://dx.doi.org/10.1083/jcb.200201098.

[125] Y. Goshima, F. Nakamura, P. Strittmatter, S.M. Strittmatter, Collapsin-induced growth cone collapse mediated by an intracellular protein related to UNC-33, Nature 376 (1995) 509–514, http://dx.doi.org/10.1038/376509a0.

[126] Y. Fukata, T.J. Itoh, T. Kimura, C. Ménager, T. Nishimura, T. Shiromizu, et al., CRMP-2 binds to tubulin heterodimers to promote microtubule assembly, Nat. Cell Biol. 4 (2002) 583–591, http://dx.doi.org/10.1038/ncb825.

[127] M. Varrin-Doyer, P. Vincent, S. Cavagna, N. Auvergnon, N. Noraz, V. Rogemond, et al., Phosphorylation of collapsin response mediator protein 2 on Tyr-479 regulates CXCL12-induced T lymphocyte migration, J. Biol. Chem. 284 (2009) 13265–13276, http://dx.doi.org/10.1074/jbc.M807664200.

[128] L. Bräutigam, L.D. Schütte, J.R. Godoy, T. Prozorovski, M. Gellert, G. Hauptmann, et al., Vertebrate-specific glutaredoxin is essential for brain development, Proc. Natl. Acad. Sci. U. S. A. 108 (2011) 20532–20537, http://dx.doi.org/10.1073/pnas.1110085108.

[129] L.H. Wang, S.M. Strittmatter, Brain CRMP forms heterotetramers similar to liver dihydropyrimidinase, J. Neurochem. 69 (1997) 2261–2269.

[130] A. Morinaka, M. Yamada, R. Itofusa, Y. Funato, Y. Yoshimura, F. Nakamura, et al., Thioredoxin mediates oxidation-dependent phosphorylation of CRMP2 and growth cone collapse, Sci. Signal. 4 (2011) ra26, http://dx.doi.org/10.1126/scisignal.2001127.

[131] M. Gellert, S. Venz, J. Mitlöhner, C. Cott, E.-M. Hanschmann, C.H. Lillig, Identification of a dithiol–disulfide switch in collapsin response mediator protein 2 (CRMP2) that is toggled in a model of neuronal differentiation, J. Biol. Chem. 288 (2013) 35117–35125, http://dx.doi.org/10.1074/jbc.M113.521443.

[132] M.E. Lönn, C. Hudemann, C. Berndt, V. Cherkasov, F. Capani, A. Holmgren, et al., Expression Pattern of Human Glutaredoxin 2 Isoforms: Identification and Characterization of Two Testis/Cancer Cell-Specific Isoforms, Antioxid. Redox Signal. 10 (2008) 547–558.

[133] L.D. Schütte, S. Baumeister, B. Weis, C. Hudemann, E.-M. Hanschmann, C.H. Lillig, Identification of potential protein dithiol–disulfide substrates of mammalian Grx2, Biochim. Biophys. Acta 1830 (2013) 4999–5005, http://dx.doi.org/10.1016/j.bbagen.2013.07.009.

[134] O.A. Bizzozero, J. Zheng, Identification of major S-nitrosylated proteins in murine experimental autoimmune encephalomyelitis, J. Neurosci. Res. 87 (2009) 2881–2889, http://dx.doi.org/10.1002/jnr.22113.

[135] J.R. Terman, T. Mao, R.J. Pasterkamp, H.-H. Yu, A.L. Kolodkin, MICALs, a Family of Conserved Flavoprotein Oxidoreductases, Function in Plexin-Mediated Axonal Repulsion, Cell 109 (2002) 887–900, http://dx.doi.org/10.1016/S0092-8674(02)00794-8.

[136] S.S.P. Giridharan, S. Caplan, MICAL-family proteins: Complex regulators of the actin cytoskeleton, Antioxid. Redox Signal. 20 (2014) 2059–2073, http://dx.doi.org/10.1089/ars.2013.5487.

[137] S.K. Krueger, D.E. Williams, Mammalian flavin-containing monooxygenases: structure/function, genetic polymorphisms and role in drug metabolism, Pharmacol. Ther. 106 (2005) 357–387, http://dx.doi.org/10.1016/j.pharmthera.2005.01.001.

[138] M. Nadella, M.A. Bianchet, S.B. Gabelli, J. Barrila, L.M. Amzel, Structure and activity of the axon guidance protein MICAL, Proc. Natl. Acad. Sci. U. S. A. 102 (2005) 16830–16835, http://dx.doi.org/10.1073/pnas.0504838102.

[139] S.S.P. Giridharan, J.L. Rohn, N. Naslavsky, S. Caplan, Differential regulation of actin microfilaments by human MICAL proteins, J. Cell Sci. 125 (2012) 614–624, http://dx.doi.org/10.1242/jcs.089367.

[140] M.R. Lundquist, A.J. Storaska, T.-C. Liu, S.D. Larsen, T. Evans, R.R. Neubig, et al., Redox modification of nuclear actin by MICAL-2 regulates SRF signaling, Cell 156 (2014) 563–576, http://dx.doi.org/10.1016/j.cell.2013.12.035.

[141] S. Etienne-Manneville, From signaling pathways to microtubule dynamics: the key players, Curr. Opin. Cell Biol. 22 (2010) 104–111, http://dx.doi.org/10.1016/j.ceb.2009.11.008.

[142] H. de Forges, A. Bouissou, F. Perez, Interplay between microtubule dynamics and intracellular organization, Int. J. Biochem. Cell Biol. 44 (2012) 266–274, http://dx.doi.org/10.1016/j.biocel.2011.11.009.

[143] D.J. Sharp, J.L. Ross, Microtubule-severing enzymes at the cutting edge, J. Cell Sci. 125 (2012) 2561–2569, http://dx.doi.org/10.1242/jcs.101139.

[144] M.K. Gardner, M. Zanic, J. Howard, Microtubule catastrophe and rescue, Curr. Opin. Cell Biol. 25 (2013) 14–22, http://dx.doi.org/10.1016/j.ceb.2012.09.006.

[145] K. Tanaka, Dynamic regulation of kinetochore-microtubule interaction during mitosis, J. Biochem. (Tokyo) 152 (2012) 415–424, http://dx.doi.org/10.1093/jb/mvs109.

[146] J.G. DeLuca, Kinetochore-microtubule dynamics and attachment stability, Methods Cell Biol. 97 (2010) 53–79, http://dx.doi.org/10.1016/S0091-679X(10)97004-0.

[147] L.C. Kapitein, K.W. Yau, C.C. Hoogenraad, Microtubule dynamics in dendritic spines, Methods Cell Biol. 97 (2010) 111–132, http://dx.doi.org/10.1016/S0091-679X(10)97007-6.

[148] D.M. Suter, K.E. Miller, The emerging role of forces in axonal elongation, Prog. Neurobiol. 94 (2011) 91–101, http://dx.doi.org/10.1016/j.pneurobio.2011.04.002.

[149] L.M. Landino, K.L. Moynihan, J.V. Todd, K.L. Kennett, Modulation of the redox state of tubulin by the glutathione/glutaredoxin reductase system, Biochem. Biophys. Res. Commun. 314 (2004) 555–560 (doi:14733943).

[150] L.M. Landino, J.S. Iwig, K.L. Kennett, K.L. Moynihan, Repair of peroxynitrite damage to tubulin by the thioredoxin reductase system, Free Radic. Biol. Med. 36 (2004) 497–506, http://dx.doi.org/10.1016/j.freeradbiomed.2003.11.026.

[151] L.M. Landino, R. Hasan, A. McGaw, S. Cooley, A.W. Smith, K. Masselam, et al., Peroxynitrite oxidation of tubulin sulfhydryls inhibits microtubule polymerization, Arch. Biochem. Biophys. 398 (2002) 213–220, http://dx.doi.org/10.1006/abbi.2001.2729.

[152] L. Bräutigam, L.D.E. Jensen, G. Poschmann, S. Nyström, S. Bannenberg, K. Dreij, et al., Glutaredoxin regulates vascular development by reversible glutathionylation of sirtuin 1, Proc. Natl. Acad. Sci. U. S. A. 110 (2013) 20057–20062, http://dx.doi.org/10.1073/pnas.1313753110.

[153] W. Chen, T. Seefeldt, A. Young, X. Zhang, Y. Zhao, J. Ruffolo, et al., Microtubule S-glutathionylation as a potential approach for antimitotic agents, BMC Cancer 12 (2012) 245, http://dx.doi.org/10.1186/1471-2407-12-245.

[154] G. Bansal, D. Das, C.-Y. Hsieh, Y.-H. Wang, B.A. Gilmore, C.-M. Wong, et al., IL-22 activates oxidant signaling in pulmonary vascular smooth muscle cells, Cell. Signal. 25 (2013) 2727–2733, http://dx.doi.org/10.1016/j.cellsig.2013.09.001.

[155] M. Sparaco, L.M. Gaeta, F.M. Santorelli, C. Passarelli, G. Tozzi, E. Bertini, et al., Friedreich's ataxia: oxidative stress and cytoskeletal abnormalities, J. Neurol. Sci. 287 (2009) 111–118, http://dx.doi.org/10.1016/j.jns.2009.08.052.

[156] S. Zahid, R. Khan, M. Oellerich, N. Ahmed, A.R. Asif, Differential S-nitrosylation of proteins in Alzheimer's disease, Neuroscience 256 (2014) 126–136, http://dx.doi.org/10.1016/j.neuroscience.2013.10.026.

[157] L. Lefièvre, Y. Chen, S.J. Conner, J.L. Scott, S.J. Publicover, W.C.L. Ford, et al., Human spermatozoa contain multiple targets for protein S-nitrosylation: an alternative mechanism of the modulation of sperm function by nitric oxide? Proteomics 7 (2007) 3066–3084, http://dx.doi.org/10.1002/pmic.200700254.

[158] H. Stroissnigg, A. Trancíková, L. Descovich, J. Fuhrmann, W. Kutschera, J. Kostan, et al., S-nitrosylation of microtubule-associated protein 1B mediates nitric-oxide-induced axon retraction, Nat. Cell Biol. 9 (2007) 1035–1045, http://dx.doi.org/10.1038/ncb1625.

[159] C. Hudemann, M.E. Lönn, J.R. Godoy, F. Zahedi Avval, F. Capani, A. Holmgren, et al., Identification, expression pattern, and characterization of mouse glutaredoxin 2 isoforms, Antioxid. Redox Signal. 11 (2009) 1–14, http://dx.doi.org/10.1089/ars.2008.2068.

[160] J.W. Fawcett, R.A. Asher, The glial scar and central nervous system repair, Brain Res. Bull. 49 (1999) 377–391.

[161] G. Yiu, Z. He, Glial inhibition of CNS axon regeneration, Nat. Rev. Neurosci. 7 (2006) 617–627, http://dx.doi.org/10.1038/nrn1956.

[162] J.W. Prineas, F. Connell, Remyelination in multiple sclerosis, Ann. Neurol. 5 (1979) 22–31, http://dx.doi.org/10.1002/ana.410050105.

[163] B. Ferguson, M.K. Matyszak, M.M. Esiri, V.H. Perry, Axonal damage in acute multiple sclerosis lesions, Brain J. Neurol. 120 (Pt 3) (1997) 393–399.

[164] A. Boyd, H. Zhang, A. Williams, Insufficient OPC migration into demyelinated lesions is a cause of poor remyelination in MS and mouse models, Acta Neuropathol. (Berl.) 125 (2013) 841–859, http://dx.doi.org/10.1007/s00401-013-1112-y.

[165] T. Koda, T. Okuno, K. Takata, J.A. Honorat, M. Kinoshita, S. Tada, et al., Sema4A inhibits the therapeutic effect of IFN-β in EAE, J. Neuroimmunol. 268 (2014) 43–49, http://dx.doi.org/10.1016/j.jneuroim.2013.12.014.

[166] Y.A. Syed, E. Hand, W. Möbius, C. Zhao, M. Hofer, K.A. Nave, et al., Inhibition of CNS remyelination by the presence of semaphorin 3A, J. Neurosci. Off. J. Soc. Neurosci. 31 (2011) 3719–3728, http://dx.doi.org/10.1523/JNEUROSCI.4930-10.2011.

[167] G. Piaton, M.-S. Aigrot, A. Williams, S. Moyon, V. Tepavcevic, I. Moutkine, et al., Class 3 semaphorins influence oligodendrocyte precursor recruitment and remyelination in adult central nervous system, Brain J. Neurol. 134 (2011) 1156–1167, http://dx.doi.org/10.1093/brain/awr022.

[168] S.M. Smerjac, O.A. Bizzozero, Cytoskeletal protein carbonylation and degradation in experimental autoimmune encephalomyelitis, J. Neurochem. 105 (2008) 763–772, http://dx.doi.org/10.1111/j.1471-4159.2007.05178.x.

[169] I. de la Pena, M. Pabon, S. Acosta, P.R. Sanberg, N. Tajiri, Y. Kaneko, et al., Oligodendrocytes engineered with migratory proteins as effective graft source for cell transplantation in multiple sclerosis, Cell Med. 6 (2014) 123–127, http://dx.doi.org/10.3727/215517913X674144.

[170] A. Arvidsson, T. Collin, D. Kirik, Z. Kokaia, O. Lindvall, Neuronal replacement from endogenous precursors in the adult brain after stroke, Nat. Med. 8 (2002) 963–970, http://dx.doi.org/10.1038/nm747.

[171] K. Jin, M. Minami, J.Q. Lan, X.O. Mao, S. Batteur, R.P. Simon, et al., Neurogenesis in dentate subgranular zone and rostral subventricular zone after focal cerebral ischemia in the rat, Proc. Natl. Acad. Sci. U. S. A. 98 (2001) 4710–4715, http://dx.doi.org/10.1073/pnas.081011098.

[172] M. Sparaco, L.M. Gaeta, G. Tozzi, E. Bertini, A. Pastore, A. Simonati, et al., Protein glutathionylation in human central nervous system: potential role in redox regulation of neuronal defense against free radicals, J. Neurosci. Res. 83 (2006) 256–263, http://dx.doi.org/10.1002/jnr.20729.

[173] M.Y. Aksenov, M.V. Aksenova, D.A. Butterfield, J.W. Geddes, W.R. Markesbery, Protein oxidation in the brain in Alzheimer's disease, Neuroscience 103 (2001) 373–383.

[174] L.M. Landino, S.H. Robinson, T.E. Skreslet, D.M. Cabral, Redox modulation of tau and microtubule-associated protein-2 by the glutathione/glutaredoxin reductase system, Biochem. Biophys. Res. Commun. 323 (2004) 112–117 (doi:15351709).

[175] H.S. Kim, S.L. Ullevig, H.N. Nguyen, D. Vanegas, R. Asmis, Redox regulation of 14-3-3ζ controls monocyte migration, Arterioscler. Thromb. Vasc. Biol. 34 (2014) 1514–1521, http://dx.doi.org/10.1161/ATVBAHA.114.303746.

[176] M.J. Reed, A.C. Corsa, S.A. Kudravi, R.S. McCormick, W.T. Arthur, A deficit in collagenase activity contributes to impaired migration of aged microvascular endothelial cells, J. Cell. Biochem. 77 (2000) 116–126.

[177] J.E. Mogford, N. Tawil, A. Chen, D. Gies, Y. Xia, T.A. Mustoe, Effect of age and hypoxia on TGFbeta1 receptor expression and signal transduction in human dermal fibroblasts: impact on cell migration, J. Cell. Physiol. 190 (2002) 259–265, http://dx.doi.org/10.1002/jcp.10060.

[178] S. Cané, S. Ponnappan, U. Ponnappan, Altered regulation of CXCR4 expression during aging contributes to increased CXCL12-dependent chemotactic migration of CD4(+) T cells, Aging Cell 11 (2012) 651–658, http://dx.doi.org/10.1111/j.1474-9726.2012.00830.x.

[179] S.T. Nikkari, J. Koistinaho, O. Jaakkola, Changes in the composition of cytoskeletal and cytocontractile proteins of rat aortic smooth muscle cells during aging, Differ. Res. Biol. Divers. 44 (1990) 216–221.

[180] M.J. Reed, N.S. Ferara, R.B. Vernon, Impaired migration, integrin function, and actin cytoskeletal organization in dermal fibroblasts from a subset of aged human donors, Mech. Ageing Dev. 122 (2001) 1203–1220.

[181] R. Blakytny, L.J. Erkell, G. Brunner, Inactivation of active and latent transforming growth factor beta by free thiols: potential redox regulation of biological action, Int. J. Biochem. Cell Biol. 38 (2006) 1363–1373, http://dx.doi.org/10.1016/j.biocel.2006.01.017.

[182] M.H. Barcellos-Hoff, T.A. Dix, Redox-mediated activation of latent transforming growth factor-beta 1, Mol. Endocrinol. Baltim. Md. 10 (1996) 1077–1083, http://dx.doi.org/10.1210/mend.10.9.8885242.

[183] V. Byles, L. Zhu, J.D. Lovaas, L.K. Chmilewski, J. Wang, D.V. Faller, et al., SIRT1 induces EMT by cooperating with EMT transcription factors and enhances prostate cancer cell migration and metastasis, Oncogene 31 (2012) 4619–4629, http://dx.doi.org/10.1038/onc.2011.612.

[184] R. Kunimoto, K. Jimbow, A. Tanimura, M. Sato, K. Horimoto, T. Hayashi, et al., SIRT1 regulates lamellipodium extension and migration of melanoma cells, J. Invest. Dermatol. 134 (2014) 1693–1700, http://dx.doi.org/10.1038/jid.2014.50.

[185] M.A.E. Almgren, K.C.E. Henriksson, J. Fujimoto, C.L. Chang, Nucleoside diphosphate kinase A/nm23-H1 promotes metastasis of NB69-derived human neuroblastoma, Mol. Cancer Res. MCR. 2 (2004) 387–394.

[186] L. Han, X.-H. Liang, L.-X. Chen, S.-M. Bao, Z.-Q. Yan, SIRT1 is highly expressed in brain metastasis tissues of non-small cell lung cancer (NSCLC) and in positive regulation of NSCLC cell migration, Int. J. Clin. Exp. Pathol. 6 (2013) 2357–2365.

[187] E. Lee, J. Jeong, S.E. Kim, E.J. Song, S.W. Kang, K.-J. Lee, Multiple functions of Nm23-H1 are regulated by oxido-reduction system, PLoS One 4 (2009) e7949, http://dx.doi.org/10.1371/journal.pone.0007949.

[188] J. Li, E. Wang, F. Rinaldo, K. Datta, Upregulation of VEGF-C by androgen depletion: the involvement of IGF-IR-FOXO pathway, Oncogene 24 (2005) 5510–5520, http://dx.doi.org/10.1038/sj.onc.1208693.

[189] A.G. Mustafa, J.A. Wang, K.M. Carrico, E.D. Hall, Pharmacological inhibition of lipid peroxidation attenuates calpain-mediated cytoskeletal degradation after traumatic brain injury, J. Neurochem. 117 (2011) 579–588, http://dx.doi.org/10.1111/j.1471-4159.2011.07228.x.

[190] J.M. Fukuto, S.J. Carrington, HNO signaling mechanisms, Antioxid. Redox Signal. 14 (2011) 1649–1657, http://dx.doi.org/10.1089/ars.2010.3855.

[191] C.H. Switzer, W. Flores-Santana, D. Mancardi, S. Donzelli, D. Basudhar, L.A. Ridnour, et al., The emergence of nitroxyl (HNO) as a pharmacological agent, Biochim. Biophys. Acta 1787 (2009) 835–840, http://dx.doi.org/10.1016/j.bbabio.2009.04.015.

[192] W.D. Gao, C.I. Murray, Y. Tian, X. Zhong, J.F. DuMond, X. Shen, et al., Nitroxyl-mediated disulfide bond formation between cardiac myofilament cysteines enhances contractile function, Circ. Res. 111 (2012) 1002–1011, http://dx.doi.org/10.1161/CIRCRESAHA.112.270827.

[193] C.C. Rohena, S.L. Mooberry, Recent progress with microtubule stabilizers: new compounds, binding modes and cellular activities, Nat. Prod. Rep. 31 (2014) 335–355, http://dx.doi.org/10.1039/c3np70092e.

[194] J.J. Field, A. Kanakkanthara, J.H. Miller, Microtubule-targeting agents are clinically successful due to both mitotic and interphase impairment of microtubule function, Bioorg. Med. Chem. 22 (2014) 5050–5059, http://dx.doi.org/10.1016/j.bmc.2014.02.035.

[195] A. Nürnberg, A. Kollmannsperger, R. Grosse, Pharmacological inhibition of actin assembly to target tumor cell motility, Rev. Physiol. Biochem. Pharmacol. 166 (2014) 23–42, http://dx.doi.org/10.1007/112_2013_16.

[196] S.M. Wilson, R. Khanna, Specific Binding of Lacosamide to Collapsin Response Mediator Protein 2 (CRMP2) and Direct Impairment of its Canonical Function: Implications for the Therapeutic Potential of Lacosamide, Mol. Neurobiol. (2014), http://dx.doi.org/10.1007/s12035-014-8775-9.

[197] K. Hensley, K. Venkova, A. Christov, W. Gunning, J. Park, Collapsin response mediator protein-2: an emerging pathologic feature and therapeutic target for neurodisease indications, Mol. Neurobiol. 43 (2011) 180–191, http://dx.doi.org/10.1007/s12035-011-8166-4.

[198] C.E. Schutt, J.C. Myslik, M.D. Rozycki, N.C. Goonesekere, U. Lindberg, The structure of crystalline profilin-beta-actin, Nature 365 (1993) 810–816, http://dx.doi.org/10.1038/365810a0.

V. Manuscript

Molecular dynamics simulations and *in vitro* analysis of the CRMP2 thiol switch

Daniel Möller*, **Manuela Gellert***, Walter Langel, Christopher Horst Lillig

submitted to Molecular BioSystems

submission ID: MD-ART-03-2017-000160

* These authors contributed equally to this work.

Molecular dynamics simulations and in vitro analysis of the CRMP2 thiol switch

Daniel Möller[+1], Manuela Gellert[+2], Walter Langel[1], Christopher Horst Lillig[*2]

[+] These authors contributed equally to this work.

* corresponding author: horst@lillig.de

[1] Biophysical Chemistry, Institute of Biochemistry, University Greifswald, 17489 Greifswald, Germany

[2] Institute for Medical Biochemistry and Molecular Biology, University Medicine, University Greifswald, 17489 Greifswald, Germany

Abstract

Collapsin response mediator protein CRMP2 (gene: DPYSL2) is crucial for neuronal development. The homotetrameric CRMP2 complex is regulated via two mechanisms, first by phosphorylation at, and second by reduction and oxidation of the Cys504 residues of two adjacent subunits. Here, we analyzed the effects of this redox switch on the protein *in vitro* combined with force field molecular dynamics (MD). Earlier X-ray data contain the structure of the rigid body of the molecule but lack the flexible C-terminus with the important sites for phosphorylation and redox regulation. An *in silico* model for this part was established by replica exchange simulations and homology modelling, which is consistent with results gained from CD spectroscopy with recombinant protein. Thermofluor data indicated that the protein aggregates at bivalent ion concentrations below 200 mM. In simulations the protein surface was covered at these conditions by large amounts of ions, which most likely prevent aggregation. A tryptophan residue (Trp295) in close proximity to the forming disulfide allowed the measurement of the structural relaxation of the rigid body upon reduction by fluorescent quenching. We were also able to determine the second order rate constant of CRMP2 oxidation by H_2O_2. The simulated solvent accessible surface of the hydroxyl group of Ser518 significantly increased upon reduction of the disulfide bond. Our results give first detailed insight in the profound structural changes of the tetrameric CRMP2 due to oxidation and indicate a tightly connected regulation by phosphorylation and redox modification.

Keywords: collapsin response mediator protein 2, thiol switch, redox regulation, molecular dynamics simulation (MD), replica exchange MD, TIGER2, tryptophan fluorescence, CD spectroscopy

Introduction

CRMP2 is an essential component of the semaphorin 3A signaling pathway and crucially involved in cell polarization and migration and thus indispensable for neuronal development and cell mobility[1,2]. This CRMP2 pathway controls, for instance, ureteric and vascular patterning[3], axon guidance[4], and the migration and polarization of T-cells[5,6]. The protein was implied in various physiological disorders, for instance a hyper phosphorylated form was found in protein deposits during Alzheimer's disease[7,8]. The regulation of CRMP2 and the biological effects triggered by this signaling hub are complex.

The crystal structures[9,10] and further analyses[11] demonstrated a homotetramer as the native conformation of CRMP2. The full sequence of a human CRMP2 monomer (Q16555) consists of 572 amino acids (aa). Unfortunately, none of the two crystal structures known to us cover the full protein, but only Asp15 - Ala489 for 2GSE[9] or Ser14 - Glu490 for 2VM8[10]. The steric structure is stabilized by four bivalent ions such as Ca^{2+} or Mg^{2+}.

A thiol-disulfide switch[11,12] regulates the protein. Two Cys504 residues of two monomers form an inter-molecular disulfide bond[11]. Closing and opening of these bonds yield an oxidized and a reduced form of CRMP2, respectively. This dithiol-disulfide switch of CRMP2 profoundly affects its structure and function. In most cases only one of the two possible disulfide bonds in a tetrameric complex is formed. Our previous work suggested significant conformational changes in the homo-tetrameric CRMP2 complex upon oxidation, leading to a decreased exposure of hydrophobic aa at the surface[11]. The protein is regulated not only via the redox switch[11-13], but also by direct phosphorylation at multiple sites via protein kinases[14-16]. The Rho kinase ROCK phosphorylates CRMP2 at Thr555, cycline-dependent kinase 5 (CDK5) at Ser522. While these two steps are thought to be independent, interconversion of CRMP2 by glycogen synthase kinase 3 beta (GSK3β) at Thr509, Thr514, and Ser518 strictly requires the priming phosphorylation at Ser522 by CDK5[14,16]. The phosphorylation of CRMP2 controls its binding to other proteins, for instance tubulin[4], and the Cyfip1/WAVE1 (cytoplasmic FMR1-interacting protein 1/WASP family verprolin-homologous protein-1) complex[17], a regulator of actin branching and polymerization. All of these experimentally verified phosphorylation sites are localized within the flexible C-terminus of the protein downstream of the Cys504 redox switch.

According to Majava et al. and Stenmark et al., the CRMP2 homotetramer has to be stabilized by four bivalent ions such as Ca^{2+} or Mg^{2+}, which are integrated into the molecular structure, and the removal of these ions will induce denaturation[9,10].

Additionally, the bivalent ions attach to the charged surface side chains, resulting in shifts in the electrostatic surface potentials and an increase of the surface areas around the C-termini. Under the conditions of the work of Majava et al., ionic concentrations around 20 mM had a stabilizing effect, whereas 200 mM or higher again resulted in protein unfolding[10].

In this study, we modelled and compared the completely oxidized and reduced states of CRMP2 and analyzed the changes in the secondary structure, the solvent accessible surface area (SASA) and the composition of defined aa properties at the surface. By tryptophan fluorescence, the transition between oxidized and reduced states of CRMP2 was probed. We further studied the stability of CRMP2 in ionic environments and the location of the bivalent ions on specific amino acids.

Results

We hypothesized that CRMP2s regulation by oxidation and reduction leads to profound structural and conformational changes. These changes were investigated by analyses of CRMP2 *in silico* and *in vitro* using a variety of experimental methods and force field molecular dynamics.

Secondary structure and conformational changes between reduced and oxidized CRMP2 assayed by MD simulations and CD spectroscopy

The steric structure of CRMP2 was analyzed using three methods. Results from CD spectroscopy (**Figure 1**) average over the full protein with 572 amino acids per monomer, including the flexible parts of the C- and N-termini with unknown secondary structures. Molecular dynamics simulations cover residues 16 to 531, and the X-ray results reproduce the rigid part of the protein only (14-490). Taking into account these differences, experimental data and simulations yield consistent distributions of the secondary structure motifs.

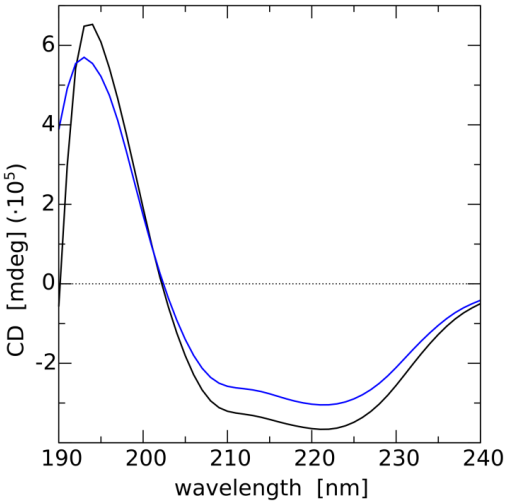

Figure 1: CD spectra of oxidized (black) and reduced (blue) recombinantly expressed CRMP2, at 10 µM in 20 mM Mg^{2+} solution. The traces clearly indicate a shift in the overall secondary structure upon oxidation. We estimated the secondary structure contents of the spectra by the method of Raussens et al.[18].

Both experimental crystal structures of CRMP2, 2VM8[10] and 2GSE[9] are rather similar with 56.5 % helical structure (α-helices and turns) as largest structured part (**Table 1**). The MD calculations are based on these X-ray data, and yield a major extent of helical structure elements.

Helices and turns are very similar, and it is not possible to distinguish between them in CD spectra. The total contribution of these two motifs increases from 57 % to 62 % upon reduction. Similarly to CD, the simulation qualitatively also yields an enhancement of helical structures in the reduced conformation of the protein, but the effect is rather small, increasing from 57.6 % to about 58.5 %.

The β-sheets contribute 23 % to the crystal structure, which decreases to a constant value of 20 % in the MD simulations in solution. CD spectroscopy revealed even lower values of only 10-13 % and significant parts of the structure are assigned to coil (28 %). *In silico*, about 20 % are random coil, and a small shift from this disordered to a helical structure is observed when switching from the oxidized to the reduced protein conformation.

The comparison between crystal, *in silico*, and the data from CD spectroscopy suggests that the C-terminus, which is missing in the crystal structure, mainly adds helical elements to the *in silico* and *in vitro* protein. Remaining amino acids are unstructured or helical, resulting in a decrease of the relative amount of β-sheet and an increase of the helical proportion. No correlation was detected between secondary structure and ionic concentrations in the MD.

Exposure of surfaces to solvent

The traces for the SASA in **Figure 2** show a steep increase within 50 ns indicating structural relaxation. After this time, the values fluctuate around a constant value. We thus assume that the simulation times of 200 to 300 ns were sufficient for sampling equilibrated systems. The highest SASA is found for the protein molecules with the four stabilizing bivalent ions (blue and black traces). The run without bivalent ions shows a large fluctuation, whereas the systems with higher ion concentrations have smaller areas and may be shrinking under the influence of the surface charge, yielding more compact protein structures. The results for the radius of gyration (Supporting Information **Figure SI 3**) of these systems seem to confirm this picture. Further inspection of the data demonstrates that the fluctuation or 'breathing' of the relaxed surface is mainly due to a fluctuation of the SASA of the flexible C-terminal area.

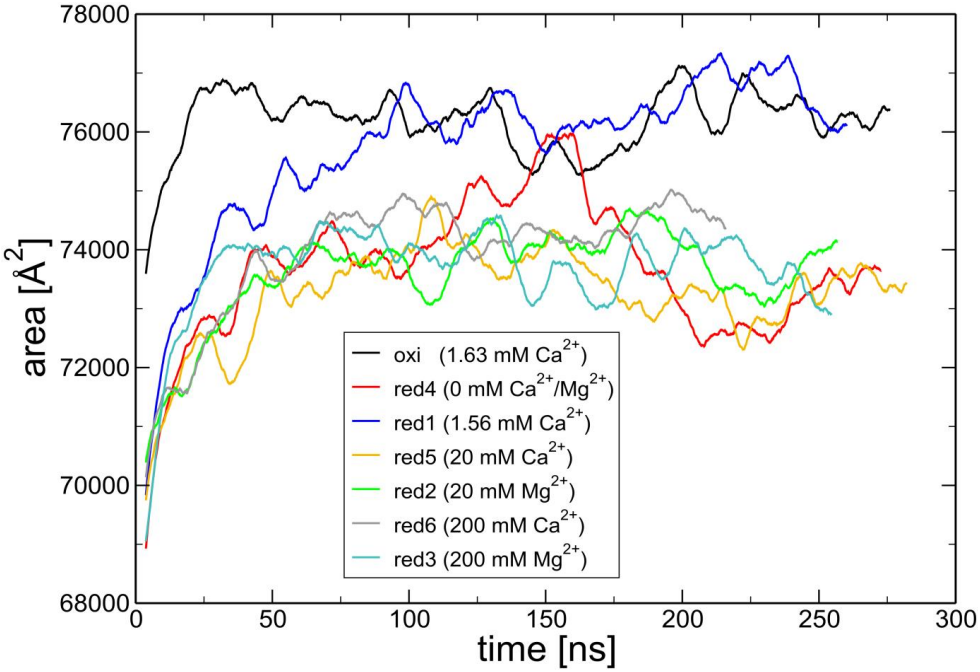

Figure 2: Solvent accessible surface area (SASA) of the CRMP2 homotetramer as a function of time from the MD simulations: Oxidized with four structure stabilizing bivalent ions (black), reduced without any bivalent ions (red), with four structure stabilizing bivalent ions (blue), with 20 mM (Mg^{2+} green, Ca^{2+} yellow) and with 200 mM bivalent ions (Mg^{2+} cyan, Ca^{2+} grey). The curves are running averages of the raw data with a window of 7.5 ns.

We consider the amino acids Ala, Ile, Leu, Met, Phe, Pro, Trp, Val as hydrophobic and evaluate the ratio of their solvent exposed area to the total SASA. During reduction and with enhanced the ion concentration from 0 to 200 mM, this ratio increased by less than 1 % (**Table 1**).

SASA of the CRMP2 phosphorylation sites Thr509, Thr514, Ser517, Ser518 and Ser522

In a previous study, we used HeLa cells expressing Grx2c, which leads to the complete reduction of the normally oxidized CRMP2 *in vivo* [REF: Gellert et al., Cancer Research submitted]. In these cells, an increased CRMP2 phosphorylation at Thr509, Thr514, and Ser518 was described. These three residues are the target sites for phosphorylation by the kinase GSK3β. For a side chain, which may be phosphorylated *in vivo*, the simulation should yield a structure, in which the hydroxyl group is well accessible.

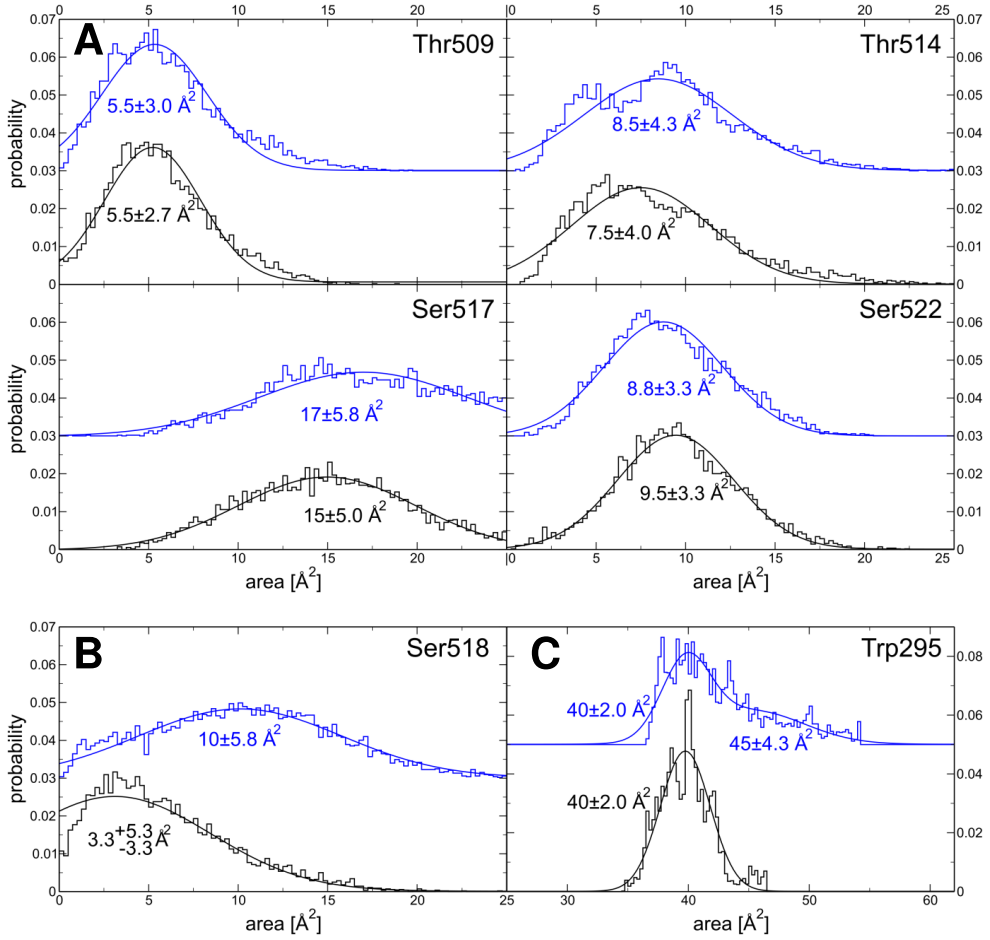

Figure 3: Distributions of the SASA:

(A) **hydroxyl groups of CRMP2s phosphorylation sites at the C-terminus in MD simulations. The molecules contained four bivalent ions. All values show significant fluctuations due to thermal motion. Centers and widths of the Gaussian fits are indicated in the figures. The distributions for oxidized (black) and reduced CRMP2 (blue) are not significantly different for Thr509, Thr514, Ser517 and Ser522.**

(B) **Only the hydroxyl group of Ser518 is significantly more exposed to the solvent in the reduced conformation compared to the oxidized form.**

(C) **The distribution of the full Trp295 SASA in the oxidized state is well described by a Gaussian centered at 40 Å². In the reduced system, a second Gaussian at 45 Å² with about the same intensity has to be added indicating an increase of the average SASA due to the relaxation of the protein.**

In our model, the five side chains are all in contact with the solvent (**Figure 3**). The hydroxyl group of Ser517 has a significantly higher SASA than the other four amino acids. Four of the hydroxyl groups do not show a significant response to reduction and protein relaxation. However the SASA of Ser518

significantly decreased after oxidation of Cys504, suggesting that this serine loses contact to the solution and therefore GSK3β accessibility. The variation of bivalent ion concentrations did not significantly affect the SASA data.

It may depend on the structure of the respective enzyme, if phosphorylation of serine affords solvent exposure of its hydroxyl group only, or of the full side chain. The inspection of the SASA for the full amino acids shows that Ser522 seems to be buried in all systems and is less exposed to the solvent than the other four amino acids. We speculate that this is consistent with the previously described observation that Ser522 is phosphorylated by another kinase, CDK5, than the other residues[14,16].

Oxidation of CRMP2 by H_2O_2 in vitro *and Quenching of Tryptophan Fluorescence*

The Trp295 is part of the rigid body of CRMP2, but is located in close proximity to the flexible C-terminus (**Figure 4.A**). We assume that the observed changes in tryptophan fluorescence (**Figure 4.B**) are mainly based on the changes in the environment of Trp295. During oxidation of the recombinant protein by H_2O_2 *in vitro*, the tryptophan fluorescence (**Figure 4.B**) was quenched. Obviously, the environment of the Trp295 residue in the CRMP2 body was affected by the oxidation reaction in the flexible C-terminus resulting in fluorescence quenching. The MD showed that because of this rearranging the SASA of this residue is slightly smaller after the formation of the disulfide bridge (**Figure 3**). *In vitro* we detected a continuous red shift of the emission maxima during the oxidation, also indicating changes of Trp295s environment (Insert of **Figure 4.B**). The displacement from 340.85 to 343.10 nm corresponded to a decrease of the quantum energy by 2.3 kJ/mol (**Figure 4.C**). It is well known that tryptophan fluorescence depends on the environment of the residue. Therefore we assign this red shift to a shift of the energy levels of the fluorescent indole ring of the corresponding Trp295 (supplementary **Figure SI 4**).

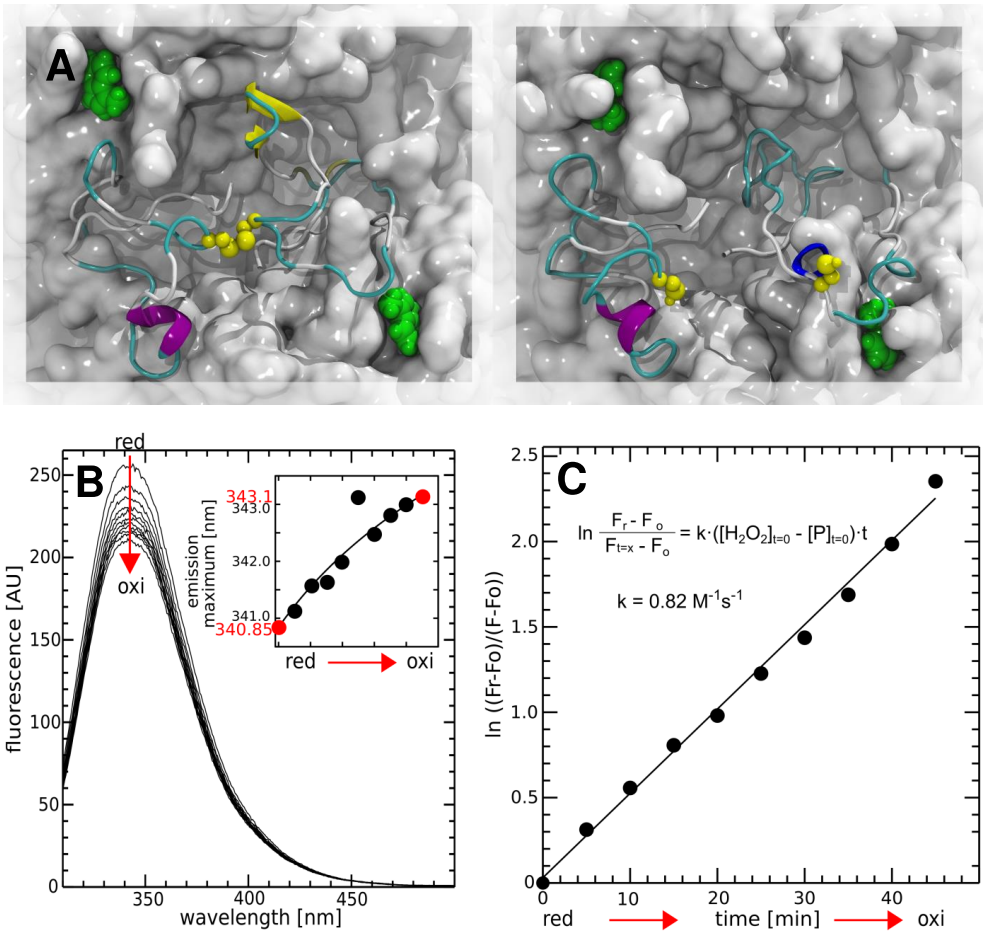

Figure 4: Fluorescence quenching of the Trp295.

(A) **Snapshots of the structures of Trp295 (green) on the surface of oxidized (right) and reduced CRMP2 (left) from MD. The 41 aa of C-termini are shown with their secondary structure (helix: purple and blue; sheet: yellow arrows; turn: cyan; coil: white) and the Cys504 residues as ball-and-stick in yellow.**

(B) **Fluorescence spectra of CRMP2 after excitation at 296 nm, measured every 5 min. The intensity continuously decreases during the oxidation with H_2O_2. The insert shows the red shift of the emission maxima over time.**

(C) **Evaluation of the decrease of the emission at 340 nm according to the inserted equation. The slope of the straight line corresponds to a pseudo first order rate constant of $8.2 \cdot 10^{-4}$ s^{-1}. With the concentration of 10^{-3} mol/l for H_2O_2, we obtained a second order rate constant of 0.82 +/- 0.06 M^{-1} s^{-1} (n=3).**

Correlation of Trp295 fluorescence wavelength and electrostatic energies of CRMP2s oxidized and reduced state

In the frame of a force field model, the shift of an electronic state relative to vacuum energy is given by the sum of the products of the atomic point charges q_a of the atoms *a* and the electrostatic potential V_a of the atomic charges of the surrounding molecules[19]:

$$E = e * (\sum_a V_a * q_a) \quad (1)$$

The smooth particle-mesh Ewald method (PME) in VMD yielded a grid for the electrostatic potential with a resolution of 0.5 Å and an Ewald factor of 0.25, which was interpolated at the positions of the tryptophan atoms a yielding V_a. This analysis afforded the knowledge of the partial charges q_a and positions of the atoms a, which were only known for the electrostatic ground state. These energies E thus only refer to this ground state.

The analysis of the E from the Trp295 side chain (**Figure SI 4**) yielded two results. By oxidizing the molecule, the electrostatic energy of the ground state of the indole ring increased by 1.1 kJ/mol, which may contribute to the observed red shift of the emission maxima. We further analyzed the electrostatic energy of indole and its benzene and pyrrole components as a function of the ionic strength of the solution. The addition of ions to the solution provoked a shift of the electrostatic energies of the ground state of Trp295. The overall electrostatic energy of the indole ring is nearly independent of ion type or concentrations, but benzene and pyrrole rings responded in opposite directions to the ions. The energy of the benzene part increases with increasing Ca^{2+} concentration, but decreases with increasing Mg^{2+} concentration. In contrast, the pyrrole part shows an increase of energy with Mg^{2+} and a decrease with Ca^{2+}.

Ion-interactions and Influences of divalent cations on the thermal stability of CRMP2

We analyzed the effects of the concentration of divalent cations, *i.e.* Mg^{2+} or Ca^{2+}, on the thermal stability of the recombinant protein in a thermofluor assay[20]. Re-buffering of the protein in 10 mM HEPES buffer (2-[4-(2-hydroxyethyl)piperazin-1-yl]ethane sulfonic acid; pH 8.0) using gel filtration chromatography, resulted in precipitation. This could only be prevented by the immediate addition of 200 mM Mg^{2+} ions. We thus eluted the protein in HEPES buffers containing either 300 mM Mg^{2+} or Ca^{2+} ions, which prohibited the precipitation completely. The ion concentrations for the thermofluor

assay were then adjusted by addition of appropriate concentrations of the EDTA, which efficiently chelates divalent cations.

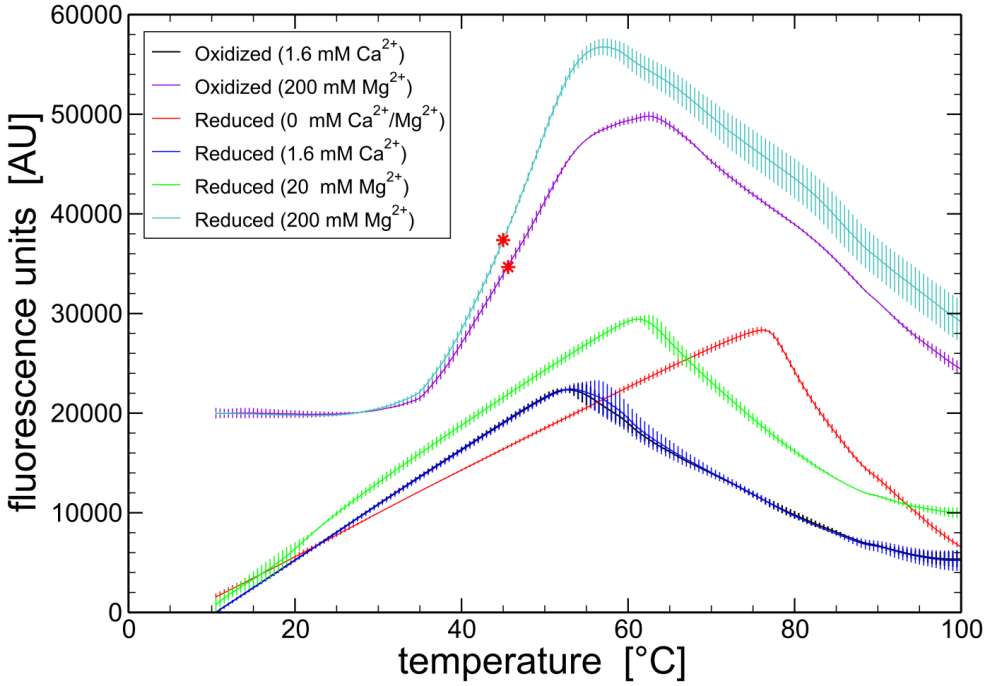

Figure 5: Differential scanning fluorimetry of recombinant CRMP2 at different ion concentrations. The protein was kept at 300 mM ion concentration, before EDTA was added to set the conditions to the ion concentrations indicated. The standard deviation was included with the curves (n=3). The curves of oxidized and reduced CRMP2 at 200 mM Mg^{2+} (violet and cyan) were shifted by 20000 au.

The fluorescence curves of all samples showed a strong increase in the temperature range from 10-60 °C (**Figure 5**). The data recorded with 200 mM Mg^{2+} were fitted by the standard Boltzmann model[21] for the intensity I at the temperature T:

$$I(T) = I_L + \frac{I_H - I_L}{1 + \exp\left(\frac{T_m - T}{I'}\right)} \quad (2).$$

I_H and I_L are the respective maximum and minimum fluorescence intensities and I´ is related to the maximum slope. Both reduced and oxidized CRMP2 are obviously stable under these conditions with melting temperatures of T_m = 45 and 45.6 °C (red stars in **Figure 5**), respectively. At lower Ca^{2+} or Mg^{2+} concentrations, the intensity nearly linearly increased over a larger temperature range, likely due to precipitation of the proteins.

It may be possible that the degradation of the samples at low ion concentrations in this experiment are not due to spontaneous denaturation of single homotetramers but due to their aggregation, which was beyond the scope of the MD simulation. Onset of protein denaturation should be indicated in the simulations by an increase of the hydrophobic area exposed to the solvent (**Table 1**). Thus was less than 1 %, and did not suggest the induction of CRMP2s denaturation.

Cation distribution on CRMP2

For each of the bivalent ions Ca^{2+} and Mg^{2+} we distinguish two layers around CRMP2 (**Figure 6.A**). At lower concentrations one very well defined shell is found, which contains ions interacting directly with the amino acid side chains and probably may be assigned as rigid Helmholtz plane. The second layer is much less occupied and has a broader distance distribution than the first one, possibly being more flexible. Mg^{2+} has a smaller ion radius than Ca^{2+} and has a shorter distance to the amino acids.

In the frame of the force field model, the bivalent ions interact mainly with the negative oxygen atoms on the protein surface. The predominant interaction centers are the deprotonated carboxyl groups of Asp and Glu (**Figure 6.B, C**). Especially at low ion concentrations, Ca^{2+} ions also attach to the oxygen atom in the Gln side chain. In the data for the first two shells, some ions are found close to amino acids which do not contain negative centers in the side chains such as Arg, Ile, Leu, Pro and Thr. Inspection of the steric structures reveals unspecific interactions of the cations with the backbone carboxyl groups (**Figure 6.C**).

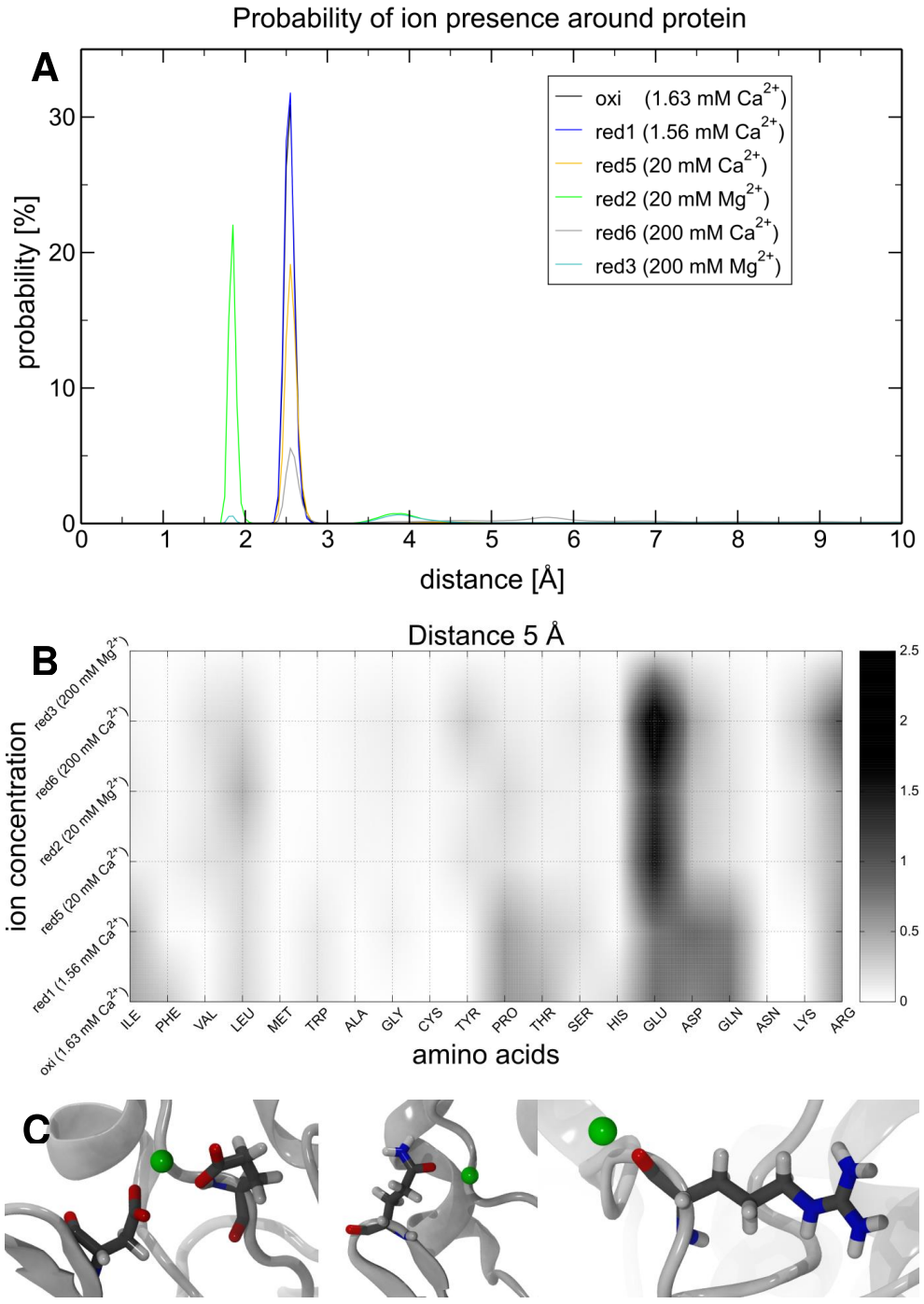
Probability of ion presence around protein
A
probability [%]
distance [Å]
oxi (1.63 mM Ca2+)
red1 (1.56 mM Ca2+)
red5 (20 mM Ca2+)
red2 (20 mM Mg2+)
red6 (200 mM Ca2+)
red3 (200 mM Mg2+)
B
Distance 5 Å
ion concentration
amino acids
ILE PHE VAL LEU MET TRP ALA GLY CYS TYR PRO THR SER HIS GLU ASP GLN ASN LYS ARG
C

Figure 6: Bivalent cations interacting with CRMP2.

(A) **Normalized distribution of cation distances to the protein. The first well defined shells are clearly distinguished for Mg^{2+} at 1.8 Å (green) and Ca^{2+} at 3 Å (orange). At 200 mM concentration broader second shells are found with respective distances of 3.8 to 4 Å for Mg^{2+} and for Ca^{2+}.**

(B) **Probability of the interaction of an amino acid with a bivalent ion up to distances of 5 Å. Data are normalized with respect to the number of occurrences of the respective amino acid at water exposed surface, the number of free ions and the simulation time. The amino acids are arranged according to their hydropathy[22,23]. Asp, Asn, Glu and Gln are sorted in order of functionality.**

(C) **Snapshots of the interactions between bivalent ions and amino acids. From left to right: Predominant attachment to the highly negative carboxyl groups of Asp and Glu, weaker interaction with the oxygen in the Gln side chain and weak adhesion to the carboxyl groups of several amino acids.**

Discussion

Secondary structure

The structure of CRMP2 used in this work is based on X-ray data. However they do not cover the chemical most important part of the protein, the C-terminus containing the regulatory phosphorylation sites and the disulfide forming cysteine residues. The C-terminus revealed to be very flexible and probably could not attain an ordered structure in the crystal. On the other hand, the regulatory sites must show high flexibility for structural rearrangements. We assembled a structure using molecular dynamics, which is consistent with experimental data and permitted further analysis of the protein. SASA data show that the fluctuation (also described as breathing) of the protein surface as well as the radius of gyration is mainly due to the flexible C-terminus rather than to the rigid body.

Tryptophan fluorescence

However, also parts other than the C-termini are affected by the structural rearrangement of the molecule after oxidation. The SASA of the Trp295 decreases upon oxidation, resulting in a quenched and red shifted fluorescence. Our simulations reveal an increase of the electrostatic energy of the ground state of about 1.1 kJ/mol. The observed red shift of 2.3 kJ/mol is reproduced, assuming a down shift of the excited state by 1.2 kJ/mol (**Figure 7**). We have no estimation for the upper state, since the charge distribution in the upper state[24] is not accessible in our calculations. We do not know the fluorescing electronic state (L_a or L_b) [25,26], but the shift of the fluorescence quantum energy of Trp295 during oxidation is the same order of magnitude as the shift for the ground state from our force field data.

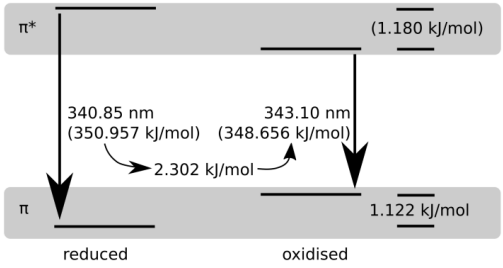

Figure 7: Possible change in ground (π) and excitation state (π*) of the Trp295 fluorescence

Ionic environment

Our results demonstrated a more distinct response of CRMP2 to the bivalent Mg^{2+} and Ca^{2+} ions compared to the literature. We aimed to reproduce the results of Majava et al.[10] regarding the protein stability with two different bivalent ions (Ca^{2+} or Mg^{2+}) in various concentrations. A stabilizing effect

with 20 mM $CaCl_2$ or $MgCl_2$ was reported, but a concentration of 200 mM destabilized the protein significantly.

Our *in vitro* studies do not confirm these effects on CRMP2s structure, *e.g.* the postulated beginning of denaturation[10]. We saw a fast precipitation at lower ion concentrations up to 20 mM and, on the contrary, stabilizing effects at 200 mM. We propose is that the adsorption of these ions to the protein results in a positive zeta-potential, which is only high enough to stop aggregation at high ion concentrations in the solution.

Mechanism

The molecular modeling of the CRMP2 thiol switch through our MD simulations suggested profound structural changes as a consequence of oxidation and reduction. These changes were confirmed *in vitro*. The fluorescence quenching of Trp295 could also be used to determine its redox state and to determine the rate constant of the oxidation of the protein by hydrogen peroxide. Moreover, our results suggest a complex cross talk between the redox switch and other post-translational mechanisms that regulate CRMP2s biological activity (**Figure 8**). We have previously demonstrated that all three target sites of the GSK3β kinase showed significantly increased levels of phosphorylation in cells in which CRMP2 was kept in the reduced conformation by Grx2c [REF: Gellert et al., Cancer Research submitted]. The molecular dynamics simulations as presented here further support and expand this hypothesis.

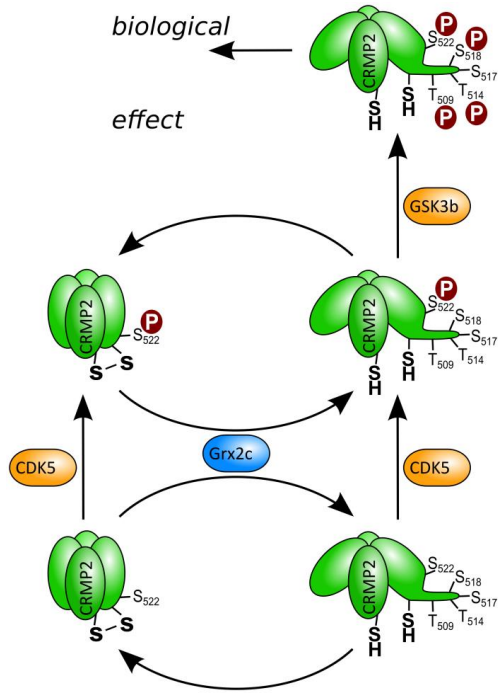

Figure 8: Model of the posttranslational regulation of CRMP2's biological activity. Phosphorylation of Ser522 by the priming kinase CDK5 appears to be independent of the redox switch. However, the subsequent phosphorylation steps by the GSK3β kinase may require the reduction of the thiol switch first, followed by phosphorylation of Ser518 and its neighboring residues, i.e. Thr509, Thr514, and Ser517.

While the hydroxyl group of Ser522 did not show significant differences, the hydroxyl group of Ser518 was significantly more surface exposed

in the reduced conformations compared to the oxidized conformations. We thus propose that the phosphorylation of Ser522 by the priming kinase CDK5[8] may be independent of the redox state of CRMP2 (**Figure 8**). However, the subsequent phosphorylation steps by GSK3β[8] may require the protein to be in the reduce form, to allow phosphorylation of Ser518 followed by the other neighboring residues. Hence, the results presented here suggest a complex cross talk between the thiol switch and interconversion by phosphorylation in the semaphorin 3A signaling pathway.

Acknowledgements

We thank Norman Geist (Greifswald) for continuous assistance, programming of some our analyzes tools and useful discussions during the simulations. CHL appreciates financial support of the Deutsche Forschungsgemeinschaft (DFG SPP 1710 (LI984/3-1)). The replica exchange MD simulations have been performed in part on the computers of the North-German Supercomputing Alliance (HLRN), project mvc00007.

Tables

Table 1: Overview of CRMP2-simulations with color scheme for Figure 2, Figure 3, Figure 5, Figure 6 and SI 2, SI 3. Oxidation status, bivalent ion concentration, box dimensions and simulation time. Secondary structure elements: for X-ray data, MD simulation (with 2064 amino acids) of the oxidized CRMP2 (oxi) and reduced forms with different ion concentrations (red1 to red6) as an average over the last 25 ns (of every simulation) per element and for oxidized and reduced recombinant CRMP2 with CD-spectroscopy. Composition of the water exposed surfaces (SASA) for every simulation from hydrophobic amino acids to total SASA of the protein.

	oxidized	reduced					
Run: color scheme	oxi: black	red4: red	red1: blue	red2: green	red3: cyan	red5: orange	red6: grey
Bivalent ions	1.63 mM Ca^{2+} 4 Ca^{2+}-ions*	0 mM no bivalent ions	1.56 mM Ca^{2+} 4 Ca^{2+}-ions*	20 mM Mg^{2+} 46 Mg^{2+}-ions	200 mM Mg^{2+} 459 Mg^{2+}-ions	20 mM Ca^{2+} 46 Ca^{2+}-ions	200 mM Ca^{2+} 459 Ca^{2+}-ions
Box-size in Å x y z	159.0 156.6 178.8	155.8 167.5 160.3	159.3 175.1 166.3	159.8 167.5 160.3	155.1 166.7 159.6	155.8 167.5 160.3	155.3 167.0 159.8
Water molecules	136207	127468	142211	127438	126217	127434	126355
Counter ions	44 Na^+	52 Na^+	44 Na^+	40 Cl^-	866 Cl^-	40 Cl^-	866 Cl^-
Simulation time	280 ns	275 ns	260 ns	260 ns	260 ns	285 ns	220 ns
Secondary structure elements from MD during the last 25 ns							
Helix	31.5 %	32.9 %	31.7 %	33.4 %	32.8 %	33.2 %	32.9 %
Turn	26.1 %	25.2 %	27.1 %	25.5 %	25.7 %	25.0 %	25.2 %
Total helix and turn	57.6 %	58.1 %	58.8 %	58.9 %	58.5 %	58.2 %	58.1 %
Sheet	20.4 %	20.3 %	20.5 %	20.2 %	20.2 %	20.9 %	20.3 %
Coil	22.0 %	21.6 %	20.8 %	20.8 %	21.3 %	21.0 %	21.7 %
Secondary structure content from CD spectroscopy of the recombinant protein							
Helical	57.4 %			62.9 %			
Sheet	12.8 %			10.4 %			
Random	28.0 %			26.5 %			
Secondary structure content in the X-ray data of reduced CRMP2 crystals							
					2VM8 (1905 aa)		2GSE (1901 aa)
Helix					37.5 %		37.7 %
Turn					19.0 %		18.8 %
Total helix and turn					56.5 %		56.5 %
Sheet					23.3 %		24.3 %
Coil					20.2 %		19.3 %
Composition of water exposed surfaces during the last 25 ns of MD							
Hydrophobic aa	29.1 %	29.0 %	29.4 %	29.6 %	29.7 %	29.5 %	29.6 %

*concentration of the four (structure supporting) Ca^{2+}-ions in the simulation box for comparison to *in vitro* experimental concentrations

References

1. Z. Chen, D. Borek, S. B. Padrick, T. S. Gomez, Z. Metlagel, A. M. Ismail, J. Umetani, D. D. Billadeau, Z. Otwinowski and M. K. Rosen, *Nature*, 2010, **468**, 533-538.
2. Y. Kawano, T. Yoshimura, D. Tsuboi, S. Kawabata, T. Kaneko-Kawano, H. Shirataki, T. Takenawa and K. Kaibuchi, *Molecular and Cellular Biology*, 2005, **25**, 9920-9935.
3. K. Reidy and A. Tufro, *Pediatr Nephrol*, 2011, **26**, 1407-1412.
4. E. F. Schmidt and S. M. Strittmatter, *Semiaphorins: Receptor and Intracellular Signaling Mechanisms*, 2007, **600**, 1-11.
5. D. A. Mendes-da-Cruz, L. Linhares-Lacerda, S. Smaniotto, M. Dardenne and W. Savino, *Exp Physiol*, 2012, **97**, 1146-1150.
6. P. Vincent, Y. Collette, R. Marignier, C. Vuaillat, W. Rogemond, N. Davoust, C. Malcus, S. Cavagna, A. Gessain, I. Machuca-Gayet, M. F. Belin, T. Quach and P. Giraudon, *J Immunol*, 2005, **175**, 7650-7660.
7. K. Hensley and P. Kursula, *J Alzheimers Dis*, 2016, **53**, 1-14.
8. Y. Uchida, T. Ohshima, Y. Sasaki, H. Suzuki, S. Yanai, N. Yamashita, F. Nakamura, K. Takei, Y. Ihara, K. Mikoshiba, P. Kolattukudy, J. Honnorat and Y. Goshima, *Genes to Cells*, 2005, **10**, 165-179.
9. P. Stenmark, D. Ogg, S. Flodin, A. Flores, T. Kotenyova, T. Nyman, P. Nordlund and P. Kursula, *Journal of neurochemistry*, 2007, **101**, 906-917.
10. V. Majava, N. Loytynoja, W. Q. Chen, G. Lubec and P. Kursula, *The FEBS journal*, 2008, **275**, 4583-4596.
11. M. Gellert, S. Venz, J. Mitlöhner, C. Cott, E.-M. Hanschmann and C. H. Lillig, *Journal of Biological Chemistry*, 2013, **288**, 35117-35125.
12. L. Brautigam, L. D. Schutte, J. R. Godoy, T. Prozorovski, M. Gellert, G. Hauptmann, A. Holmgren, C. H. Lillig and C. Berndt, *Proceedings of the National Academy of Sciences of the United States of America*, 2011, **108**, 20532-20537.
13. L. D. Schutte, S. Baumeister, B. Weis, C. Hudemann, E. M. Hanschmann and C. H. Lillig, *Bba-Gen Subjects*, 2013, **1830**, 4999-5005.
14. N. Arimura, N. Inagaki, K. Chihara, C. Menager, N. Nakamura, M. Amano, A. Iwamatsu, Y. Goshima and K. Kaibuchi, *Journal of Biological Chemistry*, 2000, **275**, 23973-23980.
15. A. R. Cole, A. Knebel, N. A. Morrice, L. A. Robertson, A. J. Irving, C. N. Connolly and C. Sutherland, *Journal of Biological Chemistry*, 2004, **279**, 50176-50180.
16. A. R. Cole, F. Causeret, G. Yadirgi, C. J. Hastie, H. Mclauchlan, E. J. McManus, F. Hernandez, B. J. Eickholt, M. Nikolic and C. Sutherland, *Journal of Biological Chemistry*, 2006, **281**, 16591-16598.
17. K. Hensley, K. Venkova, A. Christov, W. Gunning and J. Park, *Mol Neurobiol*, 2011, **43**, 180-191.
18. V. Raussens, J.-M. Ruysschaert and E. Goormaghtigh, *Analytical Biochemistry*, 2003, **319**, 114-121.
19. J. T. Vivian and P. R. Callis, *Biophysical Journal*, 2001, **80**, 2093-2109.
20. F. H. Niesen, H. Berglund and M. Vedadi, *Nat. Protocols*, 2007, **2**, 2212-2221.
21. U. B. Ericsson, B. M. Hallberg, G. T. DeTitta, N. Dekker and P. Nordlund, *Analytical Biochemistry*, 2006, **357**, 289-298.
22. D. Eisenberg, R. M. Weiss, T. C. Terwilliger and W. Wilcox, *Faraday Symposia of the Chemical Society*, 1982, **17**, 109-120.
23. H. R. Horton, L. A. Moran, K. G. Scrimgeour, M. D. Perry, J. D. Rawn and C. Biele, *Biochemie*, Pearson Studium, München [u.a.], 4., aktualisierte Aufl. edn., 2008.
24. A. L. Sobolewski and W. Domcke, *Chemical Physics Letters*, 1999, **315**, 293-298.
25. P. R. Callis, in *Methods in Enzymology*, Academic Press, 1997, vol. Volume 278, pp. 113-150.
26. E. Gindensperger, A. Haegy, C. Daniel and R. Marquardt, *Chemical Physics*, 2010, **374**, 104-110.

Molecular dynamics simulations and in vitro analysis of the CRMP2 thiol switch

Daniel Möller[+1], Manuela Gellert[+2], Walter Langel[1], Christopher Horst Lillig[*2]

[+] These authors contributed equally to this work.

* corresponding author: horst@lillig.de

[1] Biophysical Chemistry, Institute of Biochemistry, University Greifswald, 17489 Greifswald, Germany

[2] Institute for Medical Biochemistry and Molecular Biology, University Medicine, University Greifswald, 17489 Greifswald, Germany

Supporting Information

Methods

Homology search

The most complete experimental structure 2VM8 covers 477 amino acids from Ser14 to Glu490. For our study, the N-terminus was not relevant, and we omitted the first 15 aa up to Arg16. This structure still lacks the C-terminal residues 491-577, which include the major regulatory and phosphorylation sites of the protein[1-3]. We thus had to extend the structure by *in silico* methods up to the postulated cleavage site of the protease calpain, i.e. by 41 amino acids (Lys491 - Val531) with the sequence LRGVPRGLYACEVSVTPKTVTPASSAKTSPAKQQAPPV. Marked are Cys504 in red for the dithiol-disulfide redox switch; Thr509, Thr514, Ser517, Ser518 and Ser522 in brown as phosphorylation sites; and the calpain cleavage site highlighted in grey. By homology search (SWISS-Model[4-7]), we only found a template structure for the next nine aa Lys491-Tyr499 in human dihydropyrimidinase (Q14117) with the structure 2VR2[8].

Force-field package, REMD algorithm and solvent models

We now had a structure for Arg16 to Tyr499. For further simulations, a structure model covering the next 32 aa at the C-terminus till residue 531 was necessary and we used different kinds of force field based molecular dynamics (MD) to predict *in silico* the structure of the remaining 32 aa (Asp500 to Val531). Geometry optimization and molecular dynamics simulations were done using the NAMD package[9] with the AMBER-force field (ff14SB)[10,11]. For the short-range non-bonded interaction, van der Waals and electrostatic interactions were calculated until a 10 Å direct-space cutoff including a smoothing function for the potentials. Particle Mesh Ewald (PME) was used for the long-range electrostatics under periodic boundary conditions. Energy minimization was achieved by a conjugate gradient and line search algorithm in NAMD.

In MD simulations, all covalent bonds to hydrogen atoms were constrained to their nominal lengths by the RATTLE algorithm. Molecular dynamics applied a Verlet integrator with a dual time step of 2 fs for the bonded and van der Waals interactions and 4 fs for PME. A Langevin thermostat was used with a damping time every 1 ps in NVT (constant particle **N**umber, cell **V**olume and **T**emperature of 300 K) and NPT (constant **P**ressure of 1 bar) or every 100 ps in NVE (constant **E**nergy) calculations. The NPT protocol used a Langevin piston constant pressure control[12,13] with an oscillation period of 200 fs and a damping time of 100 fs in combination with a thermostat. The visualization package VMD was

used with its plugins[14-20] to analyze secondary structure, electrostatic potentials (PME), SASA and radius of gyration of the simulated structures.

Protein folding in implicit and explicit solvent

This sequence of 32 amino acids has acetyl and N-methyl protection groups at its N- and C-termini, respectively. Two different secondary starting structures were generated, one strand and an α helix. Thereby, we wanted to avoid that the result for folding is correlated to the starting structure. We used both implicit solvent (GBSA)[21-24] and explicit water (TIP3P-water model for force field)[25] as solvents respectively.

REMD in implicit water

We started with a standard replica-exchange molecular dynamics (REMD) [26,27] algorithm to map the energy surfaces of the molecules and to find the structure with minimal energy. An exchange between two replica at nearby temperatures with a similar potential energy is triggered by fulfilling the Metropolis criterion. The system contained twelve replica over a temperature range of 270 to 700 K. This number of replica is sufficient for the distributions of potential energies of replica at neighboring temperatures, to achieve their overlapping facilitating a significant probability of exchange. The calculation was accelerated by omitting the solvent molecules and counter ions as well as by working in implicit solvent (GBSA). Each replica contained only the 461 atoms of the peptide.

Verification of exchange was done in intervals of 1 ps. After 100 ns all replicas had frequently switched between different structures even at low temperatures. The folding in implicit water only attained conformations with a small number of secondary structure elements[28]. We used the results as initial configuration for simulations in explicit water.

TIGER2 with explicit water

We switched to the recently developed TIGER2 (temperature intervals with global exchange of replicas) algorithm[29,30]. In contrast to standard REMD, all replica are cooled down to the basis temperature before verifying an exchange, which minimizes the influence of temperature on the potential energy in favor of structural differences. Consequently, a smaller number of replica is needed compared to standard REMD, and the calculation is better adapted to the hardware. All further simulations ran under periodic boundary conditions with TIP3P-water as explicit solvent. In explicit solvent, the temperature range is limited to 280 to 600 K. The TIGER2-algorithm was customized combining pressure control[12,13] with explicit solvent as NPT simulations. The set point of the pressure

was chosen to be significantly higher than the respective vapor pressure of the solvent avoiding partial evaporation of the water and bubbles.

The two replicas, one from strand (now 7008 atoms including 2182 water molecules) and one from helical starting structures (now 7479 atoms including 2339 water molecules), were taken as initial structures for two TIGER2 simulations. Booth structures had the most secondary structure elements and hydrogen bonds at the end of the two implicit solvent calculations. Each of these two optimized structures gave rise to twelve replica, with a simulation time 500 ns each. The Metropolis criterion was applied each 2 ps. The overall charge of the peptide is +1 e (e is the positive elementary charge), which was compensated by one Cl^-. For the following simulations, we chose the structure among the 24 with the highest amount of secondary structure elements and highest count of hydrogen bonds.

Folding at the protein surface

We connected the residue Asp500 of the final structure from the TIGER2 runs with the residue Tyr499 of the homology search structure and got a peptide of 41 amino acids (Lys491-Val531), which is linked to the body of the CRMP2 monomer (chain A) at the residue 490 of the C-terminus. We cut this structure maintaining only the residues neighboring to the new C-terminus (**Figure SI 1.B**). The C_α atoms of the CRMP2 main body were fixed during further calculations, in order to conserve the natural environment of the C-terminus.

Following energy minimization, we equilibrated the system during three simulations at 300 K. We used the protocol NVT (1 ns), NVP (0.5 ns) and NVT (1 ns) for equilibration of the system, followed by 6 ns NVE. The resulting structure was subjected to a second TIGER2-NPT simulation with eight replicas and a temperature range of 280 to 600 K with heating for 1 ps, sampling at different temperatures for 1 ps and quenching to 280 K for 2.4 ps. During the folding simulation the peptide at the C-terminus of chain A reoriented by external restraints into a position, which permitted a later closing of the disulfide bond to chain D and the formation of the oxidized homotetramer. Therefore, we pulled the Cys504 to the place of the disulfide bond via constant force of 10 kcal/ (mol·Å) (0.7 nN) and then restrained the displacement of Cys504 with 500 kcal/ (mol·Å) out of this environment for a total of 66 ns per replica. During the last 330 ps the system relaxed shortly.

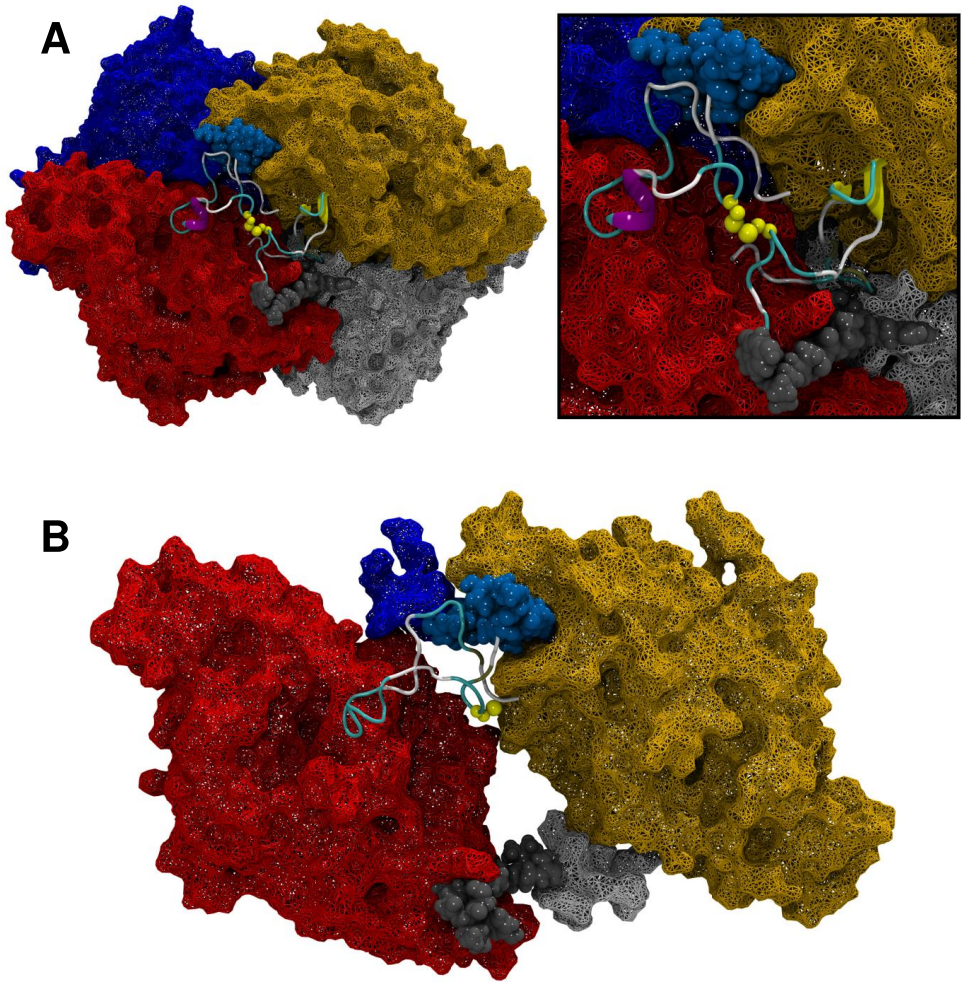

Figure SI 1: Steric view of CRMP2:

(A) **Snapshot of the oxidized CRMP2 homotetrameric structure. The four monomers are distinguished by colors (blue, red, yellow, and grey respectively). The mesh surface is based on the experimental crystal structure[31,32]. The monomers are extended by 41 amino acids at each C-terminus. The fragment with nine amino acids from the homology search is shown as van der Waals surface in colors related to the respective monomer (blue or grey, respectively). The structure of the remaining C-terminus fragment with 32 amino acids is presented with secondary structure elements (helix: purple and blue; sheet: yellow arrows; turn: cyan; coil: white) (cf. Table 1 in paper text). The Cys504 residues form the disulfide bonds (ball-and-stick, yellow).**

(Insert to A) **Magnification of in to the disulfide bond between the Cys504 residues of chain A (blue) and D (grey).**

(B) **Protein fragment for TIGER2 calculations of the peptide at the C-terminus as cut from similar structure as in** (A).

We connected a copy of the replica with the most advanced folding state to each monomer, obtaining a CRMP2 homotetramer with four C-termini with 41 additional residues each. As a result, we got an extended structure of 518 aa per monomer (Arg16-Val531).

Homotetrameric CRMP2

In the reduced structures, the cysteine 504 residues of each subunit have protonated side chains. An oxidized structure was generated by connecting the final cysteine residues (504) of each two adjacent monomers. Two cysteine bridges between monomer 1 (chain A) and 4 (chain D) and between 2 and 3 (chains: B and C) (**Figure SI 1.A**) were formed.

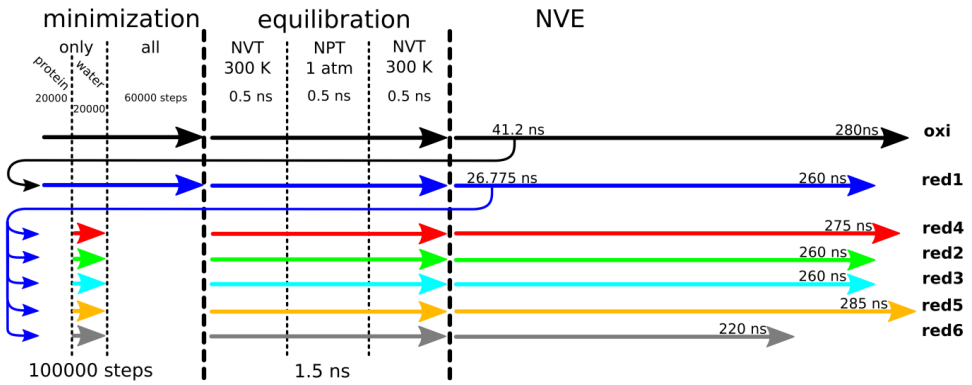

Figure SI 2: Schematic overview of simulations with the full CRMP2 molecules (oxi, red1 to red6):

Energy minimization of the system with water fixed in the box for 20000 steps, with the protein fixed for 20000 steps, with all atoms free for 60000 steps.

Molecular dynamics simulations for thermal equilibration: Heating up to 300 K, NPT run at 1 atm and 300 K, a second heating to 300 K for 500 ps respectively, NVE production runs for analysis.

Arrows indicate the flow of the simulation: originated red1 from the structure of oxi at 41 ns, with changes to the oxidized Cys504 and a new water box (plus counter ions). red2-red6 results of the structure of red1 at 27 ns, but with a new water box each and adapted concentrations of bivalent and counter ions.

The homotetramers have negative charges of -13 e per monomer, or totally -52 e. We aimed at reproducing the *in vitro* solutions from Stenmark et al. and Majava et al.[31,32] and performed simulations with 4 Ca^{2+}- ions (1.6 mM) in the oxidized and reduced states, and with 0 mM, 20 mM and 200 mM Ca^{2+} or Mg^{2+}-ions in the reduced state only. The resulting total negative or positive charges of the system were compensated by monovalent Na^{+} or Cl^{-} counter ions, respectively (see **Table 1** in paper text). The first simulation was the oxidized state with 4 Ca^{2+}-ions. After around 41 ns in NVE, we used a snapshot of its structure to build the reduced state by restoring the thiol groups of the Cys504

residues. The structure of this state after around 27 ns in NVE was used for the simulations with other bivalent cation concentrations (**Figure SI 2**).

All systems were subjected to an energy minimization of 20000 steps, or 100000 steps for the calculations with 4 Ca^{2+}-ions, before MD simulations were performed. Equilibration simulations consisted of three parts, NVT, NPT and another NVT for 0.5 ns each. The NVE calculations, with scanning times of 200-300 ns at temperatures around 300 K, were used for further analyses.

Recombinant expression and purification of CRMP2

For recombinant protein expression, E. coli cells were propagated in a 3 l conical flask. The LB-medium (400 ml), containing the selective antibiotics, was inoculated at 37 °C with 2 % of an overnight culture of E. coli BL21 (DE3) codon-plus (Life technologies) harboring the pET15b-CRMP2. At OD 0.6, expression was induced by addition of 0.5 mM IPTG (isopropyl-β-D-thiogalactopyranoside) and by lowering the temperature to 10 °C. The cells were harvested after 24 hours by centrifugation. Bacteria were lysed by incubation with 1 mg/ml lysozyme and 0.05 mg/ml DNase I for 20 minutes at room temperature (RT) and subsequent ultrasonic treatment for 2-times 2.5 minutes, 75 % intensity, 0.5 s cycle time (50 % cycling) using a Sonopuls HD2070 ultrasonic processor (Bandelin, Berlin, Germany). Recombinant His-tagged CRMP2 was purified by immobilized metal affinity chromatography using an Äkta FPLC system as suggested by the manufacturer (GE healthcare, Buckinghamshire, UK) at 4 °C.

CD spectroscopy

Circular dichroism spectra were recorded in a Jasco 810 instrument (Tokyo, Japan). Freshly purified CRMP2 was reduced with 5 mM DTT (dithiotreithol), 5 mM pH-neutralized TCEP (tris(2-carboxyethyl)phosphine), and 0.8 µM human Grx2c (glutarexdoxin 2)[1] for 30 minutes at RT. To remove all reductants, the protein solution was re-buffered using NAP-5 columns (GE healthcare). Next, the protein was oxidized by 200 µM H_2O_2 for 30 minutes at RT. H_2O_2 was removed by re-buffering in 10 mM KPO_4 buffer including 20 mM $MgCl_2$ at pH 7.4 as before. The oxidized sample (6 µM) was analyzed in a 1 mm cuvette, scanning 0.2 nm steps, averaging 10 iterations. Subsequently, the protein was oxidized by addition of 1 mM H_2O_2 and incubated for 30 minutes at RT and analyzed again. All spectra were corrected by subtraction of the respective baselines.

Differential scanning fluorimetry (thermofluor assay[33])

The thermal stability of reduced and oxidized CRMP2 was studied using the thermofluor assay as outlined in ref.[33]. 10 µM protein was reduced and oxidized as outlined above and re-buffered in 10 mM HEPES (2-[4-(2-hydroxyethyl)piperazin-1-yl]ethane sulfonic acid) pH 8, containing either 300 mM $MgCl_2$ or $CaCl_2$. Immediately after the starting temperature of 10 °C was reached, EDTA was added to adjust the concentrations of the ions to 0, 1.6, 20, or 200 mM Ca^{2+} or Mg^{2+}. SYPRO Orange was added (1:100 diluted, Sigma-Aldrich) and triplicates of the samples were heated in a CFX96 Real Time System from BioRad in 0.5 K increments from 10 to 100 °C. The increase in fluorescence due to binding of the dye to hydrophobic regions exposed during heating of the samples was recorded using the instrument's "FRET" settings.

Fluorescence spectroscopy

Time dependent quenching of tryptophan fluorescence was measured using a LS50B Fluorimeter (PerkinElmer, Boston, MA, USA). Recombinant CRMP2 was reduced with 5 mM DTT, 5 mM pH-neutralized TCEP for 30 minutes at RT. To remove all reductants, the protein solution was re-buffered in PBS (phosphate buffer saline) containing 20 mM $MgCl_2$ using NAP-5 columns (GE healthcare). 3 µM CRMP2 were used to measure the tryptophan fluorescence after excitation at a wavelength of 296 nm. The protein was oxidized using 1 mM H_2O_2 and the fluorescence quenching was recorded every 5 minutes.

We assumed second order kinetics in the pseudo first order limit, and derived rate constants k of the oxidation reaction according to equation (1) (see in following derivation):

$$\ln\left(\frac{F_r - F_o}{F_{t=x} - F_o}\right) = k \cdot \left([H_2O_2]_{t=0} - [P]_{t=0}\right) \cdot t \qquad (1)$$

We calculated first order rates $k \cdot \left([H_2O_2]_{t=0} - [P]_{t=0}\right)$ by a linear regression of the left hand expression in (1) against the time t. The ordinate values are the natural logarithms of the maximum difference between the fluorescence intensities F_r and F_o of fully reduced and oxidized proteins, respectively, over the difference between the fluorescence $F_{t=x}$ at t=x and F_o. Division of the slope by the difference of initial concentrations of H_2O_2, $[H_2O_2]_{t=0}$ and the reduced protein $[P]_{t=0}$ yields the second order rate constant k. At our conditions, $[P]_{t=0}$ is negligible with respect to the initial hydrogen peroxide concentration.

Derivation of pseudo first order kinetics for the quenching of the Trp295 fluorescence

The oxidation of any given protein or protein complex by hydrogen peroxide follows a second order reaction:

$$P_r + H_2O_2 \rightarrow P_o + H_2O_2$$

(P_r: reduced protein, P_o: oxidized protein)

The reaction rate can be calculated as expressed in equation (2):

$$-\frac{\delta[P_o]}{\delta t} = \frac{\delta[P_r]}{\delta t} = -k \cdot [P_r] \bullet [H_2O_2] \tag{2}$$

The concentrations of the reactants at t=x may also be expressed as follows:

$$[P_r] = [P_r]_{t=0} - [P_o]$$
$$[H_2O_2] = [H_2O_2]_{t=0} - [P_o]$$

The reaction rate can thus be expressed as:

$$-\frac{\delta[P_o]}{\delta t} = -k \cdot \left([P_r]_{t=0} - [P_o]\right) \bullet \left([H_2O_2]_{t=0} - [P_o]\right) \tag{3}$$

$$\Leftrightarrow \frac{\delta[P_o]}{\left([P_r]_{t=0} - [P_o]\right) \cdot \left([H_2O_2]_{t=0} - [P_o]\right)} = k \cdot \delta t \tag{4}$$

$$\Rightarrow \int_0^{[P_o]} \frac{\delta[P_o]}{\left([P_r]_{t=0} - [P_o]\right) \cdot \left([H_2O_2]_{t=0} - [P_o]\right)} = k \cdot \int_0^t \delta t \tag{5}$$

Integration using the method of partial fractions:

$$\Rightarrow \frac{1}{[H_2O_2]_{t=0} - [P_r]_{t=0}} \cdot \left(\ln\left(\frac{[P_r]_{t=0}}{[P_r]_{t=0} - [P_o]} \right) - \ln\left(\frac{[H_2O_2]_{t=0}}{[H_2O_2]_{t=0} - [P_o]} \right) \right) = k \bullet t \tag{6}$$

$$\Leftrightarrow \frac{1}{[H_2O_2]_{t=0} - [P_r]_{t=0}} \cdot \ln\left(\frac{[H_2O_2] \cdot [P_r]_{t=0}}{[P_r] \cdot [H_2O_2]_{t=0}} \right) = k \bullet t \tag{7}$$

$$\Leftrightarrow \ln\left(\frac{[H_2O_2] \cdot [P_r]_{t=0}}{[P_r] \cdot [H_2O_2]_{t=0}} \right) = k \cdot \left([H_2O_2]_{t=0} - [P_r]_{t=0}\right) \bullet t \tag{8}$$

Since the concentration of H_2O_2 greatly exceeds the concentration of P_r, the concentrations of $[H_2O_2]_{t=0}$ and $[H_2O_2]_{t=x}$ are essentially equal and the fraction on the left site can be reduced as follows:

$$\Rightarrow \ln\left(\frac{[P_r]_{t=0}}{[P_r]} \right) = k \cdot \left([H_2O_2]_{t=0} - [P_r]_{t=0}\right) \bullet t \tag{9}$$

Using Trp fluorescence quenching at the emission of 340 nm, $[P_r]_{t=0}$ and $[P_r]$ at t=x can be expressed as:

$$[P_r]_{t=0} \propto F_r - F_o$$
$$[P_r] \propto F_{t=x} - F_o$$

While F_r is the fluorescence of the reduced protein and F_o of the oxidized one. Equation (9) can thus be expressed as:

$$\Rightarrow \ln\left(\frac{F_r - F_o}{F_{t=x} - F_o}\right) = k \cdot \left([H_2O_2]_{t=0} - [P_r]_{t=0}\right) \bullet t \qquad (10)$$

Thus, equation (10) can be used for linear regression of a plot of the natural logarithm of the maximal difference between the fluorescence of fully reduced and fully oxidized protein over the difference between the fluorescence at t=x and the fluorescence of the fully oxidized protein, against the time. The rate constant can now be calculated from the slope of the curve.

Results

Exposure of surfaces to solvent

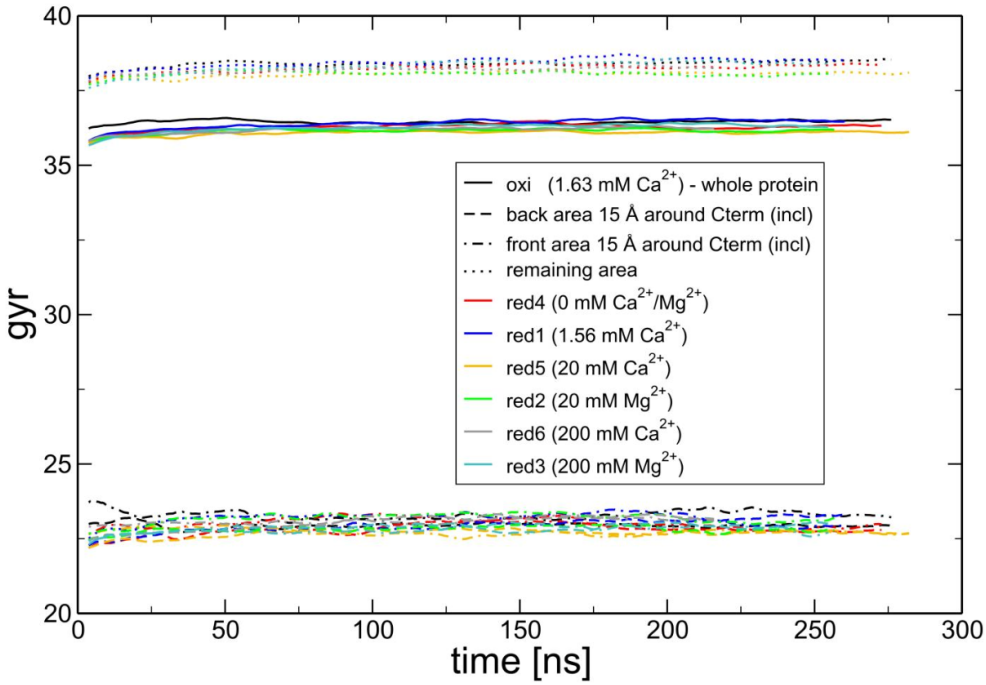

Figure SI 3: Gyradius of CRMP2 homotetramer as a function of time from the MD simulations: Oxidized with four structure stabilizing bivalent ions (black), reduced without any bivalent ions (red), with four structure stabilizing bivalent ions (blue), with 20 mM (Mg^{2+} green, Ca^{2+} yellow) and with 200 mM bivalent ions (Mg^{2+} cyan, Ca^{2+} grey). The full lines depict the whole protein, the broken lines only the area around C-termini (including them) with a maximal distance of 15 Å (separated to front- and backside), and the dotted line the remaining protein. The curves are running averages of the raw data with a window of 7.5 ns.

Correlation of Trp295 fluorescence wavelength and electrostatic energies for oxidized and reduced state

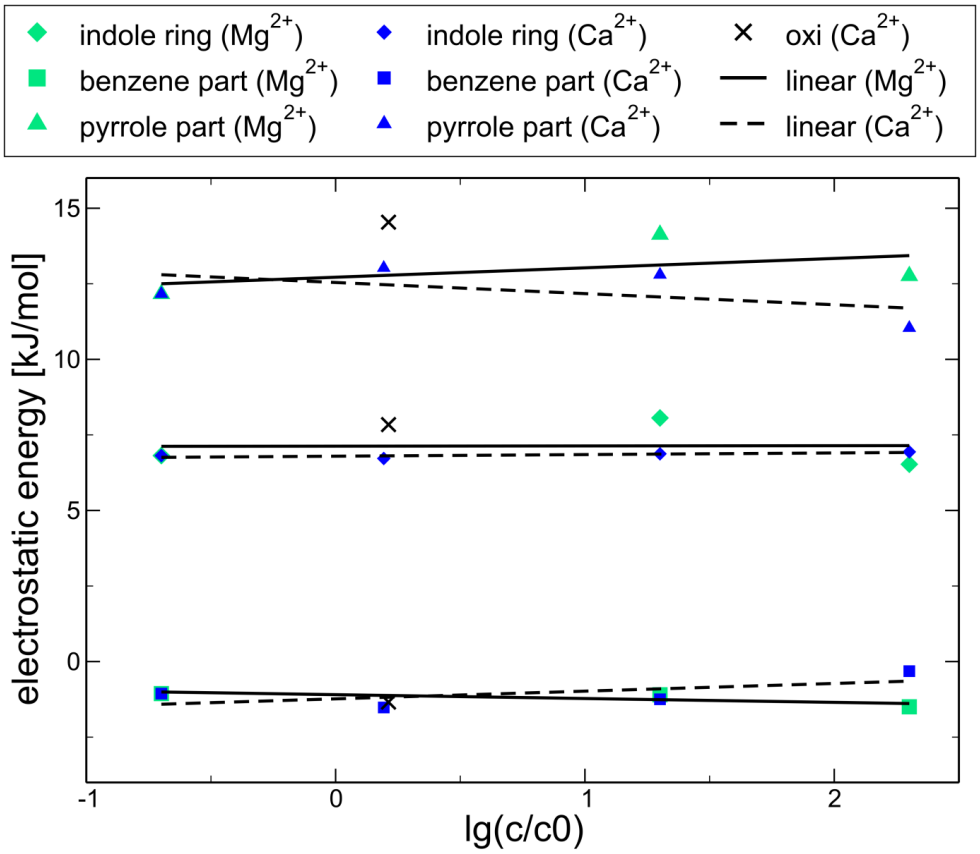

Figure SI 4: Electrostatic energy of components of the side chain of the Trp295 in the oxidized molecule (x) and at several ionic concentrations for the reduced state (colored symbols). Components are the indole ring, and its benzene and pyrrole parts. The electrostatic energy in kJ/mol was averaged over the four Trp295 residues and over 30 frames with a 0.5 ns stride.

References

1. M. Gellert, S. Venz, J. Mitlöhner, C. Cott, E.-M. Hanschmann and C. H. Lillig, *Journal of Biological Chemistry*, 2013, **288**, 35117-35125.
2. Y. Gu, N. Hamajima and Y. Ihara, *Biochemistry*, 2000, **39**, 4267-4275.
3. N. Yamashita, T. Ohshima, F. Nakamura, P. Kolattukudy, J. Honnorat, K. Mikoshiba and Y. Goshima, *The Journal of Neuroscience*, 2012, **32**, 1360-1365.
4. K. Arnold, L. Bordoli, J. Kopp and T. Schwede, *Bioinformatics*, 2006, **22**, 195-201.
5. D. T. Jones, *Journal of Molecular Biology*, 1999, **292**, 195-202.
6. J. J. Ward, J. S. Sodhi, L. J. McGuffin, B. F. Buxton and D. T. Jones, *Journal of Molecular Biology*, 2004, **337**, 635-645.
7. E. M. Zdobnov and R. Apweiler, *Bioinformatics*, 2001, **17**, 847-848.
8. M. Welin, Karlberg, T., Andersson, J., Arrowsmith, C.H., Berglund, H., Busam, R.D., Collins, R., Dahlgren, L.G., Edwards, A.M., Flodin, S., Flores, A., Graslund, S., Hammarstrom, M., Herman, M.D., Johansson, I., Kallas, A., Kotenyova, T., Lehtio, L., Moche, M., Nilsson, M.E., Nyman, T., Persson, C., Sagemark, J., Svensson, L., Thorsell, A.G., Tresaugues, L., Van Den Berg, S., Weigelt, J., Wikstrom, M., Nordlund, P., Human Dihydropyrimidinase, http://www.rcsb.org/pdb/explore/explore.do?structureId=2vr2, DOI: http://dx.doi.org/10.2210/pdb2vr2/pdb).
9. J. C. Phillips, R. Braun, W. Wang, J. Gumbart, E. Tajkhorshid, E. Villa, C. Chipot, R. D. Skeel, L. Kalé and K. Schulten, *Journal of Computational Chemistry*, 2005, **26**, 1781-1802.
10. D. A. D. Case, T.A.; Cheatham III, T.E. ; Simmerling, C.L.; Wang, J.; Duke, R.E.; Luo, R.; Walker, R.C.; Zhang, W.; Merz, K.M.; Roberts, B.; Hayik, S.; Roitberg, A.; Seabra, G.; Swails, J.; Goetz, A.W.; Kolossváry, I.; Wong, K.F.; Paesani, F.; Vanicek, J.; Wolf, R.M.; Liu, J.; Wu, X.; Brozell, S.R.; Steinbrecher, T.; Gohlke, H.; Cai, Q.; Ye, X.; Wang, J.; Hsieh, M.-J.; Cui, G.; Roe, D.R.; Mathews, D.H.; Seetin, M.G.; Salomon-Ferrer, R.; Sagui, C.; Babin, V.; Luchko, T.; Gusarov, S.; Kovalenko, A.; Kollman, P.A., *Journal*, 2012.
11. P. Li, L. F. Song and K. M. Merz, *Journal of chemical theory and computation*, 2015, **11**, 1645-1657.
12. S. E. Feller, Y. Zhang, R. W. Pastor and B. R. Brooks, *The Journal of Chemical Physics*, 1995, **103**, 4613-4621.
13. G. J. Martyna, D. J. Tobias and M. L. Klein, *The Journal of Chemical Physics*, 1994, **101**, 4177-4189.
14. A. Aksimentiev and K. Schulten, *Biophysical Journal*, 2005, **88**, 3745-3761.
15. J. Eargle, D. Wright and Z. Luthey-Schulten, *Bioinformatics*, 2006, **22**, 504–506.
16. D. Frishman and P. Argos, *Proteins: structure, function and genetics*, 1995, **23**, 566–579.
17. W. Humphrey, A. Dalke and K. Schulten, *Journal of Molecular Graphics*, 1996, **14**, 33–38.
18. M. Sanner, A. Olsen and J.-C. Spehner, in *Proceedings of the 11th ACM Symposium on Computational Geometry*, ACM, New York, 1995, pp. C6-C7.
19. J. Stone, 1998.
20. A. Varshney, F. P. Brooks and W. V. Wright, *IEEE Computer Graphics and Applications*, 1994, **14**, 19–25.
21. A. Onufriev, D. Bashford and D. A. Case, *Proteins: Structure, Function, and Bioinformatics*, 2004, **55**, 383-394.
22. D. E. Tanner, K. Y. Chan, J. C. Phillips and K. Schulten, *Journal of chemical theory and computation*, 2011, **7**, 3635-3642.
23. D. E. Tanner, J. C. Phillips and K. Schulten, *Journal of chemical theory and computation*, 2012, **8**, 2521-2530.
24. J. Weiser, P. S. Shenkin and W. C. Still, *Journal of Computational Chemistry*, 1999, **20**, 217-230.
25. W. L. Jorgensen, J. Chandrasekhar, J. D. Madura, R. W. Impey and M. L. Klein, *The Journal of Chemical Physics*, 1983, **79**, 926-935.
26. D. J. Earl and M. W. Deem, *Physical Chemistry Chemical Physics*, 2005, **7**, 3910-3916.
27. Y. Sugita and Y. Okamoto, *Chemical Physics Letters*, 1999, **314**, 141-151.
28. Y. M. Rhee, E. J. Sorin, G. Jayachandran, E. Lindahl and V. S. Pande, *Proceedings of the National Academy of Sciences of the United States of America*, 2004, **101**, 6456-6461.
29. X. Li, R. A. Latour and S. J. Stuart, *The Journal of Chemical Physics*, 2009, **130**, -.
30. W. J. Menz, M. J. Penna and M. J. Biggs, *Computer Physics Communications*, 2010, **181**, 2082-2085.
31. V. Majava, N. Loytynoja, W. Q. Chen, G. Lubec and P. Kursula, *The FEBS journal*, 2008, **275**, 4583-4596.

32. P. Stenmark, D. Ogg, S. Flodin, A. Flores, T. Kotenyova, T. Nyman, P. Nordlund and P. Kursula, *Journal of neurochemistry*, 2007, **101**, 906-917.
33. F. H. Niesen, H. Berglund and M. Vedadi, *Nat. Protocols*, 2007, **2**, 2212-2221.

VI. Manuscript

The cytosoloc isoform of glutaredoxin 2 promotes cell migration and invasion

Manuela Gellert, Erik Richter, Jörg Mostertz, Liane Kantz, Kai Masur, Eva-Maria Hanschmann, Silvia Ribback, Nils Kröger, Falko Hochgräfe, and Christopher Horst Lillig

submitted to Cancer Research

submission ID: CA-17-1219

The cytosolic isoform of glutaredoxin 2 promotes cell migration and invasion

Manuela Gellert[1], Erik Richter[2], Jörg Mostertz[2], Liane Kantz[3], Kai Masur[3], Eva-Maria Hanschmann[1], Silvia Ribback[4], Nils Kröger[1,5], Falko Hochgräfe[2], and Christopher Horst Lillig[1*]

From the Institute for Medical Biochemistry and Molecular Biology, University Medicine, Ernst Moritz Arndt University Greifswald, Germany (1), Competence Center Functional Genomics, Junior Research Group Pathoproteomics, Ernst Moritz Arndt University Greifswald, Germany (2), the Center for Innovation Competence plasmatis, Leibniz Institute for Plasma Science and Technology (INP), Greifswald, Germany (3), the Institute for Pathology (4), and the Clinic for Urology, University Medicine Greifswald, Germany (5).

* Corresponding author: Christopher Horst Lillig, University Medicine, Institute for Medical Biochemistry and Molecular Biology J.03 33, Ferdinand-Sauerbruch-Straße, DE-17475 Greifswald, Germany, phone: +49 3834 865407, fax: +49 3834 865402, e-mail: horst@lillig.de

Running title: Cancer-specific Grx2c promotes migration and invasion

Keywords: glutaredoxin, redox regulation, cell motility, invasiveness, clear cell renal cell carcinoma

Additional information: This work was supported by grants from the Deutsche Forschungsgemeinschaft (to CHL: SFB593-N01, LI 984/3-1 (SPP 1710), LI 984/4-1, GRK1947-A1), and the Bundesministerium für Bildung und Forschung (to FH: 03Z1CN21, to KM: 03Z2DN11). The authors declare no conflicts of interest.

Manuscript statistics: Word count: 4391; 1 table; 5 figures; 2 supplementary videos; 1 supplementary sheet file (proteomic data sets); 5 supplementary figures (in one file)

Abstract

Cytosolic glutaredoxin 2 (Grx2c) controls axonal outgrowth and is specifically induced in many cancer cell lines. We thus hypothesized that Grx2c promotes cell motility and invasiveness. Cell lines expressing Grx2c showed dramatic alterations in morphology. These cells migrated two-fold faster and gained the ability to infiltrate a collagen matrix. We combined stable isotope labeling, phosphopeptide enrichment, and high-accuracy mass spectrometry to characterize the underlying mechanisms. The most prominent associations were found with actin dynamics, cellular adhesion, and receptor-mediated signal transduction. Grx2c is expressed with significantly higher frequency in clear cell renal cell carcinoma compared to normal kidney tissue with strong trends in decreased cancer specific survival and more locally advanced tumor stages in Grx2c expressing tumors. These findings of our clinical pilot study are backed by data from ‘The Cancer Genome Atlas’. Our results imply critical roles of the protein in cytoskeletal dynamics and cell adhesion and imply the promotion of carcinogenesis and invasiveness by Grx2c.

Introduction

Cell motility and invasion, hallmark features of disseminating and metastasizing cancer cells, require an orchestrated interplay of signalling and effector molecules that regulate the continuous re-arrangement of the actin cytoskeleton. These dynamics are directly controlled by numerous actin-binding proteins that stabilize filaments, and promote elongation, severing, or nucleation of filaments (1) (2) (3)

(4). The spatio-temporal regulation of these effectors, for instance through receptor-associated kinases or small GTPases of the Rho family, facilitates the formation of cellular protrusions, the contraction of filament bundles, and the re-modeling of cell-cell as well as cell-matrix contacts. A key regulator of actin re-modeling is the actin-related protein 2 and 3 (Arp2/3) complex, a nucleation/branching factor essential for the formation and dynamics of lamellopodia and invadopodia (5) (4). The activity of this hetero-heptameric protein complex is controlled by nucleation-promoting factors, mostly members of the Wiskott-Aldrich syndrome protein (WASP) family protein complexes, such as WASP, N-WASP, and WAVE 1-3. These complexes are recruited to the membrane and activated by Rho GTPases, most notably Rac1 and CDC42, phosphoinositide binding, and other protein-protein interactions (6) (7). Further on, cytoskeletal dynamics, cell motility, and invasion are intimately connected to the interactions of a cell with other cells and the extracellular matrix. These interactions are mediated by integral membrane proteins, for instance cadherins and integrins, that assemble intracellular signalling complexes and serve, via mediator proteins, as an anchor for the organization of actin filaments (8) (9).

Glutaredoxins (Grxs) are glutathione-dependent oxidoreductases that catalyze the reduction of protein disulfides, for instance in ribonucleotide reductase (10), and the reversible formation and reduction of protein-glutathione mixed disulfides (11), see also (12) (13) (14). Mammalian genomes encode four Grxs and some Grx domain containing proteins (15). The gene for glutaredoxin 2 (Grx2, GLRX2) gives rise to alternative transcript variants through mechanisms of alternative splicing and transcription initiation (16) (17) (18). Three protein isoforms of human Grx2 were described, mitochondrial Grx2a, and the cytosolic/nuclear Grx2b and Grx2c; while Grx2a is expressed ubiquitously in all tissues, Grx2b and Grx2c could only be detected in spermatogenic and cancer cells in adult humans (17). In mice, Grx2a and Grx2c are conserved and both transcribed ubiquitously (18) and also the genomes of other vertebrate species, like zebrafish, contain genes that encode homologues to cytosolic Grx2c. Zebrafish with silenced expression of cytosolic Grx2 fail to develop an axonal scaffold and lose essentially all types of neurons by apoptotic cell death (19). These defects could be rescued by re-introduction of wildtype Grx2c, but not by the introduction of mutants that could not catalyze the reduction of protein disulfides (19). The process of axonal path-finding is facilitated by growth cones, actin-based structures at the tip of the growing axons or neurites, and guided by external permissive and repulsive signals that lead to the remodeling of the growth cone (20). These processes resemble in many aspects the migration of entire cells.

The functions of the cytosolic Grx2c in the establishment of axonal scaffolds and spermatogenesis (19) (17), a process that includes the transmigration of spermatogenic cells through the close Sertoli cell formation, led us to hypothesize that Grx2c may promote both the motility and invasion behavior of cells in general. To test this hypothesis, we have generated cell lines that expresse cytosolic Grx2c (21) at low to moderate levels – with dramatic effects on cytoskeletal dynamics, morphology, motility, and invasion. We performed high-accuracy mass spectrometry to characterize the influence of Grx2c expression on the levels and phosphorylation of proteins controlling cytoskeletal dynamics, cell adhesion, and migration. Our clincal pilot sttudy implies roles of Grx2c during carcinogenesis.

Materials and Methods

Materials - Chemicals and enzymes were purchased from Sigma-Aldrich (St. Louis MO, USA), unless otherwise stated, and were of analytical grade or better. Antibodies: CRMP2 (Sigma-Aldrich, C2993); GAPDH (Sigma-Aldrich, G9545); α-Tubulin (Sigma-Aldrich, T9026); additional antibodies were listed in the suppl. materials.

Electrophoresis and Western blotting - SDS-PAGE and Western blots were run using pre-casted TGX stain-free gels (4-20%, Biorad, Hercules CA, USA), and PVDF membranes (Macherey & Nagel, Düren, Germany), blue native electrophoresis using pre-casted NativeBlueNovex gels and buffers (Life technologies, Paisley, UK), according to manufacturers' instructions. Western blots were developed by enhanced chemiluminescence staining using a Chemidoc XRS+ documentation system (Biorad) or the Odyssey CLx near infrared detection system (LI-COR Biosciences).

Quantitative PCR - RNA isolation was performed using the NucleoSpin® RNA II kit (Macherey-Nagel, Düren, Germany). First strand cDNA was prepared using the RevertAid™ First Strand cDNA Synthesis Kit (Thermo Scientific). All qPCRs were performed using the BioRad CFX96 Real Time System and the SensiMix™ SYBR HI-ROX kit (Bioline, London, UK); GAPDH was used as reference. GAPDH: 5‘-CAAGGTCATCCATGACAACTTTG, 5’-GTCCACCACCCTGTTGCTGTAG; Grx2c: 5‘-CGAGATAAGCAAGATGGAGAGCAATAC, 5‘-GCCTATGAGTGTCAGTTGCACC.

Cell culturing - All media and reagents were purchased from PAA (Cölbe, Germany), serum (FCS) from Pan-Biotech (Aidenbach, Germany), disposable plastics from Sarstedt (Nümbrecht, Germany). Cells were propagated in DMEM 1 g/l glucose (HeLa), or RPMI (786-O, Panc1), supplemented with penicillin (100 U/ml)/streptomycin (0.1 mg/ml), and 10% (v/v) FCS.

Cell were transfected by electroporation. Conditions: HeLa/Grx2c: $3.5 \cdot 10^6$ cells, 250 V, 1500 µF, 500 Ω; 786-O: $5.0 \cdot 10^6$/250/1600/500; Panc1: $3.5 \cdot 10^6$/330/1600/500. For protein analysis, cells were harvested by trypsination, washed with PBS, and lysed in either 40 mM HEPES, 50 mM NaCl, 1 mM EDTA, 1 mM EGTA, 100 mM NEM, 2% (w/v) CHAPS, pH 7.4 (for SDS PAGE) or 10 mM Tris/HCl, 0.1% (v/v) NP40, 10 mM NaCl, 3 mM $MgCl_2$, pH 7.4 (for blue native gel electrophoresis). Lysis buffers contained proteinase inhibitors (Roche, Basel, Switzerland) and phosphatase inhibitors (Sigma-Aldrich).

Cell motility and invasion - HeLa cell lines were seeded to confluent density into a µ-dish (Ibidi, Martinsried, Germany), after 24 hours the inset was removed, and serum reduced (5%, v/v) medium was added. The width of the gap between the chambers was recorded every 4 hours by light microscopy. For the analysis by live cell microscopy, a 24-well plate was prepared with a collagen matrix, 25000 cells/well were seeded in 200 µl of the collagen mixture on top of the prepared matrix. The collagen was covered with DMEM and the migration was monitored over a period of 12 hours (4 frames/10 min) with the Axiovert 40 CFL microscpe (Carl Zeiss, Oberkochen, Germany). Individual cells were tracked using the Axiovision 4.8 software (Carl Zeiss) and/or the Gradientech Tracking Tool 1.02 software (Gradientech, Uppsalla, Sweden).

Quantitative proteomics and phosphoproteomics - SILAC and sample preparation

For SILAC-based quantitative proteome analyses, HeLa wild type and HeLa-Grx2c cells were propagated in SILAC RPMI 1640 (PAA), supplemented with 220 µM L-lysine and 114 µM L-arginine either in light or heavy isotope-labeled forms ($^{13}C_6{}^{15}N_2$-L-lysine/lys-8 and $^{13}C_6{}^{15}N_4$-L-arginine/arg-10, Silantes, Munich, Germany), 2 mM L-glutamine, 10% dialyzed serum (Sigma-Aldrich) and penicillin/streptomycin. Two biological replicates were created by reversing the heavy

and light labels.

At 50% confluence, cells were lysed in 8 M urea, 10 mM sodium fluoride, 2.5 mM sodium pyrophosphate, 1 mM β-glycerol phosphate, 1 mM sodium orthovanadate, 1 mM Tris (2-carboxyethyl) phosphine (TCEP), 1 mM EDTA, and 20 mM HEPES, pH 8.0). Thiols were alkylated with 5 mM iodoacetamide for 20 minutes at room temperature. The samples were centrifuged (8,700 x *g*, 15 min), the protein concentrations were determined by Bradford assay (Bio-Rad). Equal amounts of light and heavy labeled protein were mixed. For protein expression analysis, 20 µg protein mixture were fractionated into 10 gel slices after SDS-PAGE followed by trypsin in-gel digestion. For phosphopeptide enrichments, 10 mg (TiO_2-based enrichment) and 14 mg (phosphotyrosine peptide immunoprecipation) SILAC mix were diluted eight-fold with 20 mM HEPES, pH 8.0, digested with trypsin, purified with Sep-Pak Plus C18 cartridges (Waters) and lyophilized. For TiO_2-based enrichment, samples were dissolved in 5 mM KH_2PO_4, 30 % acetonitrile, pH 2.7 and separated in 15 fractions by cation exchange chromatography (ResourceS SCX 1 ml, GE) using a linear gradient with 5 mM KH_2PO_4, 350 mM KCl, 30 % acetonitrile, pH 2.7 on an Äkta Avant system (GE). Samples were lyophilized, dissolved in 14 ml 73% acetonitrile, 10% lactic acid, 2% TFA and incubated for 20 minutes with 100 µl 30 mg/ml Titansphere TiO_2 Bulk Material in acetonitrile (GL Sciences). After centrifugation, beads were washed four times with 80% acetonitrile, 2% TFA. Phosphopeptides were eluted with 5% NH_4OH and 30% acetonitrile. For enrichment of tyrosine-phosphorylated peptides by immunoprecipitation, 300 µg per sample anti-phosphotyrosine antibody (P-Tyr-100, Cell Signalling Technology) was coupled to rec-Protein G-Sepharose 4B beads (Life Technologies). Samples were dissolved in 50 mM MOPS, 10 mM Na_2HPO_4, 130 mM NaCl, 0.5% NP40, pH 7.5 and incubated with P-Tyr-100 beads at 4°C overnight. Peptides were eluted, twice with 50 µl 0.1% TFA and once with 15% acetonitrile, 0.1% TFA. All eluates were dried in a vacuum centrifuge and purified with C18 StageTips (Thermo Scientific).

Mass spectrometry and data analysis

LC-MS/MS analyses were performed using an EASY-nLCII nanoflow HPLC system coupled directly to an LTQ Orbitrap Velos Pro hybrid mass spectrometer (Thermo Fisher Scientific). Peptide samples were dissolved in 20 µl 5% acetonitrile, 0.1% acetic acid and loaded onto a 20 cm C18 analytical column (Aeris Peptide 3.6 µm, pore size 100 Å; Phenomenex). Peptides were eluted with a linear gradient from 1% acetonitrile/0.1% acetic acid to 75% acetonitrile/0.1% acetic acid. MS/MS analyses were performed with collision induced dissociation (CID) or higher-energy collisional dissociation (HCD).

Resulting spectra were analyzed with MaxQuant version 1.3.0.5 including the Andromeda search engine (45). Briefly, the MS spectra of all measurements including protein quantitation and phosphorylation analyses were searched against a Homo sapiens protein database (extracted from UniProt/Swiss-Prot release 2013_04; 20,252 sequences). Proteins in the output tables were only considered if at least one unique peptide was identified. Identified phosphorylation sites were filtered for localization probabilities greater than 75% and score differences greater than five.

Annotations were based on gene ontology classification (http://www.geneontology.org) using GO-FAT categories and KEGG pathways (DAVID Bioinformatics Resources 6.7) (46), the PhosphoSitePlus database (www.phosphosite.org; released September 3, 2013) (22) and visualized with Cytoscape version 2.8.3 (47) and Adobe Illustrator CS6.

Microscopy - For indirect immunofluorescence, cells were washed with PBS, fixated with 4% paraformaldehyde and permeabilized for 1 hour in 10 mM HEPES, 3% BSA, 0.3% Triton X-100, in PBS. Primary antibodies were applied over night at 4°C. Alexa Fluor-488 and -633-labeled secondary antibodies were used (Invitrogen, Carlsbad, USA). F-actin was stained using phalloidin-

Alexa Fluor-546 (0.3 µM, Invitrogen), nuclei were counterstained with 5 µg/ml DAPI (Invitrogen). Confocal laser scanning microscopy was performed with a Leica TCS SP2 instrument using a 40 x oil plan apochromat lens (Leica, Heidelberg, Germany). Deconvolution, 3-D reconstruction and maximum intensity projection were computed using Huygens (Scientific Volume Imaging, Hilversum, The Netherlands).

Patients, tumor sample preparation, analysis, and statistics - The study cohort comprised 55 patients from the Department of Urology, University Medicine Greifswald. The study was approved by the local review board (IRB protocol #BB 81a/12). Patients were treated for clear cell renal cell carcinoma (RCC) with open or laparoscopic radical or partial nephrectomy between 2012-2015. Tumor samples were immediately frozen at -80°C until use. Clinicopathological features included gender, age, the 7th edition of AJCC/UICC tumor, node, and metastasis classification (TNM) 2010 (48), Fuhrman grade (49), sarcomatoid features, tumor size, and the cancer specific survival time (CSS). RNA was extracted using 100 µl peqGOLD TriFast (Peqlab, Erlangen, Germany) per 10 mg tissue, the TissueLyser II system, and 5 mm stainless steel beeds (Qiagen, Hilden, Germany) according to the manufacturer's instructions. Primer specificity was confirmed by product sequencing. Descriptive statistics included medians and interquartile ranges (IQR). Differences in clinicopathological features were investigated with Fisher’s exact test. Survival times were estimated with the Kaplan Meier method and analyzed with the log rank test. The CSS was calculated from the date of surgery to the date of death from RCC, patients were censored in case of none-RCC related death or when alive at last follow up.

Results

We hypothesized that cytosolic Grx2c contributes to the development of cancer cells by promoting cell migration and invasion. To investigate this assumption, we have analyzed transiently transfected cell lines as well as a stably transfected clone of the HeLa cell line (HeLa-Grx2c) that expresses low levels of the cytosolic Grx2c in addition to the ubiquitous mitochondrial isoform Grx2a (Fig. 1A-B) (21). Wildtype HeLa cells express only the mitochondrial isoform Grx2a, but not the cytosolic Grx2c (Fig. 1A) (17).

Grx2c-induced changes in cellular morphology and motility – The expression of these low levels of Grx2c had a dramatic effect on the phenotype of the cells (Fig. 1 C-D). HeLa-Grx2c cells were elongated by a factor of two and formed long extensions of the cell body (Fig.1D) containing both actin and tubulin filaments. Grx2c induced the formation of numerous thin (~ 80 nm diameter) actin-based, filopodia-like extensions (Fig.1D). Another defining feature of the HeLa-Grx2c cells was their ability to migrate across each other (Fig.1C). To verify the specificity of the changes in morphology and motility for the presence and activity of Grx2c, we have tested their reversibility by silencing the expression of Grx2 in the HeLa-Grx2c cells by siRNA (Fig. 1E). In fact, siRNA treatment fully reversed the morphological changes induced by the expression of Grx2c (Fig. 1F-G).

We have assayed the effect of Grx2c on cell migration using a variant of the scratch or wound healing assay (Fig. 2A-B) as well as single cell tracking by live-cell microscopy (Fig. 2C). HeLa-Grx2c cells closed the gap opened by the removal of a barrier approximately two times faster compared to wildtype HeLa cells under the same conditions (Fig. 2A-B). As for the morphological changes, siRNA-mediated silencing of Grx2 in the HeLa-Grx2c cell line fully rescued this pehontype (Fig. 2B). Individual tracking of ≥ 60 cells confirmed the increased motility of HeLa-Grx2c cells on the plain surface of a culture vessel (Fig.2C, suppl. video 1). To exclude that this effect was specific for the cervical cancer cell line HeLa, we analyzed 786-O (renal cell adenocarcinoma) and PANC1 (pancreatic carcinoma of ductal origin)

cells. Independent of the initial migration velocities of these cell lines, the expression of Grx2c doubled the migration velocities of these different cancer cell lines (Fig.2C).

Next, we have analyzed the behavior of the Grx2c-expressing cell line embedded in a three dimensional collagen network (Fig. 3A-C, suppl. video 1-2). Unlike on the plain surface of a culture vessel, wildtype HeLa cells displayed a spherical phenotype and were neither able to infiltrate the collagen network, nor to migrate within (Fig. 3A, C, suppl. video 1). In contrast, HeLa-Grx2c cells kept their distinctive phenotype, infiltrated the collagen network, and actively migrated within this matrix (Fig.2B, C, suppl. video 2).

Grx2c-induced changes in the proteome and phosphoproteome - To further elucidate the role of Grx2c in the promotion of cell migration and invasion, we surveyed protein expression and signalling networks of HeLa-Grx2c cells on a global basis by quantitative proteomics and phosphoproteomics.

Using metabolically labeled Grx2c-expressing HeLa cells and corresponding controls, we reproducibly determined ratios for 4073 proteins (Fig.4A, suppl. tables). Furthermore, from our corresponding phosphopeptide analyses, phosphorylation events for 4327 sites (3695 serines, 474 threonines and 158 tyrosines) in 1682 proteins were quantitatively monitored (Fig.4B, suppl. tables). Together, both data sets resulted in 3414 phosphorylation sites with parallel quantification of protein expression, which corresponded to an overlap of approximately 75% between both sets (Fig.4C). We confirmed the changes in protein abundance and phosphorylation as identified by mass spectrometry for various proteins, *e.g.*, cyclin dependent kinase 5 (CDK5), glutaredoxin 1 and 5 (GLRX1, GLRX5), thioredoxin reductase 1 (TRXR1), and vinculin (VINC), by Western Blotting using available antibodies directed against proteins and specific phosphosites of the identified targets (suppl. Fig.1).

We primarily focused our analysis on those proteins and phosphosites with a reproducibly determined difference between HeLa-Grx2c and HeLa wildtype cells of at least two-fold. The proportion of significantly altered proteins at the level of protein abundance or phosphorylation thereby corresponded to approximately 8% (5% up, 3% down) and 25% (16% up, 9% down), respectively (Fig.4A-B). To understand the Grx2c-mediated molecular and cellular alterations, we assessed overrepresented functions and pathways with Gene Ontology (GO) enrichment analyses. The most prominent association was found with processes related to the actin cytoskeleton and cellular adhesions as well as the localization of the affected proteins primarily at cell-matrix and cell-cell contacts (Fig.4D). Additionally, altered phosphorylation sites were enriched in proteins closely linked to receptor-mediated signal transduction. (Phospho-) Proteomic enrichment analysis with the Kyoto Encyclopedia of Genes and Genomes (KEGG) pathway database resulted, in line with the results of the GO-based analysis, in the identification of corresponding major pathways. Highest significance was reached for ‘focal adhesion’ ($p = 2 \cdot 10^{-5}$, Benjamini-Hochberg corrected), ‘adherence junctions’ ($p = 4 \cdot 10^{-5}$) and ‘regulation of actin cytoskeleton’ ($p = 4 \cdot 10^{-5}$).

The adjustment of the phosphosite ratios demonstrated that approximately half of all altered phosphosites were changed at the phosphorylation level independent of changes in protein amounts (Fig.4C). This observation indicates effective phosphorylation-mediated perturbations in cellular signalling as a hallmark of Grx2c expression. To extract characteristic nodes altered in Grx2c-mediated signalling, we specifically interrogated our data sets for alterations in protein kinases. For approximately 150 different kinases quantitative information regarding protein expression or changes at phosphosites (234) was received by our profiling strategy (suppl. tables). Seven kinases showed a more than two-fold change in expression in HeLa-Grx2c vs. control cells, including trio Rho guanine nucleotide exchange factor (TRIO/*ARHGEF23*, 4.8-fold), the

epidermal growth factor receptor (EGFR, 2.3-fold) and the STE20-like serine/threonine-protein kinase (SLK, 0.5-fold). Thirty-three sites from 25 kinases were noticeable altered with an at least two-fold change in phosphorylation, the majority even after normalization to the corresponding protein ratio. For several of them a direct implication in kinase activity is known. The mitogen-activated protein kinase 1 MK01 (ERK2/*MAPK1*, pY187 2.6-fold after normalization), *e.g.*, is thus likely to be induced in down-stream activity in HeLa-Grx2c. The hepatocyte growth factor receptor MET (pY1003 0.2-fold, pY1234 0.3-fold), on the other hand, and Src-family kinases (pY419 0.4-fold) are likely repressed. Furthermore, in relation to the changes in protein expression, the receptor tyrosine kinase EGFR showed decreased phosphorylation at down-stream activation site pY1197 (0.3-fold) and increased phosphorylation at sites implicated in receptor internalization (pT693 2.0-fold; pS695 2.2-fold) (see suppl. Figs.2-3).

We utilized the PhosphositePlus database (22), which contains experimentally verified phosphorylation events and kinase substrate relationships, to match the kinases to their targets but also to track back additional potentially regulated up-stream kinases not identified in our screening (suppl. Fig. 2). Besides already deduced kinase modulations, such as increased activity for ERK2, further kinases including the cyclin-dependent kinases CDK1/2 and 5, the serine/threonine-protein kinase PAK1, the glycogen synthase kinase 3 β (GSK3β) and the mitogen-activated protein kinase 14 (p38α) can be anticipated with induced activity. Furthermore, the analysis suggests that the activity of the RAC-alpha serine/threonine-protein kinase AKT1 is repressed in consequence of Grx2c expression. Guided by these findings, we confirmed the elevated phosphorylation at kinase activation sites relative to protein expression in HeLa-Grx2c for CDK5, ERK, GSK3β, p38α, and PAK1 as well as the relative reduction in EGFR and MET by Western Blotting (suppl. Fig. 1).

Clinical data, Grx2c in clear cell renal cell carcinoma (ccRCC) – To study the potential role of Grx2c in tumor development and patient survival, we have initiated a pilot study addressing the presence of Grx2c in ccRCC, with a study cohort of 55 patients; patient characteristics were summarized in table 1. Grx2c expression was significantly more often detected in cancer compared to normal tissue (23/27 (85.2%) vs. 4/27 (14.8%); ($p<0.001$)). There was also a strong trend for more locally advanced tumor stages in Grx2c positive tumors (52.2% vs. 31.3%; $p=0.165$). Patients with vs. without detectable Grx2c had a clear tendency for a decreased cancer-specific survival (CSS) time (mean 19.1 vs. 30.5 months; median not reached, see Fig.5), albeit statistical significance for the CSS was not yet reached ($p=0.159$) due to the small cohort size and yet too short follow-up times. This tendency, however, is backed by data from ‘The Cancer Genome Atlas’ (23). In this ccRCC data set, with longer follow-up time and 462 patients included, a highly significant correlation between high mRNA expression levels of Grx2 and a decrease in cancer-specific survival probability was identified (suppl. Figure 4).

Discussion

Our study provides strong evidence that Grx2c does not only control axonal outgrowth and guidance (19) (24), but may also promote both the motility and invasiveness of non-neuronal cells. The combined proteomic and phosphoproteomic approach and the specific analysis for pathways altered in the Grx2c-expressing cells, demonstrated multiple specific alterations in the two major processes controlling cell migration and infiltration: cell adhesion and control of cytoskeletal dynamics. Suppl. Fig. 3 highlights the effects of Grx2c on some major factors and processes that control cell migration: actin binding proteins, small Rho-related GTPases, nucleation-promoting factors, nucleation and branching, and membrane ties, *i.e.* cell adhesion and adherence. Essentially all proteins highlighted have been

implied in cell migration, infiltration and malignant transformation before.

Our profiling strategy revealed profound alterations at the level of protein phosphorylation, independent from changes in protein amounts, indicating Grx2c-mediated alterations in the activity of up-stream protein kinases or phosphatases. We identified multiple kinases with relative increased (CDK5, ERK2, GSK3β, MK14/p38α, PAK1) and decreased (EGFR, FAK1, MET) activity, respectively. Essentially all of these kinases are involved in the regulation of cell adhesion or actin cytoskeleton dynamics, *e.g.* (25) (26). Moreover, activation of CDK5, ERK2, GSK3β, and PAK1 were implied in the development and progression of various cancers (27) (28) (29) (30).

The function of Grx2c in axonal outgrowth depends on the reduction of a regulatory dithiol-disulfide switch that controls two conformations of tetrameric collapsin response mediator protein 2 (CRMP2) (19) (31) (24). In wildtype HeLa cells most CRMP2 was detected in the oxidized conformation, while in HeLa-Grx2c cells, essentially all CRMP2 shifts to the reduced conformation (suppl. Figure 5A). Silencing of CRMP2 induced a phenotype similar to the one induced by the expression of its negative regulator Grx2c (suppl. Figure 5B-D). CRMP2 is an effector of the semaphorin (Sem3a) signalling pathway. This pathway controls, for instance, ureteric bud branching, vascular patterning (32), the collapse of axonal growth cones and thereby axon guidance (33), the migration of thymocytes within the thymic lobules (34) and adult T-cell polarization and migration (35). Besides the critical thiol-disulfide switch in the control of CRMP2 function, the protein is regulated by direct phosphorylation via the kinases CDK5 and GSK3β (36). For the latter two, the up-regulated activity was demonstrated in Grx2c-cells, all three GSK3β target sites in CRMP2 showed significantly increased levels of phosphorylation following Grx2c expression (suppl. tables). Phosphorylated CRMP2 has been demonstrated in association with the Cyfip1/WAVE1 (cytoplasmic FMR1-interacting protein 1/WASP family verprolin-homologous protein-1) complex (37), a potent promotor of actin filament nucleation through the ARP2/3 complex. The Ras family GTPase Rac1 (Ras-related C3 botulinum toxin substrate 1), together with phospholipids, recruits the WAVE complex to the membrane, unmasks the binding domain for the ARP2/3 complex and thereby initiates actin filament branching and polymerization at the membrane (38). Supporting a regulatory role of CRMP2 in the activation of the WAVE complex, Hall et al. (39) have previously demonstrated that the overexpression of CRMP2 inhibits the effects and morphology induced by a dominantly active Rac1 mutant.

The guanine nucleotide exchange factor (GEF) TRIO has been characterized as an activator of Rac1 and other Rho GTPases. The N-terminal domain, characterized as the Rac1 GEF, promotes actin cytoskeleton reorganization, especially lamellopodia dynamics, cell migration and spreading in a Rac1-dependent fashion (40) (41). Neural-specific targeted disruption of the TRIO gene in mice led to severe defects in both axonal guidance and cell migration and an attenuation of Rac1, RhoA, and Cdc42 activation (42), the three GTPases that orchestrate cell migration. Apparently, TRIO bears a central role in the transduction of extrinsic signals to Rho GTPases controlling the re-organization of the cytoskeleton (43). Our quantitative proteomics/phosphoproteomics approach highlighted a 4.8-fold elevation of TRIO levels and a 15-fold increase in phosphorylation at S2429, *i.e.* a 3.1-fold increase in phosphorylation over protein (suppl. tables and supplemantary Fig.7). Although so far only phosphorylation of Tyr residues of TRIO have been characterized in detail, these data suggest a central role of TRIO in the Grx2c-induced, CRMP2-dependent phenotype.

Clear cell RCC most likely originates from the terminal part of proximal tubules, but the entire process of RCC carcinogenesis is still elusive (44). The significantly higher frequency of Grx2c in RCC tissue compared to healthy kidney tissue and the strong trends in worsen cancer specific survival and more locally advanced tumor stages in the presence of Grx2c suggest a role of the protein in the carcinogenesis of RCC. The low patient numbers in subgroups and the overall short follow-up time explain why these results did not reach significance at the moment of our analyses. We plan to expand our cohort including samples with longer follow-up periods. However, already now, our data are strongly backed by the data from 'The Human Genome Cancer project'.

In synopsis, the presence of Grx2c in HeLa cells induced profound changes in cytoskeletal dynamics, significantly increased the motility of different cancer cells, and enabled the cells to invade a model matrix – key features of spreading cancer cells. Our proteomic and phosphoproteomic analysis revealed specific changes in proteins and pathways regulating cytoskeletal dynamics, in particular filo- and lamellopodia formation and cell adhesion. The clinical data imply a potential role of Grx2c in the carcinogenesis of ccRCC. Our results suggest a critical function of Grx2c in cell morphology, migration, matrix invasion, and possibly cancer development and progression.

Acknowledgments

The authors express their gratitude to C. Cott, M. Harms, K. Ventz, S. Oesteritz, and M. Werling for support and assistance.

References

1. Pollard TD, Blanchoin L, Mullins RD. Molecular mechanisms controlling actin filament dynamics in nonmuscle cells. Annu Rev Biophys Biomol Struct. 2000;29:545–76.
2. Pollard TD, Cooper JA. Actin, a central player in cell shape and movement. Science. 2009;326:1208–12.
3. Bravo-Cordero JJ, Hodgson L, Condeelis J. Directed cell invasion and migration during metastasis. Curr Opin Cell Biol. 2012;24:277–83.
4. Nürnberg A, Kitzing T, Grosse R. Nucleating actin for invasion. Nat Rev Cancer. 2011;11:177–87.
5. Pollard TD. Regulation of actin filament assembly by Arp2/3 complex and formins. Annu Rev Biophys Biomol Struct. 2007;36:451–77.
6. Soderling SH. Grab Your Partner with Both Hands: Cytoskeletal Remodeling by Arp2/3 Signaling. Sci Signal. 2009;2:pe5.
7. Kurisu S, Takenawa T. WASP and WAVE family proteins: friends or foes in cancer invasion? Cancer Sci. 2010;101:2093–104.
8. Lyons AJ, Jones J. Cell adhesion molecules, the extracellular matrix and oral squamous carcinoma. Int J Oral Maxillofac Surg. 2007;36:671–9.
9. Yilmaz M, Christofori G. EMT, the cytoskeleton, and cancer cell invasion. Cancer Metastasis Rev. 2009;28:15–33.
10. Holmgren A. Glutathione-dependent synthesis of deoxyribonucleotides. Purification and characterization of glutaredoxin from Escherichia coli. J Biol Chem. 1979;254:3664–71.
11. Gravina SA, Mieyal JJ. Thioltransferase is a specific glutathionyl mixed disulfide oxidoreductase. Biochemistry (Mosc). 1993;32:3368–76.
12. Mieyal JJ, Gallogly MM, Qanungo S, Sabens EA, Shelton MD. Molecular mechanisms and clinical implications of reversible protein S-glutathionylation. Antioxid Redox Signal. 2008;10:1941–88.

13. Lillig CH, Berndt C, Holmgren A. Glutaredoxin systems. Biochim Biophys Acta BBA - Gen Subj. 2008;1780:1304–17.
14. Lillig CH, Berndt C. Glutaredoxins in thiol/disulfide exchange. Antioxid Redox Signal. 2013;18:1654–65.
15. Hanschmann E-M, Godoy JR, Berndt C, Hudemann C, Lillig CH. Thioredoxins, glutaredoxins, and peroxiredoxins--molecular mechanisms and health significance: from cofactors to antioxidants to redox signaling. Antioxid Redox Signal. 2013;19:1539–605.
16. Jurado J, Prieto-Alamo M-J, Madrid-Rísquez J, Pueyo C. Absolute gene expression patterns of thioredoxin and glutaredoxin redox systems in mouse. J Biol Chem. 2003;278:45546–54.
17. Lönn ME, Hudemann C, Berndt C, Cherkasov V, Capani F, Holmgren A, et al. Expression Pattern of Human Glutaredoxin 2 Isoforms: Identification and Characterization of Two Testis/Cancer Cell-Specific Isoforms. Antioxid Redox Signal. 2008;10:547–58.
18. Hudemann C, Lönn ME, Godoy JR, Zahedi Avval F, Capani F, Holmgren A, et al. Identification, expression pattern, and characterization of mouse glutaredoxin 2 isoforms. Antioxid Redox Signal. 2009;11:1–14.
19. Bräutigam L, Schütte LD, Godoy JR, Prozorovski T, Gellert M, Hauptmann G, et al. Vertebrate-specific glutaredoxin is essential for brain development. Proc Natl Acad Sci U S A. 2011;108:20532–7.
20. Hou ST, Jiang SX, Smith RA. Permissive and repulsive cues and signalling pathways of axonal outgrowth and regeneration. Int Rev Cell Mol Biol. 2008;267:125–81.
21. Enoksson M, Fernandes AP, Prast S, Lillig CH, Holmgren A, Orrenius S. Overexpression of glutaredoxin 2 attenuates apoptosis by preventing cytochrome c release. Biochem Biophys Res Commun. 2005;327:774–9.
22. Hornbeck PV, Kornhauser JM, Tkachev S, Zhang B, Skrzypek E, Murray B, et al. PhosphoSitePlus: a comprehensive resource for investigating the structure and function of experimentally determined post-translational modifications in man and mouse. Nucleic Acids Res. 2012;40:D261-270.
23. Cancer Genome Atlas Research Network. Comprehensive molecular characterization of clear cell renal cell carcinoma. Nature. 2013;499:43–9.
24. Gellert M, Venz S, Mitlöhner J, Cott C, Hanschmann E-M, Lillig CH. Identification of a dithiol-disulfide switch in collapsin response mediator protein 2 (CRMP2) that is toggled in a model of neuronal differentiation. J Biol Chem. 2013;288:35117–25.
25. Dhavan R, Tsai LH. A decade of CDK5. Nat Rev Mol Cell Biol. 2001;2:749–59.
26. Sun T, Rodriguez M, Kim L. Glycogen synthase kinase 3 in the world of cell migration. Dev Growth Differ. 2009;51:735–42.
27. Eggers JP, Grandgenett PM, Collisson EC, Lewallen ME, Tremayne J, Singh PK, et al. Cyclin-dependent kinase 5 is amplified and overexpressed in pancreatic cancer and activated by mutant K-Ras. Clin Cancer Res Off J Am Assoc Cancer Res. 2011;17:6140–50.
28. Kim EK, Choi E-J. Pathological roles of MAPK signaling pathways in human diseases. Biochim Biophys Acta. 2010;1802:396–405.
29. Mishra R. Glycogen synthase kinase 3 beta: can it be a target for oral cancer. Mol Cancer. 2010;9:144.
30. Eswaran J, Li D-Q, Shah A, Kumar R. Molecular pathways: targeting p21-activated kinase 1 signaling in cancer--opportunities, challenges, and limitations. Clin Cancer Res Off J Am Assoc Cancer Res. 2012;18:3743–9.
31. Schütte LD, Baumeister S, Weis B, Hudemann C, Hanschmann E-M, Lillig CH. Identification

of potential protein dithiol-disulfide substrates of mammalian Grx2. Biochim Biophys Acta. 2013;1830:4999–5005.

32. Reidy K, Tufro A. Semaphorins in kidney development and disease: modulators of ureteric bud branching, vascular morphogenesis, and podocyte-endothelial crosstalk. Pediatr Nephrol Berl Ger. 2011;26:1407–12.
33. Schmidt EF, Strittmatter SM. The CRMP family of proteins and their role in Sema3A signaling. Adv Exp Med Biol. 2007;600:1–11.
34. Mendes-da-Cruz DA, Linhares-Lacerda L, Smaniotto S, Dardenne M, Savino W. Semaphorins and neuropilins: new players in the neuroendocrine control of the intrathymic T-cell migration in humans. Exp Physiol. 2012;97:1146–50.
35. Vincent P, Collette Y, Marignier R, Vuaillat C, Rogemond V, Davoust N, et al. A role for the neuronal protein collapsin response mediator protein 2 in T lymphocyte polarization and migration. J Immunol Baltim Md 1950. 2005;175:7650–60.
36. Cole AR, Causeret F, Yadirgi G, Hastie CJ, McLauchlan H, McManus EJ, et al. Distinct priming kinases contribute to differential regulation of collapsin response mediator proteins by glycogen synthase kinase-3 in vivo. J Biol Chem. 2006;281:16591–8.
37. Hensley K, Venkova K, Christov A, Gunning W, Park J. Collapsin response mediator protein-2: an emerging pathologic feature and therapeutic target for neurodisease indications. Mol Neurobiol. 2011;43:180–91.
38. Ridley AJ. Rho GTPases and actin dynamics in membrane protrusions and vesicle trafficking. Trends Cell Biol. 2006;16:522–9.
39. Hall C, Brown M, Jacobs T, Ferrari G, Cann N, Teo M, et al. Collapsin response mediator protein switches RhoA and Rac1 morphology in N1E-115 neuroblastoma cells and is regulated by Rho kinase. J Biol Chem. 2001;276:43482–6.
40. Seipel K, Medley QG, Kedersha NL, Zhang XA, O'Brien SP, Serra-Pages C, et al. Trio amino-terminal guanine nucleotide exchange factor domain expression promotes actin cytoskeleton reorganization, cell migration and anchorage-independent cell growth. J Cell Sci. 1999;112 (Pt 12):1825–34.
41. van Rijssel J, Hoogenboezem M, Wester L, Hordijk PL, Van Buul JD. The N-terminal DH-PH domain of Trio induces cell spreading and migration by regulating lamellipodia dynamics in a Rac1-dependent fashion. PloS One. 2012;7:e29912.
42. Peng Y-J, He W-Q, Tang J, Tao T, Chen C, Gao Y-Q, et al. Trio is a key guanine nucleotide exchange factor coordinating regulation of the migration and morphogenesis of granule cells in the developing cerebellum. J Biol Chem. 2010;285:24834–44.
43. van Rijssel J, van Buul JD. The many faces of the guanine-nucleotide exchange factor trio. Cell Adhes Migr. 2012;6:482–7.
44. Büttner F, Winter S, Rausch S, Reustle A, Kruck S, Junker K, et al. Survival Prediction of Clear Cell Renal Cell Carcinoma Based on Gene Expression Similarity to the Proximal Tubule of the Nephron. Eur Urol. 2015;68:1016–20.
45. Cox J, Neuhauser N, Michalski A, Scheltema RA, Olsen JV, Mann M. Andromeda: a peptide search engine integrated into the MaxQuant environment. J Proteome Res. 2011;10:1794–805.
46. Huang DW, Sherman BT, Lempicki RA. Systematic and integrative analysis of large gene lists using DAVID bioinformatics resources. Nat Protoc. 2009;4:44–57.
47. Saito R, Smoot ME, Ono K, Ruscheinski J, Wang P-L, Lotia S, et al. A travel guide to Cytoscape plugins. Nat Methods. 2012;9:1069–76.
48. Edge SB, Compton CC. The American Joint Committee on Cancer: the 7th edition of the

AJCC cancer staging manual and the future of TNM. Ann Surg Oncol. 2010;17:1471–4.

49. Fuhrman SA, Lasky LC, Limas C. Prognostic significance of morphologic parameters in renal cell carcinoma. Am J Surg Pathol. 1982;6:655–63.

Tables

Table 1 – Clinical pilot study, Grx2c in clear cell renal cell carcinoma, patient and tumor characteristics. The study cohort comprised 55 patients treated at the Department of Urology of the University Medicine Greifswald, Germany in the years 2012-2015.

Feature	Parameter	Patients
Age	Median (IQR)	70 (59–74)
Follow-up	Median (IQR)	11.2 (0.23–19.1)
Gender (%)	Male Female	38 (69.1) 17 (30.9)
T-Stage (%)	T1a T1b T2a T2b T3a T3b T3c T4	16 (29.1) 13 (23.6) 3 (5.5) 1 (1.8) 19 (34.5) 2 (3.6) 0 1 (1.8)
N-Stage (%)	N0 N1	52 (94.5) 3 (5.5)
M-Stage (%)	M0 M1	39 (70.9) 16 (29.1)
Fuhrman Grading (%)	G1 G2 G3 G4	9 (16.4) 28 (50.9) 15 (27.3) 3 (5.5)
Sarcomatoid Features (%)	Yes No	7 (12.7) 48 (87.3)
Cancer-specific death (%)		22 (20.0)

Figure legends

Figure 1 – Influence of Grx2c on the phenotype of HeLa cells

(A) Western-blot of HeLa and HeLa-Grx2c cell extracts stained with an antibody that identifies both the mitochondrial Grx2 isoform (Grx2a), as well as the cytosolic isoform (Grx2c). **(B)** Qunatitative PCR for Grx2c ($n \geq 9 \pm SD$). Together, these demonstrate the specific but low expression level of Grx2c in the HeLa-Grx2c cells. **(C)** HeLa-Grx2c actively migrated one upon the other; maximum intensity projection of the confocal series shown in (D, right side). **(D)** HeLa-Grx2c cells showed an increased cell length and possess various filopodia-like extensions; 3D-reconstruction of confocal image series, red: DNA, blue: actin, green: tubulin. **(E)** RT-PCR controls for the successful silencing of the Grx2 expression in HeLa-Grx2 cells. The phenotype of HeLa-Grx2c cells, transfected with a control siRNA **(F)**, is rescued to the normal HeLa phenotype by silencing the expression of Grx2 in this cell line **(G)**.

Figure 2 – Grx2c expression enhances cell migration

(A-B) The velocity of cell migration was first assayed using a modified protocol of the "scratch-type assay". Cells were seeded into µ-dishes (Ibidi coorp.) containing serum-reduced medium. Migration was induced by opening a 500 µm cleavage. The distance between the two cell layers was measured every four hours. **(B)** Quantification - HeLa-Grx2c cells closed the gap more than two-times faster compared to WT cells. **(C)** Migration velocity of HeLa, 786-O, and Panc1 cells, transfected with either control plasmid or a construct that leads to the transient expression of Grx2c, determined by live cell microscopy and tracking of ≥ 60 individual cells.

Figure 3 – Grx2c expression enables cells to infiltrate and migrate within a collagen matrix

Cell phenotypes and migration of HeLa **(A)** and HeLa-Grx2c cells **(B)** inside a collagen matrix, snapshots recorded during live cell tracings, see also suppl. videos. **(C)** Migration velocity of individually tracked HeLa and HeLa-Grx2c cells inside the 3 dimensional collagen matrix analyzed by live cell microscopy. n ≥ 60, 3 independent experiments.

Figure 4 – Grx2c-induced changes in the proteome and phosphoproteome of HeLa cells

(A-B) Frequency distribution of the HeLa-Grx2c vs. HeLa WT cells SILAC ratios of both replicates as identified by the protein expression (A) and phosphosite profiling (B) (replicate 1: white bars, replicate 2: black, overlay: grey). Numbers indicate phosphoproteins or phosphosites with fold-changes greater than two-fold in both replicates. **(C)** Correlation of the average SILAC phosphosite ratios and the same ratios normalized to their corresponding protein expression SILAC ratios. Adjusted phosphosite ratios greater than 1.5 (green dots) or less than 0.67 (red dots) in HeLa-Grx2c vs. WT cells are highlighted. Numbers indicate phosphosites consistently above the threshold in both replicates. **(D)** Gene ontology enrichment analysis of proteins with two fold difference at the level of protein expression (white bars) or phosphorylation (grey) between HeLa-Grx2c and WT cells. Enriched classifications for GO ‘Molecular Function’, ‘Biological Processes’, and ‘Cellular Compartments’ with Benjamini-Hochberg corrected p-values smaller than 0.005 are shown.

Figure 5 – Kaplan Meier analysis for the cancer specific survival (CSS) of patients with vs. without detectable Grx2c expression.

Patients with Grx2c had a clear but yet not significant trend for a decreased CSS. For details, see text and also suppl. Figure 5.

Figure 1

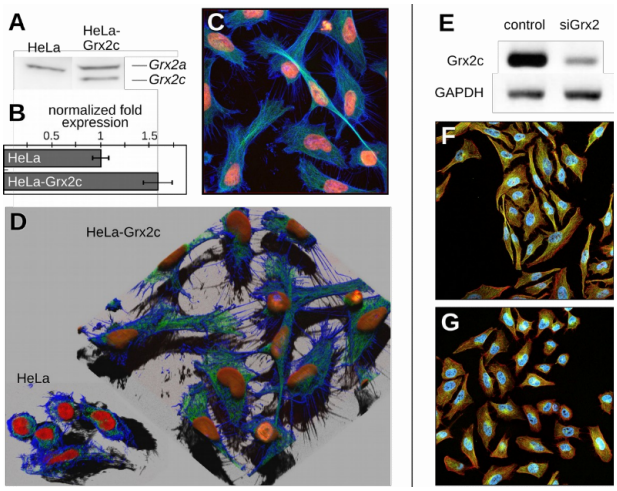

Figure 2

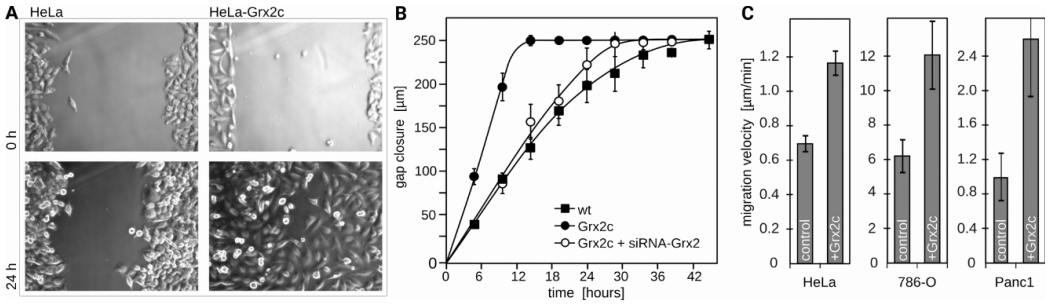

Figure 3

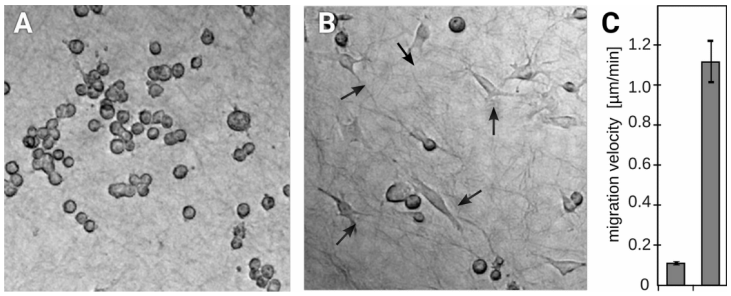

Figure 4

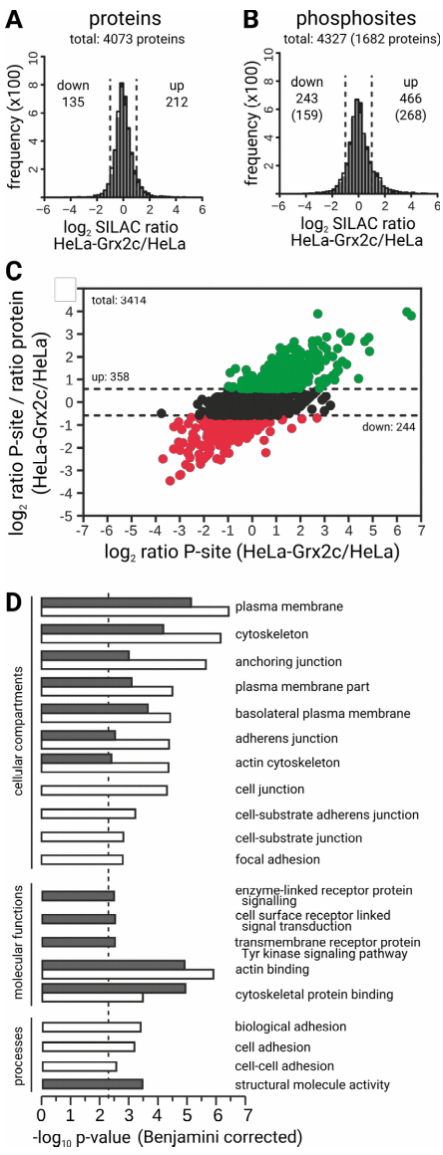
A
proteins
total: 4073 proteins
down
135
up
212
frequency (x100)
log2 SILAC ratio
HeLa-Grx2c/HeLa
B
phosphosites
total: 4327 (1682 proteins)
down
243
(159)
up
466
(268)
frequency (x100)
log2 SILAC ratio
HeLa-Grx2c/HeLa
C
total: 3414
up: 358
down: 244
log2 ratio P-site / ratio protein
(HeLa-Grx2c/HeLa)
log2 ratio P-site (HeLa-Grx2c/HeLa)
D
cellular compartments
plasma membrane
cytoskeleton
anchoring junction
plasma membrane part
basolateral plasma membrane
adherens junction
actin cytoskeleton
cell junction
cell-substrate adherens junction
cell-substrate junction
focal adhesion
molecular functions
enzyme-linked receptor protein signalling
cell surface receptor linked signal transduction
transmembrane receptor protein Tyr kinase signaling pathway
actin binding
cytoskeletal protein binding
processes
biological adhesion
cell adhesion
cell-cell adhesion
structural molecule activity
-log10 p-value (Benjamini corrected)

Figure 5

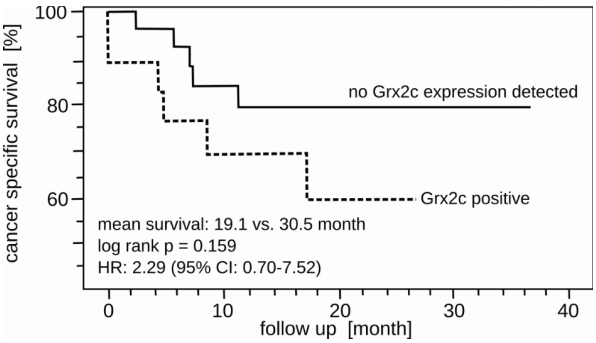
100
80
60
cancer specific survival [%]
no Grx2c expression detected
Grx2c positive
mean survival: 19.1 vs. 30.5 month
log rank p = 0.159
HR: 2.29 (95% CI: 0.70-7.52)
0
10
20
30
40
follow up [month]

Supplementary figures to:

The cytosolic isoform of glutaredoxin 2 promotes cell migration and invasion

Manuela Gellert[1], Erik Richter[2], Jörg Mostertz[2], Liane Kantz[3], Kai Masur[3], Eva-Maria Hanschmann[1], Silvia Ribback[4], Nils Kröger[1,5], Falko Hochgräfe[2], and Christopher Horst Lillig[1*]

From the Institute for Medical Biochemistry and Molecular Biology, University Medicine, Ernst Moritz Arndt University Greifswald, Germany (1), Competence Center Functional Genomics, Junior Research Group Pathoproteomics, Ernst Moritz Arndt University Greifswald, Germany (2), the Center for Innovation Competence plasmatis, Leibniz Institute for Plasma Science and Technology (INP), Greifswald, Germany (3), the Institute for Pathology (4), and the Clinic for Urology, University Medicine Greifswald, Germany (5).

Content:

Suppl. Fig. 1 – Western blots confirming the proteomic datasets

Left site: HeLa wildtype, right site: HeLa-Grx2c cells. SDS-PAGE and Western blots were run using the pre-casted TGX stain-free gels (4-20%, Biorad), and PVDF membranes (Machery & Nagel) according to the manufacturers' instructions (proteomics: SILAC ratios as determined by proteomics and phosphoproteomics).

The antibodies were purchased from the following companies: MK1/3 (Erk1/2, Cell Signalling Technology, #9102 , #9106); MK14 (p38, Cell Signalling Technology, # 9212 , # 9211); Met (Cell Signalling Technology, #4560 , #3077); Pak1 (abcam #ab131522 , Cell Signalling Technology, #2606); EGFR (Santa Cruz, #sc-16563); CDK5 (abcam #ab54926 ; Santa Cruz #sc-12919); GSK3 beta (abcam #ab131356); GSK3 alpha/beta pY216/pY279 (abcam 4797); VINC (vinculin, abcam #ab18058); NXN (proteintech, Chicago, IL, USA, #16128-1-AP); TrxR1, Grx1, and Grx5 (Godoy et al. *Biochim. Biophys. Acta* 1810: 2-92, 2011).

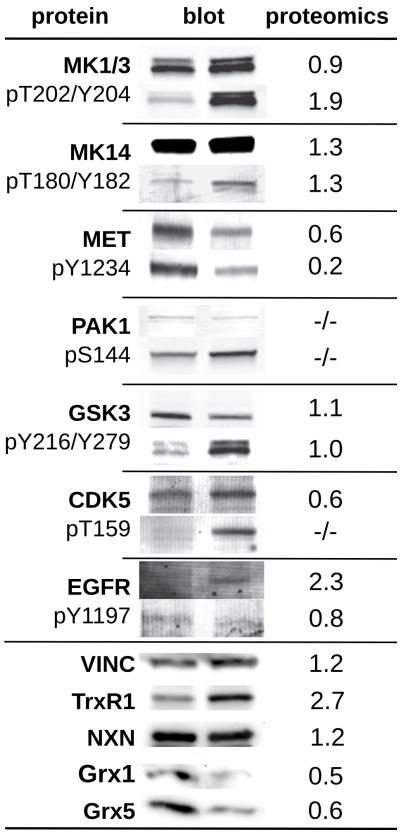

Suppl. Fig. 2 - Kinase substrate relationship analysis.

Substrate target sites with adjusted phosphosite ratios greater than 1.5 (green dots) or smaller than 0.67 (red dots) in HeLa-Grx2c vs. wildtype cells were mapped to their up-stream kinases using the PhosphoSitePlus database. Kinases (diamond shape) and substrates (elipse shape) were shown in a force-directed network if at least three events per kinase were consistently up- or down-regulated. For exact amino acid positions, please see supplementary tables.

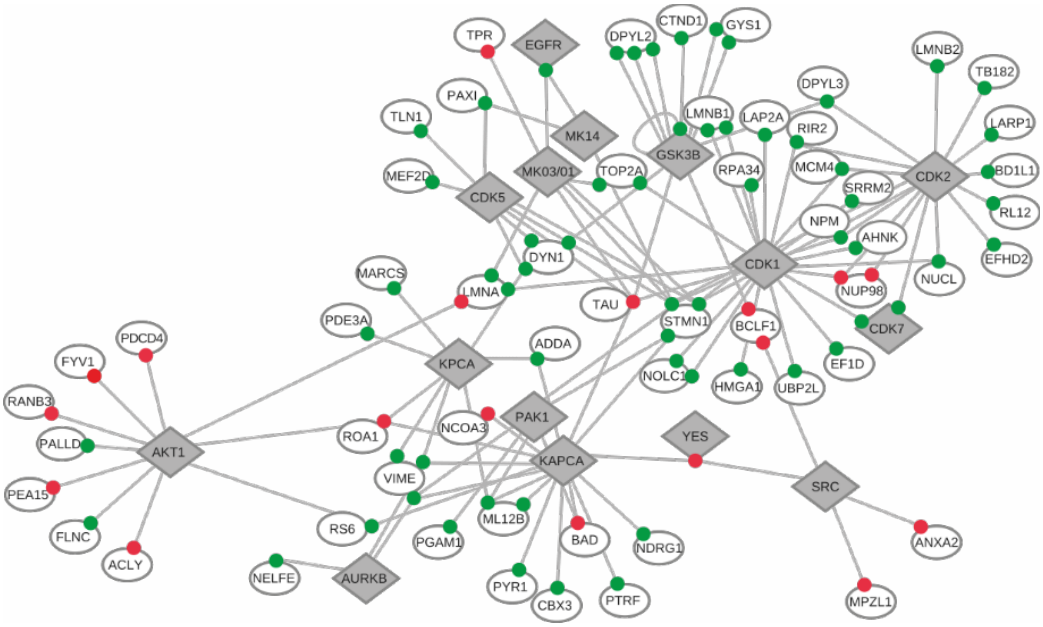

Suppl. Fig. 3 – Effect of Grx2c on the levels and phosphorylation status of proteins controlling actin dynamics

The level of increase or decrease in protein levels or phosphorylation status (normalized to the levels of the respective proteins) are indicated in shades of green (higher) or red (lower), see color code bar on the bottom right. Proteins of which the levels could not be determined by mass spectrometry are depicted in white (with total phosphorylation status). The uniprot entry IDs and, sometimes in addition, definite common trivial names were used to identify the proteins.

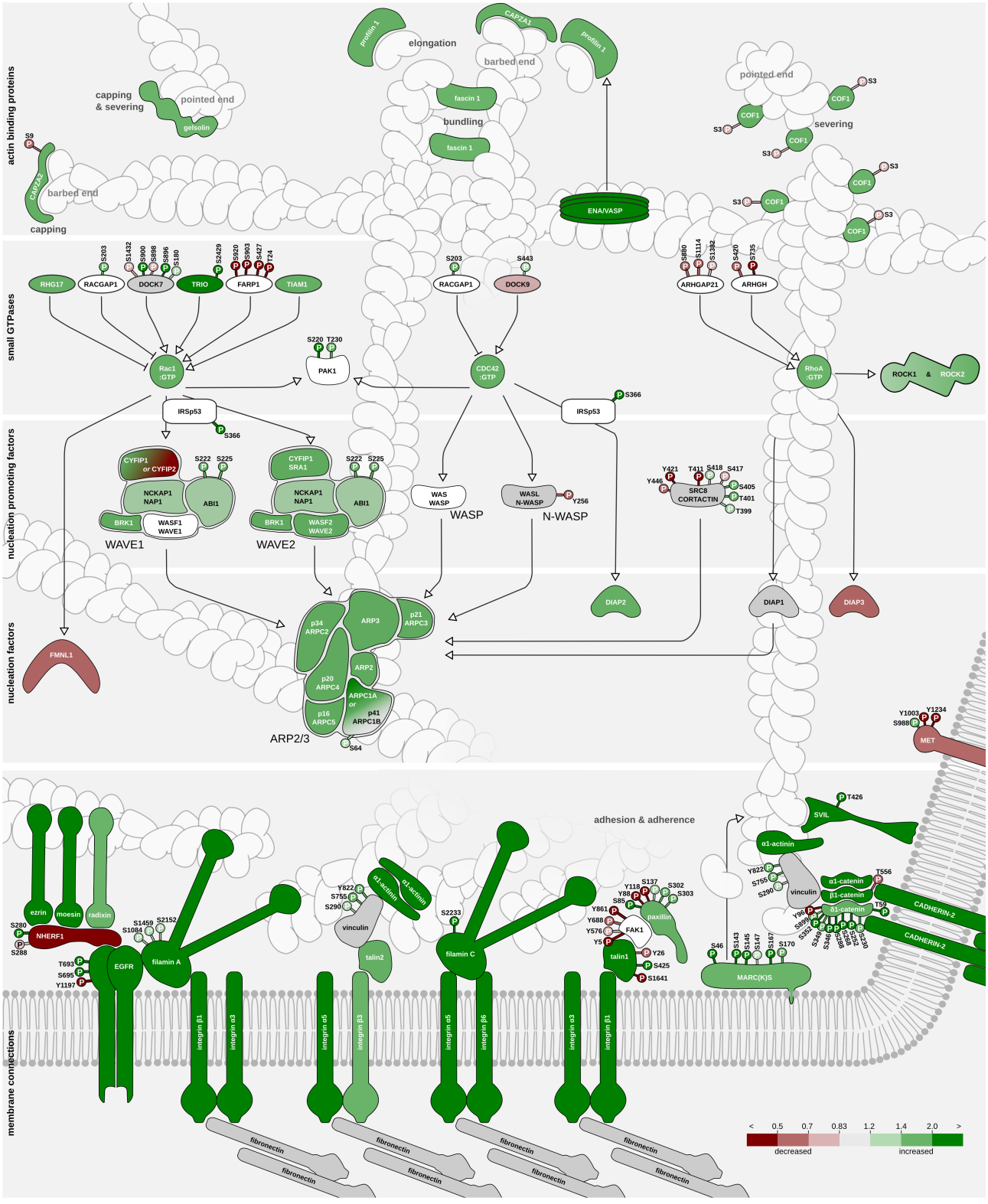

Suppl. Fig. 4 – Grx2-expression dependent cancer-specific survival probability in 'The Cancer Genome Atlas' data set.

The TCGA data set for clear cell renal cell carcinoma (KIRC, see Nature. 2013;499:43–9) was analyzed for the Grx2 expression-dependent cancer-related survival probability. Depicted is the Kaplan Meier analysis. Grx2 expression highly specifically correlates to the cancer-specific survival of ccRCC patients.

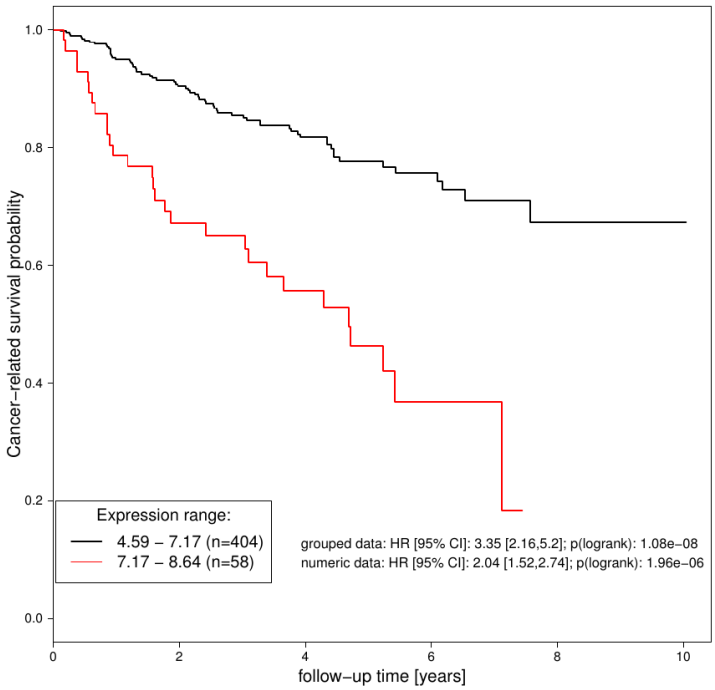

Suppl. Fig 5 – Potential role of the collapsin response mediator protein 2 (CRMP2) in the Grx2c-induced phenotype

A: Redox-dependent conformation of CRMP2 in HeLa and HeLa-Grx2c cells: Blue native PAGE stained by Western blotting for CRMP2. The lower signal in HeLa-Grx2c cells indicates the reduced (red) conformation, whereas CRMP2 in WT HeLa cells appeared to be present almost exclusively in the oxidized (ox) conformation, i.e. the higher signal (for details see: Gellert et al., J Biol Chem. 2013;288:35117–25). **B:** Evaluation of the silencing in HeLa and HeLa-Grx2c cells by Western blotting. Below: sequences of the three siRNA tested for the silencing of CRMP2 expression. The siRNA IDs as defined by the supplier Thermo Fisher (Ambion), Darmstadt, Germany, were included in front of the sequences. SiRNA2 was used for all subsequent experiments. **C:** Phenotype of HeLa cells transfected with a control siRNA and the siRNA2 targeting CRMP2. Depicted are layers derived from confocal microscopy. Yellow: F-actin, blue: DNA. **D:** Effects of CRMP2 silencing on HeLa cell motility. Cells were seeded confluently into the two inset chambers in a µ-dish (Ibidi). After 24 hours the inset was removed, opening a 500 µm cleavage. Fresh, serum reduced (5%, v/v) medium was added to suppress cell division. After removal of the inset, the width of the gap between the chambers was recorded every 6 hours by light microscopy.